

# **A study on the performance of Organic Light Emitting Diode Using bilayer anode**

By

**Dhrubajyoti Saikia**

Under Supervisor of

**Dr Ranjit Sarma**, Associates Professor, Physics Department

Jagannath Barooah College, Jorhat

Assam, 785001 India

THESIS SUBMITTED TO THE  
DIBRUGARH UNIVERSITY  
FOR THE DEGREE OF  
**DOCTOR OF PHILOSOPHY**  
IN PHYSICS



**DEPARTMENT OF PHYSICS**

**Dibrugarh University**

**Dibrugarh, Assam**

**2018**

## **Acknowledgement**

First and foremost, I want to thank my research advisor, Associate Professor Dr Ranjit Sarma for his guidance during my research work at Jagannath Barooah College. I am thankful to him for not only giving me an opportunity to work in his laboratory but also for being a great mentor. He was always accessible and willing to help. He unhesitatingly provided all the resources and assistance required for successful execution of this research goal.

Further, I am very grateful to Dr Lakhi Saikia, Professor of the material science department of North-East Institute of Science and Technology (NEIST), Jorhat for his valuable suggestion and also his effort to provide me with his laboratory facilities for FE-SEM images during the PhD period.

I would like to extend my gratitude to the Professor Parameshwar Kumar Iyer, Centre of Organic Electronics IIT-Guwahati and his research scholars specially Dipjyoti Das for providing me with the characterization facility of OLED devices. I am grateful for their efforts and untiring helping hands.

Thanks also go to my parents for their unflagging love and support throughout my life and never letting me forget where I come from. I want to give many thanks for them for truly understanding who I am and always supporting me no matter what the situation. Their loves and company always help me to weather the toughest times and make me want to become a better person.

## **Declaration**

This work has not previously been submitted to satisfy any of other degree requirements at this or any other university. This thesis contains no material published or written by another person except where due reference is made in this thesis itself.

## Urkund Analysis Result

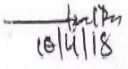
Analysed Document: Final Thesis of Dhrubajyoti Saikia13.doc (D37387652)  
Submitted: 4/10/2018 7:33:00 AM  
Submitted By: library@dibru.ac.in  
Significance: 1 %

Sources included in the report:

[https://en.wikipedia.org/wiki/Organic\\_electronics](https://en.wikipedia.org/wiki/Organic_electronics)  
<https://www.silvaco.co.kr/content/kbase/An.Organic.Light-Emitting.Diode.pdf>

Instances where selected sources appear:

11

  
10/4/18  
Deputy Librarian  
L. N. B. Library  
Dibrugarh University



Dibrugarh University, Dibrugarh

Annexure-V

LNB Library, DU  
Date: 10/04/18

Plagiarism Verification

Title of the Thesis: A study on the performance of organic light emitting diode using bilayer anode.....Page: 254.....

Researcher: Mr. Dhrubajyoti Saikia.....

Supervisor: Dr. Ranjit Sarma, Associate Professor, Jagannath Barooah College, Jorhat .....

Department: Registration under Department of Physics.....

Institution: Dibrugarh University, Dibrugarh, Assam .....

This is to report that the above thesis was scanned for similarity detection excluding bibliography and references. Process and outcome is given below:

Software used: URKUND.....Date: 10-04-2018.....

Similarity Index: 01%.....Total word count.....

The complete report is submitted for review by the Supervisor/ HOD.

Checked by

Similarity Index: 01%.....Total word count.....

The complete report is submitted for review by the Supervisor/ HOD.

Checked by

Date: 10-04-2018

Place: Dibrugarh

(Signature)  
Deputy Librarian &  
University Coordinator

The complete report of the above thesis has been reviewed by the undersigned.  
(Tick Check Box)

- The similarity index is below accepted norms.
- The similarity index is above accepted norms, because of the following reasons:

- 1.....
- 2.....
- 3.....
- 4.....
- 5.....

The thesis may be considered for the award of degree. (Relevant documents attached).

Signature of the Student

Signature of the Supervisor

# CERTIFICATE

It is certified that the six questions which are raised by the thesis expert have been properly addressed in the corrected version of the thesis entitled “A study on the performance of organic light emitting diode using bilayer anode” of Mr Dhrubajyoti Saikia.

(Dr Pankaj Dutta)

Head, Department of Physics and Chairperson, DRC

Dibrugarh University

(Dr Ranjit Sarma)

Associate Professor

Department of Physics,

Jagannath Barooah College

(Autonomous)

Date:25<sup>th</sup> January 2019

Date: 12/04/2018

## **Supervisor Clearance Certificate**

This is to certify that Mr. Dhrubajyoti Saikia a Ph.D. student of Dibrugarh University doing research work under my supervision at the Research Centre Department of Physics, Jagannath Barooah College has abided by the Ph.D. rules and regulations of Dibrugarh University. His work is original.

( Dr. Ranjit Sarma)

Associate Professor

Department of Physics, Jagannath

Barooah College

Dibrugarh University

## **List of figures**

Figure 1.1: Schematic representation of OLED

Figure 1.2 (a): Bottom emitting OLED structure

Figure 1.2 (b): Top-emitting OLED structure

Figure 1.3: Hybridization picture of Carbon atoms

Figure 1.4: Schematic representation of fluorescence and phosphorescence

Figure 1.5: Graphical representation of Forster energy transfer

Figure 1.6: Graphical representation of Dexter energy transfer

Figure 1.7: Emission of a light wave from the organic layer

Figure 1.8: Energy level alignment at the ideal situation of no dipole

Figure 1.9: Energy level alignment of modified metal/organic interface

Figure 1.10: Formation of the interfacial dipole at the metal/organic interfaces

Figure 2.2 (a): Spin coating set up for solution process film deposition

Figure 2.3 (a): Mask for buffer layer and organic layer deposition

Figure 2.3 (b): Mask for cathode layer deposition

Figure 2.5 (a): Vacuum coating set up of OLED fabrication under laboratory environment

Figure 2.5 (b): Fabricated structure of OLED over FTO electrode

Figure 2.5 (c): A photograph of OLED samples

Figure 2.5.9 (a) : Chemical structure of TPD

Figure 2.5.9 (b) : Chemical structure of Alq3

Figure 2.5.9.(c) : Chemical structure of Perylene



Figure 2.5.9 (d) : Chemical structure of Pentacene

Figure 2.5.9 (e) : Chemical structure of Rubrene

Figure 2.5.9 (f) : Chemical structure of PEDOT:PSS

Figure 2.5.9 (g) : Chemical structure of vanadium pentoxide

Figure 2.5.9 (h) : Chemical structure of molybdenum trioxide

Figure 2.5.9 (i) : Chemical structure of tungsten oxide

Figure 2.7 ( a): Block diagram of the UV-visible double beam spectrophotometer

Figure 2.7 (b): Field emission SEM setup

Figure 2.7(c): Gold coating unit under vacuum

Figure 2.8 (a): Chemical structure of ITO

Figure 2.8 (b): Chemical structure of TPD, m-MTDATA, NPB, and TAPC

Figure 2.8 ( c): Chemical structure of B-Phen, PBD, BALq, and TPBi

Figure 3.1 (a): Schematic representation of  $V_2O_5$  based OLED structure

Figure 3.1 (b): Energy level alignment of OLED structure

Figure 3.1 (c): Graph of applied voltage vs current density

Figure 3.1(d): Graph of applied voltage vs luminance

Figure 3.1 (e): Graph of applied voltage vs current efficiency

Figure 3.1 (f): Graph of applied voltage vs power efficiency

Figure 3.1 (g): Graph of the standard deviation of OLED at different thickness of  $V_2O_5$

Figure 3.1 (h): Graph of variation of sheet resistance and transmittance with a  $V_2O_5$  thickness

Figure 3.1 (i): FE-SEM images of bare FTO surface

Figure 3.1 (j): FE-SEM images of FTO/ $V_2O_5$  surface

Figure 3.1 (k): A cross-sectional SEM image of the device

Figure 3.2 (a): Schematic representation of NiO based OLED structure

Figure 3.2 (b): Energy band structure of OLED device

Figure 3.2 (c): Graph of applied voltage vs current density

Figure 3.2 (d): Graph of applied voltage vs luminance

Figure 3.2 (e): Graph of applied voltage vs. current efficiency

Figure 3.2 (f): Graph of applied voltage vs power efficiency

Figure 3.2 (g): Standard deviation of the efficiency of the OLED devices at different thickness of buffer layer over FTO surface

Figure 3.2 (h): Variation of sheet resistance and maximum optical transmittance with buffer layer thickness over FTO surface

Figure 3.2 (i): FE-SEM images of bare FTO surface

Figure 3.2 (j): FE-SEM images of FTO+NiO surface

Figure 3.2 (k): A crosssectional view of Nickel oxide layer over FTO surface

Figure 3.3 (a) Schematic representation of MoO<sub>3</sub> based OLED structure

Figure 3.3 (b): Energy band structure of OLED device

Figure 3.3 (c) Graph of applied voltage vs current density

Figure 3.3 (d): Graph of applied voltage vs luminance

Figure 3.3 (e): Graph of applied voltage vs. current efficiency

Figure 3.3 (f): Graph of applied voltage vs power efficiency

Figure 3.3 (g): Variation of optical transmittance and sheet resistance at different thickness of buffer layer over FTO surface

Figure 3.3 (h): FE-SEM images of bare FTO surface

Figure 3.3 (i): FE-SEM images of the FTO+MoO<sub>3</sub> surface

Figure 3.4 (a) Schematic representation of OLED structure

Figure 3.4 (b): Energy band structure of OLED device

Figure 3.4 (c) Transmission spectrums and a sheet resistance of bilayer FTO/WO<sub>3</sub> film

Figure 3.4(d): Graph of applied voltage vs current density

Figure 3.4 (e): Graph of applied voltage vs luminance

Figure 3.4 (f): Graph of applied voltage vs current efficiency

Figure 3.4 (g): Graph of applied voltage vs power efficiency

Figure 3.4 (h): FE-SEM images of bare FTO surface

Figure 3.4 (i): FE-SEM images of the FTO+WO<sub>3</sub> surface

Figure 3.5 (a): Variation of current density with time (in days) of FTO+V<sub>2</sub>O<sub>5</sub> OLED

Figure 3.5 (b): Variation of current density with time (in days) of FTO+NiO OLED

Figure 3.5 (c): Variation of current density with time (in days) of FTO+MoO<sub>3</sub> OLED

Figure 3.5 (d): Variation of current density with time (in days) of FTO+WO<sub>3</sub> OLED

Figure 3.5 (e): Variation of luminance with time (in days) of FTO+V<sub>2</sub>O<sub>5</sub> OLED

Figure 3.5 (f): Variation of luminance with time( in days) of FTO+NiO OLED

Figure 3.5 (g): Variation of luminance with time (in days) of FTO+MoO<sub>3</sub> OLED

Figure 3.5 (h): Variation of luminance with time (in days) of FTO+WO<sub>3</sub> OLED

Figure 3.5 (i): Variation of maximum current efficiency vs time in days

Figure 4.1 (a) Schematic representation of OLED structure

Figure 4.1 (b): Energy band structure of OLED device

Figure 4.1 (c): Graph of applied voltage vs current density

Figure 4.1 (d): Graph of applied voltage vs luminance

Figure 4.1 (e): Graph of applied voltage vs current efficiency

Figure 4.1 (f): Graph of applied voltage vs power efficiency

Figure 4.1 (g): Variation of maximum optical transmittance and sheet resistance at different thickness of buffer layer over FTO surface

Figure 4.1 (h): FE-SEM images of bare FTO surface

Figure 4.1 (i): FE-SEM images of FTO+Pentacene surface

Figure 4.2 (a): Schematic presentation of Perylene base OLED structure

Figure 4.2 (b): Energy band structure of OLED device

Figure 4.2 (c): Variation of optical transmittance and sheet resistance with Perylene thickness

Figure 4.2 (d): Graph of applied voltage vs current density

Figure 4.2 (e): Graph of applied voltage vs luminance

Figure 4.2 (f): Graph of applied voltage vs current efficiency

Figure 4.2 (g): Graph of applied voltage vs power efficiency

Figure 4.2 (h): Electroluminescence (EL) spectrum of all the OLED devices

Figure 4.2 (i): FE-SEM images of FTO surface

Figure 4.2 (j): FE-SEM images of FTO+Perylene surface

Figure 4.3 (a): Schematic representation of Rubrene based Organic Light Emitting Diode

Figure 4.3 (b): Energy level alignment of OLED structure

Figure 4.3 (c) Transmission spectrum and a sheet resistance of bilayer FTO/Rubrene film

Figure 4.3 (d): Graph of applied voltage vs current density

Figure 4.3 (e): Graph of applied voltage vs luminance

Figure 4.3 (f): Graph of applied voltage vs current efficiency

Figure 4.3 (g): Graph of applied voltage vs power efficiency

Figure 4.3 (h): Graph of standard deviation vs OLED devices

Figure 4.3 (i): FE-SEM images of single FTO surface

Figure 4.3 (j): FE-SEM images of FTO+Rubrene surface

Figure 4.4 (a): Schematic representation of PEDOT: PSS based OLED

Figure 4.4 (b): Energy band diagram of OLED

Figure 4.4 (c): Solution of Perylene doped PEDOT: PSS with 2-propanol solvent

Figure 4.4 (d): Graph of variation of optical transmittance vs wavelength of a polymer film with different concentrations of dopant

Figure 4.4 (e): Graph of doping concentrations vs sheet resistance of the polymer film

Figure 4.4 (f): Graph of current density vs voltage

Figure 4.4 (g): Graph of Luminance vs voltage

Figure 4.4 (h): Graph of current efficiency vs applied voltage

Figure 4.4 (i): Graph of power efficiency vs applied voltage

Figure 4.4 (j): FE-SEM images of bare FTO surface

Figure 4.4 (k): the FE-SEM image of non annealing doped polymer film over FTO surface

Figure 4.4 (l): the FE-SEM image of annealing doped polymer film over FTO surface

Figure 4.5 (a) : Variation of current density vs applied voltages w.r.t time (in days) for sample no.1

Figure 4.5 (b) : Variation of current density vs applied voltages w.r.t time (in days) for sample no.2

Figure 4.5 (c): Variation of current density vs applied voltages w.r.t time (in days) for sample no.3

Figure 4.5 (d): Variation of current density and voltage w.r.t time of sample-4

Figure 4.5 (e): Variation of luminance and voltage w.r.t time of sample-1

Figure 4.5 (f): Variation of luminance and voltage w.r.t time of sample-2

Figure 4.5 (g): Variation of luminance and voltage w.r.t time of sample-3

Figure 4.5 (h): Variation of luminance and voltage w.r.t time of sample-4

Figure 4.5 (i): Variation of maximum device efficiency w.r.t time (in days) for four different OLED sample

**List of tables:**

**Table -3.1:** Luminance and efficiency characteristics of the devices with different  $V_2O_5$  buffer layer thicknesses at the current density of  $30 \text{ mA/cm}^2$ .

**Table -3.2:** Luminance and efficiency characteristics of the devices with different NiO buffer layer thicknesses at the current density of  $20 \text{ mA/cm}^2$ .

**Table -3.3:** Luminance and efficiency characteristics of the devices with different  $MoO_3$  buffer layer thicknesses at the current density of  $20 \text{ mA/cm}^2$ .

**Table -3.4:** Luminance and efficiency characteristics for the devices with different buffer layer thicknesses at the current density of  $20 \text{ mA/cm}^2$ .

**Table -4.1:** Luminance and efficiency characteristics of the devices with different pentacene buffer layer thicknesses at the current density of  $30 \text{ mA/cm}^2$ .

**Table 4.2:** Summary of the property of OLED devices at a current density of  $20 \text{ mA/cm}^2$

**Table -4.3:** Luminance and efficiency characteristics for the devices with different buffer layer thicknesses at the current density of  $40 \text{ mA/cm}^2$ .

**Table 4.4:** Summary of the properties of OLED devices during the working period

**Table-5** Turn-on voltage, current efficiency and power efficiency of the Organic Light Emitting Diode (OLED) in bilayer anode structure by other workers.

**List of Abbreviations used:**

OLED: Organic Light Emitting Diode

LED: Inorganic Light Emitting Diode

MPD: Multiple Pump Down

SPD: Single Pump Down

CVD: Chemical Vapour Deposition

LCD: Liquid Crystal Display

U-V visible : Ultra-violet Visible

CB: Conduction Band

VB: Valence Band

EA: Electron Affinity

IP: Ionization Potential

TVEU: Thermal Vacuum Evaporation Unit

HOMO: Highest Occupied Molecular Orbital

LUMO: Lowest Unoccupied Molecular Orbital

ETL: Electron Transport Layer



HBL: Hole Blocking Layer

LEL: Light Emitting Layer

HTL: Hole Transport Layer

ETL: Electron Transport Layer

HIL: Hole Injection Layer

ALQ<sub>3</sub>: Tris ( 8-hydroxy quinolinato) Aluminium

TPD : N,N'-bis ( 3-methyl phenyl )-N,N'(phenyl)- benzidine

ITO: Indium-Doped Tin Oxide

FTO: Fluorine-doped Tin Oxide

V<sub>2</sub>O<sub>5</sub>: Vanadium Pentoxide

NiO: Nickel Oxide

MoO<sub>3</sub>: Molybdenum Trioxide

WO<sub>3</sub>: Tungsten Oxide

I-V: Current and Voltage

J-V: Current density and Voltage

L-V: Luminance and Voltage

EL: Electroluminescence

# FE-SEM: Field Emission-Scanning Electron Microscope

## List of contents

<b>Chapter 1: Introduction</b>	<b>Page</b>
<b>No.</b>	
1.1 Introduction to organic optoelectronics.....	
1.2 Introduction to Organic Light Emitting Diode (OLED).....	
1.3 Classification of OLEDs.....	
1.4 A literature review of the organic light emitting diodes (OLEDs).....	
1.5 Introduction to organic semiconductors.....	
1.6 Photo-physics of organic semiconductors.....	
1.6.1 Singlet and triplet excited state.....	
1.6.2 Fluorescence.....	
1.6.3 Phosphorescence.....	
1.7 Energy transfer mechanism.....	
1.7.1 Forster energy transfer.....	
1.7.2 Dexter energy transfer.....	
1.8 Device Physics.....	
1.8.1 Theory of operation.....	
1.8.2 Charge Injection.....	
1.8.3 Metal/Organic interfaces.....	
1.8.3.1 Work function.....	
1.8.3.2 Schottky Contacts.....	

1.8.3.3	Electronic properties of the interface.....
1.8.3.4	Origin of interface dipole.....
1.9	Organic compounds: Small molecules and polymers.....
1.10	Comparison of organic and inorganic light emitting diode.....
1.11	OLED applications and advantages.....
1.12	Useful impact on social life .....
1.13	Motivation of the present OLED research work.....
	<b>Chapter 2: Methodology Section.....</b>
2.1	Introduction to evaporation sources.....
2.2	Method of preparation of thin film.....
2.2.1	Vacuum evaporation.....
2.2.1.1	Single pump down (SPD) Procedure.....
2.2.1.2	Multiple pump-down (MPD) Procedure .....
2.2.2	Spin coating.....
2.2.3	Sputtering .....
2.3	Evaporation mask for vacuum deposition.....
2.3.1	Fabrication of evaporation masks.....
2.3.2	Evaporation mask for the buffer layer deposition.....
2.3.3	Evaporation mask for organic layer deposition.....
2.3.4	Evaporation mask for cathode electrode deposition.....
2.4	Cleaning of the evaporation masks.....

2.5 Fabrication and Characterization of OLED.....	
2.5.1 Thermal Evaporator System: Model-VT-2015 .....	
2.5.2 Cleaning of the vacuum unit and filaments.....	
2.5.3Substrates preparation.....	
2.5.4Heating of the substrates.....	
2.5.5Evaporation of the buffer layer over electrode surface.....	
2.5.6Evaporation oforganic ayers.....	
2.5.7Evaporationof the cathode electrode.....	
2.5.8Organic light emitting diode.....	
2.5.9 Materials used for OLED fabrication.....	
2.6 Important parameters of OLED.....	
2.6.1 Current-density characteristics.....	
2.6.2 Luminance-voltage characteristics.....	
2.6.3 Current efficiency.....	
2.6.4 Power efficiency.....	
2.6.5 Maximum luminance.....	
2.6.6 Turn-on voltage.....	
2.7 OLED characterization facility .....	
2.7.1 Device characterization facility .....	
2.7.2 Surface characterization facility.....	
2.8 Commonly used materials for OLEDs.....	

### **Chapter 3**

A study of the effect of both single and double layer anode regarding the performance of organic light emitting diode (OLED) using inorganic-inorganic bilayer structure.

#### **3.1 A comparative study of the influence of Vanadium Pentoxide layer on the FTO surface of the organic light emitting diode**

3.1.1 Device fabrication  
.....

3.1.2 Schematic representation and energy level alignment.....

3.1.3 Results and Discussion .....

3.1.4 Conclusions.....

#### **3.2 Comparative study of the organic light emitting diode with Nickel Oxide interlayer on FTO surface for anode modification**

3.2.1 Device fabrication .....

3.2.2 Schematic representation and energy level alignment.....

3.2.3 Results and Discussion .....

3.2.4 Conclusions.....

#### **3.3 Improve performance of organic light emitting diode using molybdenum trioxide (MoO<sub>3</sub>) interlayer between the electrode and organic interface**

3.3.1 Device fabrication .....

3.3.2 Schematic representation and energy level alignment.....

3.3.3 Results and Discussion .....

3.3.4 Conclusions.....

#### **3.4 Performance improvement of an organic light emitting diode using tungsten oxide (WO<sub>3</sub>) interlayer between the electrode and organic interface**

3.4.1 Device fabrication .....

3.4.2 Schematic representation and energy level alignment.....

3.4.3 Results and Discussion .....

3.4.4

Conclusions.....

**3.5 Stability of the devices.....**

**3.6 Observation and conclusion.....**

#### **Chapter 4.**

A study of the effect of both single and double layer anode regarding the performance of organic light emitting diode (OLED) using inorganic-organic bilayer structure.

**4.1 Effect of Pentacene interlayer between the electrode and organic interface of organic light emitting diode**

4.1.1 Device fabrication .....

4.1.2 Schematic representation and energy level alignment .....

4.1.3 Result and discussion.....

4.1.4 Conclusions.....

**4.2 Fabrication and characterization of organic light emitting diode with Perylene doped PEDOT: PSS interlayer on FTO surface for anode modification**

4.2.1 Device fabrication .....

4.2.2 Schematic representation and energy level alignment .....

4.2.3 Result and discussion.....

4.2.4 Conclusions.....

**4.3 Performance improvement of the organic light emitting diode with Rubrene interlayer on FTO surface for anode modification**

4.3.1 Device fabrication .....

4.3.2 Schematic representation and energy level alignment .....

4.3.3 Result and discussion.....

4.3.4 Conclusions.....

**4.4 Organic Light Emitting Diode with Fluorine-doped Tin Oxide (FTO)/  
Perylene doped PEDOT: PSS bilayer electrode**

4.4.1 Device fabrication .....  
4.4.2 Schematic representation and energy level alignment .....  
4.4.3 Result and discussion.....  
4.4.4 Conclusions.....  
**4.5 Stability of the devices.....**

**4.6 Observation and  
conclusion.....**

**Chapter 5: Conclusion**

5.1 Summary and conclusion.....  
5.2 Recommendations for Future Work.....  
5.3 Paper published and papers presented.....  
5.4 Workshop attended.....  
5.5 Bibliography.....

**Abstract**

An organic light-emitting diode (OLED) is a light-emitting diode (LED) in which the emissive electroluminescent layer is a thin film of organic compound which emits light in response to an electric current. A typical OLED consists of cathode, electron transport layer(ETL), emissive layer(EML), a hole transporting layer(HTL) and anode layer grown sequentially on the substrate surface, which emits light under forward biased. To achieve high quantum efficiency for electroluminescence (EL), it is necessary to attain three attributes: (i) efficient charge injection from electrodes at low voltage (ii) good charge balance & (iii) confinement of the injected charge carrier within the light emitting region. This work is based on the charge confinement phenomenon within the quantum tunneling region. Below I have summarized all chapter of my thesis.

## **Chapter 1: Introduction**



In the first chapter, I have given a brief introduction about the importance of organic semiconductor and their use in optoelectronic devices. Light emission process from organic materials is discussed in two forms, i.e., Fluorescence and Phosphorescence along with their mechanisms. Device physics is also mention in details. Literature review and motivation of the work is presented in the last portion of the first chapter.

The attraction to organic materials for lighting & display application had started during 1950-1960s, because of the high fluorescence quantum efficiency exhibited by some organic molecules. Study of electroluminescence in an organic semiconductor has started in the 1950s by Bernamose using dispersed polymer films. In the year 1960 Pope discovered EL of organic materials. Next step in the evolution towards efficient OLED was made in the 1970s through the use of vacuum vapor deposition techniques to prepare thin organic films. Two decades later, Patridge reported the first EL from polymeric materials, which was shortly followed by Tang & Van Slykes' discovery in 1987 the first working OLED. This work had stimulated a very intense activity in the field of organic electroluminescence. In 1990, Burroughs introduced the first polymer-based OLED where polyphenylene vinylene (PPV) was used as the active element in a large area LED. Braun & Heager followed it in 1991 in which they observed EL from diodes produced with MEH-PPV, soluble derivatives of PPV. Thus the development of OLED was continuously progressed with the advancement of time because it has many advantages, such as a simple fabrication process, a wide view angle, a quick switching speed, and low-cost production compared to the conventional LCD. One of the major areas of development has been in the field of interfacial engineering. The interface between the organic layer and the electrodes plays an important role in the

organic light emitting diode (OLED) performance because it determines the efficiency of the charge carrier injection from the electrode into the emitting layer. To improve the interface characteristics, the insertion of a buffer/injection layer between anode and hole transport layer (HTL) is one of the simple and effective methods to improve the device performances. Interfacial engineering often involves tailoring the electron energy levels of the materials that are in contact with one another, to minimize or eliminate the charge-injection barrier. Different works are carried out on Indium tin oxide (ITO) substrates. However, there are published reports that indium tends to diffuse into the emissive organic layer under device operation which may in turn influence the quantum efficiency and lifetimes of organic LEDs. Also, it is known that the performance of ITO-based organic LEDs is highly dependent on the chemical condition of the ITO electrode, which is affected, during any particular method used to clean the ITO surface for the device fabrication. Also, the work function of the ITO surface depends upon the cleaning method employed. On the other hand, a high work function does not mean a low turn-on voltage in organic LEDs because the surface and interfacial chemistry are essential for determining the charge injection across the organic layers. From the literature report, it is found that Fluorine-doped tin oxide (FTO) electrode is not widely used to fabricate the EL devices in OLED society because of their less conductivity and transparency than ITO. However, in the visible region, it is found that the optical transmission of FTO is independent of the fluorine doping. Furthermore, FTO is less expensive to produce compared with ITO. Similarly, work function and the chemical composition of FTO is independent of the cleaning methods. Therefore based on the literature report here we have decided to address the

fabrication of OLED over this non –conventional FTO surface using bilayer anode concept. Following points give the beneficial direction of bilayer anode OLED over single layer anode.

- A. Bilayer anode enhances the positive charge carrier injection tendency into the organic layer from a high energy level compared with that of a single electrode surface.
- B. Hole injection layer or buffer layer prevents the diffusion of the metallic ion into the organic layer from the anode side.
- C. Also reduces the probability of an electrical breakdown of the device.

## **Chapter 2: Methodology**

In the second chapter, I have discussed the methodology of fabrication in which two methods - Thermal vacuum deposition & Spin coating are employed. In this work, all devices are fabricated on FTO (fluorine-doped tin oxide) coated glass. Thermally deposited aluminum (AL) is used as the cathode. The FTO glasses are ultrasonically cleaned with acetone, isopropanol and deionized water for 20 min and then dried by an air gun before the fabrication of OLED devices. This cleaning step is used to remove the surface contaminants and to provide a clean FTO surface to enhance the adhesion of another layer onto its substrates. It is pre-patterned using an etching process (combination of zinc dust and dilute HCl). In our work, the filaments and boats are also flash-cleaned in a vacuum by momentarily passing a heavy current. Flash-cleaning of filaments and boats is essential for removal of contaminants adhering to them. After cleaning and etching step, we deposited the different layer of OLED

device on the substrate sequentially up to the cathode layer with proper shadow masking system (prepared in the laboratory). In this work, all the depositions are carried out at a base pressure of less than  $2 \times 10^{-6}$  Torr. The organic and the inorganic layers are evaporated at the rate of  $10 \text{ \AA} / \text{s}$  except for the polymer layer which was carried by a spin coating process. All the devices are fabricated by using Thermal Vacuum Evaporation Unit (TVEU), and the corresponding film thicknesses are recorded by a digital and interconnected thickness monitor inside the vacuum chamber (Model DTM-10) and further confirmed by a profilometer. Finally, the samples are stored kept in a desiccator charged with  $\text{CaCl}_2$  for 3-4 days for stabilization. Optical transmittances are measured by UV–Visible double beam spectrophotometer unit. The current-voltage-luminance characteristics of the fabricated OLEDs are measured by digitally controlled source-meter unit (SMU) and luminance meter unit. All tests are performed in air at room temperature under dark room condition without any encapsulation. The materials are purchased from Sigma-Aldrich Company (USA) and are used without further purification. We have fabricated and characterized the standard OLEDs samples using the following configuration.

*FTO(anode)/Buffer layer/ Hole transport layer/Light emitting layer/Electron transport layer/Cathode*

The Current density–Voltage–Luminance characteristics of respected OLEDs are compared with the different thickness of buffer layer and also that of without any buffer layer. Here we used lithium fluoride (Lif) as an electron injection layer and TPD [N, N'-Bis(3-methyl phenyl)-N, N'-diphenylbenzidine] as a hole transport layer. Without

this layer, it is difficult for electron injection from AL cathode to the Alq<sub>3</sub> [Tris-(8-hydroxyquinoline)aluminum] layer as the dissociation of the alkali halide into the organic layer leads to the enhancement of electron injection.

### **Chapter 3: The effect of both single and double layer anode on the performance of Organic Light Emitting Diode (OLED) using inorganic-inorganic bilayer structure.**

The third chapter explains the experimental observation, findings, and calculation relating to inorganic-inorganic bilayer anode based OLED configurations. For this purposes, inorganic metal oxide especially transitions metal oxides, i.e., V<sub>2</sub>O<sub>5</sub> ( vanadium pentoxide), NiO (nickel oxide), MoO<sub>3</sub> (molybdenum trioxide) and WO<sub>3</sub> ( tungsten oxide ) are used as buffer layer because of their high work function value and higher optical transmission within the visible wavelength region. The structures of all the bottom light emitting OLED devices used in this study are shown below:

Device 1: FTO/ V<sub>2</sub>O<sub>5</sub>/ TPD/Alq<sub>3</sub>/Lif/AL

Device 2: FTO/ NiO/ TPD/Alq<sub>3</sub>/Lif/AL

Device 3: FTO/ MoO<sub>3</sub>/ TPD/Alq<sub>3</sub>/Lif/AL

Device 4: FTO/WO<sub>3</sub>/TPD/Alq<sub>3</sub>/Lif/AL

I have investigated the performance improvement of OLED using an optimized layer of hole injection or buffer layer with the help of thickness variation method. In this

work, OLED performances are studied by current density, luminance, current efficiency and power efficiency characteristics along with their standard deviation value of device efficiency, in which highest current efficiency is found to be 8.42 cd/A for  $\text{WO}_3$  based OLED device with an optimized thickness of 12nm over FTO electrode. Similarly, other values of current efficiency are found to be 2.83 cd/A, 7.32 cd/A and 7.62cd/A for the devices with  $\text{V}_2\text{O}_5$ , NiO, and  $\text{MoO}_3$  based OLED devices. The maximum values of power efficiency values are 0.73 lm/W, 1.62 lm/W, 1.71 lm/W and 2.32 lm/W respectively for the devices with  $\text{V}_2\text{O}_5$ , NiO,  $\text{MoO}_3$ , and  $\text{WO}_3$  layer based OLED devices.

We have also studied the surface morphology of both the single and double layer electrode surface with the help of Field Emission Scanning Electron Microscope (FE-SEM). The stability of the fabricated OLED devices with time for inorganic based hole injection layer over FTO surface is also studied.

#### **Chapter 4: The effect of both single and double layer anode on the performance of organic light emitting diode (OLED) using inorganic-organic bilayer structure.**

Inorganic-organic layer based bilayer anode OLED devices are presented in the fourth chapter. For this purpose, organic materials, i.e., Pentacene, Perylene, Rubrene, and PEDOT: PSS [poly (3, 4-ethylenedioxythiophene: poly (4-styrenesulfonate))] are used as a buffer layer over the non-conventional FTO electrode surface.

The structures of all the bottom light emitting OLED devices used in this section are shown below:

Device 5: FTO/ Pentacene/ TPD/Alq3/Lif/AL

Device 6: FTO/ Perylene/ TPD/Alq3/Lif/AL

Device 7: FTO/ Rubrene/ TPD/Alq3/Lif/AL

Device 8: FTO/ PEDOT: PSS/ TPD/Alq3/Lif/AL

The investigation of the performance improvement of OLED by using an optimized layer of hole injection layer or buffer layer with the help of thickness variation method is used here. For polymer film(PEDOT: PSS) doping process is used to optimize the film. OLED performances are studied by current density, luminance, current efficiency and power efficiency characteristics. Here highest current efficiency is found to be 6.38 cd/A for doped PEDOT: PSS based bilayer anode OLED device over FTO electrode. Similarly, other values of efficiency are found to be 4.12 cd/A, 5.25 cd/A, and 6.35 cd/A respectively for the devices with Pentacene, Perylene, and Rubrene based bilayer anode. Similarly, the maximum values of power efficiency are found to be 0.874 lm/W, 1.39 lm/W, 2.23 lm/W and 1.58 lm/W respectively for the device 5, device 6, device 7 and device 8. We also calculate the standard deviation of device efficiency of each device. We have also studied the surface morphology of both the single and double layer electrode surface with the help of Field Emission Scanning Electron Microscope (FE-SEM). The stability of the fabricated OLED devices on time for the organic buffer layer based is also studied.

## **Chapter 5: Summary and conclusion**

In the fifth chapter, I have included the summary and conclusion of the thesis. The present investigation reported the enhanced charge carrier injection in OLED devices by placing a thin buffer layer between electrode and the organic hole transport layer. We have fabricated and characterized both single and double layer electrode based organic light emitting diode( OLED) using both inorganic and organic materials by using proper instrumentation. Our work is based on eight bilayer anode OLED configuration, and we found that device parameters including current density, luminance, current efficiency and power efficiency are improved by employing buffer layer compared to the single electrode based OLED devices. The maximum values of current efficiency for the bilayer anode OLEDs are found to be 2.83 cd/A, 7.32 cd/A, 7.62cd/A, 8.42 cd/A, 4.12 cd/A, 5.25 cd/A, 6.35 cd/A and 6.38 cd/A respectively for the devices 1, device 2, device 3, device 4, device 5, device 6, device 7 and device 8 respectively. While the maximum power efficiency values of the corresponding devices are found to be 0.73 lm/W, 1.62 lm/W, 1.71 lm/W, 2.32 lm/W, 0.874 lm/W, 1.39 lm/W, 2.23 lm/W and 1.58 lm/W respectively. Similarly, the stability of all the bilayer anode OLED devices is also noted per day decay rate for device parameters like current density, luminance, and current efficiency. The result or findings of this work demonstrated the utility of non-conventional and less popular FTO electrode towards the application of OLED society. Highly performance of FTO based OLED is realized for the first time as an outcome of this thesis.

I also included few points regarding the future direction of this research work.



## **Chapter –I**

### **1.Introduction**

#### **1.1 Introduction to organic optoelectronics:**

Organic optoelectronics is the branch of material science which deal with the characterization, and application of organic small molecules or polymers that provides electronic properties. Compared to inorganic conductors and semiconductors, organic electronic materials are constructed from organic (carbon-based) small molecules or polymers. One of the most considerable benefits of organic electronics is their possible low cost compared to conventional inorganic electronics.

Organic optoelectronic devices are electrical devices, such as light emitting diodes (LEDs), photovoltaics (PVs), or thin film transistors (TFTs), in which organic

materials with semiconducting properties are mainly used as the active materials. Because of the discrete nature of the molecular units of organic materials, there is no need for long-range order between the adjacent molecules or polymer chains. Therefore we can say that these organic semiconductors have the more advantage over conventional inorganic semiconductors materials such as Si or GaAs etc. Thus it is possible to fabricate complicated multi-layer device structures in the range of nanometer film thickness from organic materials with the help of roll-to-roll printing or vacuum coating techniques. However, there is also an important point which should be noticeable is the discrete nature of organic semiconductors. Because this nature implies that normally organic semiconducting material contain almost no intrinsic charge carriers (i.e., electrons or holes) and thus they can be considered as an insulator until electrical charges are injected into them. This fact implies that in the application of electrical devices all of the holes and electrons within a device must be injected from the anode and cathode respectively. This is again linked with the interface property between the organic materials and the electrode surface. Because this interface region has great influence on the device stability, performance and lifetime. In the literature, different reports are found regarding the importance of the electrode/organic contacts.

## **1.2 Introduction to Organic Light Emitting Diode (OLED)**

With the development of the technology of low-cost integrated circuits, the search for thin film devices also began. Integrated circuits (IC) incorporate numerous active and passive components in single crystal silicon wafers. Such types of IC are not suitable

especially for circuits for addressing flat-panel displays. Hence an alternation approach is necessary. In this regard, thin film fabrication technique is more suitable which permits the fabrication of different thin film devices on both rigid and flexible substrates. Among these thin film devices, an organic light emitting diode (OLED) has been one of the most attractive devices in Physics and materials more than last two decades. Because of the interdisciplinary nature of the organic light emitting diode, this research became more attractive and interest among the various researchers in the different period of interval. This interdisciplinary nature mainly includes synthetic and physical chemistry along with the device physics and surface engineering. Thus we can say that Organic Light Emitting Diodes (OLEDs) should develop a new and exciting technology for optoelectronic devices. It is found that this organic light emitting diode possesses several advantages. Some of which are self-light emitting tendencies, very low power consuming with a wide viewing angle (greater than 150 degrees) and having a faster response time. The organic light emitting diode is defined as the generation of light from the organic materials due to the application of electrical biasing. The organic light emitting diode has been widely studied and investigated to improve their performance which has great enormous applications in optoelectronics including flat-panel displays and solid-state lighting technology. Usually, it is possible to fabricate an OLED with one or more semiconducting organic thin films which are sandwiched between two electrodes. One of these must be transparent (i.e., anode) for emission of the generated light wave from the device, and the other electrode must always be optically reflective (i.e., cathode). During the operation of OLED, the primary function of the anode is to inject the positively charged particles into the

organic light emitting material. This charged particle is known as holes. On the other hand opposite function is performed by the cathode electrode (i.e., injection of an electron into the light emitting layer). When these opposite charge particles are reached the light emitting layer, they feeling a coulombic attraction because of which they come into close to each other. This is known as electron-hole pair recombination and is more popularly referred to as an exciton. When an exciton is formed, they can radiatively recombine to emit light. On the other hand, this emitted light is again reflected by the metallic cathode layer which finally escapes through the above mentioned optically transparent anode.

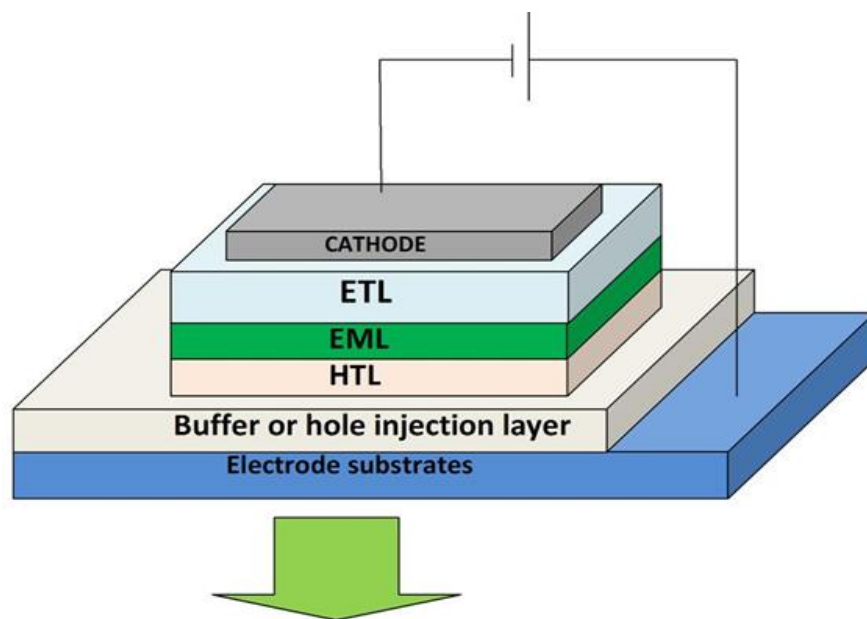


Figure 1.1: Schematic representation of OLED

A generalised schematic representation of OLED is shown in Fig. (1). In OLED society Indium tin oxide (ITO) is commonly utilised as the transparent anode and a

low work function metal is used as the cathode. With the help of shadow-mask patterning, it is possible to fabricate the device by sequentially depositing organic thin films. Similarly, this type of shadow mask is also used to deposit the thin metallic cathode layer over the organic layer to complete the OLED fabrication process. All these depositions are carried out onto a transparent substrate such as glass or flexible plastic. When we apply a forward bias, the opposite charge carriers (i.e., electrons and holes) are transported across the organic layers and which finally recombine in the organic light emitting layers to generate light. There are two major classes of organic semiconductors which are mostly used in fabricating OLEDs. First one is small molecules (low molecular weight), and another one is polymers (higher molecular weight). Now a day's every global electronics attempt to utilized OLED technology because of their wide potential .

It is important to note that although it is possible to fabricate an OLED with a single organic thin film, frequently additional organic layers are introduced as shown in figure 1.1. Single layer OLED device is the simplest structure in which only one organic material is used between the two electrodes. The efficiency of such type of single layer based OLED device will be highest if the number of holes and electrons in the device are equal. However, if either charge occurs is more in the organic layer then there is a probability that all the charges will not recombine and hence reduce the device efficiency. Therefore it is necessary to improve charge balancing factor by either adjusting the injection energy barrier for the minority or majority carriers or by blending the organic layer with materials that support the charge transport of the minority carriers. However, it is not possible to recombine all the charge carrier

because some of them can travel to the opposite electrode in single layer device. Therefore great improvement can be achieved by using some additional material layer, which increases the device efficiency. For example, a hole injection layer is used to enhance the charge injection from the anode to the HTL layer. Here again, HTL layer can perform two works simultaneously. Firstly this hole transporting layer facilitate the hole transport into the light emitting region, and secondly, it also blocks the leakage of electrons from the cathode to the anode side. Similarly, an ETL is also used in two ways, which serves in facilitating the transport of electrons from the cathode into the emissive layer and also block the leakage of holes from the anode to the cathode side. In OLEDs, the wavelength of emitted light is dependent on the electronic structure of the organic light-emissive material, i.e., the energy difference of the molecule which can be easily tuned by the chemical modification of the material, by the application of doping in it.

### **1.3 Classification of OLEDs:**

Different types of architectures and designed are used for the fabrication of organic light emitting diode. The choices of a particular design are related to a given classification. The most common method to classify the OLED is based on the position of its cathode and anode electrode concerning the organic layers. Following figure 1.2(a) and 1.2(b) shows the conventional, i.e., bottom emitting and top emitting, i.e., inverted OLED configuration respectively. Usually bottom emitting OLEDs have a bottom anode in contact with the electrode substrates while the upper layer of the device is associated with the opposite nature of the electrode (i.e., cathode). On the other hand in case of inverted OLED, the bottom electrode is always cathode, and the

upper electrode is anode in nature. Due to the presence of this difference the nature of the organic layers which constituting the device and lying between the electrodes must also be inverted for allowing the efficient carrier injection into the organic light emitting layer. Therefore the generation of light then escapes from the organic layer either through the bottom of the substrate (bottom-emitting) or the top layer of the device (top-emitting) as shown in the figure below. However, in both cases, the nature of the one electrode must be semi-transparent to escape the generated light from the device.

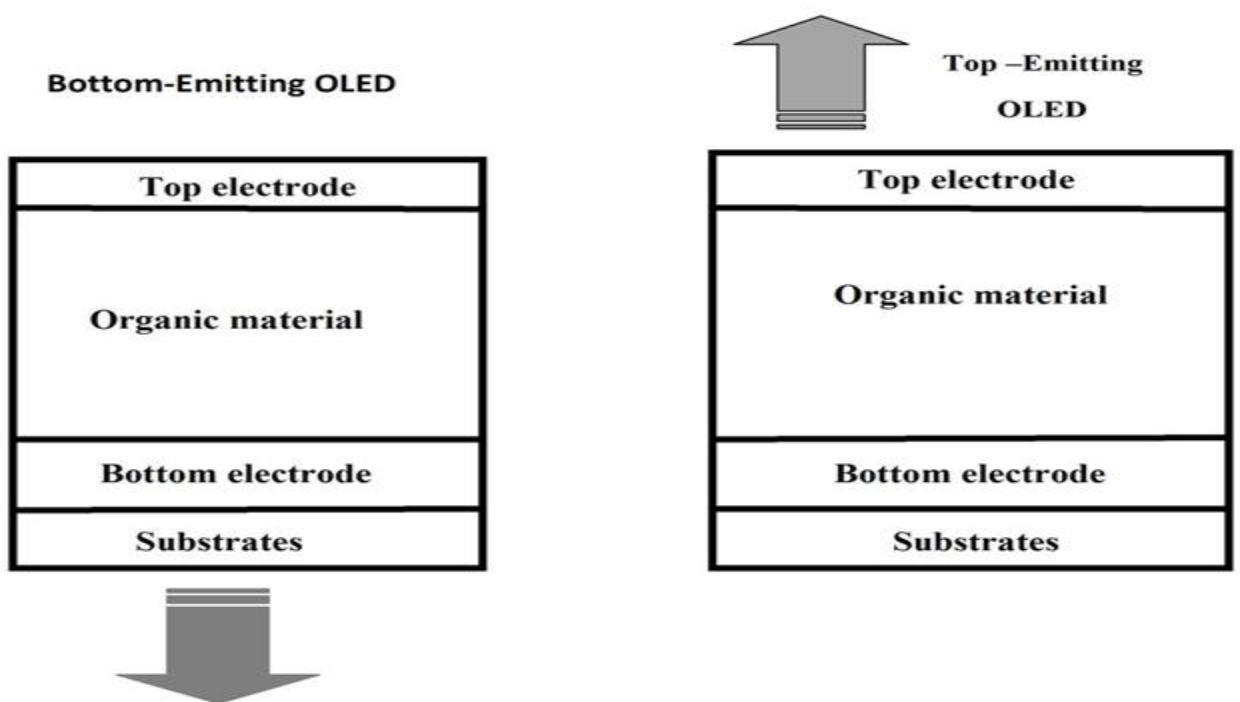


Figure 1.2 (a) : Bottom emitting OLED

Figure 1.2 (b) : Top-emitting OLED

#### 1.4 Literature review of the organic light emitting diodes (OLEDs)

The glorious chapter in organic light emitting diode back to the observation of electroluminescence (EL) from organic material in the 1960s. Electroluminescence (EL) is a phenomenon in which one can observe the light emission from certain materials due to the application of an electric field. W. Helfrich et al. [1] was the first research group who have succeeded in the injection of both types of charge carrier in anthracene crystal. Further studies were also carried out by Schwob et al. [2] on derivative materials of anthracene. Here thickness of the crystal was about 10-20  $\mu\text{m}$  containing electrodes which were prepared by silver paste. However, in their work, a several hundred of volts was required to obtain the visible EL within the crystals. This is the reason because of which their experiment did not encourage an immediate interest in the research area. After the two decades later, in 1980 again anthracene was fabricated in the form of thin film layer by thermal vacuum evaporation method [3] whose thickness was about 600nm. This leads to efficient current injection and also decreases the device operating voltage. Therefore based on these earlier reports on organic semiconductors, Tang and Vanslyke [4] from Kodak was the first group who gives the novel electroluminescent (EL) device (1987) for the OLED society. They constructed the EL device using organic materials as the light emitting elements. The fabricated diode has a double layer structure of organic thin films. For the preparation purpose, they used vapour deposition method. Proper charge carrier injection is provided from an indium-tin-oxide anode and an alloyed Mg: Ag cathode. They achieve high external quantum efficiency (1 % photon/electron), luminous efficiency (1.5lm/W) and brightness ( $> 1000 \text{ cd/m}^2$ ) at a driving voltage below 10 volts. Ching W Tang, Chin H Chen and Ramanuj Goswami (1988) give an electroluminescent device



in which luminescent zone is consists of organic host material which is capable of supporting hole-electron recombination and also capable of emitting light during the charge recombination process [5]. Steven A. VanSlyke, Ching W Tang, Luther C Roberts and Luther C Roberts (1988) works on OLEDs in which the organic hole injecting layer and the organic transporting zone was consists of a layer with porphyrinic compound [6]. Their structure also contains a hole transporting aromatic tertiary amine which was lying between the hole injecting layer and the electron injecting region. After one year again C.W. Tang, S.A.VanSlyke and C.H.Chen [7] constructed an electroluminescent device using multilayer organic thin films by doping the Alq3 layer with highly fluorescent molecules (1989). Here they report that EL efficiency has been improved by a factor of 2 in comparison with the undoped device. Ching W Tang, Steven A VanSlyke and Steven A VanSlyke [8] works on the electro-luminescence device in sequence order of an anode, hole and electron transport layer along with cathode layer respectively (1989). Here cathode is composed of alkali metals with a work function less than 4eV. On the other hand in the year 1990, Burroughs et al. [9] introduced the first polymer-based organic light emitting diode (POLED) where poly (phenylene vinylene) (PPV) was prepared by using a solution-processed precursor. This finding led to increased interest in OLEDs, following the discovery in 1991 by Braun and Heeger [10] who observed EL from diodes produced with poly( 2-methoxy, 5- ( 2'-ethyl-hexoxy ) -1, 4-phenylene- vinylene) (MEH-PPV). Again Steven A VanSlyke, Ching W Tang, Michael E O'Brien, Chin H Chen and Chin H Chen [11] works on electro-luminescence device in which the hole injecting and transporting zone includes a tertiary amine groups with two tertiary amines and

attached to a tertiary amine nitrogen atom with two fused aromatic rings (1991). Li, Changjiang, Song, and Zhigang [12] study the oxidative polymerization of transparent and conducting polypyrrole-poly, composites (1991). Zhang, Hao Li and Changjiang [13] give the Chemical synthesis of transparent and conducting ethylene terephthalate composite films (1991). G. Gustafsson, Y. Cao, G. M. Treacy, F. Klavetter, N. Colaneri & A. J. Heeger (1992) works on flexible organic light emitting diode using soluble conducting polymers [14]. Similarly P. L. Burn et al. (1992) reported an EL device with improving efficiencies by chemical tuning of EL copolymers [15]. Also, Paul L. Burn and their co-workers (1992) studied blue-shifted electroluminescence and improved efficiency [16]. Ohmori Y, Fujii A, Uchida M, Morishima C and Yoshino K [17] works on OLED using 8-hydroxyquinoline aluminium/aromatic diamine multilayer structure (1993). In the same year, Kock Yee Law [18] report on the organic photoconductive material (1993). Similarly S. Saito, T. Tsutsui, M. Era, N. Takada, C. Adachi and T. W. Y. Hamada [19] give a progressive report on organic EL devices in which multilayer organic structure is used (1993). N. Takada, T. Tsutsui, and S. Saito work [20] on organic thin film OLED by using an optical microcavity structure (1993). P.E. Burrows and V. Bulovic [21] represent an easy encapsulation technique for organic light emitting devices (1994). They study the degradation of a population of OLEDs and show that the lifetime of encapsulated devices is increased by more than two orders of magnitude compared to that of unencapsulated devices. In both cases, they found that the factor of degradation is primarily responsible for the formation of non-emissive regions or dark spot defects. Greenham NC, Friend RH and Bradley (1994) reported the angular dependence of

OLED [22]. A. Dodabalapur, L. J. Rothberg, T. Miller and E. W. Kwock [23] works on microcavity effect in OLEDs (1994). T. Tsutsui et al [24] observed sharp emission in OLED by using microcavity structure in OLEDs (1994). C Hosokawa et al [25] reported a highly efficient blue electro-luminescence OLED (1995). Similar work was also done by N.C. Greenham and R.H. Friend [26] on OLEDs in the same year (1995). On the other hand M. Onoda and K. Yoshino [27] reported the application of SPAN for the fabrication of OLEDs (1995). J. H. P. Utley et al [28] synthesis SPAN over anode material and also they prepared PDO14FV by control potential electrolysis technique (1995). J. Gao, A. J. Heeger, J. Y. Lee and C. K. Kim [29] used Polypyrrole as hole transport material in bilayer form with MEH-PPV for the OLED fabrication (1996). Christian Amatori and Florence Gaubert [30] produced a halide derivatives of poly-*p*-xylylene (PPX) via nickel complex for the application of thin film technology regarding display technology (1996). Tsuyoshi Kawai et al [31] discussed the fabrication of multilayer heterostructure of conducting polymer OLEDs (1996). While the Stanislav et al [32] discussed the formation of free charge carrier in polymers materials (1996). P.E. Burroos et al [33] give several approaches for fabrication of full colour display for example side by side patterning of discrete red, blue and green subpixel (1997). C.C. Wu et al [34] enhanced the performance of organic light emitting diode over ITO electrode by enhancing the hole injection layer using oxygen plasma treatment (1997). T. Wakimoto et al [35] discussed the fabrication of organic light emitting diode by using low work function metals such as Al or in combination of Al with other alkali metal compounds (1997). Similarly L.S. Huang et al [36] give importance on the fabrication of OLEDs using bilayer cathode such as Al/LiF (1997).

F.Li et.al [37] studied the performance improvement of OLEDs by using insulating layer of inorganic  $\text{Al}_2\text{O}_3$  layer (1997). Similar report was also given by G.E.Jaboor et.al (1998) in which they used CsF as a buffer layer for electron injection regarding the improve performance of OLED [38]. M.A. Baldo et.al [39] increases the OLED device efficiency by using green phosphorescent dyes (1998). He was the first person who works in this green phosphorescent dyes. On the other hand S.T.Lee et.al [40] works on energy level alignment mechanism at the metal and organic interface region with interface dipole barrier concept (1998). Similar work was also done by S.T.Mori et.al [41] in the same year 1998. A.Kraft et. al [42] works on the electro-luminance behavior of conjugated polymers materials (1998). While G. Parthasarathy et. al [43] works on organic devices in which organic semiconductor is metal free (1998). D.F.O. Brien et.al [44] demonstrated a highly efficient of green and red electrophosphorescent light emitters material for OLEDs in which they achieved internal quantum efficiencies closed to the level of 100% (1999). G.Gu et.al [45] studied the organic light emitting devices in which light is mainly escapes from the last deposited layer of the devices (1999). This types of light emitting OLEDs is popularly known as bottom emission OLEDs. S.K.Choi et.al [46] studied the interference effects in bilayer organic light emitting diode (1999). M.stossel et.al (1999) study the impact of the cathode metal work function on the performance of vacuum-deposited organic light emitting devices [47]. They demonstrated that there is an maximum efficiency at a work function of about 3.7 eV of metallic cathode for all the  $\text{Alq}_3$  based EL device. In the same year X. Zhou et al. [48] reported the fabrication of a vacuum deposited light-emitting device which emits light from the top surface through an Al cathode using p-

type doped silicon as the anode material (1999). They clearly demonstrated the enhanced hole injection from the p-Si anode as compared to the indium–tin–oxide (ITO) anode. They also investigated the mechanisms of hole injection from both the p-Si and ITO anodes into the organic layer and provide a possible model based on anode surface band bending. Similarly X. M. Ding et.al (2000) study the modification of the hole injection barrier in organic light-emitting devices studied by ultraviolet photoelectron spectroscopy [49]. In their work they used SiO<sub>2</sub> as hole injection layer and report that the insertion of an ultrathin SiO<sub>2</sub> layer between the organic and ITO results in reduction of the energy barrier at the interface region which enhanced the OLED performance. J.Huang et.al [50] fabricated organic light emitting diode using by alternating both doped and undoped organic materials with multiple quantum well structure (2000). J.A.E Wasey et.al [51] observed the improve efficiency from planer microcavities (2000). A.Elscher et.al [52] reported a hybrid organic light emitting diode in which PEDOT/PSS is used in their structure as a hole injection layer (2000) for improve performance. H.Fujikawa et.al [53] studied the OLEDs performances in which they used alkaline earth fluorides as an electron transport layer (2000) for better charge injection in organic layers. M.Stobel et.al study the space charge limited phenomenon in Alq<sub>3</sub> (2000). P.Piromreum et.al [54] study the role of CsF as an electron injection in conjugated polymers materials (2000) H.C.F.Marten et.al [55] gives simultaneous measurement of electron and hole mobilities in polymer light-emitting diodes(2000). A. J. Ma kinen et al. [56] gives a photoemission study (2001). Their study of the interface between spin-cast films of a conducting polymer blend consisting of poly~3,4-ethylene dioxythiophene (PEDOT), poly~4-styrenesulfonate

(PSS) and glycerol as an additive, and vacuum-evaporated hole transport layers (HTL) of 4,4'-bis(carbazol-9-yl) biphenyl, N,N'-diphenyl-N,N'-bis(1-naphthyl)-1,1'-biphenyl-4,4'-diamine and N,N'-diphenyl-N,N'-bis(3-methylphenyl)-1,1'-biphenyl-4,4'-diamine reveals a hole injection barrier between 0.5 and 0.9 eV at the glycerol-modified PEDOT-PSS/HTL interface. Similarly S. Shi [57] developed a new method for fabrication of OLED by using pre-doped materials (2001). C. Adachi et al [58] reported a highly performed OLED with high internal quantum efficiencies (2001). While M. Ikai et al [59] developed an OLED in which highest amount of luminous efficiency is 70 lmW (2001). Junqing Zhao et al [60] developed a bilayer organic light emitting diode using flexible ITO electrode (2001). Here they fabricated the OLEDs over ITO electrode on both flexible polyester and glass substrates and compared their performance by studying the current-voltage and luminance-voltage characteristics. They reported that threshold voltage of polyester device is almost same as that of the glass-based device. Chengfeng Qiu et al [61] discussed the thickness dependence of organic layer on the OLED performance (2001). In this work they change the thickness of both the electron and hole transport layer for optimization of the device structure. Finally they concluded that buffer layer of suitable thickness effectively reduced the energy barrier at the organic interface and hence improves the device efficiency. Ji Cui, Qinglan Huang, Jonathan and C. G. Veinot [62] reported the integrity of anode/organic interfacial (2002). This contact is found to be critical for the performance and stability of archetypical small molecule organic light-emitting diodes (OLEDs). In their contribution, they show that vapor-deposited hole transporting TPD and NPB thin films undergo decohesion on ITO anode surfaces under mild heating.

A. Maria et.al (2002) study the energy transfer mechanism from organic materials to rare –earth oxide complexes [63]. Here reported materials are found to be obtained in the form of spin-cast films. In this work they reported that the energy transferring of organic PBD to europium complexes is more capable than from PVK. Also these materials are easy for fabrication and hence they should be the good candidate for monochromatic light emitting diode. Ji Cui et.al [64] study the interface engineering of anode/hole transporting layer to cheque the charge injection in OLEDs (2002). They used Cu(Pc) as hole injection layer in the interface region and reported that this layer actually suppress, rather than enhancing the hole injection across the device which finally reduces the thermal stability of OLEDs. S.J.Kang et.al [65] study the effect of NaCl regarding the enhancement of electron injection in OLED (2002). Y.Qui et.al [66] works on the multiple quantum well structure of OLED (2002). Qui Chengfeng et.al [67] used Praseodymium oxide over anode surface to increase device efficiency (2002). Here they reported that this material is suitable for enhancing both current and power efficiency of the device. They obtained the best result of the OLED device at the thickness of 1nm of this buffer layer. W. H. Kim, G. P. Kushto, H. Kim and Z. H. Kafafi [68] showed that the surface resistance of conducting films of glycerol-doped poly(3,4- ethylene oxy-thiophene)–poly(styrene sulfonate) is largely dependent on the annealing temperature (2003). They also report that the device performance of organic light emitting diodes using this modified poly (3,4- ethylenedioxy-thiophene)– poly(styrene sulfonate) as an anode is also greatly affected by the baking conditions of the conducting films. In their work they found that the maximum light output, current density and luminous power efficiency are observed

from devices using anodes baked at a high temperature close to the boiling point of glycerol. J. Lee et.al [69] fabricated high efficiency OLED using Al/NaF bilayer cathode (2003). They said that NaF can be effectively used to improve the device performance. They also study the Photoelectron spectroscopy at the Al/NaF/Alq3 interface regarding the performance improvement of the device. J. Campbell Scott [70] study the metal-organic interface and charge injection in organic electronic devices (2003). Here they discussed the formation of metal-organic contact and all the parameters which affect the current injection. They said that Fermi level in organic semiconductors depends directly on the interface offset region. I-Min Chan and Franklin C.Hong (2003) study the improve performance of OLED using nickel oxide layer over ITO surface [71]. Here they found that the value of luminance and the current density of NiO coated layer were significantly increased compared to the single ITO surface device. Their results strongly indicate that the NiO/ITO is an excellent anode structure for increasing device efficiency. Beat Ruhstaller et.al [72] works on the optical and electronic simulating processes in multiwall organic light emitting diode (2003). They also discussed the optimization of emission intensity and color of red OLEDs. Here they analyzed the thin film interface effect with the help of optical model. M. Pfeiffer et.al [73] reported a highly improved organic light emitting diode in which efficiency is significantly enhanced (2003). They used doped hole transport layer for improving the device performance. Z. H. Kafafi et.al [74] study the annealing treatment on electrical and morphology properties of conducting polymers , which is used as an anode in OLEDs (2003). They observed the maximum current density and output light at the high temperature close to the boiling point of polymer



material. Zhang Zhi-Feng et. al (2003) reported the characterization of bilayer anode OLED with a nanostructured TiO<sub>2</sub> layer at the interface between ITO and NPB layers [75]. They achieve the nanostructured TiO<sub>2</sub> layer by the Sol-Gel method. They concluded that compared to the different thickness of the buffer layer, the OLEDs with the 6 nm buffer layer showed the highest efficiency. The enhancements in efficiency result from an improved balance of hole and electron injections and a more homogeneous adhesion of the buffer layer inserted. In the same year Heike Riel et.al (2003) study the role of Copper-Phthalocyanine in Multilayer Organic LEDs Based on Small Molecules [76]. Their systematic current—voltage and impedance measurements revealed a redistribution of the internal electric field of the CuPc/NPB/Alq<sub>3</sub> three-layer structure compared to that of the NPB/Alq<sub>3</sub> bilayer OLED. It was demonstrated that the hole transport is mainly controlled by the internal energy barrier at the CuPc/NPB interface. W.H. Kim et. al (2003) investigated Zr-doped ZnO (ZZO) thin films as an anode material, to make an alternative to indium tin oxide (ITO), for organic light emitting devices [77]. They study the electrical and optical properties of these films as a function of substrate temperature and oxygen pressure during deposition. For a 200-nm-thick ZZO film grown at 250 °C in 1 mTorr of oxygen, a resistivity of 5.631024 Vcm was measured and an average optical transmittance of 84% was measured in the visible range ~400–700 nm. In the next year Lin Ke et.al (2004) study the performance improvement of organic light emitting devices by inserting thin perylene layer between electrode and organic interface [78]. To deposited the perylene layer they used chemical vapour deposition (CVD) at low temperature. Such a structure gives off higher efficiency, a smaller number and

smaller size dark non-emissive areas, slower growth rate of the dark areas and a longer device lifetime compared to one without the parylene layer. Haifeng Wang et. al [79] fabricated an efficient Organic Light-Emitting Diodes with Teflon as buffer layer (2004). In this study, they report a high-performance of organic light-emitting diodes (OLEDs) with a buffer layer of polytetrafluoroethylene (Teflon). Their results indicate that the OLEDs with a 1.5-nm-thick Teflon buffer layer had a markedly enhanced performance with an efficiency of 9.0 cd/A at a current density of 100 mA/cm<sup>2</sup>. Abhishek, P. Kulkarni, Christopher and J. Tonzola [80] gives a nice presentation of wide-ranging review of the literature on electron transport materials (ETMs) used to enhance the performance of organic light-emitting diodes (OLEDs) (2004). They report the relationships among the structure-property-performance of many classes of ETMs, both small molecule and polymer-based materials to improve OLED performance. S. T. Zhang et.al [81] study the electron blocking and hole injection properties of NPB in OLED devices (2004). They study the current-voltage and luminance-voltage characteristics at the different thickness of hole injection layer. Here they report that improve device performance is due to the electron blocking behavior of NPB material. P. Abhishek et.al [82] gives a review picture of all the electron transport materials in OLEDs (2004). They discussed the electron affinity and electron mobility of the materials. They also discussed the design of multifunctional electroluminescent polymer for OLEDs along with brief challenges of important research in which further research can be done. R.M. Montoreali et.al [83] study the morphological, electrical and optical properties of organic light-emitting diodes with a LiF/Al cathode (2004). They conclude that due to the presence of LiF layer luminance

was greater than 30,000 cd/m<sup>2</sup> at a operating voltage 25 volt with a maximum luminous efficiency greater than 46 lm/W at 20 volt. Aparna Misra et.al [84] study the greenish- blue organic light emitting diode by using lithium tetra (2- methyl 8- hydroxy-quinolinato) boron complex (2004). In their work their devices emits light in the greenish-blue region. This complex material was synthesis by them in their laboratory which was characterized by different spectroscopic methods. S.H.Jung et.al [85] study the different pixel structures for successful implantation of organic light emitting diode (2004). Lee and J.H. Boo (2004) insert zinc oxide thin film in indium tin oxide anode for organic electroluminescence devices [86]. In their work Zinc oxide thin films were prepared by using the method of rf magnetron sputtering on glass substrates with designed ZnO target using high-purity of zinc oxide (99.99%) powder. This bilayer anode was used for OLED fabrication. At this structure, the lowest turn-on voltage was achieved and also the good brightness (6200 cd/m<sup>2</sup>) of the emission light from the devices. Jingze Li et.al [87] demonstrated an enhanced performance of organic light emitting device by insertion of conducting/insulating WO<sub>3</sub> anodic buffer layer (2005).They showed that the buffer thickness of 0.5 nm better enhance the hole injection in OLED. The device performance was further enhanced after the as-deposited WO<sub>3</sub> film was thermally treated. H. J. Peng et.al [88] constructed a high efficiency organic light emitting diode by considering semi-transparent silver as a anode (2005).They showed that this modified anode provide better light outcoupling and hole injection property with maximum current efficiency of 81 cd/A and power efficiency of 79 lm/W, compared to the 46 cd/A and 39 lm/W for an ITO anode device. J. X. Sun et.al [89] study the effect of intermediate layers on the performance

of stacked organic light emitting diode (2005). They said that this types of devices showed superior performance compared to the conventional single-unit devices. They found that this types of stacked OLEDs with intermediate layers i.e. LiF/Ca/Ag and LiF/Al/Au give highest efficiency of 19.6 cd/A and 17.5 cd/A, respectively at current density of 20mA/cm<sup>2</sup>. Similarly Adriano R. V. Benvenho et.al (2005) study the effects of light out-coupling efficiencies and device performance of fluorine doped tin oxide based OLED using sulphonated polyaniline as hole transport layer [90]. Yu Mingxin et.al [91] synthesis the several OLED materials of triarylamine using the lighting properties of palladium catalysts (2005). Here they examined the physical properties of the materials by UV-visible, PL and DSC spectra. Yoon-Chang Kim and Young Rag Do [92] fabricated the organic light emitting diode on nanohole template by using laser interfering lithography (2005). In this paper they experiment and analysis the electro-optical characteristics and showed that there was a shrinking of OLED takes place at the sub-wavelength scale region which has only minimum effect on their optical properties. Shengwei Shi and Dongge Ma [93] represent a bilayer cathode which is combination of Al and Ni that is Al/Ni. With the help of this bilayer cathode they improve the electroluminescent (EL) efficiency and stability in N, N-bis(1-naphthyl)-N,N-diphenyl-1,1 biphenyl 4,40- dimaine (NPB)/tris-(8-hydroxyquinoline) aluminum (Alq3)-based organic light-emitting diodes (2006). They found that the device with LiF/Al/Ni cathode achieved a maximum power efficiency of 2.8 lm/W at current density of 1.2 mA/cm<sup>2</sup>, which is 1.4 times than the efficiency of device with the state-of-the-art LiF/Al cathode. Li Jianfeng et.al (2006) et.al works on organic light emitting diode using carbon nanotube over flexible PET substrates [94].

Here they obtained the maximum output light of  $3500 \text{ cd/m}^2$  and a current efficiency of  $1.6 \text{ cd/A}$ , which is better than the ITO/PET substrates. Bernard Geffroy et.al [95] give a review report on organic light emitting diodes (2006). They informed that red, green and blue devices in the combined matrices form is the core of a display technology. M.Katlyar [96] works on organic ultraviolet light emitting diode (2006). The main aim of their work was to developed polysilane based OLEDs for the application in display technology. Here they converted the ultraviolet emission from polysilanes to the visible emission and also to white light for home applications. By Sean W et.al [97] study the effect of hole mobility on the stability of blue organic light emitting diode (2006). They used transient OLED technique to measure the hole mobilities. The resulted hole mobilities are found to be  $3.1 \times 10^{-4}$ ,  $8.9 \times 10^{-5}$  and  $3.6 \times 10^{-6} \text{ cm}^2 \text{ V}^{-1} \text{ s}^{-1}$  for three different blue OLED model with different fluorene content. John E. Knox et.al [98] studied the chemical failure of Alq3-based OLEDs (2006). In this work they used Tris (8-hydroxyquinoline) aluminum(III) as an electron-transport material and emitting layer in the organic light emitting diode. They reported that the reaction of Alq3 with trace  $\text{H}_2\text{O}$  is a major reason for the failure of Alq3 based OLEDs. Y. Sun et.al [99] reported that it is possible to achieve about 100% internal quantum efficiency by harvesting both singlet and triplet molecular excitation states with the help of electro phosphorescent materials (2006). Huishan Yang et al. [100] reported an Organic light-emitting devices which was fabricated with a hole-buffer layer (HBL) 4, 4-N,N-dicarbazolebiphenyl (CBP) inserted between ITO anode and hole transporting layer (2007). In their work it was found that the present of the CBP can balance the hole and electron injections and reduce the hole-leakage to the cathode

resulting in the enhancement of the current efficiency. The highest current efficiency of the device with optimum CBP thickness of 4 nm was 5.66 cd/A at 8 V that is nearly 1.5 times than that of the device without the HBL. Juo-Hao Li, Jinsong Huang and Yang Yang (2007) reported an improved hole-injection contact for top-emitting polymeric diodes [101]. In their work the anode has a structure of metal/molybdenum oxide/ poly 3, 4-ethylenedioxythiophene poly-styrenesulfonate (PEDOT: PSS). They used an ultraviolet photoelectron spectroscopy UPS to investigate the change of work function and also the photovoltaic measurement confirmed that the improved hole injection is due to the reduction of barrier height, resulted from the addition of transition metal oxide. Pabitra K. Nayak et.al [102] studied the redshifted of electro-luminance in OLEDs (2007). In their work they used alloy of hole transport materials. They synthesise the blue fluorescent 3,6-*p*-acetophenone Nhexylcarbazole (ANHC) and this is comparable with TPD layer. They found that charge carrier injection was more enhanced in OLEDs which was blend of TPD and ANHC, compared to ANHC alone. Ping-I Shih et al [103] fabricated a novel host material for highly efficient blue OLEDs (2007). Here they reported a novel hybrid material. This is known as triphenyl-(4-(9- phenyl-9H-fluorene-9-yl)phenyl)silane (TPSi-F). They obtained a highly efficient sky-blue phosphorescent OLEDs using TPSi-F with the maximum external quantum efficiency ( E.Q.E.) as better as 15% . This reported result shows a 2-times enhancement in device efficiency compared with reference devices on the conventional host material 1,3-bis(9- carbazolyl)benzene (mCP).

Qingjiang Sun, Yongfang Li and Qibing Pei [104] study the polymer light-emitting electrochemical cells for high efficiency and low voltage electrochemical devices

(2007). They said that polymer electrochemical cells are suitable for the solid-state lighting application. They can similarly make the polymer pixel as in polymer light emitting display like ink-jet printing. Anne Kohnen et al. [105] developed a high efficiency of multilayer organic light-emitting diodes with a low-refractive-index hole-transport layer (2007). In this work, they reported a multilayer organic light-emitting diodes with internal device modification. They used a hole-transport layer with reduced optical density but slightly reduced hole-transport properties. They concluded that improve efficiency is only some extent due to enhanced outcoupling of the reduced refractive index and mainly is affected by the changing of the width of the emission zone. Kwang-Hyuk Choi et al. (2008) study the characteristics of Ni-Doped IZO Layers Grown on IZO anode for enhancing hole injection in OLEDs [106]. They can obtain a NIZO 5 nm/IZO 135 nm double-layer anode with a sheet resistance of 30.04 and an optical transmittance of 83.8% at a wavelength of 550 nm. Also, they found that the work function of the NIZO layer was higher than that of a pure IZO anode due to the presence of a NiO<sub>x</sub> phase in the NIZO layer. Their results indicate that the NIZO/IZO anode scheme is a promising anode material system for enhancing hole injection from the anode into the active layer of OLEDs. Fengxia Wang, Xianfeng Qiao, Tao Xiong and Dongge Ma (2008) study the role of molybdenum oxide as anode interfacial modification in the improvement of efficiency and stability in organic light-emitting diodes [107]. In this paper the role of MoO<sub>3</sub> and MoO<sub>3</sub> doped N,N'-di(naphthalene-1-yl)-N,N'-diphenyl-benzidine (NPB) as the interface modification layer on ITO in improvement of the efficiency and stability of OLEDs is investigated in detail by atomic force microscopy (AFM), polarized optical

microscopy, transmission spectra, ultraviolet photoemission spectroscopy (UPS) and X-ray photoemission spectroscopy (XPS). Sung-Woo Cho, Jin-A Jeong and Jung-Hyeok Bae [108] characterize the multilayer of indium zinc oxide (IZO)–Ag–IZ which was grown on a polyethylene terephthalate (PET) substrate (2008). They investigated it for flexible organic light-emitting diodes (OLEDs) and was found that the IZO–Ag–IZO (IAI) multilayer anode exhibited a surprisingly reduced sheet resistance of 6.93  $\Omega$ /square and high transmittance of 84.8%, despite the very thin thickness of the IZO (30 nm) layer. Similarly, Jin Woo Huh et al. (2008) provide fabrication and characteristics of organic light-emitting diodes with conducting polymer anodes on plastic substrates [109]. By Henk J. Bolink et al. [110] fabricated an inverted OLED by using a metal oxide as an electron injection contact (2008). Here they developed a new model and explained the experimental results and provides a way for optimization of the organic devices. They obtained the high brightness greater than the 5700cdm<sup>-2</sup> at voltages less than 8 Volt. S. Chen, X. Li and W. Huang [111] reported a top-emitting organic light emitting diode in the blue region (2008). Their structure was based on based on 4,4- bis(2,2'-diphenylvinyl)-1,1'-biphenyl. They developed the blue emitting OLED by suppressing multiple-beam interference method and using wide-angle interference. Also, their blue emission showed the stable spectra with the variation of viewing angle from 0<sup>0</sup> to 75<sup>0</sup>.

On the other hand according to Z. W. Liu, M. G. Helander, Z. B. Wang and Z. H. Lu [112] in phosphorescent organic light-emitting diodes (OLEDs), a hole transporting layer is conventionally considered to be required to make easy for hole injection into the organic host materials (2009). They said that fac-tris 2-phenylpyridine iridium Ir



ppy 3 doped into 4,4-*N, N*-di-carbazole-biphenyl can be used to directly inject and transport the positive charge carrier from the electrode surface. In their work, the efficiencies of the simplified bilayer OLEDs go beyond 41 lm/W and 57 cd/A at a brightness of 100 cd/m<sup>2</sup>. Guang-Feng Wang et al. (2009) focus on modification of conductive polymer for polymeric anodes of flexible organic light-emitting diodes [113]. Here they report that electrical conductivity increased by more than three orders of magnitude. They studied the conductivity improvement mechanism in the nanometer range by particle size analysis, field emission scanning electron microscopy (FESEM) and X-ray photoelectron spectroscopy (XPS). Jeongho Kim et al. (2009) provide an energetic interfacial layer of NaCl–organic composite for the application as an anode in OLED [114]. By using this buffer layer, they provide improved performance of OLED over indium tin oxide (ITO) anode and *N, N*-bis(naphthalene-1-yl)-*N, N*-bis(phenyl)benzidine (NPB), based OLED. Here they conclude that this type of buffer layer provides a lower energy barrier compared with that of a pure NaCl interlayer, which is comparable to the value at a bare ITO/NPB interface. Michael Thomschke et al. [115] studied the optimized efficiency and angular emission characteristics of the white organic light emitting diode (2009) for top emission. Here they discussed the influence on the optical properties of EL devices by using silver as electrode material with the help of analytical method and numerical simulations. J. Mija and M.J. Matachowski [116] discussed the operation and application of organic light diode for display technology (2009). Here they show that the main differences between the inorganic and organic EL devices is due to the difference of organic and inorganic semiconductor materials and said that no charge carrier is present in OLED

devices without any injection. In this paper, they pointed the role of OLEDs in display technology. Kanchan Saxena et al. [117] give a review of light extraction techniques in organic electroluminescent devices (2009). In this work, they reported the advancement of different light out-coupling techniques such as substrate modification methods and microcavity effect, etc. These are the methods by the help of which it is possible to enhance the external quantum efficiency of the EL devices. Yu-Cheng Chen et al. (2010) used a UV treated ultra thin NaF film as anode buffer layer on organic light emitting devices [118]. In this work, they fabricated NaF thin film by vacuum evaporation method and then treated with the ultraviolet (UV) ozone for the fabrication of organic light emitting diodes (ITO/NaF/NPB/Alq3/LiF/Al) and to study its effect on hole-injection properties. By using this buffer layer, they provide improved performance of OLED over indium tin oxide (ITO) anode and *N, N*-bis(naphthalene-1-yl)-*N, N*-bis(phenyl)benzidine (NPB), based on the studies with ultraviolet photoelectron spectroscopy and atomic force microscopy. Pabitra K Nayak et al. [119] observed blue and white emission from a multilayer OLED by using a new aluminum complex (2010). Here they used the blue emitting aluminum complex material, i.e., bis-(2-amino-8-hydroxyquinoline). This Al complex materials showed blue emission at the wavelength region of 465nm along with maximum brightness and efficiency of 425 cd/m<sup>2</sup> and 0.16 cd/A respectively. They also used another multilayer OLED device doped phosphorescent Ir complex with Al complex. This device showed the white light emission with maximum brightness 970 cd/m<sup>2</sup> and maximum current efficiency of 970cd/m<sup>2</sup> and 0.53cd/A respectively. G. Luka et al. [120] the study the properties of Alq3 based organic light emitting diode with undoped zinc oxide anode

layer (2010). In their work, they prepared the transparent and conductive undoped zinc oxide films by atomic layer deposition method and investigated the properties of the ZnO film. In this paper, they work on the standard configuration of ZnO/CuI/Alq3/polyethylene glycol dimethyl ether/Al whose turn-on voltage was found to be 7.9 volts and E.Q.E of the device was 1.5 %. N. Thejo Kalyani et al. [121] focus on the fabrication of red OLEDs using  $\text{Eu}_x\text{Y}_{1-x}(\text{TTA})_3$  Phen organic complexes (2010). From the experimental analysis of current-voltage and luminance-voltage measurement along with the electro-luminance spectrum, they concluded that the direct trapping of holes and electrons and subsequent formation of the excitation on the dopant is mainly responsible for the high efficiency of the devices at their low value of current density. Lian Duan et al. [122] give a review report on the solution processable organic light-emitting diodes which was based on small molecules (2010). Their review paper includes the development of solution processable small molecules and also the comparative study of the different characteristics of the deposited films and devices fabricated by both solution-process or by vacuum deposition methodology. Tae Gu Kim et.al [123] study the deep blue organic light-emitting diodes (2010). In this work they used doped BCzVBi with different blue host materials. Here they fabricated the OLEDs by using 5 wt% doped BCzVBi with different host materials like NPB, MADN, TPBi etc. They obtained a maximum luminescence of 4,838  $\text{cd}/\text{m}^2$ , current density of 32.7  $\text{mA}/\text{cm}^2$  and luminous efficiency of 3.3  $\text{cd}/\text{A}$  at the operating voltage of 4.5 volt.

Dongge Ma [124] focus on high-efficiency orange and white organic light emitting diodes (OLEDs) by introducing an ultra-thin undoped orange light emitting layer (less

than 1 nm) adjacent to the electron-transporting layer (2011). They informed that the orange OLEDs showed a high external quantum efficiency (EQE) of 16.4% at 1000 cd/m<sup>2</sup>. In their work, they reveal that the resulting four-colour white OLEDs emitted an EQE of 15.5% and a maximum colour rendering index (CRI) of 87 at a luminance of 1000 cd/m<sup>2</sup>. They also carried out further analysis on the EQE of the white OLEDs. In the same year 2011, S. Cheylan et al. [125] reported an OLED with indium-free metallic bilayer as a transparent anode. This bilayer electrode structure allows combining the low sheet resistance and high transparency of Cu with the excellent stability and high work function of Ni. They demonstrate that Cu–Ni bilayer based PLED devices exhibit comparable efficiency and lifetime decay behaviour to indium tin oxide (ITO) based device, with potentially significant advantages, such as easy processing, low cost, and mechanical flexibility. Jonghee Lee et al. [126] works on the interlayer engineering of blue phosphorescent organic light-emitting diodes by using different host material (2011). In their work, they used *N,N'*-dicarbazolyl-3,5- benzene as an interlayer between the hole transporting layer and light emitting layer. They also reported that triplet exciton confinement and hole/electron balance in the EML is highly dependent upon the host material. In this work, they said that the insertion of an appropriate interlayer and host materials could enhance the maximum external quantum efficiency up to 21 times from 0.79% to 17.1%. S. A. Bagnich et al. [127] works on efficient green electrophosphorescence (2011). They carried out this work on ambipolar nonconjugated polymers. They report that on the addition of a green electrophosphorescent dye to the polymer matrix gives efficient electroluminescence. Here the maximum value of current efficiency and external quantum efficiency of the

device is found to be of 35 cd/A and 10% respectively. J. Zmija and M.J. Małachowski [128] study and work on new organic electrochromic materials and their applications (2011). They pointed out some phenomenon which is important for the occurring of electrochromic effect in the organic materials and used in various organic devices. S.W. Liu et al. [129] reported improved performance of organic light-emitting diodes by using MoO<sub>3</sub> interlayer (2011). Here they deposited this oxide interlayer by oblique angle technique. The thickness of this oxide layer was about 20nm over the ITO surface. They found that the current efficiency and external quantum efficiency of the device were significantly enhanced at an oblique deposition angle of 60° for the oxide layer deposition. Kihyon Hong and Jong-Lam Lee [130] give a review report on developments in light extraction technologies of the organic light emitting diodes (2011). They said that OLEDs still have a low out-coupling efficiency of about 20% due to different factors like total internal reflection, absorption, etc. This is a major problem for the limitation of the high efficiency of OLEDs. Their paper discussed the different ways of enhancing the out-coupling efficiency for OLED devices. S. Touihria, L. Cattinb, D-T. Nguyenb and M. Morslic [131] deposited the In<sub>2</sub>O<sub>3</sub> thin films (100 nm thick) by a new evaporation method (i.e., reactive evaporation of indium), in the atmosphere of an oxygen partial (2012). It was found that by using the following experimental conditions: oxygen partial pressure = 1 ×10<sup>-1</sup> Pa, substrate temperature = 300 °C and deposition rate = 0.02 nm/s, they obtained a relatively high conductive (= 3.5 ×10<sup>3</sup> S/cm) and transparent films. They introduce the 5nm thick layers of this In<sub>2</sub>O<sub>3</sub> in AZO/In<sub>2</sub>O<sub>3</sub> and FTO/In<sub>2</sub>O<sub>3</sub> multilayer anode structures. Instead of these bilayer structures, they also focus on other both

single and bilayer structure in their work such as AZO, FTO, AZO/In<sub>2</sub>O<sub>3</sub>/MoO<sub>3</sub>, FTO/In<sub>2</sub>O<sub>3</sub>/MoO<sub>3</sub> and FTO/MoO<sub>3</sub>. Young Kwon and Ji-Hoon Kim [132] designed and synthesized a novel yellow-emitting iridium complex, bis[2-(9-ethyl-9H-carbazol-3-yl)-benzothiazole]iridium(III) acetylacetonate (Btc)<sub>2</sub>Ir(acac)], for use in phosphorescent organic light-emitting diodes (OLEDs) (2012). Tae-Hee Han et al. [133] give an extremely efficient flexible organic light-emitting diodes with modified graphene anode (2012). K. Narayan et al. [134] gives the Effect of thickness variation of hole injection and hole blocking layers on the performance of the fluorescent green organic light emitting diodes (2012). In this paper, they optimized the current and power efficiency of the OLED devices, and they obtained a maximum luminance of 5993 cd/m<sup>2</sup> when current density was 140 mA/cm<sup>2</sup>. A. Behjat and M. Neghabi [135] study the yellow organic light emitting diodes (2012). They used multilayer anode structure for OLED fabrication in the form of ZnS/Metal/ZnS. Moreover, they also investigated the effect of BCP layer on the performance of electro-luminescence spectrum of the devices. Here lowest turn-on voltage is 5.61 volt and high luminance of 1836 cd/m<sup>2</sup>. O. Rana et al. [136] study the hole injection properties in OLEDs by modifying the metal-organic interface with the help of F4-TCNQ (2012). By using this material they can change the work function at the interface region which was measured by Kelvin probe method (KPM). Here they found that work function of the substrates increases with increasing the thickness of the F4-TCNQ layer and then saturates for further increase in thickness. Yu-Fan Chang et al. [137] fabricated the solution-processed organic light-emitting diodes (2012). Here they used a vacuum-free lamination of low work function cathode. The obtained value of current efficiency was

3cd/A and luminance of 2500cd/m<sup>2</sup> for green fluorescent emitter and similarly 25 cd/A and 3200 cd/m<sup>2</sup> was achieved for green phosphorescent emitter. The lowest turn-on voltage of the device was found to be about 5 V higher. Jun Ho Youn, Su Jin Baek and Hyeong Pil Kim [138] reported a polymer light-emitting diode (PLED) (2013). For the fabrication purpose they used solution processed tungsten-oxides (WO<sub>x</sub>). It was found that the coating of a thin WO<sub>x</sub> layer on PEDOT: PSS increases the current efficiency of PLED from 9.11 to 9.90 cd A<sup>-1</sup> because of the improved conductivity of the PEDOT: PSS due to the incorporation of WO<sub>x</sub>. This improvement of conductivity of PEDOT: PSS ultimately increases the hole injection tendency into the light emission layer. Chia-Cheng Huang, Fang-Hsing Wang , Chia-Ching Wu , Hong-Hsin Huang and Huang [139] also provide another study for bilayer thin films (2013). They made a study in which radio frequency magnetron sputtering was used to deposit nickel oxide thin films (NiO, deposition power of 100 W) and titanium-doped zinc oxide thin films was used (TZO, varying deposition powers) on glass substrates. In their work, they basically investigated the structural, optical and electrical properties of the TZO and NiO thin films along with this bilayer heterojunction devices. They show that the NiO/TZO heterojunction diode was dominated by the space-charge-limited current theory. L. Zhou et. al (2013) give the performance improvement of organic light emitting diode with aluminum oxide buffer layer for anode modification [140]. They characterized the roughness, sheet resistance and surface potential ( $E_F$ ) of the Al<sub>2</sub>O<sub>3</sub> modified ITO. They also investigated the properties of Al<sub>2</sub>O<sub>3</sub> films at the device level. Here they concluded that the Al<sub>2</sub>O<sub>3</sub> buffer layer enhanced the device performance by balancing charge carrier injection in the light emitting layer. On the other hand Lucia

Petti et.al [141] reported a novel two-dimensional nanopatterned conductive PEDOT: PSS Films for organic optoelectronic applications (2013). They also fabricated a 2D nanopatterned transparent anode onto a flexible polyethylene terephthalate (PET) substrate. Their obtained results fully confirm the feasibility of the developed process of micro/nanopatterning PEDOT: PSS. Massimo Rippla et.al [142] provides a novel OLED structure (2013). In their work they used conductive polymeric photonic crystal as an electrode instead of ITO electrode. In their work, they used electron beam lithography and a plasma etching process. This photonic crystal based OLED significantly reduced the light trapping tendency in OLED and also they demonstrated that this types of electrodes surface can be used on rollable and flexible substrates. Keigo Sato et.al [143] studies the singlet and triplet excited energy state of the organic luminescent molecule for organic EL devices (2013). In this work they reported an organic molecule with a zero energy gap between the singlet and triplet excited states. Finally they reported that organic light emitting diodes with this molecule significantly increases the external electroluminescence efficiency up to 14%. Pen-Cheng Wang et.al [144] studies the conducting polymers for transparent electrodes based display technologies (2013). They said that conducting polymers should be new alternative materials for the fabrication of transparent electrodes in near future display devices. Because they offer some significant advantages which includes lightweight, low cost, mechanical flexibility and excellent compatibility with plastic substrates for the development of display technologies. Similarly Mark T Greiner and Zheng-Hong Lu [145] give a review report on thin film metal oxide for the organic semiconductor applications (2013). They said that the barrier energy at the electrode-organic interface



region depends on the work function of the electrode. Their paper provides a details review of the progress in interfacial study of oxide /organic region for the organic EL devices. In the same year, Jiajie Liang et.al [146] developed a fully solution-based flexible light-emitting diode under ambient conditions (2013). In this work they reported fabrication of solution process polymer light-emitting electrochemical cells (PLECs) with the help of spin-coating methodology. Also they used SWCNT/AgNW bilayer composite electrode as an anode instead of popularly known conventional ITO electrode. It was found that this type of fully solution based EL device shows higher performance than that of the conventional control devices fabricated on indium tin oxide anode coated on glass. In the year 2014, Y. Karzazi [147] provides a discussion of organic light emitting diode as a device and their application in display technology. While Ehsan Najafabadi (2014) focus on stacked inverted top-emitting white organic light emitting diode [148]. They represent a novel anode consisting of 1,4,5,8,9,11-hexaazatriphenylene hexacarbonitrile (HAT-CN)-modified Ag. They reported that such OLEDs can be fabricated on recyclable carbon nanocellulose (CNC) substrates, demonstrating the versatility of this inverted top-emitting architecture. Jun-Hyuk Choi et. al (2014) give a new method of enhanced photoluminescence with hybrid nanoimprinting method [149]. They developed this method for fabricating embedded metal nanopatterns with greater processability and improved reliability for enhanced photoluminescence (PL) in optoelectronic devices where they taken optical properties for all samples. Here the samples containing Ag nanopatterns provides better PL compared with reference samples without any Ag. The relative PL enhancements compared with samples with Ag dot-shaped nanoarrays were 32.2%, 36.1%, and

62.7% for pattern sizes of 150, 200, and 265 nm, respectively. Carolin Isenberg and Tobat P. I. Saragi [150] reveal the origin of magnetoresistance (MR) in unipolar amorphous organic devices (2014). Here they used low molecular weight 2,2',7,7'-tetrakis(diphenylamino)-9,9'-spirobifluorene (Spiro-TAD) in thin film form to fabricate the organic devices. In their work device fabricated on bare SiO<sub>2</sub> shows larger MR than the device fabricated on hexa-methyl disilazane treated SiO<sub>2</sub>. Kasinath Ojha et.al [151] studies the graphene-based hybrid materials (2014). Here they discussed the synthesis and unique properties of graphene and graphene-based composites in which they give special attention to the green synthetic methods and their wide applications in energy conversion, electronics and biomedical. Jun wang et.al [152] give a improve light outcoupling efficiency for OLEDs with microlens array over transparent substrate (2014). Here they design different kinds of microlens array on the substrate emission surface which were simulated using light tracing method. Finally they fabricated the organic devices with microlens array substrate which enhancing the light output about 1.64 times compared to that without any microlens array. Kazuyuki Yamae et.al [153] reported a high efficiency white OLED by controlling the wide angular distribution of incident light (2014). They investigated the optimization of angular light distribution in organic layer, based on high refractive index substrate. Here white OLED shows the high efficiency of 133 lm/W at 1,000 cd/m<sup>2</sup>. Chizu Sekine et.al [154] reported the high performance of polymer OLED and materials for organic printed electronics (2014). Here they investigated the different organic materials regarding the organic electronics field and give the guidelines for material designing and reported the progress of polymer-based organic light-emitting

diodes (OLEDs). Hongli Zhu et.al developed a transparent paper for the fabrication of organic devices in the display technology (2014). They discuss the properties and functionalization of transparent paper, such as surface roughness, printability, thermal stability, etc. In this work they also mention the advantages of transparent paper over traditional flexible plastic substrates along with its challenges [155]. Wenya Xu et.al developed a novel approach to arrange a large-diameter semiconducting single-walled carbon nanotube (sc-SWCNT) based on co-polyfluorene derivative with high yield (2014). They obtained high purity sc-SWCNTs inks by covering arc-discharge SWCNTs with poly[2,7-(9,9-dioctylfluorene)-alt-4,7-bis(thiophene-2-yl)benzo-2,1,3-thiadiazole] (PFO-DBT) aided by sonication and centrifugation in tetrahydrofuran (THF) [156]. Tae-Hee Han et. al (2015) works on flexible transparent electrodes for organic light emitting diodes [157]. They study many kinds of transparent conducting electrode (TCE). In this paper, the properties and applications of the transparent flexible electrodes classified into four categories (conducting polymer, silver nanowire, carbon nanotube and graphene) which suggests how to develop alternative TCEs for replacing the conventional ITO electrode. Bouanati Sidi Mohammed, N. E. Chabane SARI and Mostefa Kara Selma (2015) study the electrical and optical of PLED & OLEDS structures [158]. In this paper they prepared model polymer LEDs and OLEDs for studying their electrical and optical characteristics. The purpose of this modeling process is, to obtain information about the running of OLEDs, as well as the injection and charge transport mechanisms by changing some parameters such as doping concentration, thickness and electrode materials for maximum device performance. Eliot F. Gomez and Andrew J. Steckl (2015) work on Cellulose/Epoxy

Substrate for OLED fabrication by using adenine as a hole injection layer [159]. They found that adenine as a hole injection layer over gold can provide a better charge injection into the organic semiconductors and also increases the maximum OLED luminance and emission efficiency on both glass and cellulose substrates by increasing current (hole injection). Their result indicates the utility of the DNA bases for naturally based electronics and reveal practical methods to integrate cellulose as a biodegradable substrate. Xiaolong Yang et .al (2015) give a report on the advancement of emitters regarding the high performance of deep-blue organic light emitting diode[160]. Hironori Kaji et.al [161] developed a purely organic electroluminescent material with 100% conversion efficiency from electricity to generate light (2015). They reported that at approximately zero singlet-triplet energy gap and the thermal energy less than at room temperature, consequences in an organic light-emitting diode in which highest external quantum efficiency found to be 29.6%. Malte C. Gathera and Sebastian Reineke [162] give the recent development of light outcoupling from white organic light-emitting diodes (2015). In this work they reported a foreword to the physics of outcoupling in white OLEDs and also mention the progressive development towards making light extraction more efficient. In this paper they discussed the different phenomenon which affects the external and internal light out-coupling in OLED devices. Andrzej Dane et.al [163] developed a solution processable double layer organic light emitting diodes (OLEDs) (2015). They fabricated OLED based on 6-N, Narylsubstituted-1H-pyrazolo[3,4-b] quinolines. Here they synthesis three 1H-pyrazolo [3,4-b]quinolines (PQs) with N,N-diarylamine moiety which were used as dopants in poly(9-N-vinylcarbazole) (PVK) matrices. In

this work they obtained the highest luminance of about 355–806 cd m<sup>-2</sup>. Jae-Hyun Lee et.al [164] developed a functional nano-particle layer for highly efficient OLED (2015). Here they reported the light scattering films with aluminum oxide nanoparticles and matrix composite of polystyrene to obtain highly proficient OLEDs. They also characterized the optical properties and surface roughness measurement with variation of mixing concentration of Al<sub>2</sub>O<sub>3</sub> nanoparticles. Young Hoon Kim et.al works on multicolored organic and inorganic hybrid light-emitting diodes (2015). In this work they used CH<sub>3</sub>NH<sub>3</sub>PbBr<sub>3</sub> as a light emitting layer and self-organized buffer hole-injection layer (Buf-HIL). Their device configuration shows highest value of luminance, current efficiency and EQE are 417 cd m<sup>-2</sup>, 0.577 cd A<sup>-1</sup> and 0.125%, respectively [165]. Korwin M. Schelkle et.al induced solubility modulation of polyfluorene for enhancing the OLEDs performance (2015). In this work they considered  $\pi$ -conjugated polymers (polyfluorene) with side chains functionalized with hydroxycinnamic acid. Their work provides the possibility for the development of functional materials by manipulating the solubility and emissive parameters [166]. In the year 2016, Akanksha Uniyal and Poornima Mittal give a comparison of bilayer and multilayer OLED [167]. This paper defines the types of OLED on the basis of its mode of operation (Active-matrix and Passive matrix). Different characteristics and parameters of individual OLED structure are extracted and compared to show their structure dependent behavior. Bo Wang et.al (2016) worked on doped hole injection bilayers for solution processable blue phosphorescent organic light-emitting diodes [168]. They demonstrate a solution-processed composite film as the hole injection layer (HIL) in OLEDs developed by mixing HAT-CN with

2,3,5,6-tetrafluoro-7,7,8,8-tetra-cyanoquinodimethane (F<sub>4</sub>-TCNQ). The crystallization is suppressed effectively by optimizing the mixing ratio. While Yuan Li et.al (2016) reported an improving efficiency of blue organic light-emitting diode with sulfobutylated lignin doped PEDOT as anode buffer layer [169]. With PEDOT: ASLS as HIL, a highly enhanced current efficiency of 37.65 cd/A was achieved. In their device structure the result is even better than that of the control device using PEDOT: PSS as HIL. Compared with PSS with regular structure, strong aggregation and oxidation behavior of ASLS contribute to the hole injection capability of PEDOT: ASLS. E. Angioni et.al [170] developed a white-emitting organic light emitting diode based on exciplex interface emission (2016). Here they introduced a new triaryl molecule based on a benzene benzothiadiazole benzene core for the fabrication of white OLED. This fabricated OLED gives white light emission with CIE coordinates of (0.38, 0.45) and a colour temperature of 4500 K. Daniel Volz and Thomas Baumann [171] give efficient and deep-blue TADF-emitters for OLED display technology (2016). In this work they used a novel emitters based on thermally activated delayed fluorescence (TADF) technology. It was found that compared to simple fluorescent dopants, the efficiency of TADF-emitters is higher than four times. In this bottom-emitting OLED device, maximum efficiency values was close to 20%. Adam F. Henwood et.al [172] works on solubilised and bright blue-emitting OLED (2016). They fabricated OLED using iridium complexes by solution processed method. They compared this complex with two reference complexes bearing 4,4'-di-tert-butyl-2,2'-bipyridine and solution processed organic light emitting diodes (OLEDs) have been fabricated from these materials. Jin-Woong Hong et.al [173]

studied the performance of organic light-emitting diodes with an electron-transport layer of BCP (bathocuproine) (2016). They calculated the current density-voltage-luminance characteristics of the OLEDs, which shows that device performance is better than without BCP. Here it was found that the current density, luminance and luminous efficiency increased by about 22%, 50% and 2% respectively. Rafael Gomez-Bombarelli et.al [174] design efficient molecular organic light - emitting diodes (2016). They used virtual screening method and reported a designing process of integrated organic functional material which incorporates quantum chemistry, molecular characterization, device fabrication and optoelectronic testing. They identify thousands of novel OLED materials in the visible spectrum. Similarly Tae-Hee Han et.al [175] reported an ultrahigh efficiency of solution processed small-molecule organic light-emitting diodes by using universal host materials (2016). They also reveal a solution-processed flexible solid-state lighting device. Jie Yang et. al give a new approach for controlling the intramolecular conjugation and hence the optimized performance of OLED devices (2016). Their paper focused the design strategies for controlling the intramolecular conjugation effect and to understand blue emission. They also provides some outlooks on the further investigation of this field [176]. Yonggang Yao et.al developed a hybrid substrate towards high-performance optoelectronics (2016). Here they report a new substrate i.e plastic–paper, which has a high optical transmittance and high transmittance haze in a broadband wavelength. This substrates has ultra-flat surface which is mechanically flexible, durable in different solvents and also compatible with standard processing in semiconductors for OLEDs [177]. Recently in the year 2017, Y. Xu et.al [178] works on multilayer

graphene. They used multilayer graphene ( specially trilayer graphene ) as transparent conducting electrodes in organic light emitting diodes. For multilayer graphene preparation they used new method of preparing tri-layer graphene films with chemical modification and give the effect of doping and patterning process on the graphene films performance as transparent electrodes. Zhike Liu et.al (2017) works on functionalized graphene materials and other two dimensional materials for organic devices [179]. In the same year, Meiling Shan et. al (2017) reported an enhanced hole injection in organic light-emitting diodes utilizing a copper iodide-doped hole injection layer [180]. They demonstrated organic light-emitting diodes (OLEDs) by incorporating copper iodide (CuI) in 4,4',4''-tris(N-3-methyl phenyl-N-phenyl-amino)triphenylamine (m-MTDATA) as a hole injection layer (HIL) based on the emitting system of C545T–Alq<sub>3</sub>. Their device with CuI-doped m-MTDATA HIL shows a very low operating voltage of about 4.26 and 5.70 V for 1000 and 10 000 cd m<sup>-2</sup>, respectively, which reveals a great improvement over the undoped device m-MTDATA HIL (4.85 V for 1000 cd m<sup>-2</sup> and 7.72 V for 10 000 cd m<sup>-2</sup>). In the month of June 2017, Bao-Jia Li et al. report on optimization of FTO thin film by ultrasonic vibration using laser annealing treatment [181]. Heng Zang et.al [182] represented an efficient quantum dot light-emitting diodes (2017). Here they used inverted tandem structure where efficiency is greater than 100 cdA<sup>-1</sup>. They also developed a solution-processable interconnecting layer based on poly(3, 4-ethylene dioxythiophene)/polystyrene sulfonate/ZnMgO. They further optimized the fabrication process and a hybrid deposition technique which exhibit remarkable EQE over 23%, which was the highest values yet reported. Qingchen Dong et.al [183] give a report on



efficient light out-coupling in organic light-emitting diodes (2017). They used surface carbon-coated magnetic alloy nanoparticles. They said that the efficiencies of fluorescent green OLEDs can be enhanced by 47.1% and 48.5% by mixing the surface carbon-coated magnetic FePt (0.5 wt%) and CoPt (0.5 wt%) alloy NPs into PEDOT:PSS, which provides the maximum values of  $5.40 \text{ cd A}^{-1}$  and  $5.45 \text{ cd A}^{-1}$ , respectively. They also concluded that the presence of such an alloy NP-included PEDOT:PSS acts as an optical out-coupling layer which finally enhancing the device efficiency. Similar report was also found regarding the application of quantum dots in OLEDs [184,185]. Amos Egel et.al [186] study the optical simulation of nano-particle based internal scattering layers for light outcoupling from organic light emitting diodes (2017). They used infinitely extended scattering layers in order to correct the truncation error due to the presence of finite no of particles in the simulations. Here they calculated the optimal particle filling fraction for an internal scattering layer in a sensible OLED structure.

## **1.5 Introduction to organic semiconductors:**

Organic semiconducting materials are mainly composed of  $\pi$ -conjugated carbon compounds. These organic materials usually remain as insulators as they do not contain any free charge carriers under room temperature. Their band gap energies are ranges from 1.5 to 3.5eV base on their chemical structures [187, 188]. These semiconducting materials are classified into two group's i.e. low molecular weight small molecules and higher molecular weight conducting polymers. As mentioned above they are also different in their processing techniques. Thermal vacuum

deposition method is used for the deposition of small molecule devices and spin coating method is normally used for the solution process devices. There are different kind of organic semiconducting materials are available. Some of which are popularly known as small molecule organic semiconducting materials are NPB, Alq3, TPD and 2,9-dimethyl-4,7-diphenyl-1,10-phenanthroline (BCP) . Organic semiconductor materials always possess a property of alternative single and double carbon-carbon bond no matter whether they are small molecule or polymer molecules as shown in the following figure 1.2. We know that the atomic number of carbon is given as 6, so its electronic configuration in the ground state is given as  $1s^2 2s^2 2p^2$ .

Therefore it is clear that there are four valence electrons and hence for a saturated carbon atom formation, four bonds are possible. In this situation, the material behaves as a perfect insulator since all the four electrons are used to make a bond. However, for an unsaturated organic material not all of the four valence electrons are used for the bond formation. When three electrons out of four are utilized to form a chemical bond, then there will be the result of three similar  $sp^2$  hybridized orbitals which are associated at  $120^\circ$  with respect to each other as shown in the following the figure.

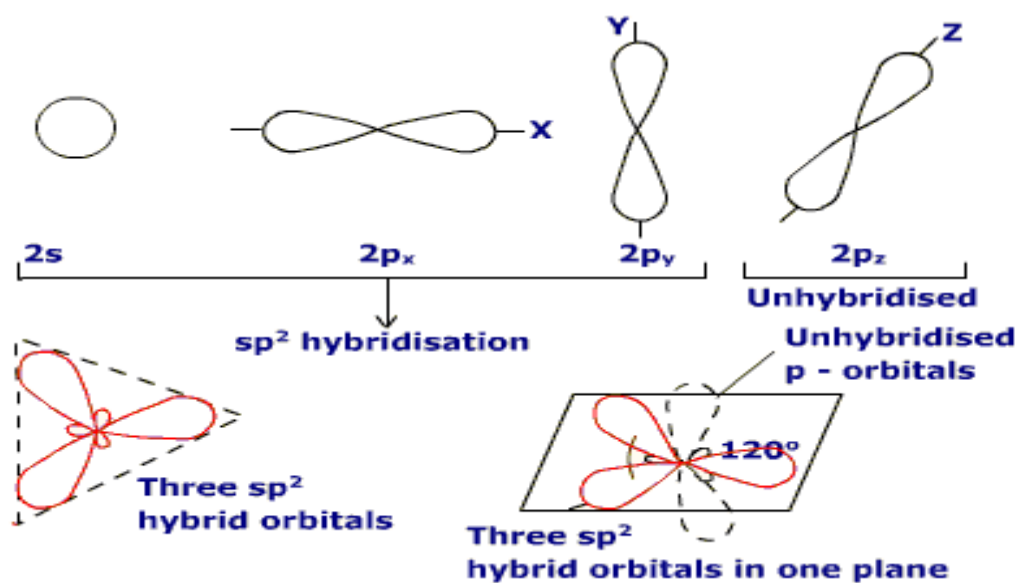


Figure 1.3: Hybridization picture of Carbon atoms

These types of orbitals can form  $\sigma$ -bonds. In these bonds, it is found that the excitation energy is very high about 8eV. This value is beyond the visible range of the spectral region. Also, in this case, the electronic property of the material due to the presence of  $\sigma$ -bond is entirely insulating behaviour. On the other hand, the residual 2s electron can jump to the vacant  $P_z$  orbital where they are lies vertically to the  $sp^2$  orbital. This unhybridized P-orbitals is responsible for the formation of  $\pi$ -bond with the adjacent carbon atoms by the electron contribution. This type of bond is found to be very weak which is responsible for the delocalization of the electron in the long chain for the polymer molecules, and also they form a closed circle in the case of small molecules. The semiconducting nature of the organic materials is only due to the presence of these delocalized or  $\pi$ - electrons and they are mainly responsible for the electronic properties of the material. It is found that in case of  $\pi$ -bonds there is a large number of structural relaxations is occur due to the addition of extra charge. This bond is also

responsible for all the electronic features of the organic materials. This type of delocalised  $\pi$ -orbitals is also known as molecular orbitals in organic electronics. In molecular orbitals, two important terms are mainly associated. One is Highest Occupied Molecular Orbital (HOMO), and the other is Lowest Unoccupied Molecular Orbital (LUMO). When a molecular orbital is found to be filled with electrons, then it is known as HOMO. Similarly, if it is found to be remaining empty, then the same orbital is known as LUMO. This terminology of the molecular orbital is similar to the valence and conduction bands of the inorganic semiconductors. The separation between the two states is called the band gap of the organic material. The energy difference of this band gap determines the nature of the emitted light from the electroluminescence device due to their recombination process. It is also possible to tune the nature of the wavelength of the emitted light by changing the chemical structure of the organic material. Because of the very low mobilities and low free charge carrier densities of organic molecules, they can be considered as an insulator. Due to the presence of different geometry and different local environment of the molecules in organic materials they are typically more disordered. As a result there exists an energy state for both neutral states and charged states. There is a strong structural relaxation that occurs when an electron is added or removed in a molecule. However, it is found that the charges in the electronic state of the molecule remain on the individual conjugated system since the transferring of electrons between the neighboring molecules are not very large. So the transport of charge carrier is taken by the process of hopping between the two localized states within the films. As already mentioned above the main reason for the presence of disorder for small molecules are due to their

molecular orientation and the different types of possible chemical defects. There is also some contribution of the dipole moments which has a different orientation towards the disorder of the material. Because of this type of orientation of the dipole moment there is a resulting random electric field that changes the energy level in the film. As a result, the mobility of the small organic molecule is found to be very low. This is the only reason why the efficiency of the OLED device is found to be very small where only a single layer is used as both electron and hole transport layer which finally increase the large driving voltage. Hence it is necessary to think about the alternate way to overcome this difficulty. For that purpose, the idea of multilayer device is presented in which different material of hole and electron mobility are introduced between the two electrode surfaces of the EL device. In the literature, it is found that normally different types of diamines such as TPD, N,N'-di (naphthalene-1-yl)-N,N'-diphenyl-benzidine (NPB) are used as hole injection or hole transport layer because they provide little opposition force to hole transport across the device. They also have a high hole mobility of about  $10^{-3}$  cm<sup>2</sup>/Vs [189, 190]. On the other hand, one of the most common examples of electron transport material is Alq<sub>3</sub>. Other metal chelates are also used as electron transport layer organic devices. However, it is found that the transport of organic material is harder because of the presence of some impurities of oxygen and water. They produce some extra energy states between the HOMO and LUMO of the organic material [191]. For example, it is possible to produce high electron mobility in Alq<sub>3</sub> only under the high electric field of about 106V/cm [192-194]. On the other hand in case of amorphous films, there are different kinds of electron transport were found to be observed depending upon the purity level

[194]. Some examples of electron transport materials (ETL) which are widely used in fabrication of OLEDs are given as 1,3-bis[2-(2,2'-bipyridine-6-yl)-1,3,4-oxadiazole-5-yl]benzene (Bpy- OXD), 6,6'-bis[5-(biphenyl-4-yl)-1,3,4oxadiazole-2-yl]-2,2'-bipyridyl (BP-OXDBpy), 3-(4-biphenyl)-4-phenyl-5-*tert*-butylphenyl-1,2,4-triazole (TAZ), 2,9-dimethyl-4,7-diphenyl-1,10-phenanthroline (BCP), 8-hydroxyquinolinolato-lithium (Liq) etc.

## 1.6 Photophysics of organic semiconductors

### 1.6.1 Singlet and triplet excited state

Quantum mechanics is used to describing the electronic state of a molecule where one electron is excited from an occupied state into an unoccupied state. Therefore a hole is generated due to this electronic excitation of the electron which implies the missing of the electron. Same nature of wave function is used to represents the electron and hole. When we considered a system of two particle consisting of  $\frac{1}{2}$  spin, then due to the Pauli Principle the eigenstate of the Hamiltonian is found to be antisymmetric with respect to the exchange of particle [195]. In quantum mechanics wave functions can be represented as the product of the spatial and spin wave function. Therefore the spin wavefunction can be either symmetric or antisymmetric on condition that the spatial wavefunction has the opposite parity. The spin part of the wave function for the electron and hole is given by  $\Psi_{spin} = |\uparrow\rangle$  or  $|\downarrow\rangle$ , where arrow sign provides the direction of the orientation of the spin. Therefore for this two-electron system, four possible combinations can be differentiated between one antisymmetric (singlet) state  $S_n$ :

$$\Psi_{\text{spin}} = \frac{1}{\sqrt{2}} (|\uparrow\rangle|\downarrow\rangle - |\downarrow\rangle|\uparrow\rangle)$$

Moreover, also three symmetric states are given by

$$\Psi_{\text{spin}} = \frac{1}{\sqrt{2}} (|\uparrow\rangle|\downarrow\rangle + |\downarrow\rangle|\uparrow\rangle)$$

$$\Psi_{\text{spin}} = |\uparrow\rangle|\uparrow\rangle$$

$$\Psi_{\text{spin}} = |\downarrow\rangle|\downarrow\rangle$$

However, it is important to note that initially the excited singlet and triplet states with the lowest energy ( $S_1$  or  $T_1$ ) are not generated, and only higher excited states ( $S_n$  or  $T_n$ ) can be generated. However these excited states have a very short lifetime so, they can quickly decay into the lowest excited states through a nonradiative process, known as internal conversion (IC) as shown in figure 1.4.

## 1.6.2 Light Emission

After the generation of an exciton in the light emitting layer, the excited electronic state of the molecule is relaxed and back into the ground state by either radiative or nonradiative decay process. The following proportionality equation gives the probability of this radiative electronic transition from the state  $\Psi_i$  to state  $\Psi_j$

$$P \propto \langle \Psi_i | M | \Psi_j \rangle = \left| \int \Psi_i M \Psi_j d\tau \right|^2$$

Where  $M$  is the dipole moment operator and the integration over  $d\tau$  cover the whole space of all  $3N$  coordinates with  $N$  the number of electrons. Hence from this equation, it is clear that only those transitions which have similar spin symmetry are responsible for the non zero transition dipole moment. Therefore with the singlet behaviour of ground state  $S_0$ , radiative transitions are only possible between the lowest singlet excited state  $S_1$  and the ground state  $S_0$ . On the other hand, the transitions from the lowest triplet excited state  $T_1$  to the ground state are restricted due to the spin quantum mechanics. These types of radiations are known as fluorescence.

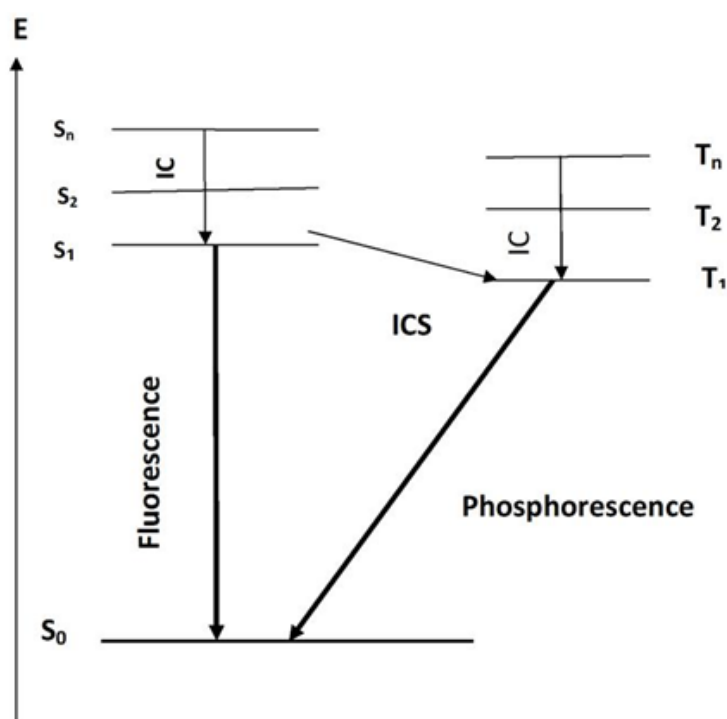


Figure 1.4: Schematic representation of fluorescence and phosphorescence

### 1.6.3 Fluorescence



According to the spin quantum mechanics, about 25% of all the excitons which are produced in an organic semiconductor reside on the singlet state of the material. It is found that although excitons tend to remain inside the higher excited state, they are usually transformed to the lower state through internal conversion (IC) because the radiative emission is strongest when transitions are taking place from the lowest excited state ( $S_1$  or  $T_1$ ) decaying to the ground state. Similarly, the nonradiative transitions of excitons are also taken place, but they are responsible for heat generation only. Therefore fluorescence is a phenomenon in which there is a resulting of radiative photon emission from singlet excited state to ground state  $S_0$ . In these types of fluorescence materials, singlet state is only responsible for the light emission because of the fact of spin selection rule in quantum mechanics which forbidden the transitions between the singlet and triplets state of the energy level. This result considerably affects the device efficiency in which only 25% of the total exciton is used for electronic transitions [196]. This fact implies that the device using these materials, the maximum value of internal quantum efficiency (IQE) is only 25%. Therefore to facilitate increasing value of this IQE, excitons from both the singlet  $S_1$  and triplet  $T_1$  states need to be addressed.

### **1.6.4 Phosphorescence**

Baldo seminal was the first person who introduces the concept of spin-orbit coupling for allowing to mixing both singlet and triplet energy state to enhanced the device performance of OLED efficiency [197]. This spin-orbit coupling was possible by introducing a heavy metal like Iridium or platinum with a high orbital angular momentum.

This types of process break the transition rules between singlet and triplet excitons and allows for singlet-to-triplet intersystem crossing (ISC) [198,199]. Therefore through this intersystem crossing, it is possible to make all the excited excitons on the singlet state  $S_1$  can transition to the triplet state  $T_1$ . Thus in this triplet state, all the excited excitons have 100% probability that can emit radiative transitions from  $T_1$  to ground  $S_0$ . So, this triplet to ground state radiative transitions process can lead to IQE of 100%. This phenomenon of radiative transition is known as phosphorescence in OLEDs.

## **1.7 Energy transfer mechanism in OLED**

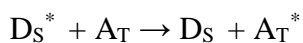
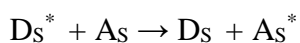
Generally, in organic phosphorescent OLED devices, some of the lowest excited states are lost due to the triplet-triplet annihilation. This is because when two triplets energy state collides with each other, then the energy of one state is transferred to the other excited state which finally decreases one excited state [200, 201].

Therefore it is not possible to produce efficient OLED with purely phosphorescent complexes due to the triplet-triplet annihilation. So to overcome this small difficulty amount of guest material is doped into this light emitting phosphorescent complexes [202]. However, however, to maintain a radiative transition it is necessary to maintain a good energy transfer from the host to the guest molecule. These types of energy transfer mechanism are mainly classified into two groups which are discussed below.

### **1.7.1 Forster energy transfer mechanism**

This type of energy transfer is due to the interaction of two electrical dipoles. It is also known as

Coulomb mechanism. The probability of this coulombic energy transfer mechanism is decreased with  $R^{-6}$  where  $R$  is the distance between the molecules. Here dipole interactions can be expected up to a distance of 10 nm [197]. Since it is a purely dipole-dipole interaction, this implies that the spin of each molecule must be conserved throughout the energy transfer mechanism which implies that the triplet transfer from a donor (D) to acceptor (A) is strictly forbidden in Förster transfer which leads to the singlet energy transfer.



This energy transfer is given below

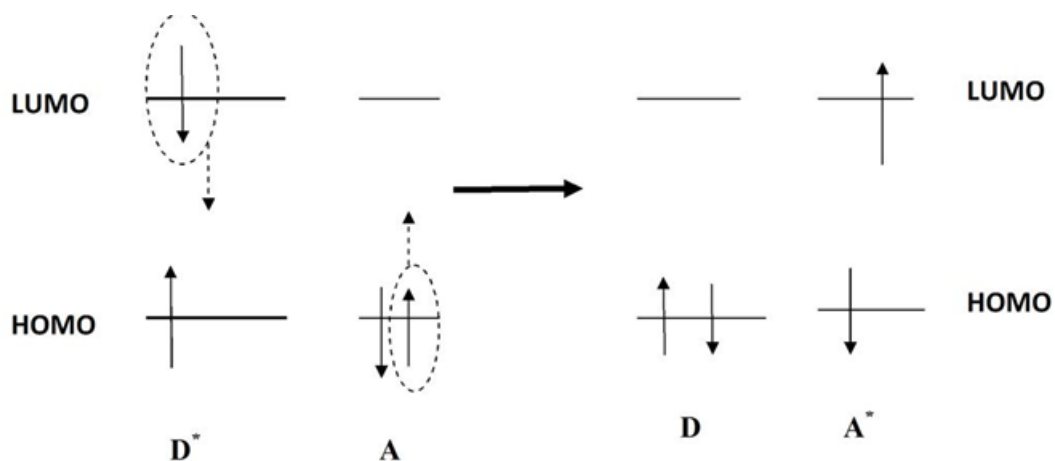
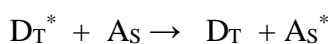
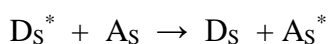


Figure 1.5: Graphical representation of Förster energy transfer

## 1.7.2 Dexter Energy Transfer

It is a purely quantum mechanical phenomenon in which overlapping of atomic orbitals is necessary for transferring of energy between the two states. For this interaction to take place the total spin of both molecules before and after the process has to exist. This leads to the spin conservation of the molecules. The possible transitions are shown in the following figure



In this Dexter energy transfer process, electrons are allowed to transfer between the molecules, whereas in case of Foster energy transfer process these electrons remain bound to the same molecule. In this Dexter energy transfers, both triplet-triplet and singlet-singlet energy transfer is taking place between molecules [203]. Energy transfer mechanism for Dexter process is given below:

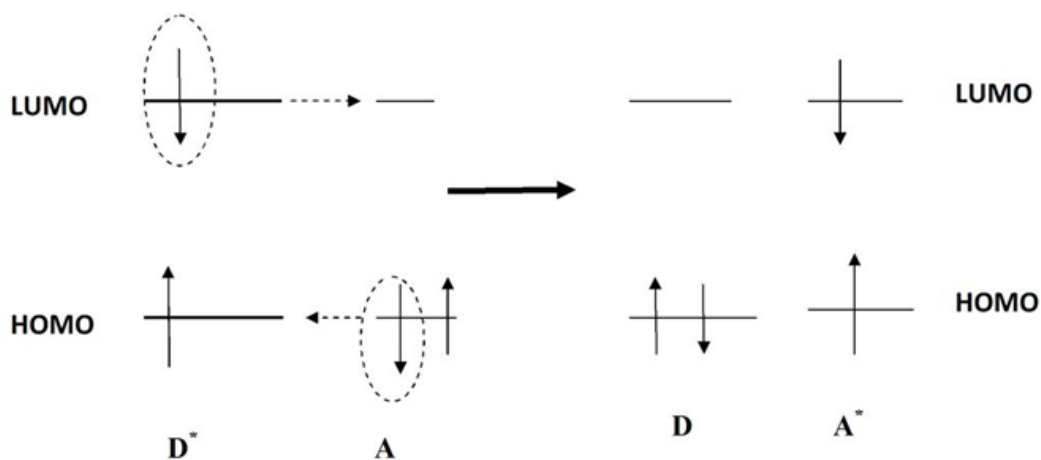


Figure 1.6: Graphical representation of Dexter energy transfer

## 1.8 Device Physics

### 1.8.1 Theory of operation

Organic light emitting diode (OLED) works on the principle of electroluminescent, i.e., emission of the light wave under the application of electric field. In an OLED, the active light emitting layer is made of organic compounds. This is electroluminescent which emits light in response to an electrical biasing. As shown in the following figure. An OLED consists of one or more organic layers which are sandwiched between two electrodes (i.e., cathode and anode). The nature of this anode is optically transparent which allows to light to escape from the device. Due to the application of the electric field both the charge carrier is transported across the device from both sides of the electrode, and finally, they recombine in the light emitting layer which emits light as shown in the following figure. The first OLED was demonstrated by

Eastman-Kodak which consists of only a single organic heterojunction between two layers of semiconducting material [204]. However, now a day's for OLEDs fabrication multiple semiconducting layers are used to make easy for charge injection and transport from both the electrode side.

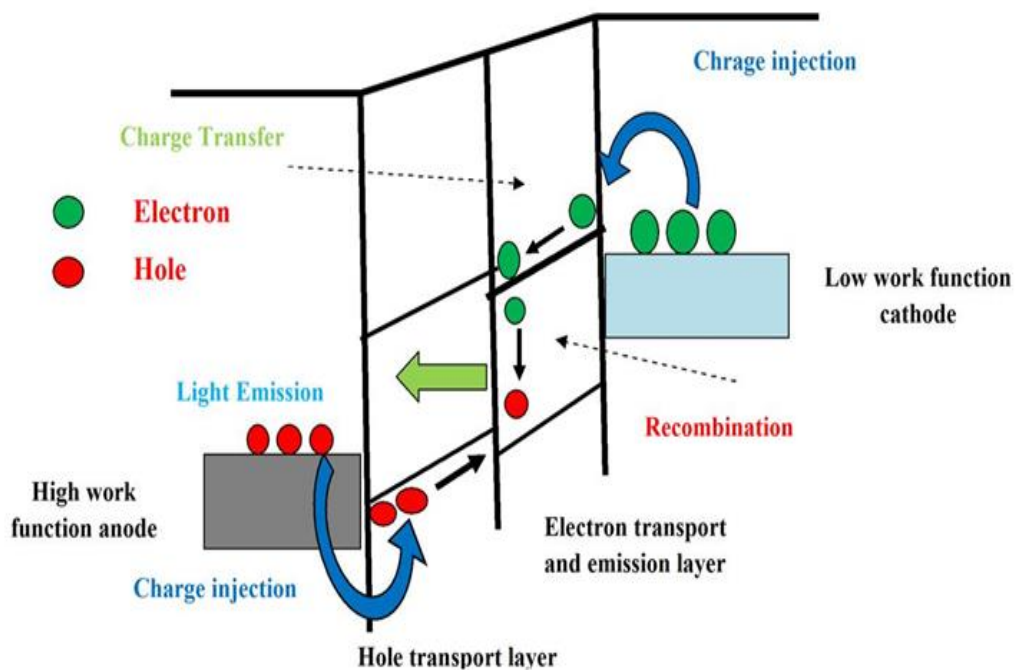


Figure 1.7: Emission of a light wave from the organic layer

The operation of OLED involves charge injection from an electrode, transport of charge carrier and recombination of holes and electrons to generate excited states called excitons, followed by the emission of light. The main factors that determine the luminance be-

1. The efficiency of charge injection from electrodes.

2. Confinement of the injected charge carrier within the emitting layer to increase the probability of desired emissive recombination.

During operation, a voltage is applied across the OLED such that the anode is positive on the cathode. A current of electrons flows through the device from the cathode to anode, as electrons are injected into the LUMO of the organic layer at the cathode and withdrawn from the HOMO at the anode. Electrostatic forces bring the electrons and the holes towards each other, and they recombine forming an exciton, a bound state of the electron and hole. It happens closer to the emissive layer because in organic semiconductors holes are more mobile than electrons. The decay of this excited state results in a relaxation of the energy levels of the electron, accompanied by the emission of radiation whose frequency is in the visible region.

### **1.8.2 Charge Injection**

From the early days of Tang and Vanslyke, it was realized that the injection of charge carrier from the metallic electrode plays an important role for the device performance. Because when the barrier height is very large at the metal/organic interface, then the charge injection process is limited. The energy barrier implies the difference of energy between the HOMO or LUMO of the semiconducting material and the work function of the metallic electrode. For better device performance the contact materials always to be chosen in such a way that the barrier energy in minimum. In this situation, a large number of charge carrier can inject into the organic materials and this type contact is known as an ohmic contact. In this situation, the device performance is limited by the transport properties of the organic materials. From the literature report, it is found that

there is a maximum amount of current which is held by organic semiconductor and is known as the space charge limited current (SCLC) which is given by the following equation.

$$J_{SCLC} = \frac{9}{8} \mu \epsilon \frac{V^2}{L^3} \dots\dots\dots (1)$$

This equation is known as Mott-Gurney equation. Here,  $\mu$  is the mobility of charge carriers,  $\epsilon$  is the permittivity of the organic semiconductor ( $\epsilon = \epsilon_0 \epsilon_r$ ) and  $V$  is the voltage across the device whose thickness is  $L$ . The efficiency factor, ( $\eta$ ) is defined as the ratio of measured current  $J$  and the SCLC current ( $J_{SCLC}$ ), where  $\eta = J/J_{SCLC}$ . It is found that when the value of efficiency is 1, then the contact behaviour is ohmic. While if its value less than 1, then charge injection is limited. On the other hand from the theoretical point of view it is calculated that when the barrier energy is less or equal to 0.3eV, the contact behaviour is ohmic [205, 206]. Similarly, when the barrier energy is greater or equal to 0.3eV, the contact is injection limited. In the case of organic semiconducting materials, it is not possible to explain the charge injection mechanism by a simple thermionic model like inorganic materials [207]. Here charge injection is influenced by different parameters of the organic materials like organic media, charge localization properties, hopping type of transport and polaronic effects. That why thermionic emission model is difficult to apply. In the case of organic semiconductors, a considerable amount of charge accumulation occurs at the interface region after the injection from the electrode surface due to the low mobility nature of charge carrier. Therefore tunnelling of charge carrier takes place across the barrier energy at the high electric field. This type of charge tunnelling is known as Fowler-



Nordheim tunnelling (FN tunnelling). This model, however, does not contain the hopping nature of the charge carrier. Due to the low mobility of charge carrier in real devices, it was realized that there is a considerable amount of backflow of charge carrier is takes place since a larger amount of charge accumulation occurs at the interface region. Therefore a model was introduced by the Scott et al. [208] by considering both these hopping nature and backflow of charge carriers. Here they modified the older models by considering the current contribution due to the backflow of charge. It is possible to measure the distance from the interface region of metal/organic away from which the electron can escape from this interface region without recombination, by comparing the columbic attraction of image charge (i.e., charge left on the metal after electron injection) along with the thermal energy of the electron. This recombination current can be calculated considering the diffusive transport of electrons. Therefore it can be said that the true value of current is the difference between the thermionic current and the recombination current. This model was already experimentally proved by considering a molecular doped polymer PC: TPD with various concentration of TPD to changes the mobility value and here current is found to be proportional to the mobility of the doped system [209]. On the other hand, hopping nature of charge carrier was also introduced in the charge injection model lately [210] by considering thermal tunnelling of charge carrier.

### **1.8.3 Metal/Organic interfaces**

The interface between the metal and the semiconductor play an important rule for the injection of charge carrier. The charge carrier injection into the organic layer is highly

dependent on energy barrier at the interface region. This interface region also controls the carrier concentration which directly affects the device performance and the operating voltage of the OLED. This barrier height is not simply the difference between the work function level of the metal and the energy of the semiconducting material because some other factors such as chemical and electronic properties of the interface region also change the energy barrier considerably. In this interface region, the barrier height is found to be dependent on various factors such as the tendency of dipole formation, charge localization, chemical reaction, metal diffusion, etc. On the other hand, the device with a buffer layer at the metal/organic interfaces maintains a higher performance during the operation time. This indicates that the stability of devices can be improved by inserting an HIL at the interface region to avoid direct contact of the organic hole transport layer and the metal electrode surface. This is because the ionization potential of the hole transport layer is the key factor which affects the stability of an EL device. Because a high potential barrier for injection of holes at the interface region produces Joule heating which finally causes a local aggregation of the molecules at the interface and hence the destruction of the barrier [211, 212]. By placing buffer or hole injection layer at the interface, this difficulty can be overcome which reduces the high energy barrier. The barrier height at the interface region depends upon several factors such as dipole formation, charge localization, etc.

### **1.8.3.1 Work function**

In metals usually, the electrons in the outer shells of the atoms are loosely bound, and they move about freely throughout the lattice of positive ions. These loosely bound electrons are called free electrons. However, these electrons are confined to the conductor and hence cannot leave its surface at ordinary temperature. Because the moment an electron comes out of a metal surface with its negative charge, the metal surface acquires an equal positive charge and pulls it back. Thus there is a potential barrier. So, the work function of a metallic conductor is defined as that minimum amount of energy which is required to escape the electrons from the conductor to just outside the surface. In this case, the word “just outside” implies that a considerable distance which is large enough so that the image force can be insignificant but should be small than the dimension of the crystal which is normally in the order of  $10^{-4}$  cm. On the other hand, work function is also defined as the energy level difference between the electrochemical potential ( $\mu$ ) of electrons and the electrostatic potential energy of an electron in the vacuum just outside the surface [213] i.e.

$$e\phi_m = -e\phi_{vac} - \mu$$

Here the term  $-e\phi_{vac}$  represents the energy level which is known as the local vacuum level ( $E_{vac}$ ). This local vacuum level is different from the vacuum level at infinity  $E_0$ , which implies that zero potential energy of the electron [214]. Also, the electrochemical potential of electrons is defined as the Fermi level  $E_F$  relative to the vacuum level at infinity  $E_0$  [215].

Hence the work function representation of above-given equation is also equivalent to the difference in potential energy of an electron between the local vacuum level ( $E_{\text{vac}}$ ) and the Fermi level ( $E_{\text{F}}$ ) i.e.

$$e\phi_{\text{m}} = E_{\text{vac}} - E_{\text{F}}$$

From this relation, it is clear that the value of work function will be changed if the local vacuum level ( $E_{\text{vac}}$ ) varies from a sample.

### **1.8.3.2 Schottky Contacts**

Due to the importance of semiconductor/metal interface in optoelectronics devices, the corresponding energy level alignment at this interface region has been extensively studied. Generally, in Schottky-Mott limit, the vacuum level of the semiconductor and metal align, at the interface region and thus form a region of net space charge. As a result of which no charges can move across this interface region, and therefore the semiconductor bands are forced to bend and hence accommodate the potential difference. The difference between the metallic work function ( $\phi$ ) and the electron affinity of the semiconductor ( $\chi$ ) is known as the Schottky barrier height.

However, this Schottky-Mott limit is most rarely observed in metal/semiconductor interfaces due to the formation of an interfacial dipole because of which charge can transfer across the interface region. Moreover, hence the Fermi level cannot move freely in the band gap of the organic and thereby pinned by the dipole layer.

On the other hand, it is found that in comparison to inorganic semiconductors, in the Schottky-Mott limit the vacuum level of the organic and metallic alignment takes place by forming a region of net space charge at the interface. Then the barrier height

for holes is given by the value of the difference between the HOMO of the organic material and the work function of the metal.

$$e\phi_{bp} = E_{\text{HOMO}} - e\phi_m$$

However, organic semiconductors possess no free charge carriers, and hence the band bending in the organic cannot entirely contain the potential difference. That is why this Schottky-Mott limit, is most rarely observed at metal/organic interfaces due to the formation of a strong interfacial dipole between the metal surface and organic molecules.

### **1.8.3.3 Electronic properties of the interface**

The following figure represents the energy level diagram of the metal-organic interface region. In this figure,  $E_{\text{vac}}$  represents the energy value close to the vacuum level of the material at 0 eV. An electron can easily remove from the surface above this energy level. The ionization potential (IE) is defined as the difference of energy between the HOMO and the  $E_{\text{vac}}$ , while the energy difference between the LUMO and the  $E_{\text{vac}}$  known as the electron affinity (EA). Also, the energy difference between the LUMO and the work function of the cathode is known as energy barrier of electron injection. Both these values can be determined by ultraviolet photoemission spectroscopy (UPS). On the other hand, the value of HOMO and LUMO energies are determined by the optical absorption spectra of the material. Hence the final value of electron affinity is determined from the values of HOMO and HOMO-LUMO gap.

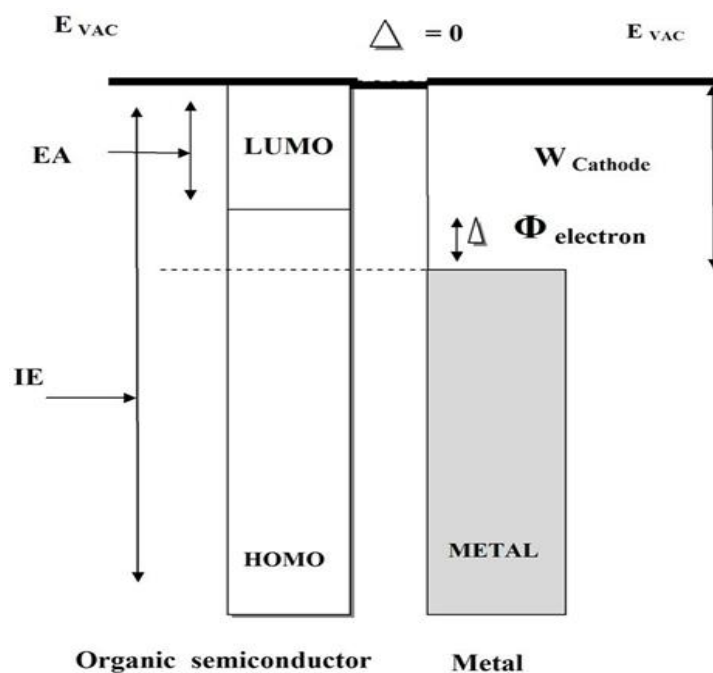


Figure 1.8: Energy level alignment at the ideal situation of no dipole

However, the situation is shown in figure 1.8 is not simple as it is like to see it is because normal vacuum energy level at the interface region is not applicable [216-218]. There are many processes which modify the interface region such as transferring of charge from metal to organic, reorganization of the electron cloud, interfacial chemical movement, etc. when two materials make their contact [216]. As a result vacuum level is a shift to the new position compared to previously measured one as shown in figure 1.9. Different studies are reported on the metal/organic interface by UPS [216-227].

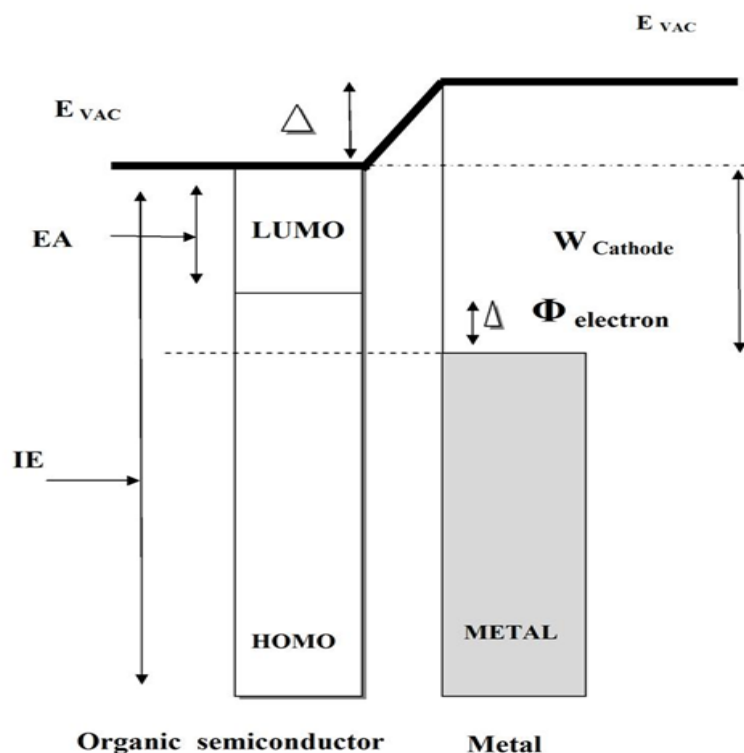


Figure 1.9: Energy level alignment of modified metal/organic interface

From all the above studies it can be concluded that the concept of common vacuum level is not truly applicable and there is always a dipole of magnitude  $\Delta$  is appear due to the shifting of  $E_{vac}$  and the HOMO-LUMO of the considered organic materials. This magnitude of the dipole barrier depends upon the work function of metal and nature of the organic material. Therefore the value of work function of the metal is lowered making the barrier height smaller.

### 1.8.3.4 Origin of interface dipole

From the studies of different previous metal-organic interfaces, it is concluded that there is a relation between the dipole formation for the organic material and the metallic work function [203-207]. Here main observation is that there is always a shifting of vacuum level is occurring negatively which causes a lowering of the vacuum level. Therefore based on this observation the formation of the dipole at the interface region was explained by Ishii et al. and the corresponding mechanism is illustrated in following figure 1.10 (taken from Ref. [228]).

The primary factor responsible for the dipole formation is the transferring of an electron from the metal to the organic surface which can form positive and negative charge at the interface region due to their separation. For the formation of the interfacial dipole, the electric field is confined to a very narrow region, normally 1-2nm [229]. This type of electron transformation is taking place for a strong combination of organic donor material and a high work function of the metallic electrode as shown in Figure 1.10(A1) or there is a strong acceptor organic material and a low work function metallic electrode as shown in Figure 1.10(A2).



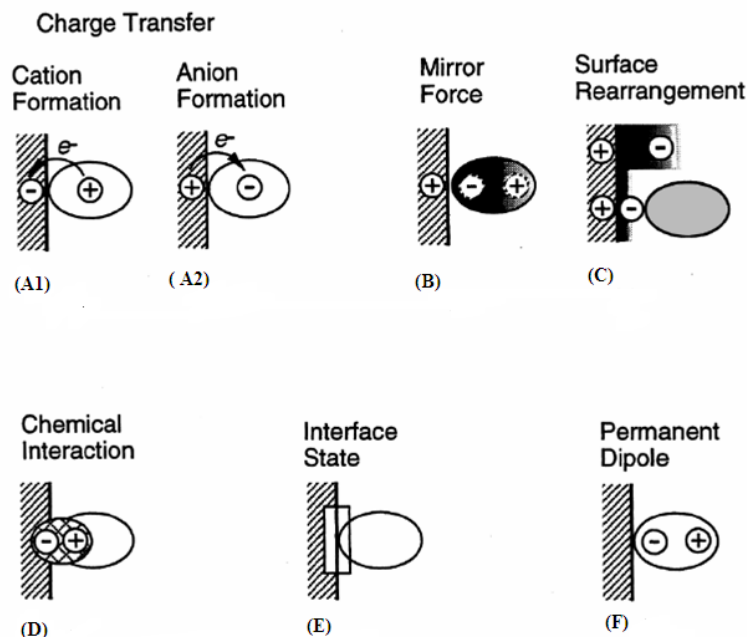


Figure 1.10: Formation of the interfacial dipole at the metal/organic interfaces

Here the second one responsible for the formation of dipole may be due to the image charge effect or the alteration of the surface dipole at the metal surface region. This is due to the polarization of electron cloud attracted by the image charge at the metal surface region as shown in figure 1.10 (B). There is also a rearrangement of the electron cloud takes place from the metal side due to the presence of molecules in this surface as shown in figure 1.10 (C). On the other hand chemical interaction as shown in figure 1.10(D), is another factor which is responsible for the origin of the dipole where either metal or organic molecule is chemically very reactive. In this situation, the presence of organic molecules on the surface results in the formation of new bonds along with the reorganization of presented local chemical bonds. In such situation, the formation of dipole direction depends upon the chemical interaction. Another factor

responsible for the dipole formation is the possible maintenance of an interfacial state. However, in organic material, the presence of such states is less possible because the weaker van der Waals forces form organic materials. In conclusion for a polar organic molecule, having a permanent dipole, the direction of this dipole can result in the formation of an interfacial dipole as shown in Figure 1.10(F).

## **1.9 Organic compounds: Small molecules and polymers**

In organic compounds, covalent bonds take an active role in the formation molecules which are consists of mostly carbon atoms. Here atoms are held together by covalent bonds by sharing some of their electrons. Organic compounds are mainly classified into two different classes for the fabrication process. First one is known as small organic molecules, and the next one is known as conducting polymer molecules. It is found that small organic molecules contain only a few carbon atoms, on the other hand, a polymer molecule consists of a long chain of repeating units which are connected to each other by sharing of neighbouring electrons, i.e., covalent bonds. Thermal vacuum evaporation unit is used for the fabrication of small molecules under high vacuum condition, while the conducting polymers can be dissolved in a solvent and then processed from that solution using well-known techniques, such as spin – coating techniques, inkjet printing [230] or screen printing [231]. These polymer molecules also possess some advantage such as they tend to become twisted together with each other in the solid state. This property makes them thermally more stable, because of which they tend to crystallize at temperatures below 100 °C [232, 233].

While the vacuum evaporation process is suitable for deposition of small molecules, this solution processing techniques are suitable for the deposition of polymer molecules. Compared to vacuum coating deposition set-up this solution process techniques have low production cost because it can be done at atmospheric pressure. This step saves the pumping time which is required for thermal evaporation process. Thus fabrication of polymer organic light emitting diode can be easily done with the help of these solutions processing set up. Further different kinds of OLED research have already been put into these both thermal evaporation and solution-processing techniques by the different research group to optimize the device performance.

## **1.10 Comparison of organic and inorganic light emitting diode**

It is found that there is a strong coupling force exist between the neighbouring atoms of the inorganic semiconductors. On the other hand, organic materials are mainly bonded by weaker Van Der Waal and London forces. From the literature report also it has been proved that carrier mobility in organic semiconducting materials is considerably lower than inorganic semiconducting materials. For example, the electron and hole mobilities in Si are found to be 1500 and 500  $\text{cm}^2/\text{V-s}$ , respectively, which are higher than the hole mobility in TPD ( $1.2 \times 10^{-3} \text{ cm}^2/\text{V-s}$ ) and electron mobility in Alq3 ( $1.4 \times 10^{-6} \text{ cm}^2/\text{V-s}$ ) [234, 235]. These reported values represents the mobilities of two selective organic materials only, the typical charge carrier mobilities among other organic light emitting materials are found to range from  $10^{-3}$  to  $10^{-5} \text{ cm}^2/\text{V-s}$  normally. The organic, materials which are used in OLED society mainly

classified into two groups first one is small molecules, and other is polymer chain molecules which are main difference with respect to their size and weight. Because of this physical difference, the fabrication of both OLEDs and PLEDs became dissimilar. Spin coating techniques are used for the deposition of Polymer materials which are initially formed an aqueous solution after combined with a solvent. This is opposite to the case of small molecules in which thermal vacuum evaporation or electron beam evaporation techniques are used for their deposition. It is found that spin coating process requires a less deposition setup typically compared with thermal evaporation because in this solution process vacuum equipment is not required. Most important features of thermal evaporation process are controlling accurate deposition rate and depositing a highly ultra-thin layer with a homogeneous pattern. However, it is found that both these categories of organic molecules have demonstrated success in OLED applications, although they have significant dissimilarities in fabrication processes.

On the other hand, there is a significant research area which is directly linked to this research area of the light emitting diode, an, i.e., an inorganic light emitting diode (ILED). This inorganic light emitting diode has an important background regarding the new research area of OLEDs which have an excellent class. In this research usually, non-coherent light sources are used which are capable of producing continuous and sufficient illumination from a simple semiconductor diode. This is commercially known as a chip. These chips are store in clear epoxy set-up. Usually, there are two semiconductor regions are present. Negative charges carrier mainly dominates one of this region. This region is known as an n-type region. Positive charges dominate the other region. Similarly, this is known as a p-type region. A current is generated across

the device due to the application of forwarding electrical biasing through the electrode. Here both the negative charge carrier and positive charge carrier are transported across the junction between the two semiconductors region and they combine with each other. This intermediate junction region between the two semiconductor chips where both the charge carriers are recombined is known as the charge depletion region.

In this charge recombination region, each combination of charges that take place is connected with a decrease in energy level. This energy level is given as the charge times the band-gap of the semiconductor chip. Due to the presence of this difference, energy (i.e., electromagnetic radiation) is released in the form of a photon whose energy is equal to the bandgap energy. These types of junction diode are normally based on a mixture of both Group III and Group V elements, such as gallium, arsenic, phosphorous, indium and aluminium. There are some advantages of inorganic light emitting diodes (ILEDs). These are given as brilliant, efficient, and stable emitters of light at different wavelengths. The band-gap of the specific materials used determines the colour of the emitting light from the device. However, however, there is one major drawback of these ILEDs is the limited used in point source applications because of their high production cost of such emitters. These devices are widely used in a broad range of applications for examples: indication lights, computer components, watches, medical devices and mobile application.

## **1.11 OLED Applications and Advantages**

Although considerable amount of success has been achieving by different type of display technology such as inorganic light emitting diode (ILED), liquid crystal

display (LCD) and plasma display technology, but the Organic Light Emitting Diode (OLED) has the more scope of bringing out a novel application for display technology in nearing future. One of the main drawbacks of ILEDs is high power consumption during their operation time, which also includes very poor resolution limit and absence of large matrix arrays. On the other hand, it is found that although LCD has a high contrast ratio, they require a separate lighting source for their operation, and also they possess a very slow response with respect to time. Similarly, another most interesting display is plasma technology, where a wide range of colour is present, and they also have a fast response time. However, the main drawback is their heavyweight due to the presence of thick glass panel, and also they have poor resolution. On the other hand, compared to above display devices organic light emitting diode needs only a low operating voltage. Also, OLED possesses a fast response time than the other display technology along with their high levels of brightness, contrast and output efficiency. They are also self-emitters and require less energy for their operation. One most prominent advantage of OLED is that they thinner than conventional LCD and also they do not require backlight system for their operation. These types of advantages increase the possibility of the formation of thinner and lighter display design. Similarly, some other advantages of OLEDs are sharper image formation tendency along with their wide viewing angles. One unique advantage of OLED is that the fabrication devices over flexible substrates. This provides an innovative potential application for bending to rollable display panels. Already different company and industries such as Universal Display Corporation and Vitex Systems have successfully produced OLED devices over flexible substrates [236].

It is observed that the performance of OLEDs on rigid substrates is comparable to that on flexible substrates, but their unique difference is observed regarding the stability of the device lifetime. Zhao et al. fabricated a polyester device [237]. However, the weaker adhesion force and larger surface fluctuation of flexible ITO films lead to the increasing possibility of device failure [238]. Therefore it can be concluded that flexible devices have more challenges compared with the rigid OLED devices. All the advantages of OLEDs are mentioned here in details as below:

1. OLEDs are self-luminous and thus do not require a backlight like LCD technology.
2. During operation, OLED consumes low power range ( i.e., 2-10 DC volts ).
3. Since there is no need of backlighting for OLED operation so they can have a thinner form and a more light-weighted.
4. The roll-to-roll manufacturing process, such as inkjet printing and screen printing, are possible for polymer OLEDs. That is why new applications like displays embedded in clothes or roll-up displays are possible.
5. There are abundant organic materials to produce a whole spectrum of visible light.
6. Lightweight, compact and thin devices: OLEDs are a thin layer in the nanometer range.
7. OLEDs can be easily fabricated on plastic substrates which are the doorway for flexible electronics.
8. OLEDs are brilliant at a low operating voltage, e.g., white OLEDs can be as bright as  $150,000 \text{ cd/m}^2$ .
9. OLED emission is Lambertian, and so the viewing angle is increased up to 160 degrees.

10. Response time is very fast: OLEDs electroluminescence decay time is less than one microsecond.

11. OLED display technology allows a broader range of operating temperature than traditional displays.

## **1.12 Useful impact on social life :**

1. Enormous energy saving for the society
2. Environmental impact associated with the reduction of the need for electricity (less air Pollution, depletion of non-renewable sources of energy, less greenhouse effect).
3. Creation of new lighting (fixture) industry.
4. New architectural designs enabled (lower ceilings, contour lighting, wall/ceiling panel lighting, space saving in aeroplanes, and tall buildings, etc.
5. Easy to read.
6. Flexibility in their designing pattern.
7. Images, graphics, and video.

## **1.13 Motivation of the present OLED research work**

We know that energy is an important factor, which critically concerns among the different countries across the globe. On the other hand from the survey of the available literature, it is found that currently lighting technology hold about 40% of total global electricity usage. Although Compact fluorescent light bulbs (CFLs) and light-emitting diodes (LEDs) have a great potential to the replacement of incandescent light bulbs, neither technology is suitable to fill the wide application across the globe, because of



their high fabrication costs and harmful effect on atmosphere (e.g., CFLs contain toxic mercury). On the other hand, it is interesting to note that organic light emitting diodes (OLEDs) composed of environmentally friendly carbon-based organic compounds. Nowadays the momentum of OLEDs has significantly increased in portable electronics, due to their better performance and lightweight in the form of thin film device. These OLED devices also have the potential application for high-efficiency lighting technology. The rapid development of organic electronics is a result of a large-scale, concerted effort from the science and engineering research community. One of the major areas of development has been in the field of interfacial engineering. The interface between the organic layer and the electrodes plays an important role in the organic light-emitting diode (OLED) performance because it determines the efficiency of the charge carrier injection from the electrode into the light emitting layer [239]. To improve the interface characteristics, the insertion of a buffer/injection layer between anode and hole transport layer (HTL) is one of the simple and effective methods to improve the device performances. These interfaces must allow charge carriers (either electrons or holes) to easily pass across the material boundary with minimal resistance [240]. Low-resistance in electrode/organic interfaces is not as easy to achieve. Interfacial engineering often involves tailoring the electron energy levels of the materials that are in contact with one another, to minimize or eliminate the charge-injection barrier [241]. From the survey of the available literature, it is found that an buffer layer or hole injection layer such as copper phthalocyanine (CuPc) [64] , CBP [100], poly (3,4-ethylene dioxythiophene) (PEDOT) [52], CuI [181], NaCl [114], NaF [69], TiO<sub>2</sub> [75] brings

an energy-band alignment between the HTL and the anode. It lowers the energy barrier, reduces the turn-on voltage and increases the OLEDs lifetime. Another inorganic insulating buffer layer such as LiF [83], Al<sub>2</sub>O<sub>3</sub> [37], SiO<sub>2</sub> [49], MoO<sub>3</sub> [107], etc. are also reported in the literature. Thus interface engineering a proper choice to enhance the performance of OLED for better display technology shortly. Some advantages of using buffer layer or hole injection layer over electrode surface in OLEDs are given below:

- ❖ When we placed the buffer layer between the anode and hole transport layer, then there is a high tendency for the positive charge carrier to inject into the organic layer from a high energy level compared with that without any buffer layer.
- ❖ There is also some hole trap may exist in the hole transport layer which should trap the holes before they come to light emitting region. However, when the holes are injected relatively from a higher energy level than the probability of their trapping is decreased.
- ❖ This interlayer also prevents the diffusion of the metallic ion into the organic layer and hence the active layer from the anode side. Therefore it reduces the probability of an electrical breakdown of the device.
- ❖ Also, the insertion of buffer layer decreases the contact resistance, provides better smoothness and uniform electric field distribution, which finally increases the charge injection into the organic layers along with better adhesion property than that of without any buffer layer. Therefore, it is easy to

understand that the device performance of bilayer anode based OLED is better than that of single electrode based OLED devices.

Therefore from the above discussion, it is clear that using of buffer layers or hole injection layer over electrode would be a better direction of OLED research to get the high performance of Organic Light Emitting Diode along with better-stabilised structure in the form of bilayer anode compared with single layer anode surface. However, in the maximum literature reports are found to be published on ITO coated electrode substrates. On the other hand although Fluorine-doped Tin Oxide (FTO) though being cost-effective than the ITO, it is not widely used to fabricate OLEDs because of its less transparency and conductivity than ITO. However, in the visible region, it is found that the optical transmission of FTO is independent of the fluorine doping [242]. Furthermore, FTO is less expensive to produce compared with ITO, and there is no indium present to possibly diffuse into the light emissive layer in the organic light emitting devices. Similarly, work function and the chemical composition of FTO is independent of the cleaning methods employed which implies that FTO is more stable to oxidation than ITO (also indium is more rare material than fluorine). Thus it is clear that FTO has greater stability, chemical inertness and high tolerance to physical abrasion compared to ITO. This indicates that FTO should also be a good agent for transparent conductive oxide compared with popularly known conventional ITO electrode. Also, most of the OLEDs reported to be successful are fabricated by Single Pump Down (SPD) method which needs sophisticated vacuum unit that involves large capital investment. On the other hand, compared to SPD, Multiple Pump Down

(MPD) method is considerably simple and permits volume production. Further MPD method facilitates the use of photolithography thereby yielding a better resolution of the patterns. Only a few reports about the OLEDs produced by MPD method are found in the literature. Therefore in this work, the OLEDs are fabricated by the MPD method, and their properties are studied from the various characteristics curves. The important OLED parameters like current density, luminance, and device efficiency are estimated from the fabricated devices. Also in our work, we considered only small organic molecule for OLED fabrication along with inorganic metal oxide which is deposited by conventional thermal vacuum evaporation. This is due to the reason that small molecular based OLEDs have a higher value of device efficiency compared to the Polymer based light emitting diode (PLEDs). Polymer light-emitting material is more sensitivity to oxidation and humidity compared with small molecule materials. Also, PLED materials have a short lifetime at high luminescence region. Therefore it can be concluded that higher performance can be obtained for small molecule-based OLEDs. On the other hand vacuum deposition of small molecule produce a more uniform organic thin film having better quality with control deposition. Thus it is possible to produce complex multi-layer OLED structures without damaging the previous layers. Therefore in our laboratory, we carry out our investigation on FTO electrode substrates for comparative study purposes by efficiency calculation. To complete our work we take the help of thickness variation method for both inorganic and organic material which are used as hole injection layer or buffer layer over electrode surface to making it bilayer anode for standard OLED

fabrication and characterization. Because thickness variation (under quantum tunnelling phenomenon) is the only method which can clearly provide the exact thickness of the buffer layer in which device performance is highly enhanced since too thin or too thick film layer does not help in increasing the device performance. In this work, we apply thickness variation on different buffer layer materials especially transition metal oxide ( like  $V_2O_5$ ,  $MoO_3$ , etc.) and small molecule based organic materials ( like Perylene, Rubrene, etc.). We consider these materials because of their nature of high work-function value along with their high optical transparency (greater than 80%) within the visible wavelength region. It is also possible to produce a thin film of these materials easily with the help of MPD procedure under relatively mild temperature and low operational voltage. Finally, we carry out the stability analysis for all the fabricated OLEDs samples with respect to time variations in our laboratory.

## **Chapter 2**

### **Methodology**

This chapter contains a brief introduction to the evaporation sources along with details discussion of the experimental procedure for the fabrication of the thin film by using different patternable shadow masks, thermal vacuum evaporation and spin coating process and hence the OLEDs. Here we also provide the details of the characterisation facilities and parameters of OLEDs. Finally, we discussed the common materials used for OLED fabrications.

#### **2.1 Introduction to evaporation sources**

For evaporation of material in a vacuum, a source is required that will supply heat of vaporization in addition to supporting the evaporant. To avoid contamination of the deposit, the support material itself must have negligible vapour and dissociation pressure at the operating temperature. The two types of support material used are refractory metals and oxides, nitrides, etc.

The metallic evaporation sources consist of either metal wire, or metal foils/wire sources are used for the evaporator, which sticks to the filament, by surface tension, on melting. Metal foils are usually designed into open boats of various shapes. Metals like tantalum, tungsten and molybdenum are commonly used for such evaporation sources. For flash-evaporation techniques various arrangement are available. One such

arrangement is called the dispenser. In this technique, a finely divided powder of the evaporator is made to fall slowly on a very hot tungsten strip, from a vibrating dispenser. On being in contact with the hot tungsten strip, the material evaporates immediately. Non-metallic crucible having high thermal conductivity are also used as evaporation sources. Wire coils heat these electrically non-conducting crucibles wound around them or by placing them on heated metal foil structure. For preparing a very pure film, one has to resort to the electron beam heating technique. In this process, a stream of electrons accelerated up to 10 KV, is focussed on the surface of the evaporator. This causes the evaporation of the material. Reactive evaporation is used to obtain oxide thin –films. In this method different metallic oxide and the organic materials are deposited on the substrates.

## **2.2 Method of preparation of thin film**

The thin film is defined as the uniform layer of materials whose thickness are ranging from nanometer ( $10^{-9}$ ) to several micrometres ( $10^{-6}$ ). Now a day's fabrication of thin film is considered as a fundamental step for many applications. For example thin metallic coating on the back side of a glass sheet to form a reflective interface and hard coatings on cutting tools and also for energy generation and storage devices. In addition to this thin film also play an important role in the improvement and study of materials with new and exclusive properties.

Physical vapour deposition method and spin coating techniques are the only effective method which is broadly used for the preparation of thin films. Physical methods include the deposition techniques, which depend on the evaporation or physical

ejection of the materials from a source. The most widely used methods such as vacuum evaporation and sputtering fall in this group. The physical methods are thought to produce films of good quality, purity, and resolution.

### **2.2.1 Vacuum evaporation**

This is a widely used method. In this method, the material is heated in vacuum to its gaseous state and then condensed on the substrate. Because of reduced pressure, the melting point of the material is sufficiently lowered, the tendency to form oxides is considerably reduced, the number of impurities in the deposited film is minimum and the evaporated material from the source to substrate follows the straight-line path, which ultimately aids in producing the good quality films. The temperature of the material may be raised either by resistive heating or electron bombardment heating. In the resistive heating process, the material is heated to its evaporation temperature either by slowly increasing the source temperature or by allowing the material to fall in a source maintained at its evaporation temperature. The later method requires the flash evaporation facilities for instant evaporation. In electron bombardment heating a stream of the electron is accelerated through high voltage and focused on to the evaporator surface. Sometimes oxygen or nitrogen gas is introduced into the chamber allowing reaction with the evaporant to obtain films of controlled composition. This technique is called the reactive evaporation. There are two processes of obtaining more than one deposition by vacuum evaporation namely (i) single pump down procedure (SPD) and (ii) multiple pump down procedure (MPD).



### **2.2.1.1 SPD Procedure**

In SPD method the step-by-step deposition of the different materials is done in one pump down of the vacuum system, i.e., without breaking the vacuum. The masks required to obtain different geometries of the films on the substrates are positioned at various suitable places inside the vacuum chamber. For deposition at various suitable places inside the vacuum chamber of different layers, the substrates are shifted from the mask to mask with the help of suitable levers operated from the outside. Again proper positioning and uncovering of the different evaporation sources containing the evaporator inside the chamber are also performed from the outside. The vacuum evaporation units having these facilities involve a large capital investment. Nevertheless, the procedure is advantageous because the ambient contamination between the deposited layers is avoided and it achieves high-quality devices showing good performance.

### **2.2.1.2 MPD procedure**

In this procedure, the vacuum is broken after each deposition step or in between some deposition steps. The main advantage of the MPD method is that devices could be produced in bulk. Since one deposition is usually done with a large mask or an array of identical masks covering the entire dimension of the chamber could be used, thus enhancing the volume of production. Moreover, such units require a far less capital investment. Another advantage of this method is that it permits the use of mechanically obtained shadow masks as well as a photolithographic process for the

deposition of the electrodes of the devices. The method of photolithography obtains the fine geometry required for the electrodes. High resolution is achieved by this method for which it is widely used in IC industry. Further, the computer-controlled electron beam technique permits the highest resolution of the pattern.

### **2.2.2 Spin coating**

Spin coating is a rapid and easiest method to produce thin and uniform organic films from organic solutions. This method is used to apply regular thin films to plane substrates. A spin-coater machine consists of a properly maintained turntable under vacuum conditions. Here a considerable amount of an organic solution is placed at the centre of the substrate, which is then rotated at high speed to broaden the organic solution by centrifugal force. As a result of rotation, the liquid solution starts spreading outwards to the boundary of the substrate and forms a relatively uniform layer of thin film. Thus spin coating is a process with the help of which it is possible to deposit a few organic solutions over the centre of a substrate and then to revolve the substrate at high angular speed. This speed is in general found to be in the order of 3000 rpm. In this process, the factor which is mainly responsible for spreading the liquid is centripetal acceleration. Because of which the boundary of the substrate leaves taking a thin film of liquid over the surface. However, the final film thickness and other properties of the thin film depend on the nature of the liquid. Some other factors are such as viscosity, drying rate, surface tension, etc. It also depends on the parameters which are chosen for the spin coating process. Different factors, for instance, final revolving speed, acceleration, and fume exhaust determine how the properties of spin-

coated thin films are distinct. Parameter variations during the spin coating process can result in severe changes in the coated film.

## **Description of the spin-coating process**

In general, a typical spin coating process consists of a two-step by the help of which the resin solution is deposited on top of the substrate surface. At first, a rapid spin step is used to thin the solution, and after that, a drying step is used to eliminate the extra solvents from the ensuing film. Usually, two common methods are popularly used. One of them is Static dispense, and the other method is known as Dynamic dispense. At first Static, dispense method involves a simple depositing a small amount of solution on or near the centre of the substrate. In this case, the required range is spread from 1 to 10 cc depending on the viscosity of the fluid and the size of the substrate on which film to be coated. To make full exposure of the substrate during the time of high-speed spin step, generally higher viscosity and larger substrates require for a larger puddle. On the other hand, Dynamic dispense is the process which involves the turning of the substrate at low speed. Commonly a speed of about 500 rpm is used during the process. This types of measures help to spread the solution over the substrate and which result in less waste of resin material because it is not required to deposit as much too wet the whole surface of the substrate. Therefore we can say that this method is a particularly advantageous method when either the fluid or the substrate itself has poor wetting abilities. Moreover, this approach also eliminates any possibility of voids formation that may otherwise form.

After completing the above step, it is necessary to accelerate to a comparatively high speed to make the fluid considerably thin and hence to near its final preferred thickness. For this step, the normal spin speeds range from 1500-6000 rpm. Also, depending on the properties of the solution as well as the substrate. To complete the process this step can take from 10 seconds to several minutes. The final thickness of the deposited film is the combined effect of spin speed and time which is selected for this step. Normally greater the revolving speeds and longer revolving times will generate thinner films. In the spin coating process, a large number of variables tend to terminate and average out. Therefore it is best for the operator to stand for sufficient time to occur. However, sometimes there is an additional drying step is used after completing the rapid spin step to drier the film without significantly thinning it. It is mainly beneficial for a thick film because longer drying times is essential to increase the physical stability of the film before treatment. In the absence of this drying step problems can occur during the time of treatment, for instance when the substrate is removing from the spin bowl there is a possibility of pouring off the side of the substrate. Here in this situation, a moderate revolving speed of about 25% of the high-speed spin will normally be enough to assist in drying the film without considerably altering the film thickness. A typical spin –coating set up is shown below:



Figure 2.2 (a): Spin coating set up for solution process film deposition

## **Spin speed**

One of the most important factors that affect the spin coating process is the spin speed. The spin speed expressed in term of revolution per minute (RPM). Moreover, this value of RPM of the substrate involves the degree of centrifugal force applied to the fluid resin in addition to the velocity and typical instability of the air immediately above it. In general, the final film thickness is determined by the high-speed spin step. If there is a slight variation of RPM (i.e.,  $\pm 30$ ) at this stage, then it will create resulting film thickness change of about 10%. Therefore it can be concluded that film thickness is mainly a balancing factor between the applied force to cut off the solution resin towards the boundary of the substrate and the drying rate which affects the viscosity of the resin. When the resin dries, the viscosity began increases until the radial force of the spin process can no longer significantly move the resin over the surface. It is found

that the film thickness will not considerably decrease with increasing spin period at this point.

### **Acceleration:**

The spin-coated film properties are also affected by the final spin speed of the acceleration of the substrate. It is necessary to control the rate of acceleration because the liquid begins to dry during the first part of the spin cycle. However, it is found that in a few processes; nearly 50% of the solvents in the liquid are lost toward evaporation in the first few seconds of the process. Also, acceleration acting a great role in the coating properties of the considerable patterned substrates. Generally, in most cases, it is found that the substrate will keep topographical features from preceding processes. Therefore it is essential to cover the resin over and through these functions homogeneously. Thus in one hand, it can say that the spin process, in general, provides an outward force to the liquid while in another hand acceleration is the factor that provides a twisting force to the liquid. Uniformity of film thickness over the substrates is suitably enhanced by the slower rate of the drying process. The fluids are constantly dry when they shift towards the substrates during the rotation of the spin coater. This observable fact is mainly responsible which leads to the thickness nonuniformities because of the fluid stickiness changes with distance from the centre of the substrates. Therefore it is possible to keep the stickiness remain more constant across the substrates by slowing the rate of the drying process. On the other hand, the film thickness is also found to be depending on the dampness condition. The change of film thickness will be large if only a few percents of moisture change takes place.

However, it is possible to preserve the stream of the solvent rotating bowl atmosphere by rotating movement. At the closing stages of the process when the cover is lifted to carry off the substrate, the entire drain is maintained to enclose and take away solvent clouds.

### **2.2.3 Sputtering**

In this method a thin uniform film of a material is deposited on a substrate by bombarding the material with highly energetic particles and then condensing the ejected atoms of the material onto the substrate to get the film. Ejection of atoms from the material takes place if they are bombarded with energetic particles. This is the main principle of sputtering. The process consists of forming positive ions of heavy, inert gas such as argon. These ions are accelerated to bombard the surface of the target material which is made the cathode of a DC glow discharge at about  $10^{-2}$  Torr. In sputtering the film formation occurs by an atom-by-atom process. As a consequence non-porous and high quality film could be easily obtained. One of the main advantages of this method is that no container contamination occurs. It is also possible to deposit alloy films which retain the composition of the parent target material. Materials having high melting point can be deposited and the use of R.F. techniques makes it possible to fabricate dielectric film. Thus a wide range of materials including carbides, oxides and nitrides can be deposited by this method.

## **2.3 Evaporation mask for vacuum deposition:**

### **2.3.1 Fabrication of evaporation masks**

For fabrication of OLEDs by vacuum deposition procedure the various selected materials were evaporated on the substrates in suitable geometrical patterns which were achieved by the use of shadow masks. For each desired deposition the substrates were placed on the masks near allow deposition of the film to the exposed substrate areas only. All the masks were processed mechanically. The different structures of the masks used in the present investigation are described below:

### **2.3.2 Evaporation mask for the buffer layer deposition**

An aluminium foil thickness 0.03 cm was cut to the circular shape of diameter 23.5 cm to suit our vacuum unit. A fine metal tip at first drew the desired geometrical patterns of the buffer layers, and then the openings were using cutting and filing tools. With sufficient precaution, the patterns were kept regular and mask plane and free of dents. The mask was then fixed over a rigid metal ring and thoroughly cleaned by the procedure as described in our section 2.4. The complete buffer layer or hole injection layer deposition mask is shown in the following the figure. Before every organic layer deposition in successive use, the mask was thoroughly cleaned.



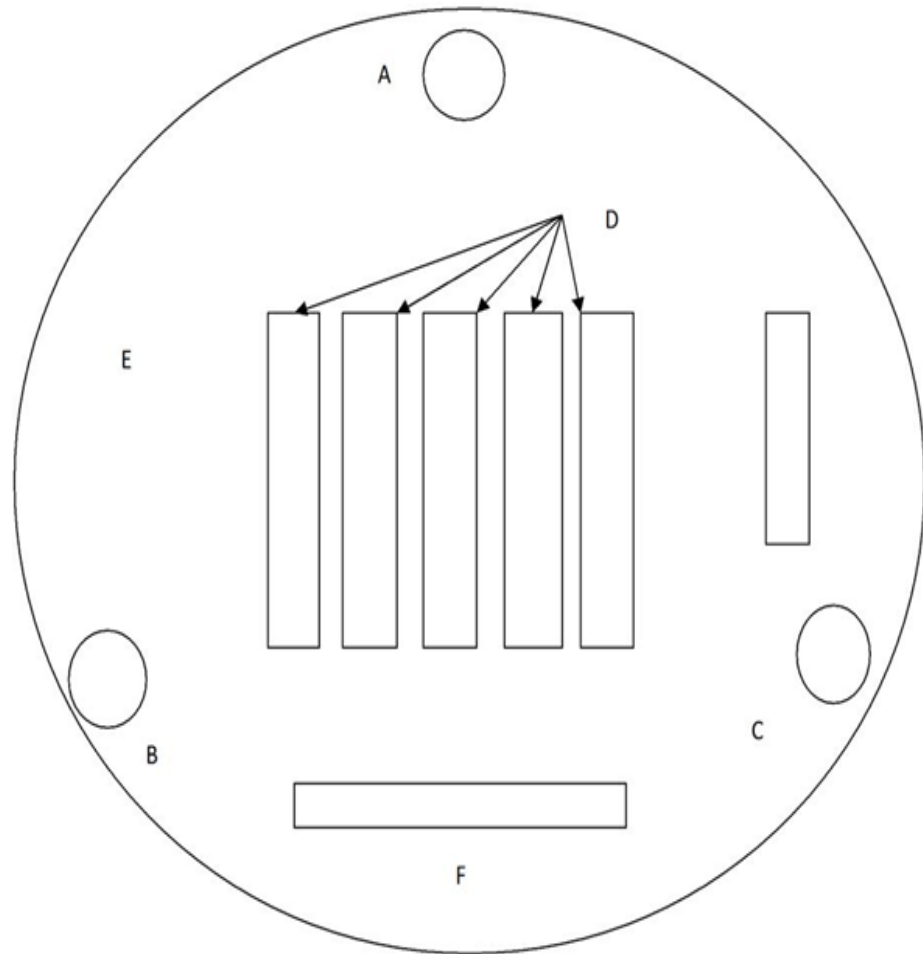


**Figure 2.3 (a): Mask for buffer layer deposition**

Where A, B and C represents the hole to fixed the mask in deposition holder.

D represents the geometrical pattern used for buffer layer deposition.

E represents the aluminum foil of the mask.

F openings for film for thickness measurement

### **2.3.3 Evaporation mask for organic layer deposition:**

The organic films were deposited over the entire buffer layer region over the electrode substrate in the OLED fabrication. In this case, also a 23.5 cm diameter and 0.03 cm thick aluminium foil was used, and the method described in above section obtained the desired patterns. The mask was then fixed on a rigid metal ring and cleaned thoroughly before use. Since the effective area of the organic layer is similar to buffer layer in OLED fabrication, so the mask is similar to that of buffer layer deposition as shown in figure 2.3(a).

### **2.3.4 Evaporation mask for cathode electrode deposition:**

Here again, the desired patterns were obtained on 23.5 cm diameter and 0.03 cm thick aluminium foil by the procedure described in section 2.3.2, fixed on a rigid metal ring and cleaned by the method to be described in section 2.4. Since the dimension of the cathode electrode is smaller than the organic layer deposition, utmost care was taken while obtaining the patterns. The dimension of cathode layer is smaller than the dimension of the organic layer to remove the possibility of shorting the two electrode terminal and hence the device failure probability. This mask is shown in the following the figure.

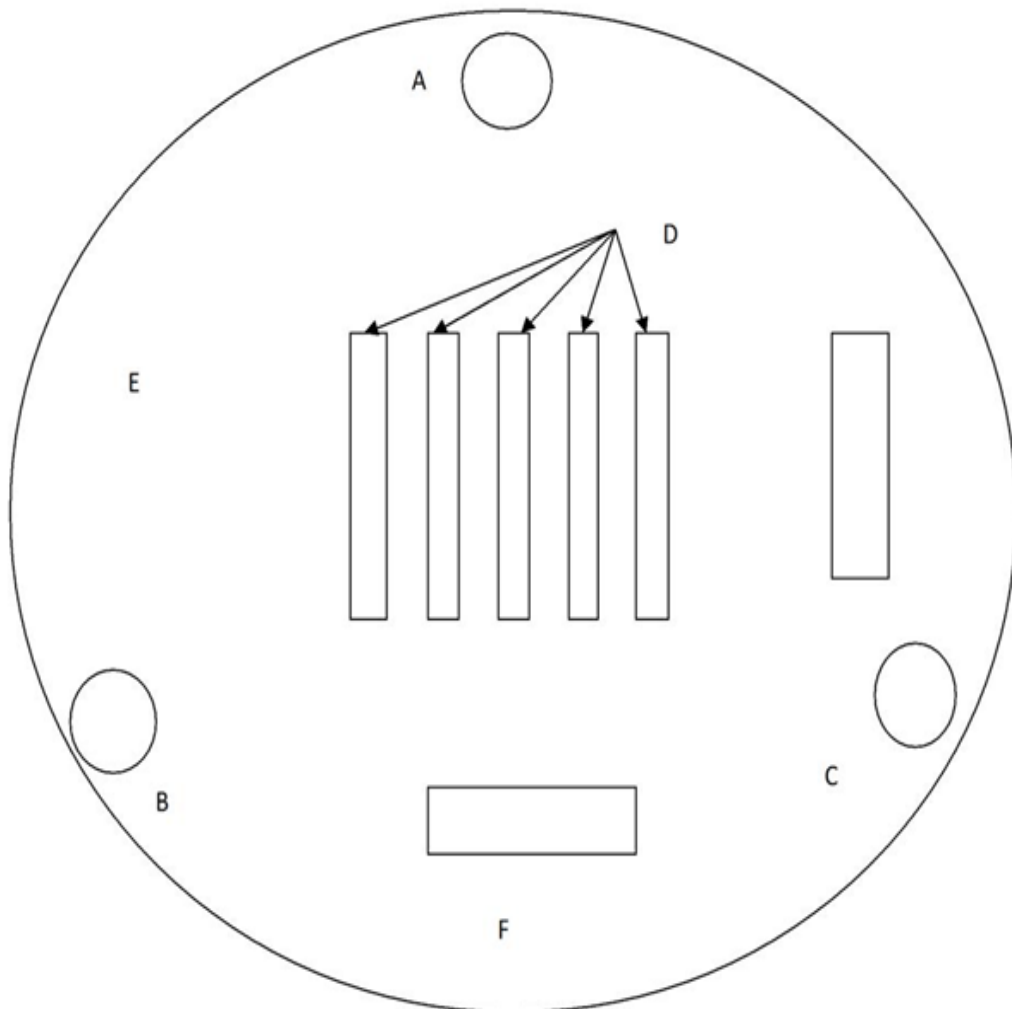


**Figure 2.3 (b): Mask for cathode layer deposition**

Where A, B and C represents the hole to fixed the mask in deposition holder.

D represents the geometrical pattern used for cathode layer deposition.

E represents the aluminum foil of the mask.

F openings for film for thickness measurement

While fabricating the above masks, a great deal of precaution was taken to keep the masks plane and dent free.

## **2.4 Cleaning of the evaporation masks**

The evaporation masks should be free from dust particles, scattered pieces of rubbing from the cutting process, fibres and any other type of contaminants to avoid possible film contamination. For cleaning the masks were treated with “Teepol” (a green-coloured detergent) and washed in running tap water. These were then washed with acetone and dried in an electric oven. The masks were finally cleaned with acetone and dried by blowing air hot air. During the investigation, the cleaning of masks was a routine procedure and was undertaken before fabrication of a batch of OLEDs.

## **2.5 Fabrication and Characterization of OLED**

In our work, the different layers of the organic and inorganic materials layers of the OLED structures were prepared by thermal vacuum deposition technique. Therefore, the description of thermal evaporation system and characterization techniques will be discussed in this section.

### **2.5.1 Thermal Evaporator System: Model-VT-2015**

The vacuum coating unit, Model-VT-2015 was used for the fabrication of OLEDs. The whole unit consists of three main parts, i.e., vacuum chamber, the pumping system, and the electrical connections. The vacuum chamber is a corning bell jar

of 13-inch diameter placed on the metal base plate. The chamber is evacuated using an oil diffusion pump backed by a double stage gas ballast rotary pump having a suction capacity of 200litre/minute. The pump alone could produce a rough vacuum of  $2 \times 10^{-3}$  Torr. The ultimate vacuum obtainable in the unit is  $10 \times 10^{-6}$  torr, which may be measured by using penning ionization gauge attached to the unit. The rough vacuum of the chamber and the diffusion backing line is measured with the help of Pirani gauge. There are seven well insulated and three earthed electrodes fitted to the base of the chamber. Each electrode was coupled to the earthed electrode electrically connected to the base. Out of this two electrode were used for heating the evaporation source of the remaining electrode, two are for either the radiant heater or the substrates heater and one for HT discharge cleaning. In addition to these, the base plate has provisions for fitting a movable shutter. The masks can be positioned with the help of stand fitted on the base plate. The transformer and the corresponding electrical circuits for passing current at required voltages through the various electrodes and gauges are contained in the compact unit. All the switches, control knobs and meters for performing different operations are fitted on the front panel of the instrument. The following figure shows the set up of the vacuum evaporation unit.



Figure 2.5 (a): Vacuum coating set up of OLED fabrication

### **2.5.2 Cleaning of the vacuum unit and filaments**

Before every deposition, the corning bell jar cleaned by carbon tetrachloride and then finally by acetone. The metal electrodes, base plate, a substrate holder, etc were cleaned using acetone. After cleaning all the components were dried by using an air gun. The cleaning of the vacuum chamber was a routine work performed before every evaporation step irrespective of evaporates. Moreover, for ensuring faultless performances of the unit, normal checking of the vacuum points and rotary pump oil level was periodically undertaken.

All new filaments and boats were flash-cleaned in vacuum by passing a heavy current momentarily. Flash-cleaning of filaments and boats are essentially for removal of contaminants adhering to them.

### **2.5.3 Substrates preparation**

In our work we used commercially available, FTO coated glass with sheet resistance less than  $25 \Omega/\text{square}$  as substrates for all of the fabrication of the device in this work. In our work, this electrode substrate was used as an anode for OLED devices. Buffer layer or hole injection layer was used over FTO coated glass to carry out our whole research work to make bilayer anode. For single anode OLED devices, all the successive layers were deposited one by one up to the cathode layer by vacuum deposition method. While in bilayer anode we initially deposited a buffer layer over metallic electrode surface and after that we deposited the successive layer as mentioned above. Here all substrates were properly cleaned with acetone, isopropanol and deionized water for 15 minutes and then dried by an air gun before fabrication of OLED. This cleaning step is used to remove the surface contaminants and to provide a clean FTO surface to enhance the adhesion of another layer onto its substrates. Therefore initially all substrates were cleaned for the better formation of another layer over it. Also before the cleaning procedure, these substrates were patterned by using the etching process which can be done with the help of zinc dust and dilute HCl. This step is necessary for the proper designing of OLED devices over these substrates.

### **2.5.4 Heating of the substrates**

A flat circular heater of diameter 19cm was made winding nichrome wire on mica sheet. The two surfaces of the heater were then covered with mica sheets of diameter 20cm, to prevent short-circuits. The heater was placed near the substrates with the help of four metallic pins, and the temperature was controlled by regulating the current

using a dimmerstat. The substrates temperature was noted by a chromel-alumel thermocouple, the tip of which just touched the glass substrate. The two mica sheets covering the heater coil were replaced with fresh sheets from time to time because during depositions evaporants were found to condense over them. Also, care was taken to keep the heater free from dust particle and another type of contaminants.

### **2.5.5 Evaporation of the buffer layer over electrode surface**

Here  $V_2O_5$ ,  $MoO_3$ ,  $NiO$ ,  $WO_3$ , Pentacene, Perylene, Rubrene, and PEDOT: PSS were used as the buffer layer or hole injection layer. We consider these materials as buffer layer because of their P-type semiconducting nature along with high work-function value. Because of which they formed better energy level alignment concerning the organic hole transport layer. These materials also provide higher optical transmittance within the visible wavelength region. Before evaporation of organic or inorganic buffer or hole injection layer, it was take utmost care to clean the vacuum chamber to make it free from any contamination and during that period the substrates was kept covered inside the dry dessicator. Each material was evaporated at constant source temperature by passing a constant current through the evaporation source utilized except the polymer layer. For this purpose we used spin coating method.

### **2.5.6 Evaporation of organic layers**

After the evaporation of buffer layer over the electrode surface, we deposited the organic hole transport layer (HTL) and the light emitting layer (EML) with the help of same type mask designing as mention above. As a result EML layer completely



overlap the HTL layer. Here we used cone filament for HTL layer deposition, and molybdenum boats were used for EML layer deposition. A similar procedure was also repeated for electron transport layer deposition over EML layer by using proper shadow masking.

### **2.5.7 Evaporation of the cathode electrode**

In our work, we used Aluminium (Al) as cathode layer to complete the OLED fabrication, for carrying out this investigation. To obtain the films, Al was evaporated from tungsten-helix filaments. The required quantity of Al was introduced inside the helical filament which was kept inside the vacuum chamber. Al was observed for complete melting, and then it was allowed exposure of the substrates through the mask to the evaporant.

### **2.5.8 The OLEDs**

All the OLEDs studied in the present investigation were fabricated as shown in figure 2.5 (b). A photograph of OLEDs samples is shown in figure 2.5(c). In our work hole injection layer or buffer layer of desired thickness were first deposited on the thoroughly cleaned FTO substrates using proper shadow masking pattern. After evaporation of the buffer layer the vacuum was broken, the unit cleaned and arrangement for next evaporation of organic hole transport layer (HTL). The hole transport film of desired thickness was then deposited through the mask covering the whole buffer layer region. Again the vacuum was broken, the unit cleaned and arrangement for next EML film evaporation made. The EML film of desired thickness was deposited over the semiconductor layer. A similar procedure was also repeated for

electron transport layer (ETL) and cathode layer deposition. During the time intervals, between the breaking of the vacuum after one deposition and making arrangements for the next deposition the substrates were kept in thoroughly cleaned Petri dishes and then placed in clean desiccators charged with  $\text{CaCl}_2$ . The time intervals were made as small as possible. It is necessary to keep the substrates in dry air to prevent the deposited films from absorbing atmospheric moisture and thereby prevent the formation of oxide.

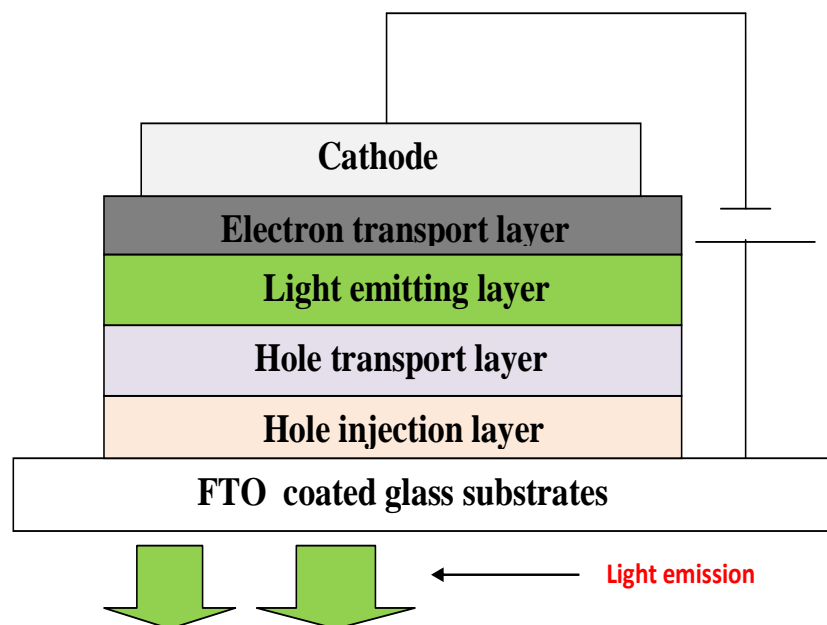


Figure 2.5 (b): Fabricated structure of OLED over FTO electrode

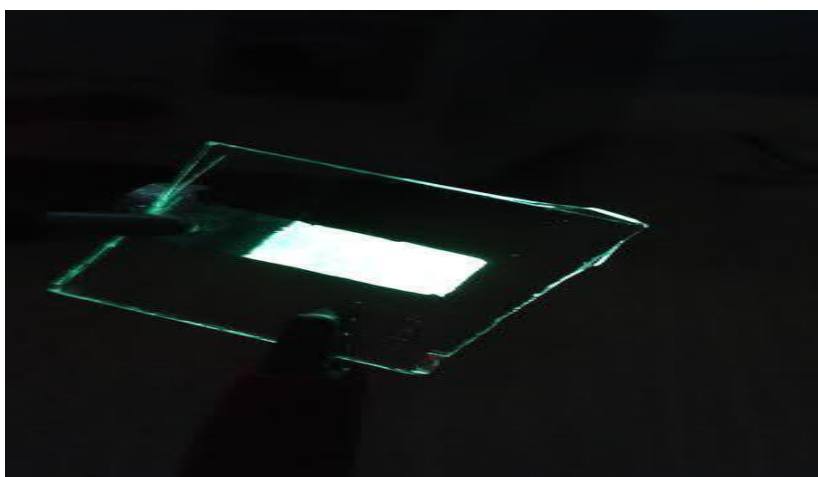


Figure 2.5 (c): A photograph of OLED samples

### **2.5.9 Materials used for OLED fabrication**

For the fabrication of Organic Light Emitting Diode we used two electrodes one is cathode and the other is anode. Between these two electrode successive layers are deposited from anode side to the the topmost layer of cathode for complete device fabrication. As mentioned above in our work device configuration is anode/buffer layer/hole transport layer/emitting layer/ electron transport layer/ cathode. For the purpose of making the bilayer anode we use different buffer materials including both organic and inorganic at the interface region of anode-hole transporting region. A brief introduction of all the materials used in this study is given below. Here we purchased all the materials from Sigma-Aldrich company.

## **(I) Introduction to cathode electrode**

Generally low work function metals are used as a cathode electrode for OLED fabrication. Different types of low work function materials such as lithium, calcium and magnesium are used mainly due to their lower value of work function. Because during the OLED operation, electron can travel from low work function side to the lowest unoccupied molecular orbital of (LUMO) of the organic semiconductor. But there is a main disadvantage of this low work function cathode is that they are highly reactive especially in ambient atmosphere. Therefore only more stable materials such as aluminum (Al) and gold (Au) are preferable as cathodes. But for low cost purposes here we used Al as cathode electrode.

## **(II) Introduction to anode electrode**

One of the most widely used anode material in OLED society is found to be transparent conductive oxide (TCO). Transparent conductive oxides are widely used because of their high work function (4.1-5.1 eV), high transparency to visible light, good electrical conductivity, excellent adhesion to the substrates and easy patterning ability. Here we used

Flourine doped tin oxide (FTO) coated glass sheets as anode substrates as mentioned in above sectioned ( sectioned no 1.13) with surface resistance less than 25 ohm/square (rectangular in size). This FTO sheet has better transparency within the visible wavelength region (85%-90%).

### (III) Introduction to TPD

The full form of TPD is (N,N'-Bis(3-methylphenyl)-N,N'-diphenylbenzidine). It is an organic material which is widely used as hole transport materials in organic electronic devices. TPD is also used as a blue-violet light emitting material or host material on the phosphorescence organic light emitting diodes for its wide energy band is about 3.2 eV with highest occupied molecular orbital (HOMO) and lowest unoccupied molecular orbital (LUMO) 5.5 eV and 2.3 eV respectively . Molecular mass of TPD is given as 516.67 g/mol with chemical formula  $C_{38}H_{32}N_2$ . The boiling point of TPD is given as  $680.1 \pm 55.0$  °C at 760 mmHg, melting point of TPD is 175-177 °C. Chemical structure is given below:

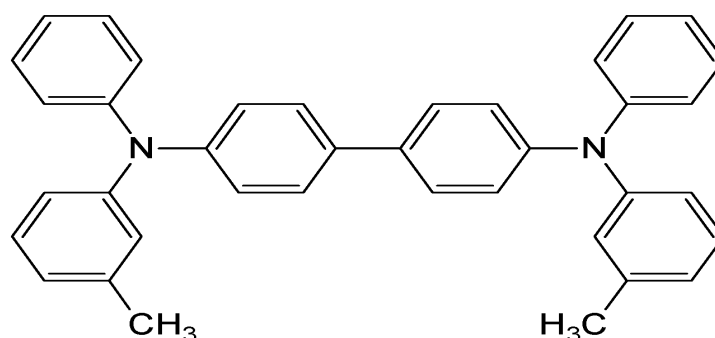


Figure 2.5.9 (a): Chemical structure of TPD

### (IV) Introduction to Alq3

The full form of Alq3 is Tris (8-hydroxyquinolato) whose chemical formula is  $Al(C_9H_6NO)_3$ . It is a coordination complex wherein aluminium is bonded in

a bidentate manner to the conjugate base of three 8-hydroxyquinoline ligands. Tris (8-hydroxyquinoline)aluminum(III) is widely used in organic light-emitting diodes (OLEDs) as an electron-transport material (ETM) and emitting layer material (ELM) due to its high thermal stability, high quantum yield of fluorescence and high electron-transport ability. Alq<sub>3</sub> as the electron-transport and emitting layer material was the first efficient low molecular weight OLED reported by Tang in 1987 [4]. Since then, metaloquinolates have become the focus of new electroluminescent materials research, with Alq<sub>3</sub> being the most studied. Molecular mass of greenish Alq<sub>3</sub> is given as 459.43 g/mol. Melting point is greater than 300 degree celcius. The highest occupied molecular orbital (HOMO) and the lowest unoccupied molecular orbital (LUMO) value of Alq<sub>3</sub> are 5.7 eV and 3.0 eV respectively. Chemical structure of Alq<sub>3</sub> is given below:

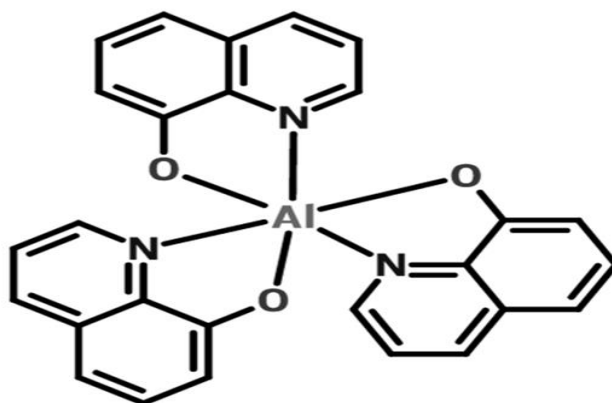


Figure 2.5.9 (b) : Chemical structure of Alq<sub>3</sub>

## (V) Introduction to Perylene

Perylene is a polycyclic aromatic hydrocarbon with the chemical formula  $C_{20}H_{12}$  having high optical transparency within the visible region. The perylene molecule consists of two naphthalene molecules connected by a carbon-carbon bond at the 1 and 8 positions on both molecules. All of the carbon atoms in perylene are  $sp^2$  hybridized. It is widely used as hole injection or hole transporting materials in organic devices. Melting point of Perylene is range from 276-279 °C. Molecular mass of Perylene is 252.316 g/mol. The highest occupied molecular orbital (HOMO) and the lowest unoccupied molecular orbital (LUMO) value of Perylene are 5.3 eV and 2.2 eV respectively. Chemical structure of Perylene is given below:

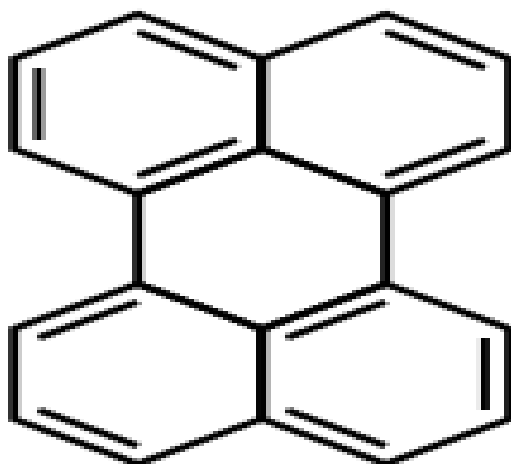


Figure 2.5.9 (c) : Chemical structure of Perylene

## (VI) Introduction to Pentacene

Pentacene is a polycyclic aromatic hydrocarbon consisting of five linearly-fused benzene rings. This highly conjugated compound is an organic semiconductor. Pentacene has drawn enormous interest in recent years as a result of both its crystals and thin film behaving as a P-type organic semiconductor which can be utilized to manufacture electronic devices in display technology such as OLED and OTFT. It is also used as a photo luminescent material. The pentacene films show good charge transport properties. The hydrogen atoms which surround the carbon backbone are less electronegative than the carbon backbone itself and lend some electron density to the delocalized pi-electron cloud. Molecular mass of pentacene is 278.354 g/mol. Melting point is found to be greater than 300 °C. The highest occupied molecular orbital (HOMO) and the lowest unoccupied molecular orbital (LUMO) value of Pentacene are 5.0eV and 3.0 eV respectively. Chemical structure of Pentacene is given below:

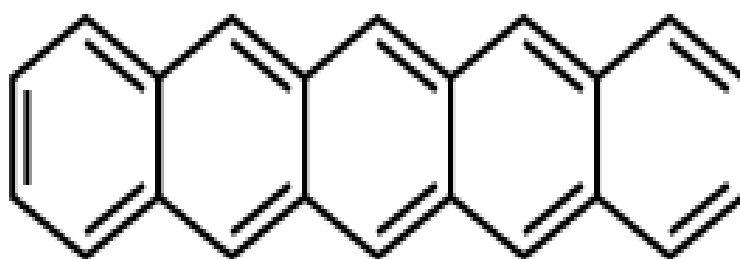


Figure 2.5.9 (d): Chemical structure of Pentacene



## (VII) Introduction to Rubrene

Rubrene (5,6,11,12-tetraphenyltetracene) is a red colored polycyclic aromatic hydrocarbon which have optical transparency within the visible region ( greater than 80%). As an organic semiconductor they are mainly used as hole injection layer in different applications. The major application of rubrene is in organic light-emitting diodes (OLEDs) and organic field-effect transistors, which are the core elements of flexible displays. Its molar mass 532.7 g/mol and melting point found to be 315 °C. It is also used in bioelectronics, biosensing and bioimaging, light emitting dopants, Fluorescent Dyes and Materials Science. The highest occupied molecular orbital (HOMO) and the lowest unoccupied molecular orbital (LUMO) value of are 5.4 eV and 3.2 eV respectively. Chemical structure of Rubrene is given below:

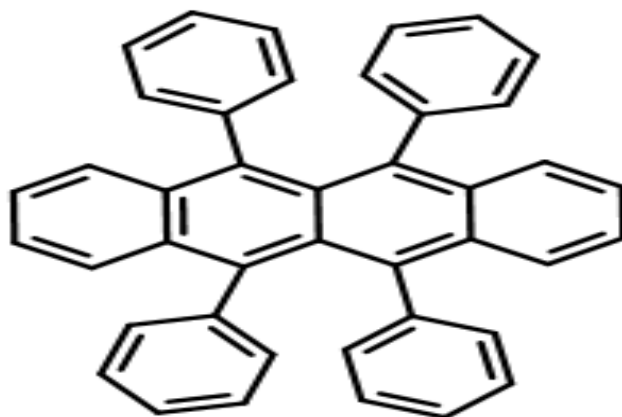


Figure 2.5.9 (e): Chemical structure of Rubrene

## (VIII) Introduction to PEDOT: PSS

The full form of PEDOT: PSS is known as poly (3,4-ethylenedioxythiophene) polystyrene sulfonate. One component in this mixture is made up of sodium polystyrene sulfonate which is a sulfonated polystyrene. The other component poly (3,4-ethylenedioxythiophene) or PEDOT is a conjugated polymer and carries positive charges. It is used as a transparent, conductive polymer with high ductility in different applications because of their transmittance property. It is also found that when organic solvent are added, then their conductivity increases by many orders of magnitude [243, 244]. Therefore they are widely used as a transparent electrode or electrode buffer layer such as touch\_screens, organic light-emitting diodes, flexible organic solar cells and electronic paper to replace the traditionally used conductive oxide. The highest occupied molecular orbital (HOMO) and the lowest unoccupied molecular orbital (LUMO) value of PEDOT: PSS are 5.2 eV and 2.4 eV respectively whose molecular mass is depend upon the composition weight ratio. Chemical structure of PEDOT: PSS is given below:

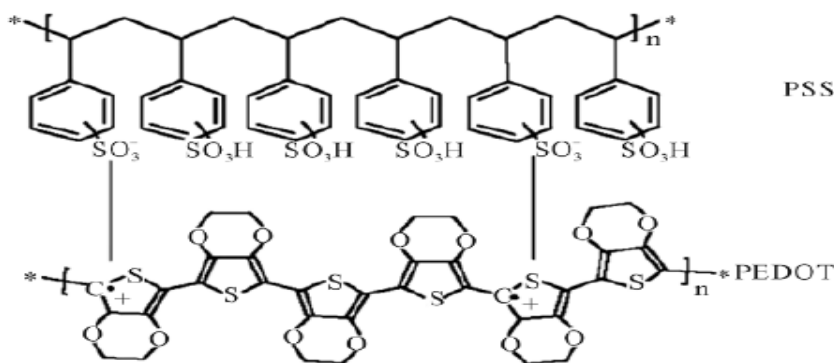


Figure 2.5.9 (f): Chemical structure of PEDOT: PSS

## **(IX) Introduction to Lithium fluoride ( LiF)**

Lithium fluoride is a white powder inorganic compound with the chemical formula LiF. Its structure is analogous to that of sodium chloride, but it is much less soluble in water. It acts as an electron transporting material between the light emitting layer and cathode electrode because lithium fluoride works as a coupling layer to enhance electron injection. Without LiF electron injection layer it is difficult for the electron to be injected from Al cathode to the Alq<sub>3</sub> layer, as the dissociation of the alkali halide into the organic layer leads to the enhancement of electron injection. Molecular mass of LiF is 25.939 g/mol. Melting point and boiling are given as 845 °C and 1676 °C respectively.

## **(X) Introduction to Vanadium pentoxide ( V<sub>2</sub>O<sub>5</sub>)**

Vanadium Pentoxide is a yellow crystalline powder and slightly soluble in water. It is a transition metal oxide whose molecular mass is 181.88 g/mol. This is widely used as a P-type semiconducting material specially as a hole injection layer for thin film device fabrication in optoelectronics due to its high optical transmittance property within the visible wavelength region. Melting point and boiling point are 690 °C and 1750 °C respectively. The highest occupied molecular orbital (HOMO) and the lowest unoccupied molecular orbital (LUMO) value of V<sub>2</sub>O<sub>5</sub> are 4.7 eV and 2.2 eV respectively. Bonding structure of Vanadium Pentoxide is given below:

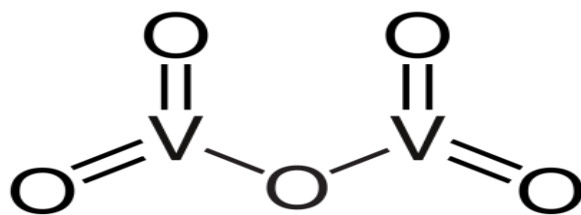


Figure 2.5.9 (g): Bonding structure of vanadium pentoxide

## **( XI) Introduction to Molybdenum trioxide**

Molybdenum trioxide is a transition metal oxide which acts as a hole injection layer in organic devices. This P-type inorganic semiconductor provide higher optical transparency ( greater than 80% ) within the visible wavelength region. The highest occupied molecular orbital (HOMO) and the lowest unoccupied molecular orbital (LUMO) value of MoO<sub>3</sub> are 5.3eV and 2.3 eV respectively. Molecular mass is 143.94 g/mol This material offer many advantages such as less contamination, easy thermal deposition and energy level matching with organic molecules. This was used for the first time by Tokito et al. in 1996 [ 245] between hole transport layer and transparent conductive oxide. In their work they reported reduced operation voltage with high device efficiency. Since then it is widely used in organic electronics research [246, 247]. As a hole injection layer it is also found to reported in both top-emitting OLEDs/PLEDs and invertible PLEDs but all are ITO based devices. In our work we focus this material over non conventional FTO surface. Bonding structure of this oxide material is given below:

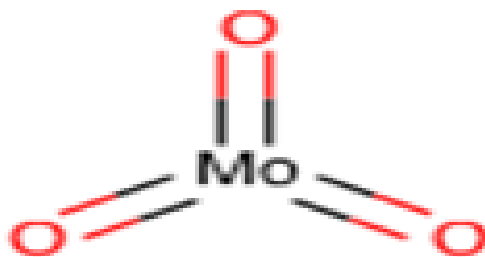


Figure 2.5.9 (h): Bonding structure of molybdenum trioxide

## (XII) Introduction to Tungsten trioxide ( $\text{WO}_3$ )

Tungsten trioxide is a chemical compound containing oxygen and the transition metal tungsten which is insoluble in water. It is a P-type inorganic semiconducting material whose appearance is light yellow. This acts as a hole injection layer in optoelectronics devices because of high work function and high transparency within the wavelength region from 390nm to 700nm [248]. The highest occupied molecular orbital (HOMO) and the lowest unoccupied molecular orbital (LUMO) value of  $\text{MoO}_3$  are 6.4eV and 4.1 eV respectively. Melting point and boiling are given as 1,473 °C and 1700 °C respectively. Molecular mass is 231.84 g/mol. Bonding structure is given below:



Figure 2.5.9 (i): Bonding structure of tungsten oxide

### **(XIII) Introduction to Nickel oxide ( NiO)**

Nickel(II) oxide is the chemical compound with the formula NiO which is soluble in Potassium Cyanide ( KCN). It is a transition metal oxide whose molecular mass is 74.6928 g/mol. It is a P-type inorganic semiconducting material whose appearance is light green. This is mainly acts as a hole injection layer at the electrode/semiconductor interface region in optoelectronics devices because of high work function and high optical transparency within the wavelength region from 390nm to 700nm . The highest occupied molecular orbital (HOMO) and the lowest unoccupied molecular orbital (LUMO) value of NiO are 5.0 eV and 3.0 eV respectively. Melting point is given as 1,950 °C .

## **2.6 Important parameters of OLED**

Different parameters have been used to measure the quality of an OLED. The most important parameters we used to measure the OLED quality in this work are discussed below:

### **2.6.1 Current density-voltage (J-V) measurement**

Current density (J) and voltage (V) measurement are primarily necessary for OLED characterization. Because by studying the J-V characteristics graph it is possible to know whether the device is working properly or not, which also provide the quality of the device. During the operation of the OLED device, current starts flowing across the device and at the same time corresponding current, or voltage response is recorded by digitally controlled source-meter-unit (SMU). This current density is defined as the

flow of current per unit area of the device. However current density can also be defined as a vector whose magnitude is the current per cross-sectional area. It is measured in the unit of milli-ampere per square centimetre ( $\text{mA}/\text{cm}^2$ ). It is possible to estimate the conductivity of the overall materials constituting the OLED and the ability of carrier injection by calculating the slope of J-V characteristics.

### **2.6.2 Luminance-voltage (L-V) measurement**

Similar to the J-V measurements, Luminance (L) and voltage (V) measurements are also necessary for the OLED characterization to know whether the device is working properly or not. During the operation of OLED, the opposite charge carrier is transported from both sides of the electrode. When these charge particles are reached the light emitting layer, they feeling a columbic attraction because of which they come into close to each other. This is known as electron-hole pair recombination and is more popularly referred to as an exciton. When an exciton is formed, they can radiatively recombine to emit light. Luminance is defined as the amount of light generated in the OLED device due to the application of electric biase at the rate of per unit solid angle. It is expressed regarding  $\text{cd}/\text{m}^2$ .

### **2.6.3 Current efficiency**

The radiated power of light-emitting diodes is reported as the luminance in  $\text{cd}/\text{m}^2$ , which describes the amount of light that is emitted from an area of  $1\text{m}^2$  and falls into a given Solid angle. The current efficiency is defined as the ratio of the light output (L) per unit the area to the current density (J) and is obtained from the slope of the linear characteristics of luminance vs current of the device, which is given as follows:

$$\gamma = L/J \dots\dots\dots (1)$$

### 2.6.4 Power efficiency

The power efficiency is defined as the ratio of the output power to the input power of the device. It is measured in the unit of lm/W. Here lumen is a measure of the total quantity of light emitted by a source. It is found that the power efficiency ( $\eta$ ) and current efficiency ( $\gamma$ ) are depending on each other, and their relation can be given by following equation of Lambertian emission pattern [13].

$$\eta = \pi \frac{L}{VJ} = \pi \frac{1}{V} \left( \frac{L}{J} \right) = \pi \gamma \frac{1}{V} \dots\dots\dots (2)$$

Where L is the luminance measured from the light emitting surface and V is the applied voltage. The value of current efficiency depends on the optical coupling and the internal quantum efficiencies. From this equation, it is clear that the term power efficiency is inversely proportional to V.

### 2.6.5 The maximum luminance

The maximum luminance is expressed regarding cd/m<sup>2</sup>. This parameter describes the highest amount of light emitted from a surface per unit area in a given forward direction over a range of operational voltage or current density. This parameter is important for an OLED device, to know the device applications because different device applications require different luminance value. For example in case of solid-state lighting requires a sufficient amount of luminance values to illuminate given



surroundings. On the other hand, a white fluorescent tube can realize a luminance of 10,000 cd/m<sup>2</sup> and most computer screens usually not brighter than 1,000 cd/m<sup>2</sup>.

### **2.6.6 Turn-On Voltage**

The term “turn-on voltage” in OLEDs is used to estimate the performance of OLEDs. For the organic light emitting diodes, this parameter (i.e., turn-on voltage) is normally defined as the voltage at which the luminescence device starts appearing on the device. This luminance value can easily be detected by the human eye. This turn-on voltage of the organic light emitting diode can be obtained from the luminance-voltage (L-V) graph of the device. Usually, a lower value of turn-on voltage is required for obtaining higher current density under lower electrical biasing. This is because luminous power efficiency of OLED device tends to become lower for a given current and luminance at higher voltages.

## **2.7 OLED characterization facility**

Characterisation facility of OLED is divided into two categories, i.e., device characterization and surface characterization facility. In this section, all such characterization facility is discussed.

### **2.7.1 Device characterization**

#### **(a) Source-meter set up**

After fabrication of OLED devices, all of them were characterized by measuring their current density-voltage and luminance-voltage characteristics graph. In this study, we used a computer controlled source-meter set up to measure or record all these

characteristics graph. This SMU instrument offers four-quadrant precision voltage and current source couple with measurement. This source-meter can simultaneously act as a source and measure current from 10 fA (1 femto ampere =  $1 \times 10^{-15}$  A) to 10 A pulse and voltage from 100nV to 200V, for 1000W pulse and 100W DC. Similarly, luminance, current efficiency, and power efficiency were also measured with the help of OLED testing set-up measurement as mentioned above set-up with connecting digital luminance meter unit.

### **(b) Thickness measurement unit**

In our work thickness of the thin films are measured by thickness monitor (**Model DTM-10**) and further confirmed by the profiler set up. The profiler poses an innovative design that enables accuracy limit of about 4Å. This profiler enables to perform at the critical nanometer-level and film thickness measurements which are widely utilized in the microelectronics, semiconductor, solar, high-brightness LED, medical, scientific and materials science. It is a widely accepted profiler for measuring thin film thickness and surface roughness measurements. It provides the ability to quickly and easily set up and run automated multi-site measurement routines to verify the precise thickness of thin films down to the nanometer scale. In this profiler system, there is a stylus exchange tool that allows to safely exchanging one stylus for another without damaging the delicate tip. This profiler system contains all of the mechanical, electrical, and optical components for sample positioning, sample viewing, and scanning/measurement. Also, its powerful single-arch bridge design reduces sensitivity to adverse environmental conditions.

## 2.7.2 Surface characterization

### (a) UV-Visible double beam spectrophotometer

UV-double beam spectrophotometer unit is used for the measurement of optical transmittance of the bilayer anode surface. This instrument incorporates a 320×320 dot matrix LCD for photometric results, easy operation and the wavelength range of 190nm to 1100nm. Here the lamp is focused on the entrance slit of the monochromator where the collimating directs the beam onto the grating. The grating disperses the light beam to produce the spectrum, a portion of which is focused on the slit of the monochromator by a collimating mirror. From here the beam is passed to a sample compartment through one of the filters, which helps to eliminate unwanted second order radiation from the diffraction grating. Upon leaving the sample compartment, the beam is passed to the silicon photodiode detector and causes the detector to produce an electrical signal that is displayed on the digital display. Block diagram of the set up is shown below:

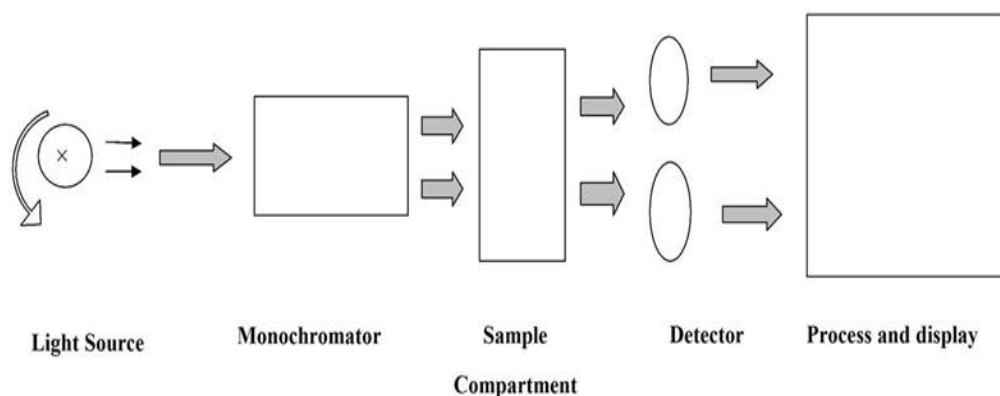


Figure 2.7 ( a): Block diagram of the UV-visible double beam spectrophotometer

### **( b) Four probe resistance measurement method:**

This four probe technology is used to measure the average sheet resistance of a thin film by passing the current through the outside two points of the probe along with the corresponding voltage measuring value across the two points of the probe which is lies inside region of the probe. In this resistance measurement system, the distance between the two probe points is constant, and thickness of the measuring layer is usually less than 40% of the spacing between two probe points.

On the other hand thickness of the measuring thin layer film and the corresponding surface resistivity value at particular, current and voltage is given by the following relation

$$R_s = \frac{\text{Resistivity of the film}}{\text{Thickness of the thin film}}$$

Therefore from the above equation, it is easy to understand that the surface resistance of a thin film is directly proportional to the resistivity and inversely proportional to the corresponding film thickness, i.e., surface resistance decreases with the increasing the thickness of the thin film. Thus it is possible to calculate the resistivity value for a thin film layer at particular thickness if the surface resistance value is known.

### **( c) Field Emission Scanning Electron Microscope (FE-SEM)**

Field Emission Scanning Electron Microscope is used to study the surface morphology of both the single and double layer of electrode surface during OLED fabrication. During the process of taking the images, initially, the film surfaces are coated with a

gold layer under a vacuum condition to make the film more conductance. By doing so, it is possible to take the FE-SEM images of better quality. The following figure shows the set up of FE-SEM facility in a laboratory environment.



Figure 2.7 (b): Field emission SEM setup Figure 2.7(c): Gold coating unit under vacuum

## **2.8 Commonly used materials for OLED applications**

### **(a) Anode materials for hole transfer**

One of the most widely used anode material in OLED society is found to be Indium tin oxide (ITO). It is widely used because of its high work function (4.3-5.1 eV), high transparency (90%) to visible light, good electrical conductivity, excellent adhesion to the substrates, and easy patterning ability. ITO surface properties are critical in the performance OLEDs. Oxygen plasma treatment combined with chemical treatment is effective in increasing hole-injection efficiency of ITO. In the literature also different types of anode such as AZO, ZnO, etc. are found to be used by a various group of the

researcher in the various period. Chemical structure of popularly known ITO electrode is given below:

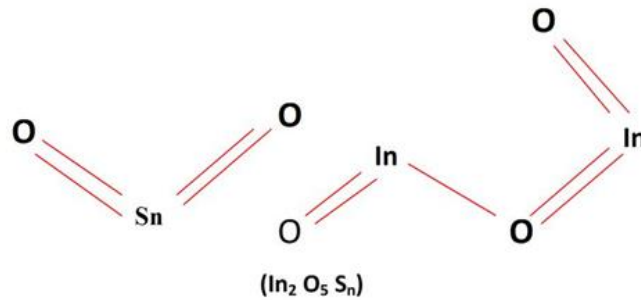


Figure 2.8 (a): Chemical structure of ITO

### **(b) Cathode materials for electron transfer**

Low work function metals are used as a cathode electrode for OLED fabrication. Different types of low work function materials such as lithium, calcium, and magnesium are used mainly due to their lower value of work function. Because during the OLED operation, an electron can travel from low work function side to the lowest unoccupied molecular orbital of (LUMO) of the organic semiconductor. However, there is the main disadvantage of this low work function cathode is that they are highly reactive especially in ambient atmosphere. Therefore only more stable materials such as aluminium (Al), silver (Ag) and gold (Au) are preferable as cathodes. However, the OLEDs which are based on these types of the cathode are found to be inefficient, and their light output is very low compared to OLEDs with a reactive metal cathode. That is why a thin film of an insulator such as lithium fluoride (LiF) deposited between the organic layer and the Al cathode for

improvement purpose. Instead of this LiF, some other materials are also available in the literature such as silicon dioxide, magnesium fluoride, calcium fluoride, sodium chloride, hexatriacontane and cesium carbonate. However, it is found that the device performance and stability of these materials are comparatively low as compared with that of LiF as a buffer layer from a characterization point of view.

### **( c ) Hole-Transporting Molecular Materials (HTL)**

Only those materials which have the electron-donating properties are known as hole-transporting materials (HTL) in the society of OLEDs. The hole transporting layer (HTL) plays the role of controlling the hole injection from the anode and transporting the injected holes to the light emitting layer by accepting them. This hole-transport layer also functions as the electron blocking layer which blocks the electrons escaping from the light emitting layer (EML). The available hole transport materials are N,N'-diphenyl-N,N-bis (3- methylphenyl) 1,1'-biphenyl- 4,4'-diamine (TPD), 4,4'-bis-1-naphthyl-Nphenylamino1- biphenyl (NPB), N,N-di (naphthalene-1-yl)-N, Ndiphenylbenzidine (NPD), m-MTDATA, N,N'-bis(naphthalen-1-yl)-N,N'-bis(phenyl)-2,7-diamino-9,9-diphenyl ( DPFL-NPB ), N,N'-bis(naphthalene 1-yl)-N,N'-bis(phenyl)-2,2'-dimethylbenzidine ( $\alpha$ -NPD ), 2,2',7,7'- tetrakis(N,N-diphenylamino)-9,9-spirobifluorene (Spiro-TAD ), 9,9-bis[4- (N,N-bis-naphthalen-2-yl-amino)phenyl]-9H-fluorene (NPAPF ), 9,9-bis[4- (N-naphthalen-1-yl-N-phenylamino)-phenyl]-9H-fluorene (NPBAPF ), 2,2',7,7'-tetrakis[N-naphthalenyl(phenyl)-amino]-9,9-spirobifluorene (Spiro- 2NPB), N,N'-bis(phenanthren-9-yl)-N,N'-bis(phenyl)-benzidine (PAPB ), 2,2'-bis[N,N-

bis(biphenyl-4-yl)amino]-9,9-spirobifluorene (2,2'-Spiro- DBP), 2,2'-bis(*N,N*-diphenyl-amino)-9,9-spirobifluorene (Spiro-BPA ), Di- [4-(*N,N*-ditolyl-amino)-phenyl]cyclohexane (TAPC ) etc. Chemical structure of TPD, NPB, m-MTDATA and TAPC are given below :

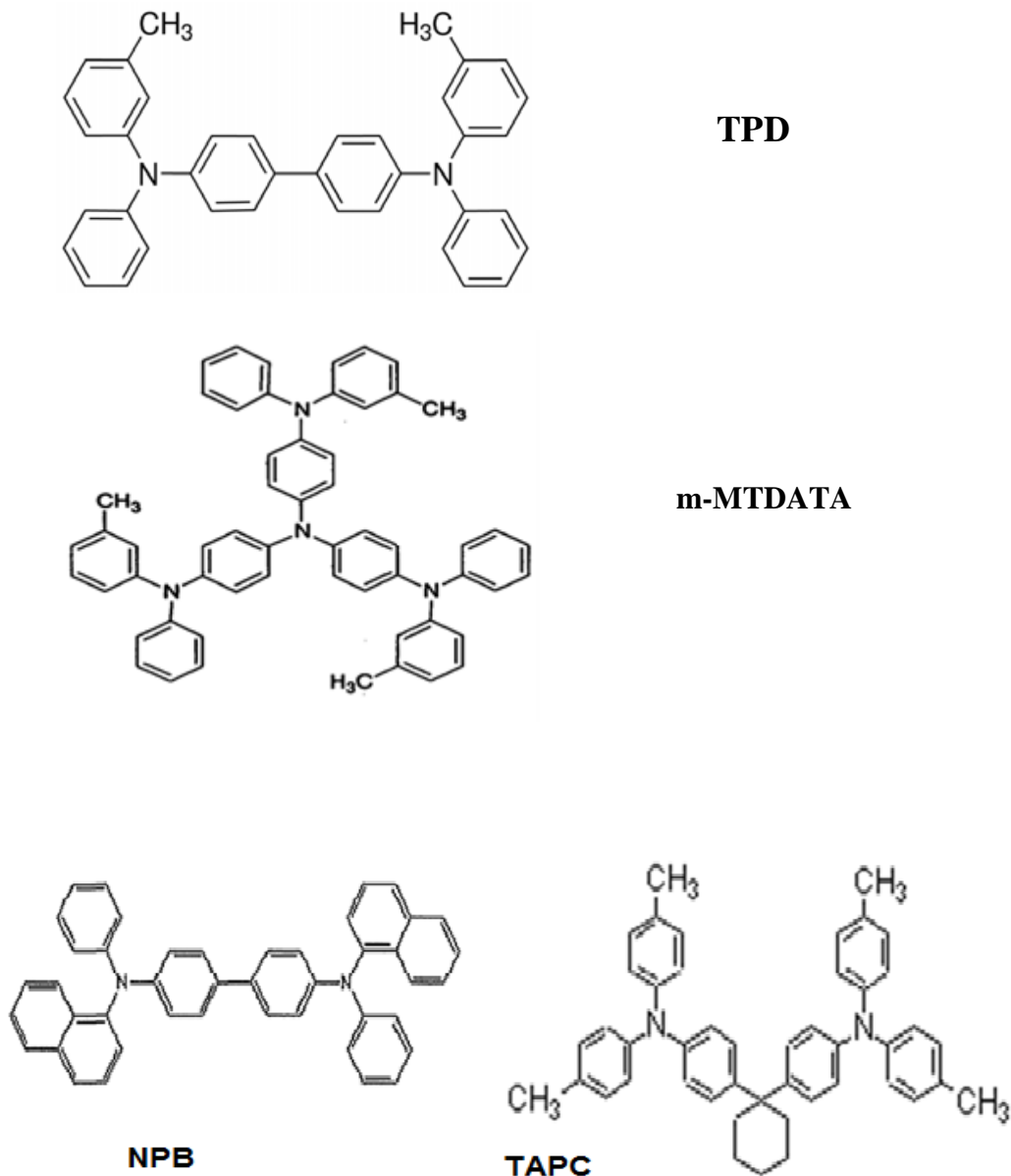


Figure 2.8 (b) : Chemical structure of TPD, m-MTDATA, NPB and TAPC



### (d) Electron-transporting Amorphous Molecular Materials

The materials which have electron-accepting properties used in OLEDs as electron-transporting materials (ETL). Similarly to HTL, the electron transporting layer (ETL) also plays the active role of controlling the electron injection from the cathode, accepting electrons, and transporting injected electrons to the emitting layer. ETL layer also functions as-is hole blocking layer that blocks holes from the emitting layer. As compared with hole transporting materials, fewer electron transporting materials have been reported in the literature. A popularly known green emitter, Tris (8-hydroxyquinoline) aluminium (Alq3) has been widely used as an excellent electron transporter. It is also thermally and morphologically found to be stable for evaporated into thin films and easily synthesized and purified. Chemical structures of some ETL layer are given below:

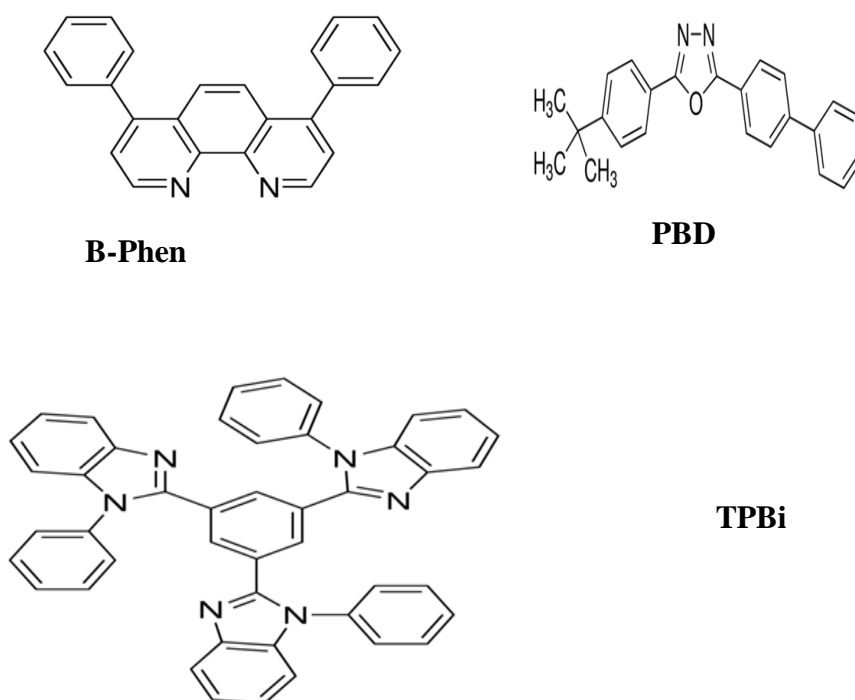


Figure 2.8 ( c): Chemical structure of B-Phen, PBD and TPBi

## ( e ) Fluorescent Host Materials

There are different types host materials are available some of these are as follows:

- Tris(8-hydroxy-quinolino)aluminium (Alq3)
- 9,10-di(naphth-2-yl)anthracene (ADN)
- 2-tert-butyl-9,10-di(naphth-2-yl)anthracene (TBADN)
- 2,7-bis[9,9-di(4-methylphenyl)-fluoren-2-yl]-9,9-di(4-methylphenyl)fluorene (TDAF)
- 2-methyl-9,10-bis(naphthalen-2-yl)anthracene (MADN)
- 2-(9,9-spirobifluoren-2-yl)-9,9-spirobifluorene ( BSBF)
- 2,7-bis(9,9-spirobifluoren-2-yl)-9,9-spirobifluorene (TSBF)
- 2-[9,9-di(4-methylphenyl)-fluoren-2-yl]-9,9-di(4-methylphenyl)fluorene (BDAF)
- 2,2'-dipyrenyl-9,9-spirobifluorene (2,2'-Spiro-Pye)
- 1,3,5-tri(pyren-1-yl)benzene (TPB3)
- 9,9-bis[4-(pyrenyl)phenyl]-9H-fluorene ( BPPF)
- 2,2'-bi(9,10-diphenyl-anthracene) (TPBA)
- 2,7-dipyrenyl-9,9-spirobifluorene (Spiro-Pye)
- 1,4-di(pyren-1-yl)benzene (p-Bpye)
- 1,3-di(pyren-1-yl)benzene (m-Bpye)
- 6,13-di-biphenyl-4-yl-pentacene (DBPenta)
- 3,9-di(naphthalen-2-yl)perylene and 3,10-di(naphthalen-2-yl) perylene mixture ( DNP)

## (f) Phosphorescent Host Materials

In the literature also different kinds of phosphorescent host materials are available.

Some of them are mentioned here:

- 1,3-bis(carbazol-9-yl)benzene (MCP)
- 1,3,5-tris(carbazol-9-yl)benzene (TCP)
- 4,4',4''-tris(carbazol-9-yl)triphenylamine (TcTa)
- 4,4'-bis(carbazol-9-yl)biphenyl (CBP)
- 4,4'-bis(carbazol-9-yl)-2,2'-dimethylbiphenyl (CDBP)
- 2,7-bis(carbazol-9-yl)-9,9-dimethylfluorene (DMFL-CBP)
- 2,2',7,7'-tetrakis(carbazol-9-yl)-9,9-spirobifluorene (Spiro-CBP)
- 2,7-bis(carbazol-9-yl)-9,9-ditolylfluorene (DPFL-CBP)
- 9,9-bis[4-(carbazol-9-yl)-phenyl]fluorene (FL-2CBP)
- 2,7-bis(carbazol-9-yl)-9,9-spirobifluorene (Spiro-2CBP)
- 1,4-bis(triphenylsilyl)benzene (UGH-2)
- 1,3-bis(triphenylsilyl)benzene (UGH-3)
- Bis(4-*N,N*-diethylamino-2-methylphenyl)-4-methylphenylmethane (MPMP)
- 2,7-bis(carbazol-9-yl)-9,9-dioctylfluorene (DOFL-CBP)
- 4,4''-di(triphenylsilyl)-*p*-terphenyl (BST)
- 4,4'-di(triphenylsilyl)-biphenyl (BSB)
- 9-(4-*tert*-butylphenyl)-3,6-bis(triphenylsilyl)-9H-carbazole (CzSi)
- 9-(4-*tert*-butylphenyl)-3,6-ditryl-9H-carbazole (CzC)

- 9-(4-tert-butylphenyl)-3,6-bis(9-(4-methoxyphenyl)-9H-fluoren-9-yl)-9H-carbazole (DFC)

Since in the case of OLED operation light emission from the device is depend on the dopant elements in the active region. It is possible to produce the different color from OLED device by choosing proper dopant materials. Here we mentioned the different class of organic dopant materials for different color light emission.

### **(g) Green Dopant Materials**

- N<sub>10</sub>,N<sub>10'</sub>-bis(4-methylnaphthalen-1-yl)-N<sub>10</sub>,N<sub>10'</sub>-di-p-tolyl-9,9'-bianthracene-10,10'-diamine (BA-MNT)
- N<sub>9</sub>,N<sub>10</sub>-diphenyl-N<sub>9</sub>,N<sub>10</sub>-di-p-tolylanthracene-9,10-diamine (An-o-TP)
- N<sub>9</sub>,N<sub>9</sub>,N<sub>10</sub>,N<sub>10</sub>-tetra-o-tolylanthracene-9,10-diamine (An-o-DT)
- N<sub>9</sub>,N<sub>10</sub>-di-m-tolyl-N<sub>9</sub>,N<sub>10</sub>-di-o-tolylanthracene-9,10-diamine (An-DT)
- N<sub>9</sub>,N<sub>9</sub>,N<sub>10</sub>,N<sub>10</sub>-tetra-m-tolylanthracene-9,10-diamine (An-m-DT)
- fac-tris(2-(3-p-xylyl)phenyl)pyridine Iridium(III) (TEG)
- 7-(diethylamino)-3-(6-methylbenzo[d]thiazol-2-yl)-2H-Chromen-2-one (Courmarin 6-M)
- 3-(2-benzothiazolyl)-7-(diethylamino)coumarin (Coumarin 6)
- 2,3,6,7-tetrahydro-1,1,7,7-tetramethyl-1H, 5H,11H-10-(2-benzothiazolyl)quinolizino[9,9a,1gh]coumarin (C545T)
- N,N'-dimethyl-quinacridone (DMQA)
- Tris(2-phenylpyridine)iridium(III) [Ir(ppy)<sub>3</sub>]
- Bis(2-phenylpyridine)(acetylacetonate)iridium(III) [Ir(ppy)<sub>2</sub>(acac)]

## (h) Blue Dopant Materials

- 4,4'-bis(9-ethyl-3-carbazovinyleno)-1,1'-biphenyl ( BCzVBi)
- Perylene
- 2,5,8,11-tetra-*tert*-butylperylene (TBPe)
- 1,4-bis[2-(3-*N*-ethylcarbazoryl)vinyll]benzene (BCzVB)
- 4,4'-bis[4-(di-*p*-tolylamino)styryll]biphenyl (DPAVBi)
- 4-(di-*p*-tolylamino)-4'-[(di-*p*-tolylamino)styryll]stilbene
- Bis(3,5-difluoro-2-(2-pyridyl)phenyl-(2-carboxypyridyl)iridium(III) (FIRPic)
- 4,4'-bis[4-(diphenylamino)styryll]biphenyl (BDAVBi)
- Bis(2,4-difluorophenylpyridinato)tetrakis(1-pyrazolyl)borate iridium(III) (FIR6)
- N,N'-bis(naphthalen-2-yl)-N,N'-bis(phenyl)-tris-(9,9- dimethylfluorenylene) (BNP3FL)
- 2,7-bis{2-[phenyl(*m*-tolyl)amino]-9,9-dimethyl-fluorene-7-yl}-9,9-dimethylfluorene (MDP3FL)
- N-(4-((E)-2-(6-((E)-4-(diphenylamino)styryll)naphthalen-2-yl)vinyll)phenyl)-N-phenylbenzenamine (N-BDAVBi)

### (i) Red Dopant Materials

- (E)-2-(2-(4-(dimethylamino)styryl)-6-methyl-4H-pyran-4-ylidene) malononitrile ( DCM)
- 4-(dicyanomethylene)-2-methyl-6-julolidyl-9-enyl-4H-pyran ( DCM2)
- 4-(dicyanomethylene)-2-methyl-6-(1,1,7,7-tetramethyljulolidyl-9-enyl)- 4H-pyran ( DCJT)
- 4-(dicyanomethylene)-2-*tert*-butyl-6-(1,1,7,7-tetramethyljulolidin-4-yl vinyl)-4H-pyran ( DCJTB)
- Tris(dibenzoylmethane)phenanthroline europium(III) (Eu(dbm)3(Phen))
- 5,6,11,12-tetraphenylnaphthacene (Rubrene)
- Bis(2-benzo[*b*]thiophen-2-yl-pyridine)(acetylacetonate)iridium(III) (Ir(btp)2(acac))
- Tris(1-phenylisoquinoline)iridium(III) (Ir(piq)3)
- Bis(1-phenylisoquinoline)(acetylacetonate)iridium(III) (Ir(piq)2(acac))
- Bis[1-(9,9-dimethyl-9H-fluoren-2-yl)-isoquinoline]

Therefore it is possible to produce the different colour of light emission from OLED devices by using a proper selection of suitable materials from available literature. Thus OLED technology should bring the new doorway for the existing display technology.

## **Chapter 3**

*A study of the effect of single and double layer anode structure regarding the performance of organic light emitting diode (OLED) using inorganic-inorganic bilayer configuration*

### **3.1 Organic Light Emitting Diode (OLED) with Alq<sub>3</sub> as light emitting material and FTO+ V<sub>2</sub>O<sub>5</sub> as bilayer anode structures**

Vanadium pentoxide layer deposited on the fluorine doped tin oxide (FTO) anode by vacuum deposition has been investigated for the Organic light-emitting diode (OLED). With an optimal thickness of V<sub>2</sub>O<sub>5</sub> (12nm), the luminance efficiency is increased by 1.66 times than the single FTO OLED. The improvement of current efficiency implies that there are a better charge injection and better controlling of hole current. To investigate the performance of OLED by the buffer layer a series of V<sub>2</sub>O<sub>5</sub> films of different thicknesses were deposited on the FTO anode and study their **J-V** and **L-V** characteristics. Further analysis was carried out by measuring sheet resistance, optical transmittance and surface morphology with FE-SEM images. Here the maximum value of current efficiency is found to be 2.83Cd/A.

#### **3.1.1 Fabrication of the OLEDs**

The OLEDs in the bottom emitting structure with the Alq<sub>3</sub> as an active layer and FTO+V<sub>2</sub>O<sub>5</sub> as bilayer anode configuration were fabricated by the Multiple Pump Down (MPD) method after cleaning the FTO coated glass substrates. In every deposition, thoroughly cleaned masks were used to achieve the different geometrical patterns. Initial substrates cleaning and the cleaning of the unit and masks after each deposition achieved by the procedure described in chapter 2. The AL cathode electrode was evaporated using tungsten helix filament while the thin layer of



Vanadium Pentoxide ( $V_2O_5$ ) was evaporated using a tungsten boat. In our work for deposition of both the inorganic and organic layer, we used a high vacuum chamber unit having vacuum better than  $8 \times 10^{-6}$  Torr. The source to substrate distance for  $V_2O_5$  was about 8cm while for other layer deposition it was about 12-14cm. The deposition rate for  $V_2O_5$  was about  $10 \text{ \AA}/\text{sec}$ , and for another layer, it was about  $15 \text{ \AA}/\text{sec}$ . Sheet resistance and optical transmittance are measured by four probe and UV-VISIBLE double beam spectrophotometer unit. The current-voltage-luminance characteristics of the fabricated OLEDs were measured by digitally controlled source-meter and luminance meter unit. All materials were purchased from Sigma-Aldrich Company and used without further purification. In our work active area of the samples was  $3 \times 6 \text{ mm}^2$  and thickness of the thin film was confirmed by the profilometer set up as mentioned in section 2.7.1(b).

We have fabricated the standard OLEDs using  $V_2O_5$  as hole injection layer(HIL), N,N'-bis ( 3-methyl phenyl )-N,N'(phenyl)- benzidine(TPD) , Tris ( 8-hydroxy quinolino) aluminium (Alq3) and lithium fluoride (LiF) are used as hole transport layer , emitting layer and electron transport layer respectively and compared the J-V-L characteristics of OLEDs with different thickness of HIL and also that of HIL free OLED. Without LiF electron injection layer it is difficult for electron injection from AL cathode to the Alq3 layer since the dissociation of the alkali halide into the organic layer leads to the enhancement of electron injection.

### 3.1.2 Backing and ageing

Clean electric oven was used to air-baked the fabricated OLEDs up to a temperature of 200°C for 3-4 hours. The OLEDs were taken in the thoroughly cleaned petridishes of suitable sizes and placed in the electric oven at the pre-set temperature for the required time of baking. These were then stored in a clean dessicator charged with fused  $\text{CaCl}_2$  for OLED characterization.

### 3.1.3 Schematic representation and energy level alignment diagram of Organic Light Emitting Diode (OLED)

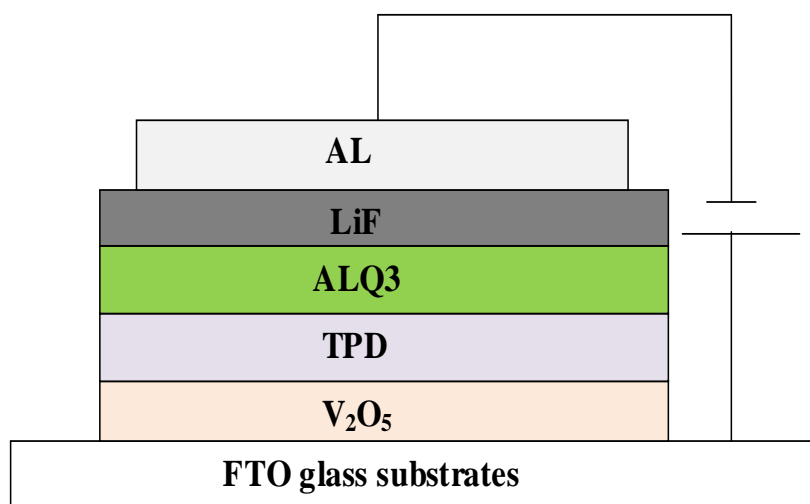


Figure 3.1 (a): Schematic representation of OLED structure

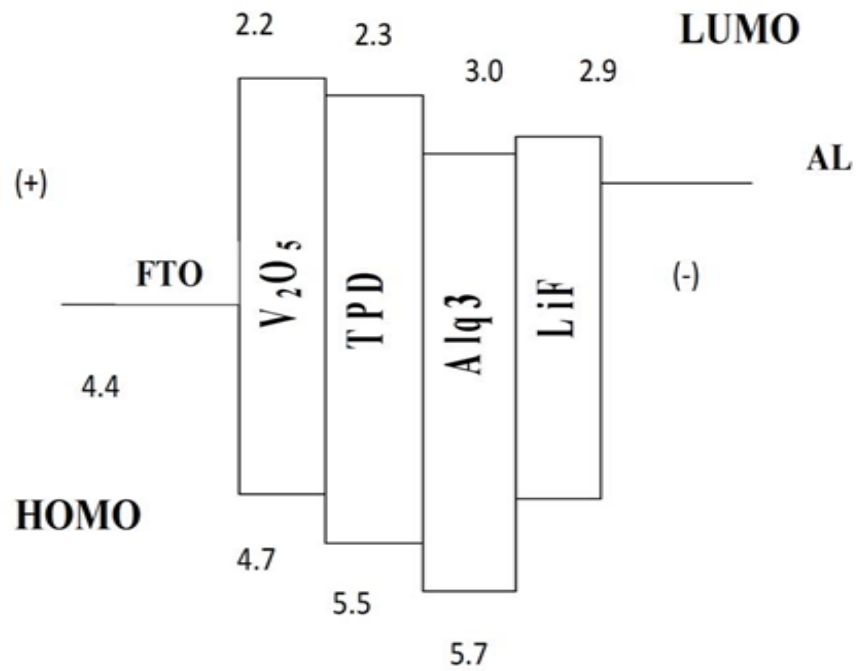


Figure 3.1 (b): Energy level alignment of OLED structure

### 3.1.4 Result and discussions

The structures of all the bottom light emitting OLEDs used in this investigation are given below

Device: A. FTO/V<sub>2</sub>O<sub>5</sub> (0nm)/ TPD (40nm)/Alq<sub>3</sub> (50nm)/LiF(5nm)/Al (110nm)

Device: B. FTO/V<sub>2</sub>O<sub>5</sub> (4nm)/TPD (40nm)/Alq<sub>3</sub> (50nm)/LiF(5nm)/Al (110nm)

Device: C. FTO/V<sub>2</sub>O<sub>5</sub> (8nm)/TPD (40nm)/Alq<sub>3</sub> (50nm)/LiF(5nm)/Al (110nm)

Device: D. FTO/V<sub>2</sub>O<sub>5</sub> (12nm)/TPD (40nm)/Alq<sub>3</sub> (50nm)/LiF(5nm)/Al (110nm)

Device: E. FTO/V<sub>2</sub>O<sub>5</sub> (16nm)/TPD (40nm)/Alq<sub>3</sub> (50nm)/LiF(5nm)/Al (110nm)

The current-voltage and luminance-voltage characteristics of FTO/  $V_2O_5$  (varying thickness)/TPD (40 nm)/Alq3 (50 nm)/LiF(5nm)/Al (110 nm) is shown in Fig 3.1 (c) and Fig 3.1 (d) respectively. To study the influence of thickness variation of  $V_2O_5$  on luminance, we kept the thickness of all layers constant except  $V_2O_5$  layer thickness, which was varied between 4 nm and 16 nm. It is found that when the thickness of buffer is continuously increased, then there is a decreasing tendency of current density. This indicated that this interlayer has the direct effect of blocking the hole current by controlling the flow of positive charge carrier. On the other hand, a good EL device should possess high luminance efficiency. In our work, it is found that the device with 12nm  $V_2O_5$  buffer layer has the highest efficiency of 2.83Cd/A compared to the other OLED devices. Therefore current efficiency increases compare to the device without buffer layer (1.70 Cd/A). With the increasing thickness of buffer layer, there is a gradual decrease of luminance and increases the efficiency of the devices which is due to the blocking of positive charge carrier current by the high thickness of  $V_2O_5$  layer [249]. This improvement in efficiency is because of the proper balancing of charge carrier injection. This interlayer also prevents the diffusion of metal and oxygen into the organic layer from the anode and hence reduces the probability of an electrical breakdown of the device. From the literature, it is known to us that the mobility of electron is lower in electron transport layer than the mobility of holes in hole transport layer [250]. As a result of which there is an accumulation of positive charge carrier at the interface of HTL/ETL layer. Therefore to enhance the

efficiency of the device we should either decrease the number of positive charge carrier mobility or increases the electron mobility. In our case, we balance the mobility of positive charge carrier by using the  $V_2O_5$  buffer layer between the FTO and TPD layer.

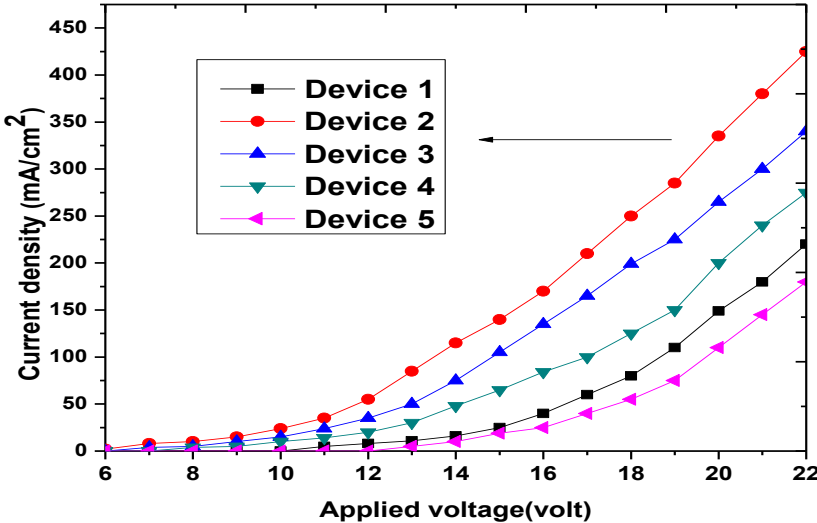


Figure 3.1 (c) : Graph of applied voltage vs current density

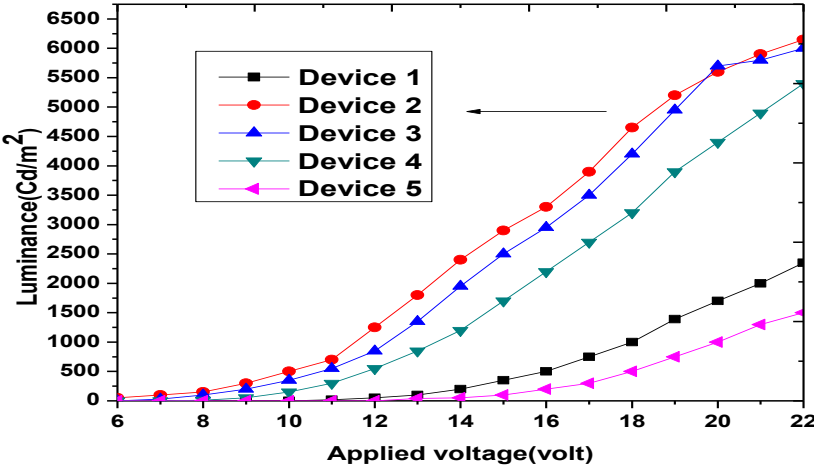


Figure 3.1(d): Graph of applied voltage vs luminance

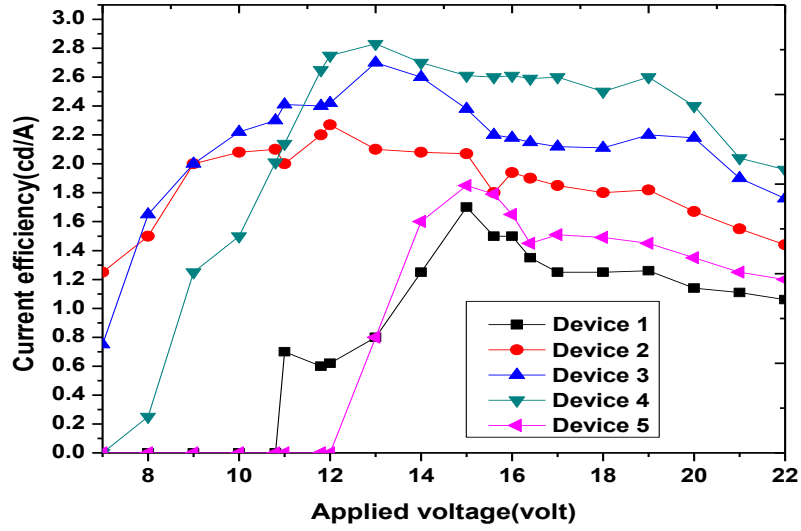


Figure 3.1 (e) : Graph of applied voltage vs current efficiency

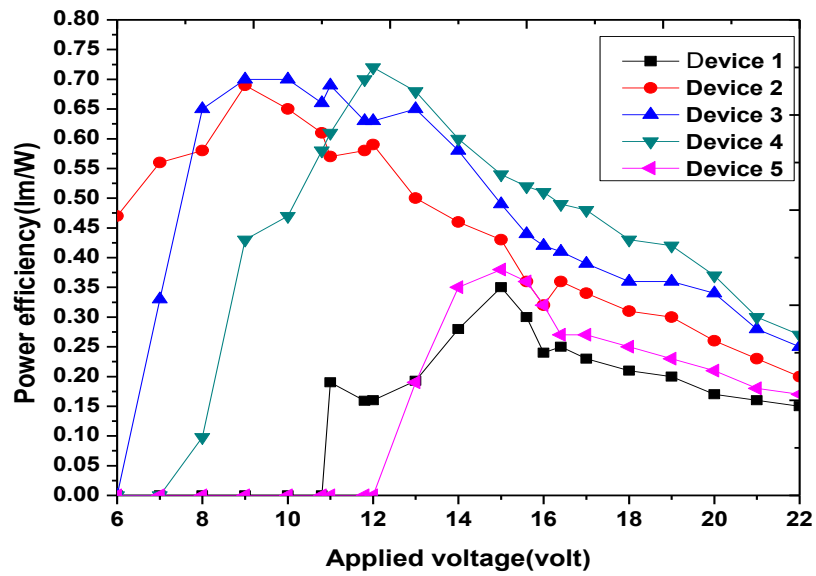


Figure 3.1 (f): Graph of applied voltage vs power efficiency

In other words, this oxide layer can help in preventing the accumulation of excess holes in the luminance layer and thus increasing the probability of electron-hole pair combination. Initially when the thickness of  $V_2O_5$  is very thin mobility of the positive charge carrier is significant increases due to the tunnelling of charge carrier from FTO surface to the TPD layer. This effect is associated with the high value of current density and luminance of the device along with the low threshold voltage. After that when we increase the thickness of the layer continuously, it is found that there is a decreasing tendency of both current density and luminance of the devices. This may be due to the reducing of tunnelling effect between the anode and hole transport layer. From the characteristics graph as shown in figure 3.1 (c, d, and e) it is clear that although the value of current density and luminance is decreased their efficiency is more improved continuously with the increasing thickness of the buffer layer. In our work maximum efficiency is provided by device four which is better than the earlier reported [90, 251]. Here the optimized thickness of the buffer layer is found to be 12nm. After that efficiency of the device is decreased due to the more reduction of tunnelling effect at a higher thickness of this buffer layer. The initial increase of luminance is may also be due to the minimized of crystal defects within the interface region of FTO and TPD layer because of the presence of oxide layer. Also when we placed the  $V_2O_5$  layer between the anode and hole transport layer, then there is a high tendency for the positive charge carrier to inject into the organic layer from a high energy level compared with that without any buffer layer as shown in figure 3.1(b). There is also some hole trap may exist in the hole transport layer which should trap the holes before they come to light emitting region. When the holes are injected relatively

from a higher energy level, then the probability of their trapping is decreased. This is the reason for device efficiency is increased with the presence of the buffer layer than the device of without any buffer layer. Figure 3.1(e) represents the variation of current efficiency of the OLED devices with respect to their applied voltage. In this figure, it is clear that device 4 shows the maximum efficiency and whereas device 1 has lower efficiency. This situation is directly linked to the proper charge injection process, i.e., exciton formation probability. Initially, when the thickness is very low, the charge tunnelling process is slightly enhanced. However, when we increase the thickness, then this process tends to more enhance because of which we get better device efficiency in our devices. This effect is maximum at the optimized thickness of 12nm (device 4) where we get the highest efficiency of 2.83 cd/A. This implies that at a 12nm thickness of buffer layer there is more balanced of positive charge injection w.r.t. negative charge from the anode side of the device. However, after the optimized thickness efficiency became decreases. This is due to the reducing of charge carrier tunnelling at a higher thickness of the buffer layer from the anode to hole transport layer.

Similarly, the variation of power efficiency vs applied voltage graph for all the devices is shown in figure 3.1(f) in which device 4 shows the highest value where the maximum balance of holes and electron injection takes place. As a result of which less energy is consumed at the anode and hole transport interface layer. It is found that the power efficiency ( $\eta$ ) and current efficiency ( $\gamma$ ) are depending on each other, and their relation can be given by equation 1 considering the Lambertian emission pattern.



$$\eta = \pi \frac{L}{VJ} = \pi \frac{1}{V} \left( \frac{L}{J} \right) = \pi \gamma \frac{1}{V} \quad \text{----- 1}$$

Where L is the luminance measured from the emitting surface and V is the applied voltage. The value of current efficiency depends on the optical coupling and the internal quantum efficiencies. From this equation, it is clear that the term power efficiency is inversely proportional to V.

The graph of standard deviation (which is a measure of the spread of their efficiency in a set of data at different voltages from their mean value) of current and power efficiency vs different thickness deposition of OLED devices is given in figure 3.1(g). Following table 1 shows the summary of the result of five OLED devices along with the electrical and optical properties of different bilayer anode film surface. From this table, it is seen that both sheet resistance and transmittance are decreasing with increasing the anode layer thickness as shown in figure 3.1 (h)

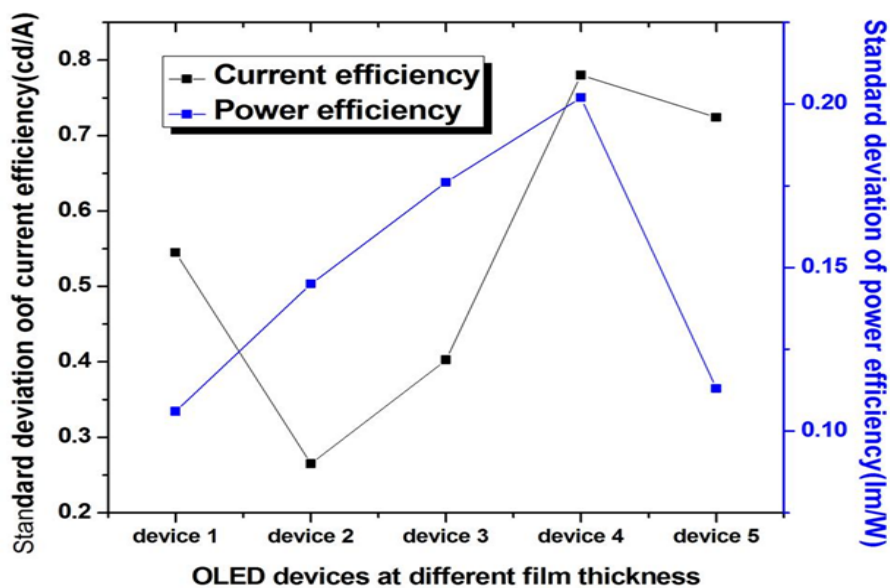


Figure 3.1 (g): Graph of the standard deviation of OLED at different thickness of  $V_2O_5$

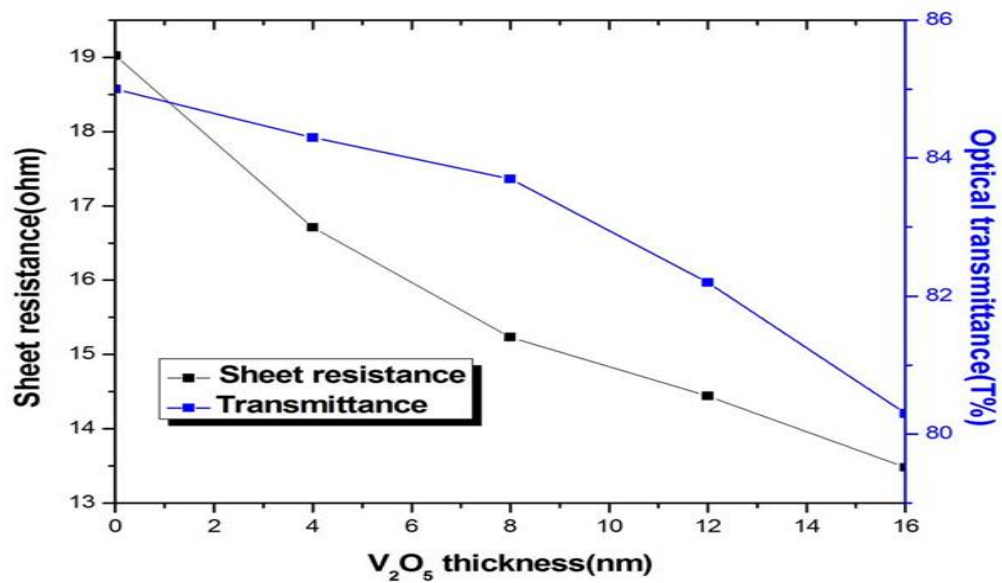


Figure 3.1 (h): Graph of variation of sheet resistance and transmittance with a  $V_2O_5$  thickness

**Table -3.1:** Luminance and efficiency characteristics of the devices with different

$V_2O_5$  buffer layer thicknesses at the current density of  $30 \text{ mA/cm}^2$ .

S.N	$V_2O_5$ thickness	Luminance ( $\text{cd/m}^2$ )	Turn-on voltage(volt)	Luminous efficiency ( $\text{cd/A}$ )	Sheet resistance of bilayer anode	Optical transmittance of bilayer anode
1	0nm	450	11.1	1.50	19.02	85.0%
2	4nm	650	6.1	2.11	16.71	84.3%
3	8nm	800	7.2	2.60	15.23	83.7%
4	12nm	850	8.1	2.83	14.66	82.2%

5	16nm	250	12.9	1.45	13.48	80.3%

From this table, it is seen that the turn-on voltages are 11.1, 6.1, 7.2, 8.1 and 12.9 for the devices with a buffer layer in 0nm, 4nm, 8nm, 12nm, and 16nm respectively. Thus the turn-on voltage of 4nm, 8nm, and 12nm is to be lower than that of the device without the buffer layer. However, there is a tendency that the turn-on voltage increases with the increase of anode layer thickness because a larger voltage is dropped across the oxide layer [252]. The surface morphology of single and double layer of FTO film is given in Figure 3.1 (i) and 3.1(j). The figure 3.1 (k) represents the cross-sectional view of the device with  $V_2O_5$ .

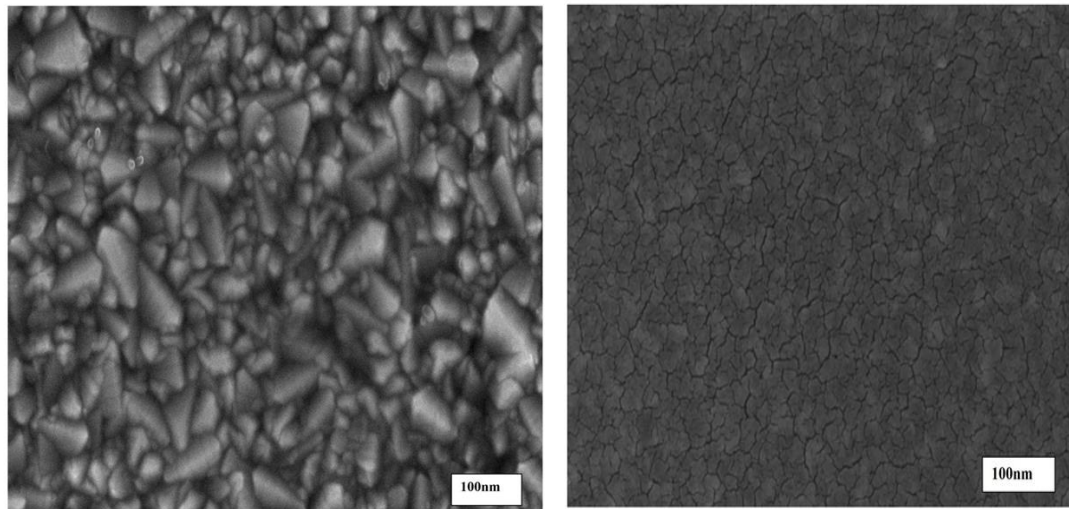


Figure 3.1 (i): FE-SEM images of bare FTO surface      Figure 3.1 (j): FE-SEM images of FTO/ $V_2O_5$  surface

From the study of SEM images, it can be concluded that the surface of bilayer anode became smoother compared to the single anode due to the presence of the oxide layer.

This implies that there is a better contact of anode surface to the organic layer. Because of which we get, the better the device efficiency when bias is applied within the tunnelling region.

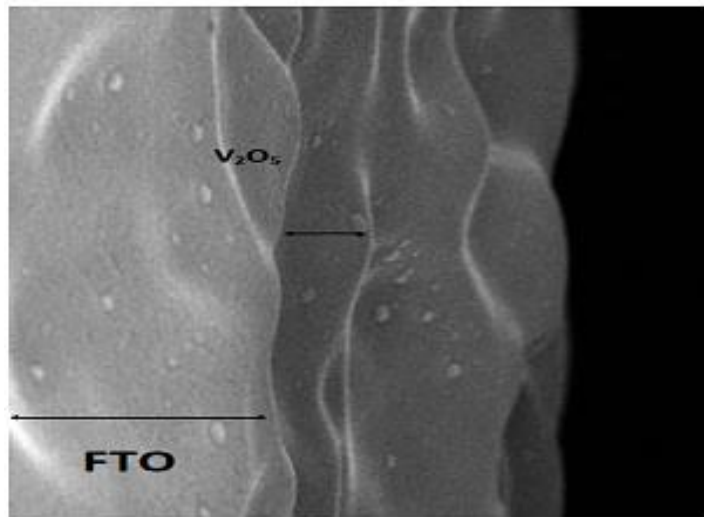


Figure 3.1 (k): A cross-sectional SEM image of the device

### 3.1.5 Conclusion:

1. Our result revealed that there is an optimum thickness of buffer layer at which the maximum OLED current efficiency can be achieved.
2. In this case, the optimum thickness of 12 nm  $V_2O_5$  buffer layer has resulted in 1.66 times enhancement in current efficiency compared to the bare FTO anode.
3. For maximum current efficiency, the thickness of LiF, Alq3, TPD, and  $V_2O_5$  are 5nm, 50 nm, 40 nm and 12 nm respectively. In this configuration, a luminance of 5400  $cd/m^2$  is obtained at a current density of 275  $mA/cm^2$ .
4. Therefore from the above study, it can be said that the performance of bilayer anode OLED is higher than the simple FTO based OLED device.

## **3.2 Organic Light Emitting Diode (OLED) with Alq3 as light emitting material and FTO+ NiO (nickel oxide) as bilayer anode structures**

Here we investigated the influence of nickel oxide (NiO) layer over the fluorine-doped tin oxide (FTO) surface regarding the performance of Organic light-emitting diode (OLED). We reported that at a 10nm thickness of nickel oxide buffer layer the luminance efficiency is found to be increased compared to the simple FTO based OLED. The performance of OLED is studied by depositing NiO films at different thicknesses over electrode surface and analyzed their **J-V** and **L-V** characteristics. Further analysis is carried out by measuring sheet resistance and optical transmittance. The surface morphology is studied with the help of FE-SEM images.

### **3.2.1 Fabrication of the OLEDs**

The OLEDs in the bottom emitting structure with the Alq3 as an active layer and FTO+NiO as bilayer anode configuration were fabricated by the Multiple Pump Down (MPD) method after cleaning the FTO coated glass substrates. In every deposition, thoroughly cleaned masks were used to achieve the different geometrical patterns. Initial substrates cleaning and the cleaning of the unit and masks after each deposition achieved by the procedure as mention in above section 3.1.1.

Here we also used aluminium as a cathode layer which was evaporated using tungsten helix filament while the thin layer of nickel oxide (NiO) was evaporated using a

tungsten boat. In our work, we carry out the deposition of both inorganic and organic layer under a high vacuum chamber unit having vacuum better than  $8 \times 10^{-6}$  Torr. The source of substrates distances for NiO was about 8cm while for other layer deposition it was about 12-14cm. The deposition rate for NiO was about  $10 \text{ \AA}/\text{sec}$ , and for another layer, it was about  $15 \text{ \AA}/\text{sec}$ . Sheet resistance and optical transmittance of bilayer anode structures are taken by four probe resistivity measurement and UV-VISIBLE double beam spectrophotometer unit. The current-voltage and luminance-voltage characteristics of the fabricated devices were measured by digitally controlled source-meter and luminance meter unit. Here we collected all the materials from Sigma-Aldrich Company and used without further purification. In our work active area of the samples was three  $3 \times 6 \text{ mm}^2$  and thickness of the thin film was confirmed by the profilometer set up as mentioned in section 2.7.1(b).

We have fabricated the standard OLEDs using NiO as hole injection layer(HIL), N,N'-bis( 3-methyl phenyl )-N,N'(phenyl)- benzidine(TPD),Tris ( 8-hydroxy quinolinato) aluminium (Alq3) as hole transport layer emitting layer and lithium fluoride (LiF) as electron transport layer respectively. We have compared the J-V-L characteristics of OLEDs with different thickness of HIL and also that of HIL free OLED.

### **3.2.2 Backing and ageing**

Clean electric oven was used to air-baked the fabricated OLEDs up to a temperature of  $200^\circ\text{C}$ . The OLEDs were taken in the thoroughly cleaned petridishes of suitable sizes and placed in the electric oven at the pre-set temperature for the required time of

baking. These were then stored in a clean dessicator charged with fused  $\text{CaCl}_2$  for OLED characterization.

### 3.2.3 Schematic representation and energy level alignment

diagram:

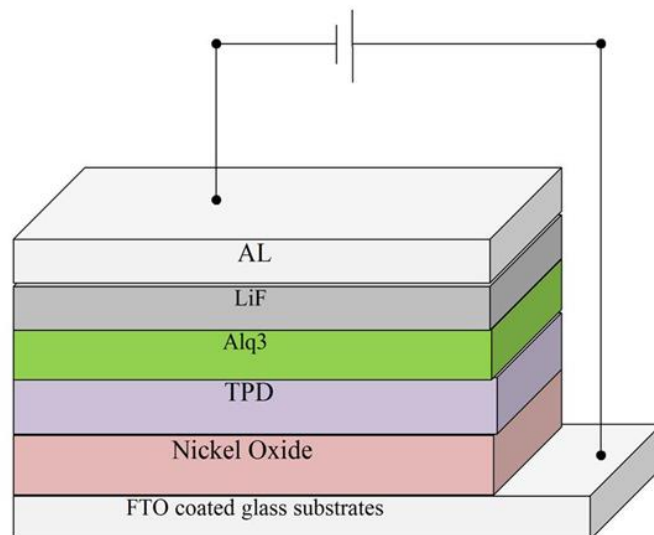


Figure 3.2 (a): Schematic representation of OLED structure

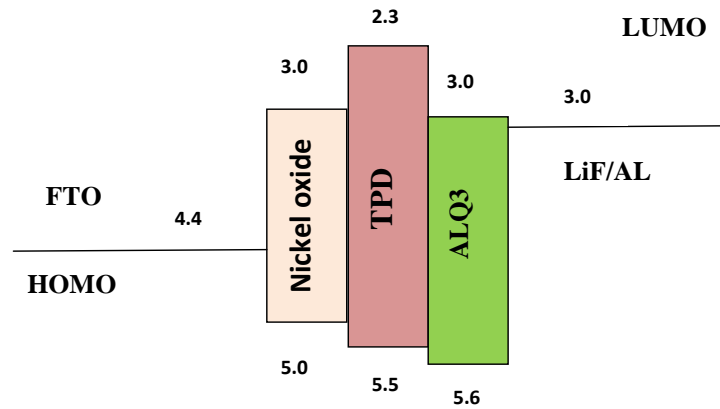


Figure 3.2 (b): Energy band structure of OLED device

### 3.2.4 Result and discussion:

To investigate the effect of nickel oxide layer on device performance here, we used following bottom light emitting OLEDs structures:

Device: A. FTO/NiO (0nm)/TPD (46nm)/Alq3 (54nm)/Lif(5nm)/Al (120nm)

Device: B. FTO/NiO (3nm)/TPD (46nm)/Alq3 (54nm)/Lif(5nm)/Al (120nm)

Device: C. FTO/NiO (6nm)/TPD (46nm)/Alq3 (54nm)/Lif(5nm)/Al (120nm)

Device: D. FTO/NiO (10nm)/TPD (46nm)/Alq3 (54nm)/Lif(5nm)/Al (120nm)

Device: E. FTO/NiO (13nm)/TPD (46nm)/Alq3 (54nm)/Lif(5nm)/Al (120nm)



The J-V-L characteristics of OLED devices having configuration FTO/ NiO (varying thickness) /TPD (46 nm) /Alq3 (54 nm) /Lif (5nm) /Al (120 nm) are given in Fig 3.2 (c) and 3.2 (d) respectively. To study the influence of thickness variation of nickel oxide layer on the light emitting tendency, we kept all the other layers thickness is constant. We observe that when the thickness of the buffer is continuously increased, then there is a decreasing tendency of current density. This observation shows that the presence of interlayer has a direct effect of blocking the hole current by controlling the flow of positive charge carrier towards the organic layer. In our work, we found that the device with 10nm NiO buffer layer provides the maximum device efficiency of 7.32Cd/A compared to the other OLED devices. Thus it is clear that the current efficiency value is increased compared to the device without a buffer layer (4.90 Cd/A). Due to the high thickness of buffer layer, there is a gradual decrease of luminance and increase of device efficiency is observed. This is due to the better controlling of positive charge carrier current by the high thickness of NiO layer [249] and hence the proper balancing of charge carrier injection. Therefore it is understood that the presence of NiO interlayer enhanced the device efficiency by blocking the hole injection. This oxide buffer layer also prevents the diffusion of oxygen and metallic ion into the organic layer from the anode and hence reduces the possibility of an electrical breakdown of the OLED device. From the earlier report, it is clear that the mobility of electron is always lower in the electron transport layer (ETL) than the mobility of holes in the hole transport layer (HTL) [251]. Because of which there

is always positive charge carrier accumulation is taking place near the interface region of HTL/ETL layer. So, to enhance the device performance, one should either increase the electron mobility in N-type ETL layer or decrease the number of positive charge carrier mobility in P-type HTL layer. Here we balance the mobility of positive charge carrier by inserting a thin nickel oxide buffer layer between the FTO and TPD layer.

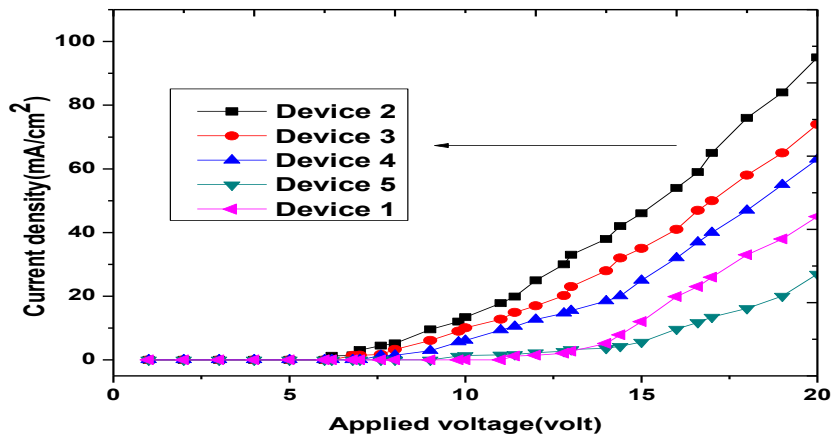


Figure 3.2 (c): Graph of applied voltage vs current density

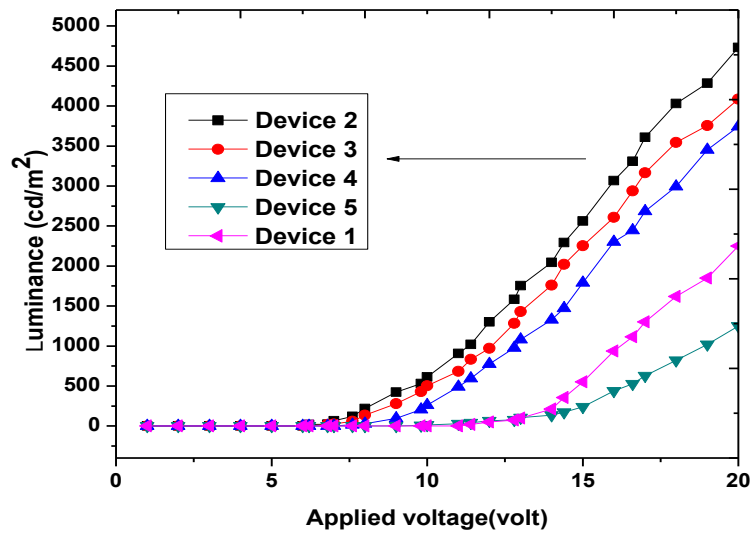


Figure 3.2 (d): Graph of applied voltage vs luminance

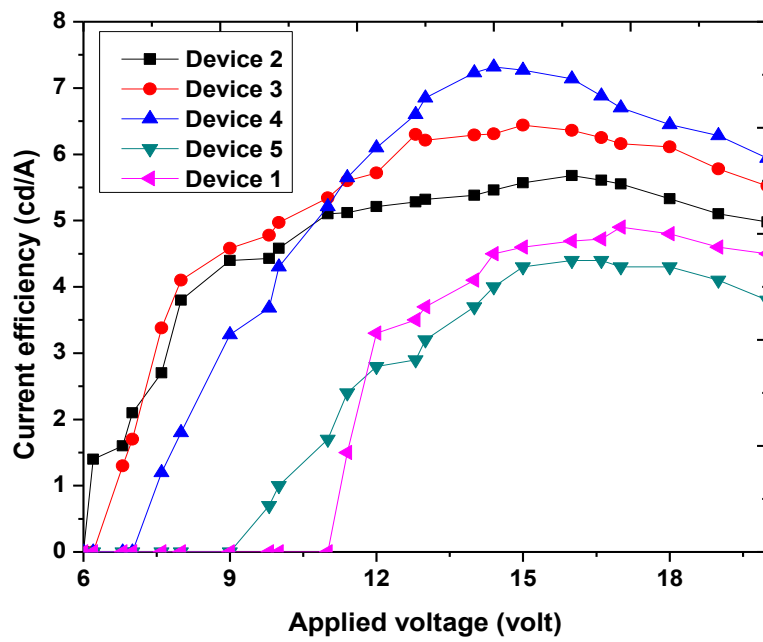


Figure 3.2 (e): Graph of applied voltage vs current efficiency

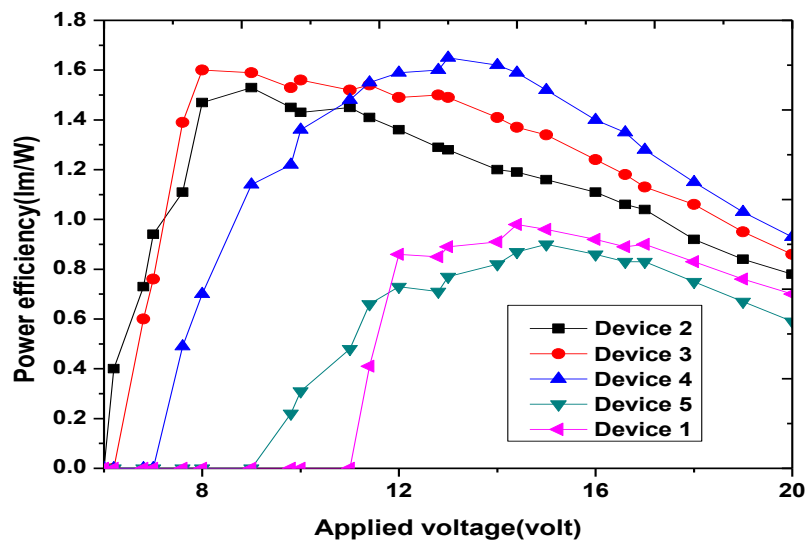


Figure 3.2 (f): Graph of applied voltage vs power efficiency

Therefore the buffer can increase the probability of electron-hole pair recombination by preventing the accumulation of excess holes in the luminescence layer. The mobility of the charge carrier is significantly balanced due to the proper charge tunnelling from the FTO surface to the organic TPD layer when the thickness of NiO is very thin. As a result of that, the high value of current density and luminance of the device is obtained along with along with lower threshold voltage. However, when we continuously increase the thickness of the NiO layer, we found that both the value of current density and luminance of the devices decrease gradually. This result is due to the reducing of charge tunnelling mechanism into the organic hole transport layer with the increasing thickness of buffer layer. From the characteristics graphs, it is clear that efficiency of the devices is found to be increased continuously although the current density and the luminance value of the devices decrease with increasing interlayer thickness. In our

work optimized result of the device is found to be at the thickness of 10nm oxide buffer layer. After this critical thickness of the buffer layer efficiency of the device is decreased considerably due to more reduction of charge tunnelling mechanism at the higher thickness. The initial increasing value of luminance of the device is also due to the minimization of crystal defects within the interface region of FTO and TPD layer under the presence of this oxide interlayer. Similarly, when we placed the NiO interlayer between the anode and hole transport layer, there is a high tendency of injection of the positive charge carrier into the HTL layer relatively from a high energy level compared with single layer anode OLED device as shown in figure 3.2 (b). Therefore when the holes are injected comparatively from a higher energy level than the probability of their trapping is decreased in the organic hole transport layer. It is the reason for better efficiency of the OLED devices compared with the single FTO based OLED device, i.e. without any buffer layer. Figure 3.2 (e) represents the current efficiency and voltage characteristics of the OLED devices. From this figure, it is clear that device 4 shows the maximum efficiency and whereas device 5 has the lowest efficiency. This situation is directly linked to the proper charge injection process from electrode to the organic layer. Initially, when the thickness of oxide layer is thin, the process of charge balancing is slightly enhanced. However, the process of charge balancing is found to be improved with increasing thickness of buffer layer which provides better efficiency in our devices. This charge balancing process is reached its maximum value at the optimized thickness of 10nm (device 4) NiO layer over FTO surface. This result gives the highest efficiency of 7.32 cd/A. This means that at a 10nm thickness of nickel oxide buffer layer there is a balance of positive charge

injection w.r.t. negative charge injection from both the electrode side of the OLED device. On the other hand, the device efficiency is found to decrease after the optimized thickness which is due to the reducing of charge carrier tunnelling at a higher thickness of the buffer. Similarly, the variation of power efficiency vs voltage characteristics for all the devices is also shown in figure 3.2 (f) in which device 4 shows the highest value where the maximum charge balancing is achieved. The variation of the standard deviation of current efficiency and power efficiency of OLED devices with different thickness of oxide layer is given in figure 3.2 (g). The following table shows the summary of the result of five OLED devices along with the electrical and optical properties with different bilayer anode combination. From this table, it is clear that the surface resistance value and optical transmittance value are decreasing with the increase of the thickness of oxide buffer layer as shown in figure 3.2 (h).

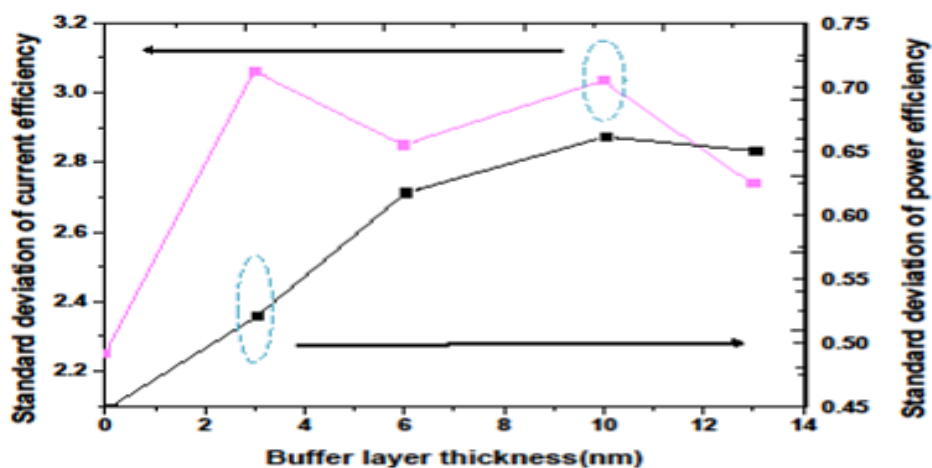


Figure 3.2 (g): Standard deviation of the efficiency of the OLED devices at different thickness of buffer layer over FTO surface

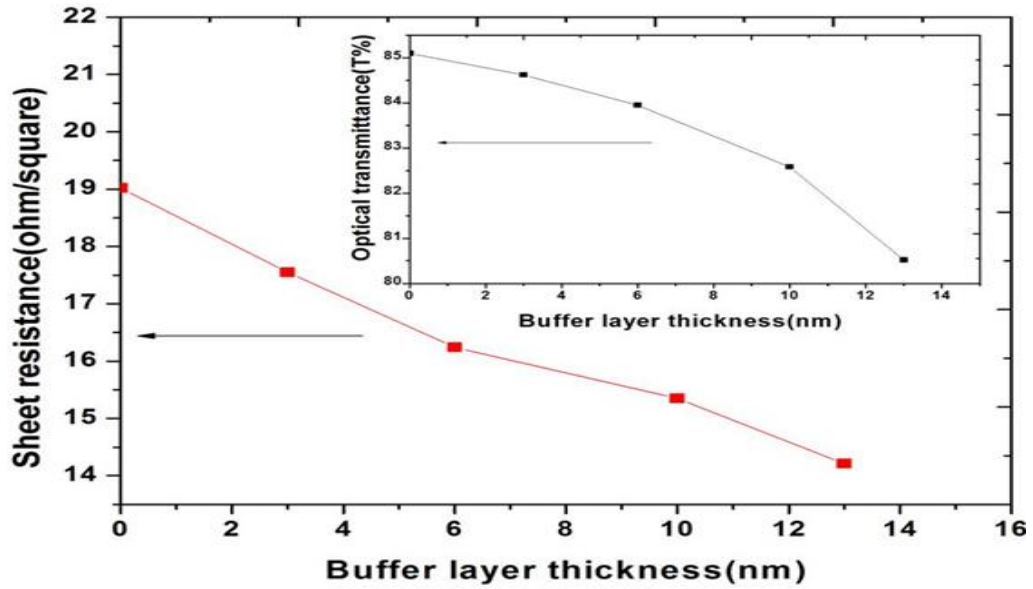


Figure 3.2 (h): Variation of sheet resistance and maximum optical transmittance with buffer layer thickness over FTO surface

**Table -3.2:** Luminance and efficiency characteristics of the devices with different NiO buffer layer thicknesses at the current density of 20 mA/cm<sup>2</sup>.

S.N	NiO thickness	Luminance (cd/m <sup>2</sup> )	Turn-on voltage(volt)	Luminous efficiency (cd/A)	Sheet resistance of bilayer anode	Optical transmittance of bilayer anode
1	0nm	938	11.4	4.69	19.02	85.10%
2	3nm	1018	6.2	5.12	17.55	84.62%
3	6nm	1282	6.8	6.35	16.24	83.95%
4	10nm	1471	7.6	7.32	15.35	82.58%

5	13nm	824	9.8	4.10	14.21	80.52%
---	------	-----	-----	------	-------	--------

Thus the turn-on voltage of 3nm, 6nm,10nm, and 13nm is to be lower than that of the device without the buffer layer. However, there is a tendency that the turn-on voltage increases with the growth of buffer layer thickness. This situation is linked to the larger voltage dropped across the oxide buffer layer [252]. On the other hand performance of the OLED is highly dependent on the surface morphology of electrode surface. For that purpose, we analyzed the surface morphology of both the single and double layer of FTO surface and is carried out with the help of FE- SEM images, which are given in figure 3.2 (i) and 3.2 (j) respectively.

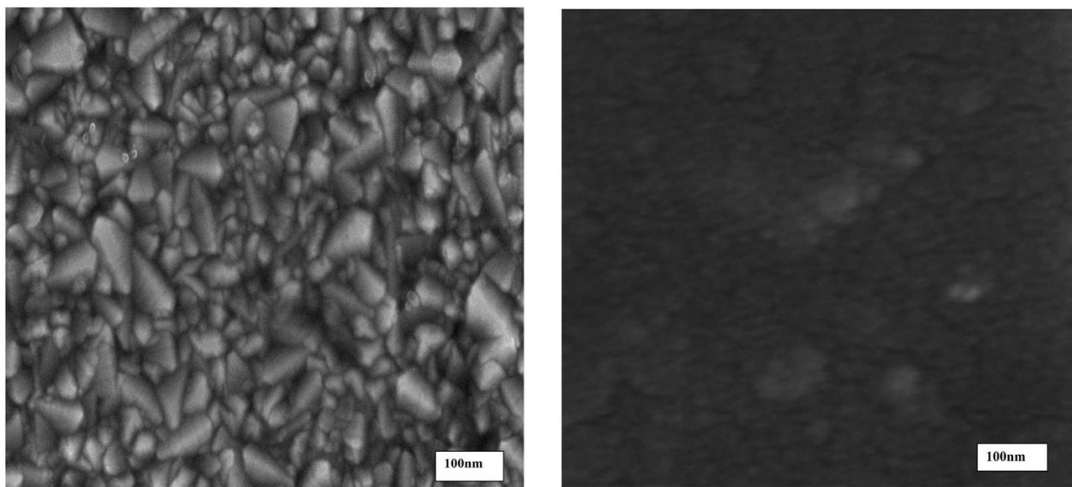


Figure 3.2 (i): FE-SEM images of bare FTO surface      Figure 3.2 (j): FE-SEM images of FTO+NiO surface



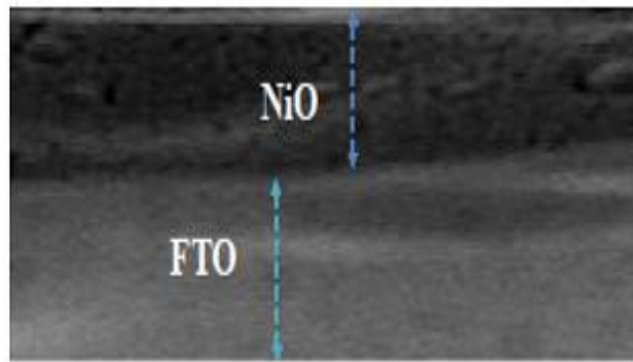


Figure 3.2 (k): A crosssectional view of Nickel oxide layer over FTO surface

From the study of SEM images, it is found that the surface of bilayer anode became smoother compared to the single anode due to the presence of the oxide layer. This provides a uniform field distribution over the entire anode region and also reduces the probability of the formation of the non-emissive area in the active region. It implies a better contact of anode surface to the organic layer. We also provide a cross-sectional view of the FE-SEM images of nickel oxide layer over an FTO surface as shown in figure 3.2 (k). From this figure, it is clear that there is a homogeneous film of NiO buffer layer is obtained over FTO surface without any presence of sharp tips or spikes inside this buffer layer. Therefore, it can be concluded that smooth uniformity of film surface for improving the interface and contact of the buffer layer with organic layer is important for the injection and controlling of charge carrier.

### **3.2.5 Conclusion**

1. In this work, we used nickel oxide as a buffer layer which has been systematically studied for FTO based OLED structure.
2. We concluded that too thick NiO films lead to higher turn-on voltage along with lower device efficiency
3. Our result revealed that there is an optimum thickness of nickel oxide at which OLED efficiency is highly enhanced.
4. In this investigation, 10nm NiO buffer layer has resulted in 1.49 times enhancement in current efficiency compared to the single layer FTO anode.

### **3.3 Improve performance of organic light emitting diode using molybdenum trioxide (MoO<sub>3</sub>) interlayer between the electrode and organic interface**

We investigated bottom-emitting organic light emitting diodes (OLEDs) with bi-layer FTO/MoO<sub>3</sub> electrodes. To study the performance of OLED by the hole injection layer, we deposited MoO<sub>3</sub> films at different thicknesses over the FTO surface and studied their **J-V** and **L-V** characteristics. We also carried out the further analysis by measuring sheet resistance, optical transmittance and surface morphology with the FE-SEM images. Finally, we concluded that MoO<sub>3</sub> (9 nm) buffer layer increases the efficiency of FTO based OLED devices within the tunnelling region. Here the maximum value of current efficiency is found to be 7.62 cd/A.

#### **3.3.1 OLEDs fabrication:**

The OLEDs in the bottom emitting structure with the Alq<sub>3</sub> as an active layer and FTO+MoO<sub>3</sub> as bilayer anode configuration were fabricated by the Multiple Pump Down (MPD) method after cleaning the FTO coated glass substrates. In every deposition, thoroughly cleaned masks were used to achieve the different geometrical patterns. In our work, we carry out the deposition of both inorganic and organic layer under a high vacuum chamber unit having vacuum better than  $8 \times 10^{-6}$  Torr. Sheet resistance and optical transmittance of bilayer anode structures are taken by four probe resistivity measurement and UV-VISIBLE double beam spectrophotometer unit. The current-voltage and luminance-voltage characteristics of the fabricated devices were measured by digitally controlled source-meter and luminance meter unit.

### 3.3.2 Schematic representation and energy level alignment diagram:

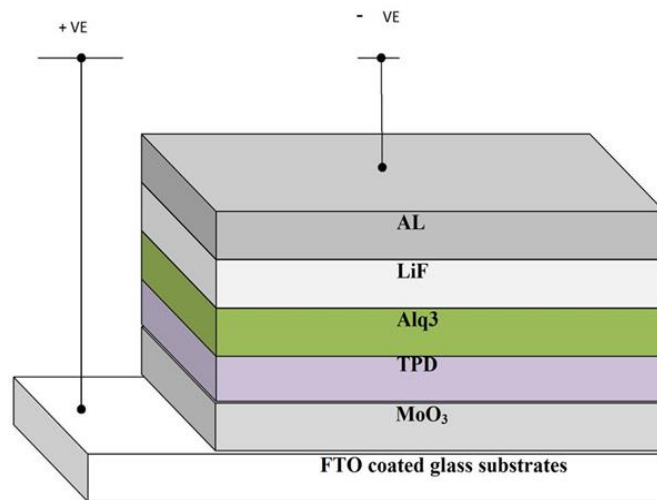


figure 3.3 (a) Schematic representation of OLED structure

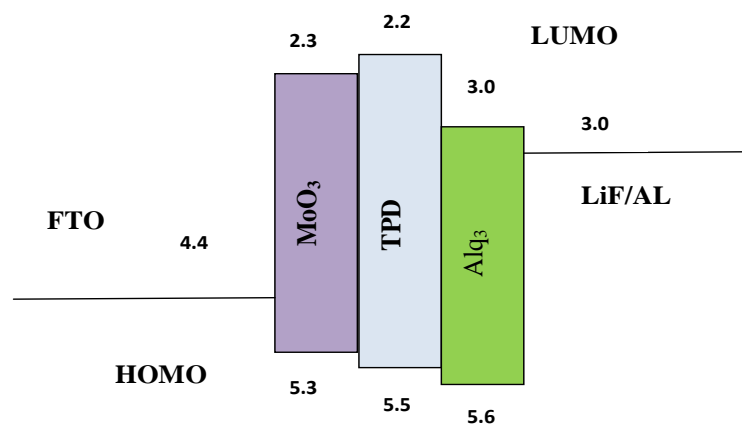


Figure 3.3 (b): Energy band structure of OLED device

### 3.3.3 Result and discussion

The output characteristics of all the OLED devices with buffer thickness of 4nm, 7nm, 9nm and 11nm are discussed in this section. The structures of the bottom light emitting OLEDs used in this study are given below:

Device: 1. FTO/ MoO<sub>3</sub> (0nm)/ TPD (36nm)/Alq<sub>3</sub> (45nm)/Lif(5nm)/Al (100nm)

Device: 2. FTO/MoO<sub>3</sub> (4nm)/TPD (36nm)/Alq<sub>3</sub> (45nm)/Lif(5nm)/Al (100nm)

Device: 3. FTO/MoO<sub>3</sub> (7nm)/TPD (36nm)/Alq<sub>3</sub> (45nm)/Lif(5nm)/Al (100nm)

Device: 4. FTO/MoO<sub>3</sub> (9nm)/TPD (36nm)/Alq<sub>3</sub> (45nm)/Lif(5nm)/Al (100nm)

Device: 5. FTO/MoO<sub>3</sub> (11nm)/TPD (36nm)/Alq<sub>3</sub> (45nm)/Lif(5nm)/Al (100nm)

The J-V-L characteristics of OLED devices having configuration FTO/ MoO<sub>3</sub> (varying thickness) /TPD (36 nm) /Alq<sub>3</sub> (45 nm) /Lif (5nm) /Al (100 nm) are given in Fig 3.3 (c) and 3.3 (d) respectively. Our observation shows that the presence of interlayer has a direct effect of blocking the hole current by controlling the flow of positive charge carrier towards the organic layer. In our work, we found that the device with 9nm buffer layer provides the maximum device efficiency of 7.62Cd/A compared to the other OLED devices. Thus it is clear that the current efficiency value is increased compared to the device without a buffer layer (4.01 Cd/A). Due to the high thickness of buffer layer, there is a gradual decrease of luminance and increase of device efficiency is observed. This is due to the proper balancing of

charge carrier injection. Therefore it is understood that the presence of MoO<sub>3</sub> interlayer enhanced the device

efficiency by blocking the hole injection. This oxide buffer layer also prevents the diffusion of oxygen and metallic ion into the organic layer from the anode and hence reduces the possibility of an electrical breakdown of the OLED device. From the earlier report, it is clear that the mobility of electron is always lower in the electron transport layer (ETL) than the mobility of holes in the hole transport layer (HTL) [251]. Because of which there is always positive charge carrier accumulation is taking place near the interface region of HTL/ETL layer. So, Here we balance the mobility of positive charge carrier by inserting a thin buffer layer between the FTO and TPD layer. Therefore the buffer can increase the probability of electron-hole pair recombination by preventing the accumulation of excess holes in the luminance layer. From the characteristics graphs, it is clear that efficiency of the devices is found to be increased continuously although the current density and the luminance value of the devices decrease with increasing interlayer thickness. In our work optimized result of the device is found to be at the thickness of 9nm oxide buffer layer. After this critical thickness of the buffer layer efficiency of the device is decreased considerably due to more reduction of charge tunnelling mechanism at the higher thickness.

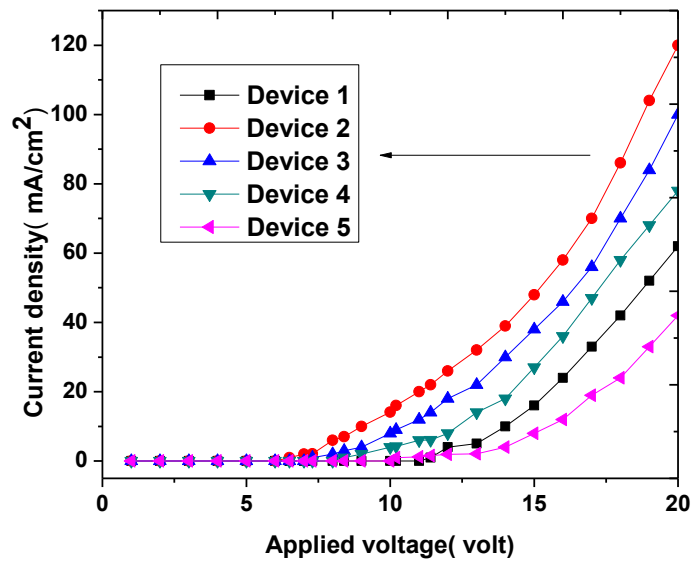


Figure 3.3 (c): Graph of applied voltage vs. current density

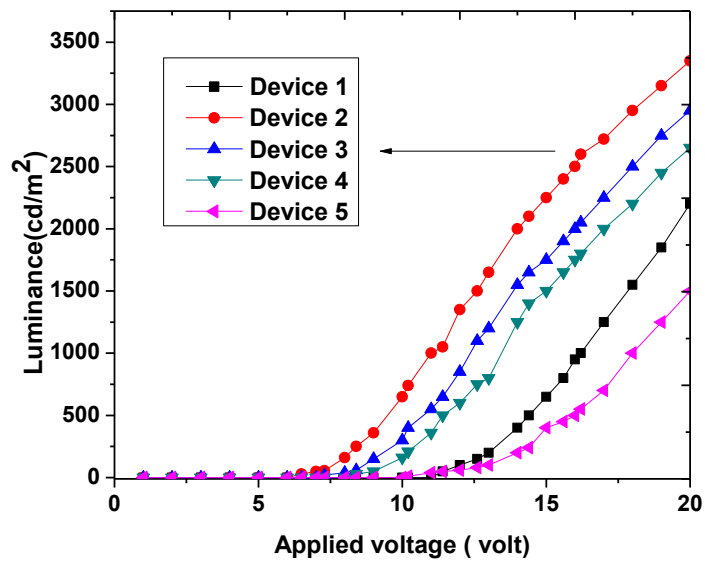


Figure 3.3 (d): Graph of applied voltage vs luminance

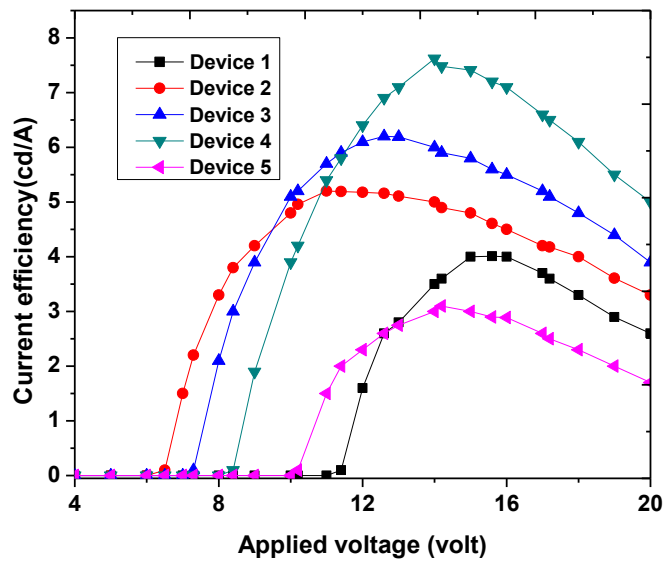


Figure 3.3 (e): Graph of applied voltage vs. current efficiency

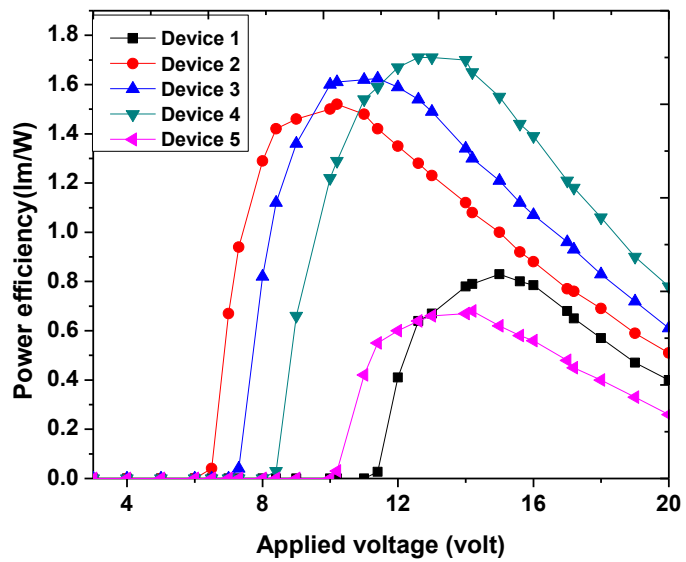


Figure 3.3 (f): Graph of applied voltage vs power efficiency



Figure 3.3 (e) represents the current efficiency and voltage characteristics of the OLED devices. From this figure, it is clear that device 4 shows the maximum efficiency and whereas device 5 has the lowest efficiency. This situation is directly linked to the proper charge injection process from electrode to the organic layer. Similarly, the variation of power efficiency vs voltage characteristics for all the devices is also shown in figure 3.3 (f) in which device 4 shows the highest value where the maximum charge balancing is achieved. The variation of optical transmittance and sheet resistance with different thickness of oxide layer over FTO film is given in figure 3.3 (g). The following table shows the summary of the result of five OLED devices along with the electrical and optical properties with different bilayer anode combination.

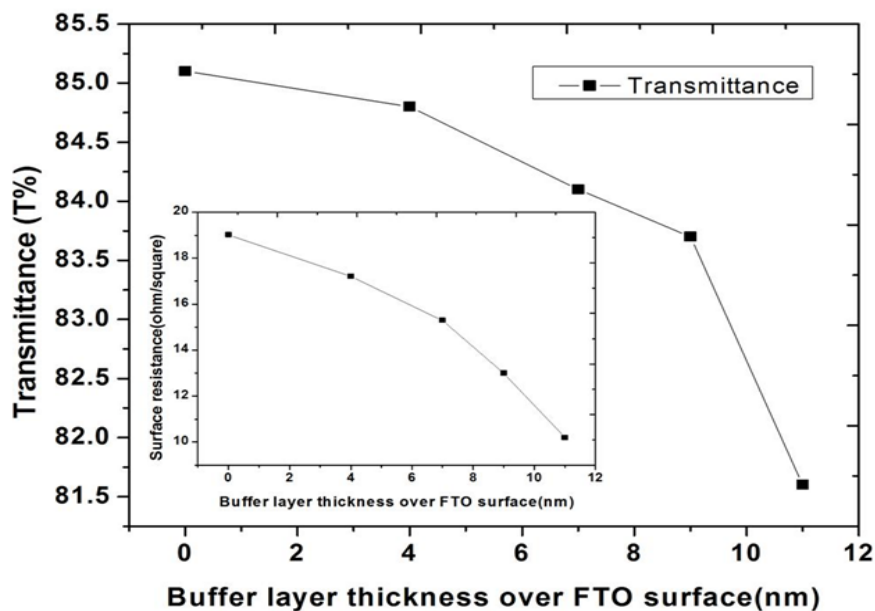


Figure 3.3 (g): Variation of optical transmittance and sheet resistance over FTO surface

**Table -3.3:** Luminance and efficiency characteristics of the devices with different MoO<sub>3</sub> buffer layer thicknesses at the current density of 20 mA/cm<sup>2</sup>.

S.N	MoO <sub>3</sub> thickness	Luminance (cd/m <sup>2</sup> )	Turn-on voltage(volt)	Luminous efficiency (cd/A)	Standard deviation of current efficiency(cd/A )	Standard deviation of power efficiency(lm/W)
1	0nm	800	11.2	4.01	1.72	0.34
2	4nm	1000	6.5	5.2	1.52	0.38
3	7nm	1100	7.3	6.2	2.02	0.51
4	9nm	1400	8.4	7.62	2.84	0.63
5	11nm	550	10.1	2.89	1.26	0.27

From this table, it is observed that the turn-on voltage of 4nm, 7nm, 9nm, and 11nm is to be lower than that of the device without the buffer layer. However, there is a tendency that the turn-on voltage increases with the growth of buffer layer thickness. This situation is linked to the larger voltage dropped across the oxide buffer layer [252]. On the other hand performance of the OLED is highly dependent on the surface morphology of electrode surface. For that purpose we analyzed the surface morphology of both the single and double layer of FTO surface and is carried out with the help of FE- SEM images, which are given in figure 3.3 (h) and 3.3 (i) respectively.

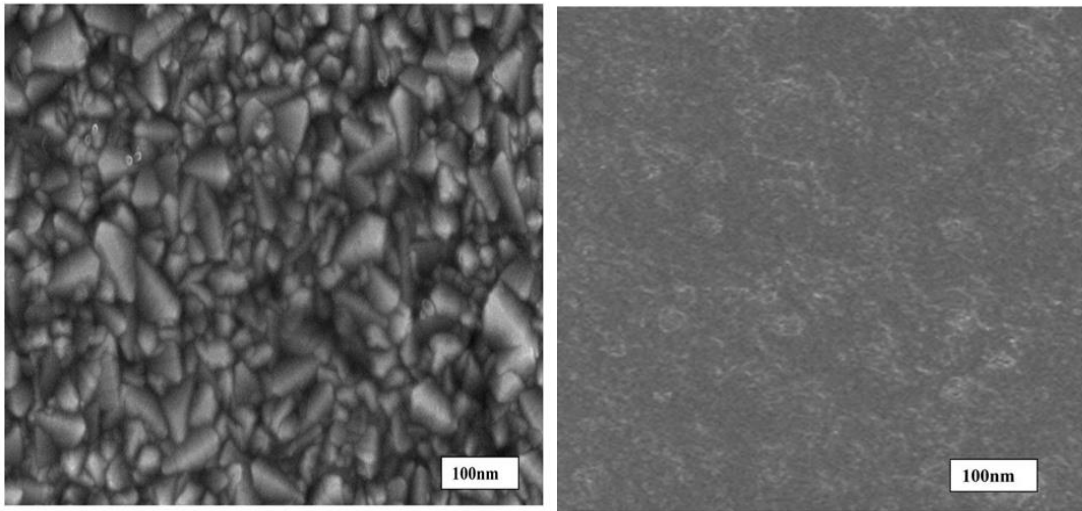


Figure 3.3 (h): FE-SEM images of bare FTO surface      Figure 3.3 (i): FE-SEM images of the FTO+MoO<sub>3</sub> surface

From the study of SEM images, it is found that the surface of bilayer anode became smoother compared to the single anode due to the presence of the oxide layer. This provides a uniform field distribution over the entire anode region and also reduces the probability of the formation of the non-emissive area in the active region. It implies a better contact of anode surface to the organic layer. Therefore, it can be concluded that smooth uniformity of film surface for improving the interface and contact of the buffer layer with organic layer is important for the injection and controlling of charge carrier.

### **3.3.4 Conclusion**

1. In this work, we used Molybdenum trioxide as a buffer layer which has been systematically studied for FTO based OLED structure.
2. We concluded that too thick MoO<sub>3</sub> films lead to higher turn-on voltage along with lower device efficiency
3. Our result revealed that there is an optimum thickness of oxide layer at which OLED efficiency is highly enhanced.
4. In this investigation, the 9nm buffer layer has resulted in enhancement in current efficiency compared to the single layer FTO anode.

### **3.4 Performance improvement of organic light emitting diode using tungsten oxide (WO<sub>3</sub>) interlayer between the electrode and organic interface**

Here in this work we fabricated bottom emitting FTO based organic light-emitting diodes (OLEDs) with bilayer FTO/WO<sub>3</sub> electrode. Compared with those of a device without a buffer layer of WO<sub>3</sub> the current and power efficiency were highly enhanced in a device with a 12nm MoO<sub>3</sub> hole injection layer inserted. To study the performance of OLED by the hole injection layer, we deposited WO<sub>3</sub> films at different thicknesses over the FTO surface and studied their **J-V** and **L-V** characteristics. We also carried out the further analysis by measuring sheet resistance, optical transmittance and surface morphology with the FE-SEM images. Finally, we concluded that WO<sub>3</sub> (12 nm) buffer layer increases the efficiency of FTO based OLED devices within the tunnelling region. Here the maximum value of current efficiency is found to be 8.42 cd/A.

#### **3.4.1 Fabrication of the OLEDs**

The OLEDs in the bottom emitting structure with the Alq<sub>3</sub> as an active layer and FTO+WO<sub>3</sub> as bilayer anode configuration were fabricated by the Multiple Pump Down (MPD) method after cleaning the FTO coated glass substrates. In every deposition, thoroughly cleaned masks were used to achieve the different geometrical patterns. Initial substrates cleaning and the cleaning of the unit and masks after each deposition achieved by the procedure as mention in above section 3.1.1.

Here we also used aluminium as a cathode layer which was evaporated using tungsten helix filament while the thin layer of tungsten oxide ( $\text{WO}_3$ ) was evaporated using a tungsten basket. In our work, we carry out the deposition of both inorganic and organic layer under a high vacuum chamber unit having vacuum better than  $6 \times 10^{-6}$  Torr. Sheet resistance and optical transmittance of bilayer anode structures are taken by four probe resistivity measurement and UV-VISIBLE double beam spectrophotometer unit. The current-voltage and luminance-voltage characteristics of the fabricated devices were measured by digitally controlled source-meter and luminance meter unit. Here we collected all the materials from Sigma-Aldrich Company and used without further purification. In our work active area of the samples was  $3 \times 6 \text{ mm}^2$  and thickness of the thin film was confirmed by the profilometer set up as mentioned in section 2.7.1(b).

### 3.4.2 Schematic representation and energy level alignment diagram:

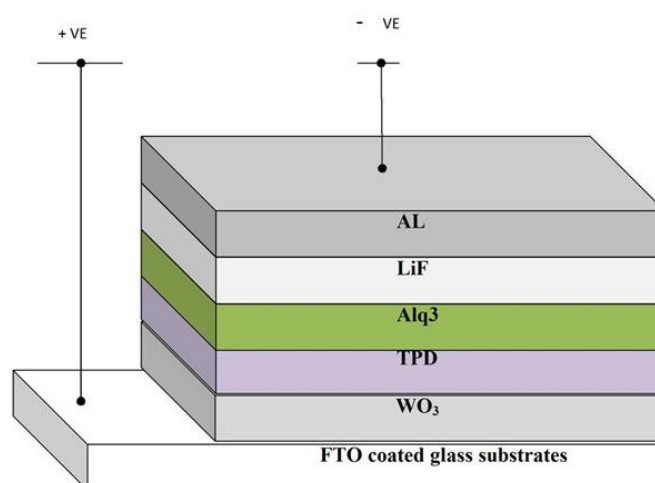


Figure 3.4 (a) Schematic representation of OLED structure

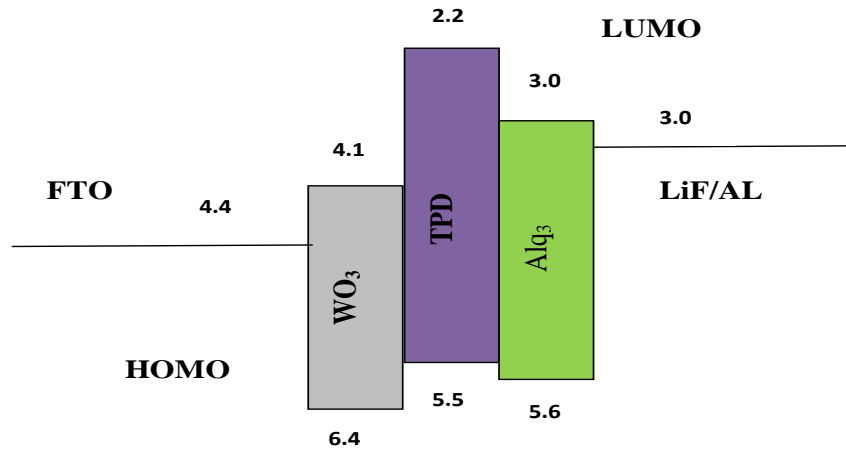


Figure 3.4 (b): Energy band structure of OLED device

### 3.4.3 Result and discussion

The output characteristics of all the OLED devices with buffer thickness of 4nm, 8nm, 12nm, and 16nm are discussed in this section. The structures of the bottom light emitting OLEDs used in this study are given below:

Device: 1. FTO/ WO<sub>3</sub> (0nm)/ TPD (30nm)/Alq<sub>3</sub> (45nm)/Lif(5nm)/Al (120nm)

Device: 2. FTO/WO<sub>3</sub> (4nm)/TPD (30nm)/Alq<sub>3</sub> (45nm)/Lif(5nm)/Al (120nm)

Device: 3. FTO/WO<sub>3</sub> (8nm)/TPD (30nm)/Alq<sub>3</sub> (45nm)/Lif(5nm)/Al (120nm)

Device: 4. FTO/WO<sub>3</sub> (12nm)/TPD (30nm)/Alq<sub>3</sub> (45nm)/Lif(5nm)/Al (120nm)

Device: 5. FTO/WO<sub>3</sub> (16nm)/TPD (30nm)/Alq<sub>3</sub> (45nm)/Lif(5nm)/Al (120nm)

Following figure 3.4 (c) represents the transmittance spectra of bilayer anode for the  $\text{WO}_3$  layer over FTO electrode. Here the maximum value of optimized FTO/ $\text{WO}_3$  bilayer anode is higher than 80% (average value of 83.85% within 530-560nm wavelength region) which is a good indicator for transparent electronics. Similarly, the variation of sheet resistance vs thickness of  $\text{WO}_3$  layer over FTO surface is also shown here. This shows a decreasing trend of surface resistance at a higher thickness of buffer layer [253].

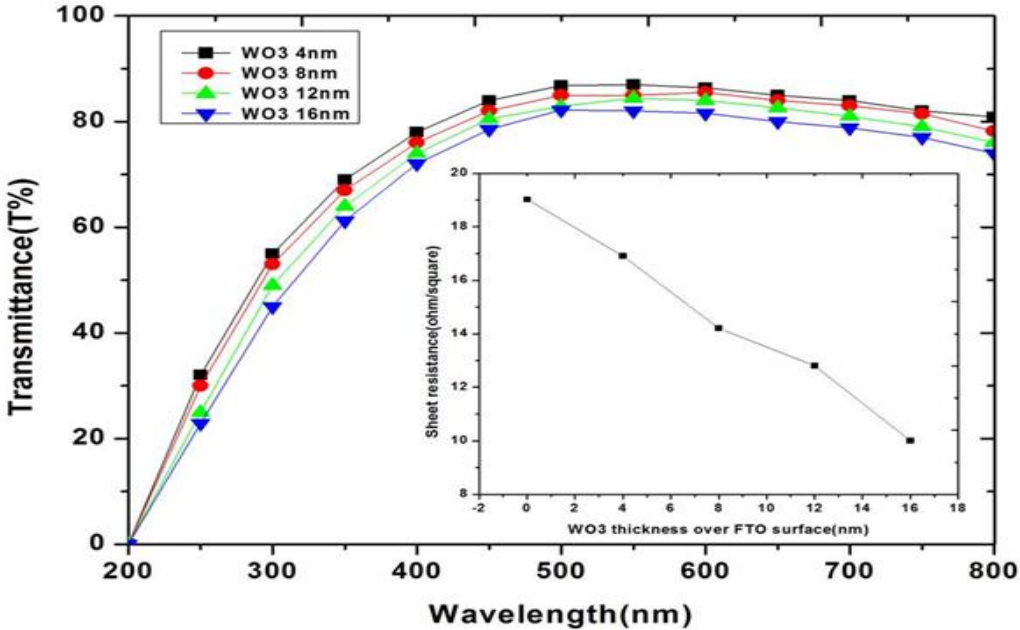


Figure 3.4 (c) Transmission spectrum and sheet resistance of bilayer FTO/ $\text{WO}_3$  film



In this work to study the J-V and L-V characteristics, we varied the operational voltage from 0 to 21 volt. It was found that OLEDs with a WO<sub>3</sub> layer at 12 nm thickness have relatively higher performance at the same applied voltage compared with other devices. Maximum device efficiency is found to be 8.41 cd/A provided by the device 4. Therefore, current efficiency increases compared to the device without a buffer layer (3.80 Cd/A). This improvement in efficiency is because of the proper balancing of charge carrier injection from electrode side to the organic layers. Output characteristics of all the devices are shown below:

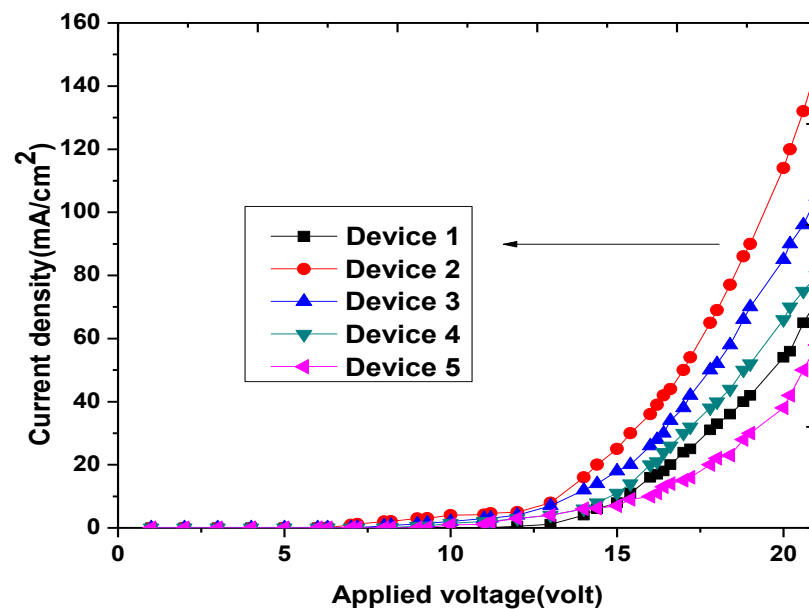


Figure 3.4(d): Graph of applied voltage vs current density

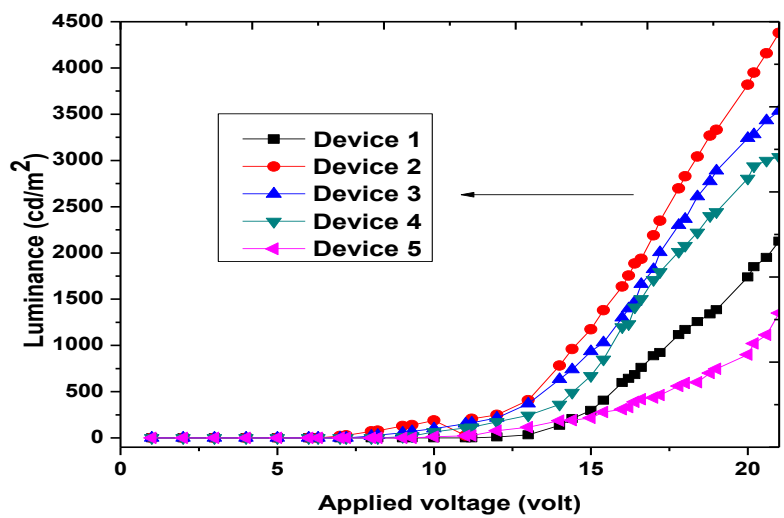


Figure 3.4 (e): Graph of applied voltage vs. luminance

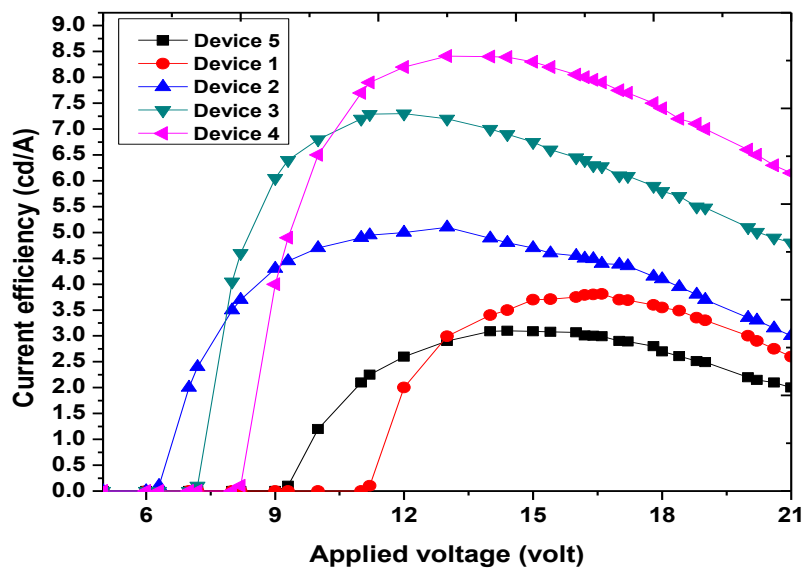


Figure 3.4 (f): Graph of applied voltage vs current efficiency

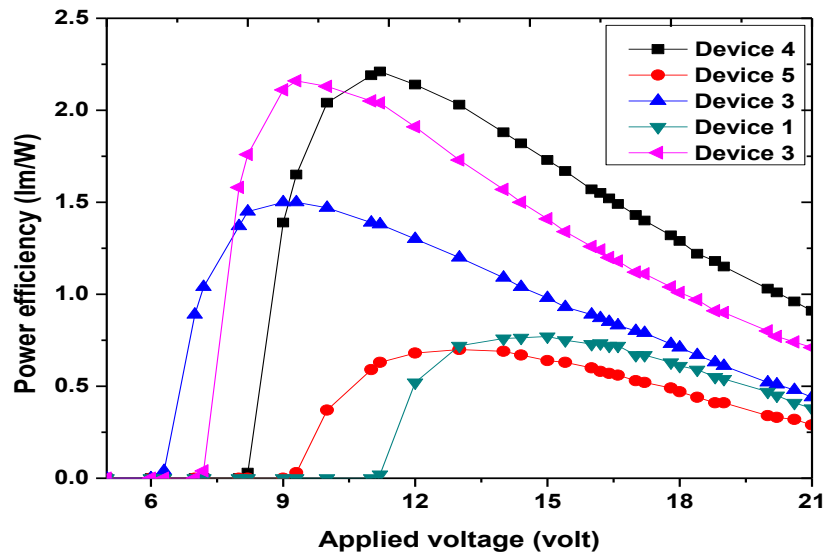


Figure 3.4 (g): Graph of applied voltage vs. power efficiency

From the above characteristics graph, it is clear that device 4 shows the maximum efficiency and whereas device 5 has the lowest efficiency. This situation is directly linked to the proper charge injection process, i.e., exciton formation probability. When the thickness is very low, the charge balancing process is slightly enhanced. However, when we increase the thickness, then this process tends to more enhance because of which we get better device efficiency in our devices. This effect is maximum at the optimized thickness of 12nm (device 4) where we get the highest efficiency of 8.41 cd/A. This implies that at a 12nm thickness of buffer layer, there is more balance of positive charge injection w.r.t. negative charge from the anode side of the device. However, after the optimized thickness, efficiency became decreases. This is due to the reducing of charge carrier tunneling at a higher thickness of the buffer layer from

the electrode to the hole transport layer. On the other hand, the variation of power efficiency vs. applied voltage characteristics for all the devices is shown in figure 3.4 (g) in which device 4 shows the highest value where the maximum balance of holes and electron injection takes place. Following table shows the summary of the result of five OLED devices along with their standard value (which is a measure of the spread of their efficiency in a set of data at different voltages from their mean value).

**Table -3.4:** Luminance and efficiency characteristics for the devices with different buffer layer thicknesses at the current density of 20 mA/cm<sup>2</sup>

<b>S.N</b>	<b>Buffer layer thickness</b>	<b>Luminance (cd/m<sup>2</sup>)</b>	<b>Turn-on voltage(volt)</b>	<b>Luminous efficiency (cd/A)</b>	<b>Sheet resistance of bilayer anode</b>	<b>Standard deviation value of current efficiency</b>
<b>1</b>	0nm	<b>762</b>	<b>11.2</b>	<b>3.81</b>	<b>19.02</b>	<b>0.830</b>
<b>2</b>	4nm	<b>960</b>	<b>6.3</b>	<b>4.80</b>	<b>16.90</b>	<b>1.050</b>
<b>3</b>	8nm	<b>1030</b>	<b>7.2</b>	<b>7.31</b>	<b>14.20</b>	<b>1.150</b>
<b>4</b>	12nm	<b>1640</b>	<b>8.2</b>	<b>8.40</b>	<b>12.80</b>	<b>1.350</b>
<b>5</b>	16nm	<b>560</b>	<b>9.3</b>	<b>2.80</b>	<b>10.01</b>	<b>0.694</b>

From this table, it is seen that the turn-on voltage of 4nm, 8nm, and 12nm is to be lower than that of the device without a buffer layer. However, there is a tendency that the turn-on voltages are increased with the increasing of anode layer thicknesses. This is due to the relatively weak modulation of the internal electric field, and hence the larger voltage is dropped across the buffer layer [252]. Also when the thickness is increased to 16 nm of the buffer layer, both the value of luminance and luminance efficiency is found to be decreased due to more reduction of a tunnelling mechanism.

The modification of the electrode/organic interface by the insertion of a thin layer of  $\text{WO}_3$  prevent the direct contact of the metal electrode with the organic TPD layer and thus preventing the unfavourable chemical reactions between organic and the electrode surface.

Also after the insertion of the  $\text{WO}_3$  layer over FTO electrode, the surface becomes smoother which is necessary for the achievement of a good OLED device and also for providing better contact with organic TPD layer. The surface morphology of both the single and double layer of FTO film is shown in figure 3.4 (h) and figure 3.4 (i) respectively.

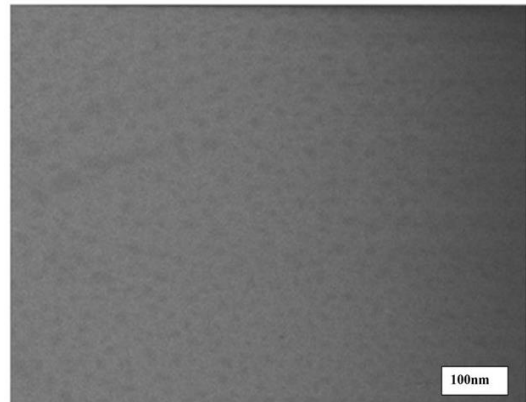
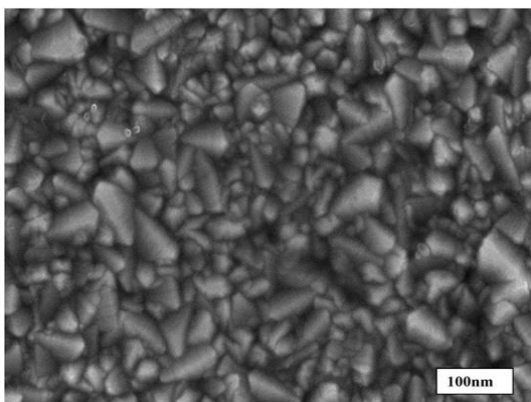


Figure 3.4 (h): FE-SEM images of bare FTO surface      Figure 3.4 (i): FE-SEM images of the FTO+WO<sub>3</sub> surface

From the above figures, it is clear that the presence of oxide buffer layer smooths the anode surface by uniformly distributing the whole rough surface region with minimizing surface traps and spikes. This lead to a more homogeneous adhesion of the hole-transporting layer over the entire anode surface. This is an important reason for reducing the contact resistance and hence the bulk resistance of the device. Because of which we get the better device efficiency when bias is applied within the tunnelling region.

### **3.4.4 Conclusion**

1. In summary, after the above investigation, our results demonstrate an organic electro-luminance device on bilayer anode in which the maximum efficiency is found to be 8.41 cd/A at the optimized thickness of 12nm WO<sub>3</sub> interlayer.
2. This result is found to be better than single layer anode under the same condition of operation.
3. Also, we concluded that thick buffer layer leads to high turn-on voltage along with decreasing the current efficiency of the OLED devices.
4. In this case, the optimum thickness of 12 nm WO<sub>3</sub> buffer layer has resulted in 2.20 times enhancement in current efficiency compared to the single layer FTO device.
5. From the above discussion we finally concluded that the performance of bilayer anode based OLED is higher compared with the single anode based device and in our work, the highest value of device efficiency is found to be FTO+WO<sub>3</sub> based device.

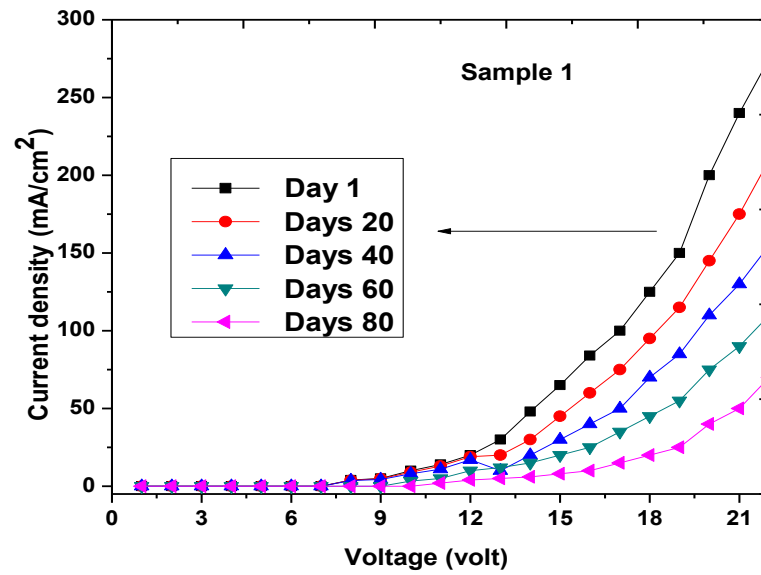
This is due to the higher value of work function of  $\text{WO}_3$  which more influenced the charge balancing tendency within the active layer region.

### 3.5 Stability of the devices

To assess the stability of the devices, all the OLED samples were stored in thoroughly cleaned desiccators (charged with fused  $\text{CaCl}_2$ ) and then the readings were noted after certain intervals of time periods in the ambient atmosphere under dark room conditions. After taking the readings, samples were again left inside the desiccators for a particular time interval. Thus in this manner, we noted the readings after 20 days, 40 days, 60 days and 80 days. The current density was found to decrease gradually with time as shown in figure 3.5 (a)-(d), for the optimized devices of  $\text{FTO}+\text{V}_2\text{O}_5$  (sample 1),  $\text{FTO}+\text{NiO}$  (sample 2),  $\text{FTO}+\text{MoO}_3$  (sample 3) and  $\text{FTO}+\text{WO}_3$  (sample 4). In the figure, a variation of current density is considered at a different voltage with respect to time. In these figures, current density variation is shown for fresh sample along with their variation after 20 days, after 40 days, after 60 days and after 80 days. The corresponding luminance values are also shown in from figure 3.5 (e)-(h). Similarly, the plots of the maximum current efficiency of the optimized devices versus time are presented in figure 3.5 (i). From this figure it is noted that the current efficiency values vary from 2.83 cd/A to 0.7 cd/A, 7.32 cd/A to 3.2 cd/A, 7.62 cd/A to 3.8cd/A and 8.41 cd/A to 4.1 cd/A respectively for the devices of  $\text{FTO}+\text{V}_2\text{O}_5$ ,  $\text{FTO}+\text{NiO}$ ,  $\text{FTO}+\text{MoO}_3$  and  $\text{FTO}+\text{WO}_3$  based bilayer anode configuration.

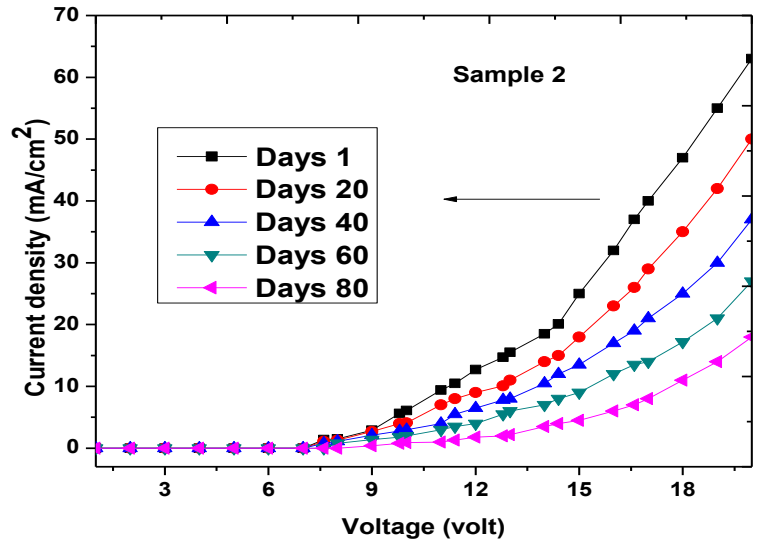
Van Calster and De Vos in 1980 [254] have pointed out the following two phenomena responsible for the low stability of the organic devices.

- (i) Mobile ions in the P-type semiconducting layer which caused a degradation of the device performance.
- (ii) Slow states at the metal/organic interface, which caused attenuation of the device efficiency.

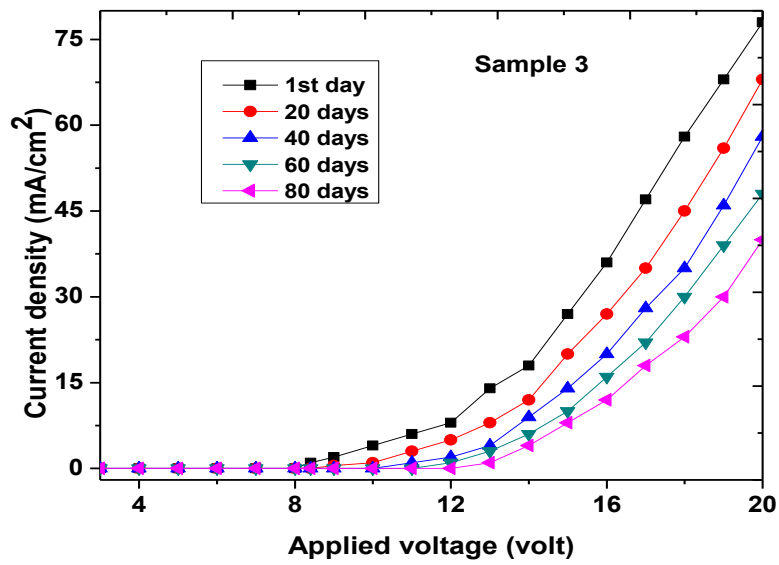


3.5 (a): Variation of current density with time (in days) of FTO+V<sub>2</sub>O<sub>5</sub>

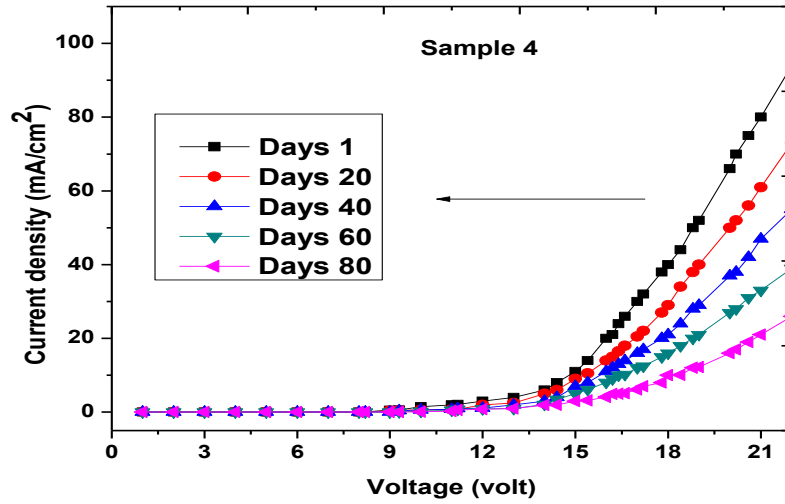




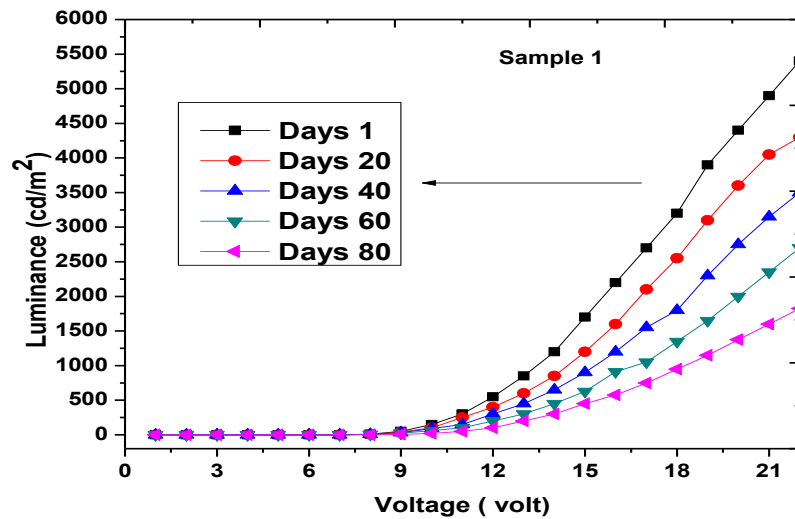
3.5 (b): Variation of current density with time (in days) of FTO+NiO



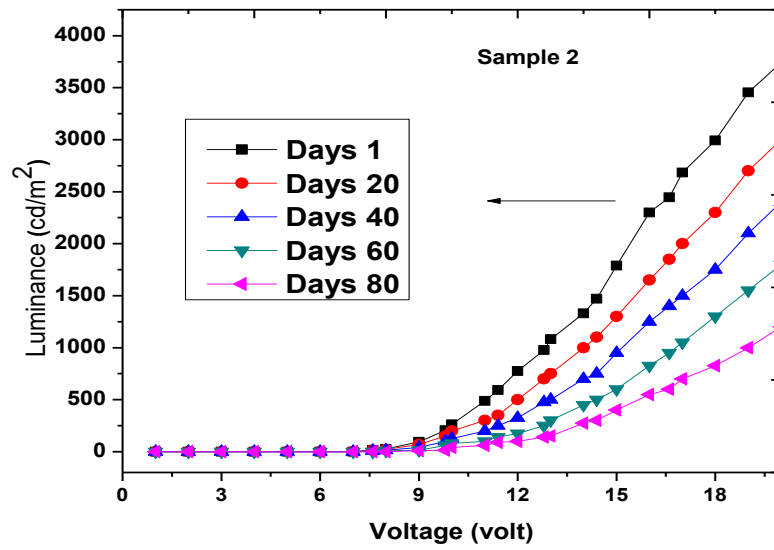
3.5 (c): Variation of current density with time (in days) of FTO+MoO<sub>3</sub>



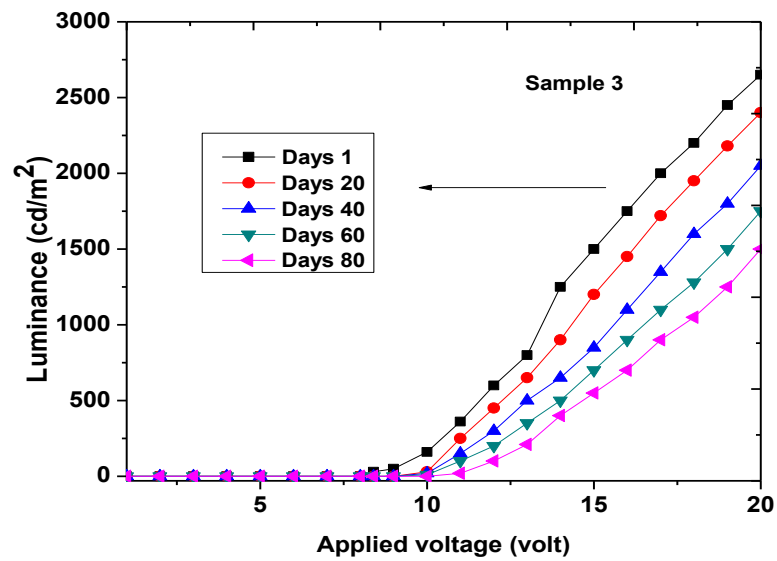
3.5 (d) : Variation of current density with time (in days) of FTO+ WO<sub>3</sub>



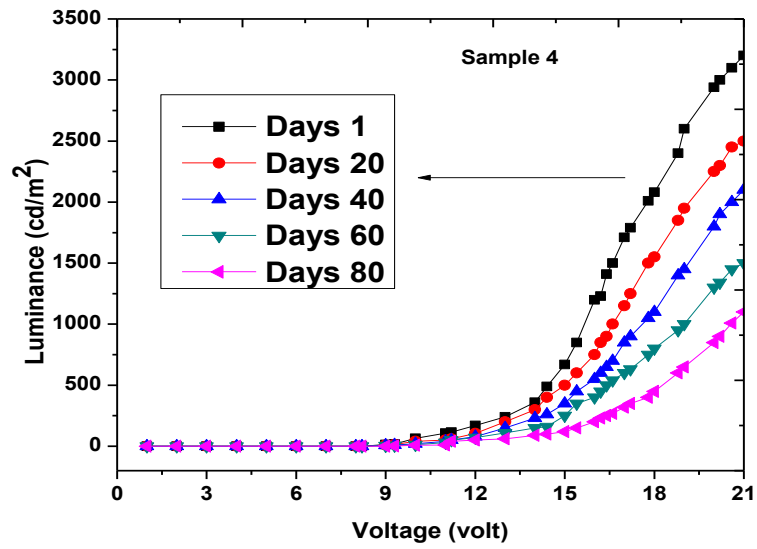
3.5 (e): Variation of luminance with time( in days) of FTO+V<sub>2</sub>O<sub>5</sub>



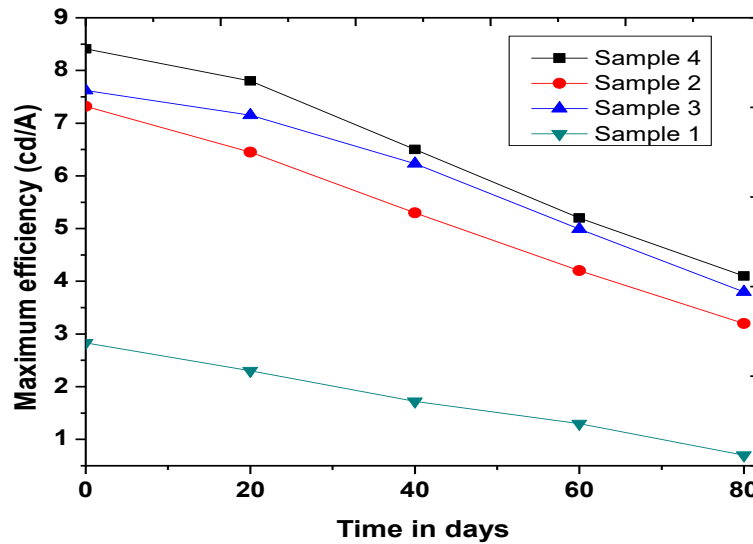
3.5 (f) : Variation of luminance with time( in days) of FTO+NiO



3.5 (g): Variation of luminance with time( in days) of FTO+MoO<sub>3</sub>



3.5 (h): Variation of luminance with time (in days) of FTO+ WO<sub>3</sub>



3.5 (i): Variation of maximum current efficiency vs time in days for four sample

On the other hand, the OLEDs materials used in this investigation though claimed to be 99.9 percent pure by the manufacturer or company, but it may be contaminated with ions, which move through the film under the influence of applied electric field. Typically charge carriers trapping at the interface region occur with evaporated or sputtered irrespective of the OLED material [255]. The existence of large surface state densities arising either due to built-in defect or some other factors often cause a reduction in charge mobility and affect reliability and performances [256]. The trapped charge at the interface region reduced the electric flux density in the semiconductor material. Therefore the increase in density of states over a period would make conductivity modulation less effective.

In the MPD method of OLED fabrication, a layer of air and other atmospheric contaminants might remain trapped in between the semiconductor and the electrode surface. Such a trapped layer might contain sufficient moisture, which would help oxidation of the semiconducting film and contribute towards the attenuation process. During ambient exposure of the semiconductor film foreign contaminants, both neutral and ionized may also enter the interface region. Some contaminants or a layer of air might also be trapped between the substrates and the buffer layer [257]. Again during the period of stability investigation, these impurities might have slightly diffused into the organic layer through the grain boundaries to increase the surface states.

Another influencing factor affecting the OLED performance is the nature of the metal-semiconductor contact. For achieving ideal characteristics, the contacts between the metallic electrode and semiconducting layer should be ohmic. Though aluminium/LiF

is known to make satisfactory ohmic contact with the Alq<sub>3</sub> film, due to the ambient exposure of these bilayer electrodes before their deposition in the present method of fabrication, a thin insulating barrier of air or other contaminants might remain trapped between these two films. Such a barrier would degrade the quality of contact between the Alq<sub>3</sub> and the cathode film, and failure to achieve good ohmic contact would consequently reduce the device performances [258]. On the other hand oxidation of the Al electrode with time is also responsible for degradation of the OLED performance [259]. In our devices, we noted that there is a fluctuation of readings along with the decreasing tendency of efficiency values with respect to time. This indicates that complete deterioration had set in these devices. It is to be noted that no encapsulation was used for the fabricated OLEDs and all the readings were taken at room temperature. Absorption of the little amount of moisture from the atmosphere during the fabrication process (i.e., MPD) and characterization as pointed out by Erskine and Cserhati [260] is also responsible for the devices degradation. The sensitivity of the OLED materials towards humidity leads to the early collapse of the devices. Chan and Hill [261] observed that the electrical properties of the thin film were unstable when the films were exposed to the atmosphere. The decrease in conductance is a result of conduction charge being captured by oxygen atoms physically absorbed on the surface. As this process continues, a depletion layer is formed, and an electrical potential is established between the negative oxygen ions on the surface and the ionized donors. This limits the arrival of charge carrier at the surface. W.J.Kim et al. study the long-term stability of thin film based organic devices encapsulated with transparent SnO<sub>2</sub> [262]. They observed that the electrical properties

of the organic film were unstable when the films were exposed to the atmosphere. Instability of organic thin film devices is caused by ambient gases such as moisture (H<sub>2</sub>O) [262] and Oxygen [263]. The decrease in conductance is a result of conduction charge being captured by oxygen atoms physically absorbed on the surface.

All the above factors discussed here are responsible for degradation of the device characteristics.

### **3.6 Observations**

(i) 12 samples (4 samples per batch ) of each bilayer anode structure OLEDs were fabricated using the proper thickness of different organic and inorganic layers with definite patterns since the masks were mechanically obtained.

(ii) The variation of current density and luminance with applied voltage was not found to be same in all the fabricated devices. Although similar nature of diode behaviour is observed in each of the fabricated devices, the maximum device efficiency was found to be in FTO/WO<sub>3</sub> bilayer anode structure based OLED device. This result is due to the higher work function value of the WO<sub>3</sub> layer which brings the energy level alignment more deeply with respect to TPD layer compared to another set of bilayer anode structure. As a result charge balancing process is more enhanced. Therefore

despite this similar diode nature of the characteristics, about each variety was observed.

(iii) Device performance is highly depending on the fabricated condition of deposition layers. Therefore making the time of exposure of thin film layers to the ambient, before deposition of the device as small as possible.

### **3.7 Conclusions**

(i) OLEDs with the bilayer anode combinations FTO+V<sub>2</sub>O<sub>5</sub>, FTO+NiO, FTO+MoO<sub>3</sub>, and FTO+WO<sub>3</sub> could be realized by the Multiple Pump Down (MPD) method.

(ii) Compared to single layer anode based OLEDs, the performance of bilayer anode OLEDs is found to be better. Because when we placed the buffer layer between the anode and hole transport layer, then there is a high tendency for the positive charge carrier to inject into the organic layer from a high energy level compared with that without any buffer layer. This interlayer also prevents the diffusion of the metallic ion into the organic layer from the anode and hence reduces the probability of an electrical breakdown of the device.

(iii) Among the above four bilayer anode combinations, the FTO+WO<sub>3</sub> structure provides the better device efficiency. This may be due to the higher value of work function, for which the energy level alignment of interface layer more suitably occurs with respect to the hole transport layer along with better hole injection tendency compared to other bilayer anode configurations.



(iv) Surface states and charge trapping near the grain boundary region are believed to play a major role in the ultimate device deterioration. Some built-in-defects which are liable to creep in the devices manufactured by MPD method are also responsible for the device degradation. Therefore in this respect, SPD might be more useful for the devices.

(v) Suitable encapsulation would resist atmospheric moisture from entering into the device, and thus the process of degradation would be reduced.

## **Chapter 4**

*A study of the effect of single and double layer anode structure regarding the performance of organic light emitting diode (OLED) using inorganic-organic bilayer anode combinations*

## **4.1) Effect of Pentacene interlayer between the electrode and organic interface of organic light emitting diode**

We investigated bottom-emitting organic light emitting diodes (OLEDs) with bi-layer FTO/ Pentacene electrodes. To study the performance of OLED by the hole injection layer, we deposited pentacene films at different thicknesses over the FTO surface and studied their **J-V** and **L-V** characteristics. Further analysis is carried out by measuring sheet resistance, optical transmittance and surface morphology with the FE-SEM images. Finally, we concluded that Pentacene (10 nm) buffer layer increases the efficiency of FTO based OLED devices within the tunnelling region. Here the maximum value of current efficiency is found to be 4.10 cd/A.

### **4.1.1 OLEDs fabrication**

The OLEDs in the bottom emitting structure with the Alq<sub>3</sub> as an active layer and FTO+Pentacene as bilayer anode configuration were fabricated by the Multiple Pump Down (MPD) method. In every deposition, thoroughly cleaned masks were used to achieve the different geometrical patterns. In our work, we carry out the deposition of both inorganic and organic layer under a high vacuum chamber unit having vacuum better than  $5 \times 10^{-6}$  Torr. Sheet resistance and optical transmittance of bilayer anode structures are taken by four probe resistivity measurement and UV-VISIBLE double beam spectrophotometer unit. The current-voltage and luminance-voltage characteristics of the fabricated devices were measured by digitally controlled source-meter and luminance meter unit.

#### 4.1.2 Schematic representation and energy level alignment diagram:

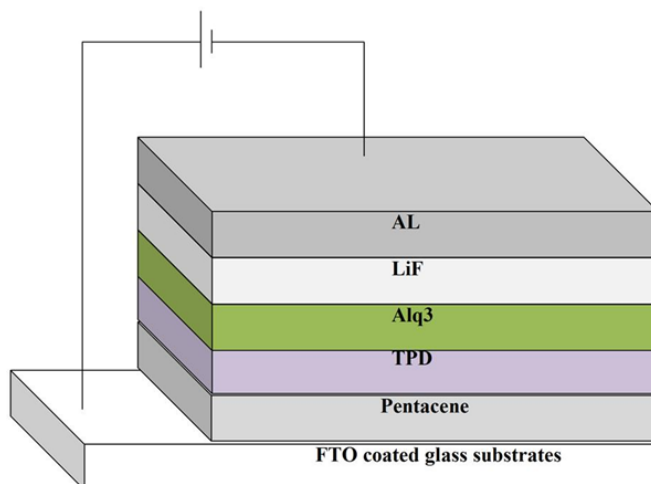


Figure 4.1 (a) Schematic representation of OLED structure

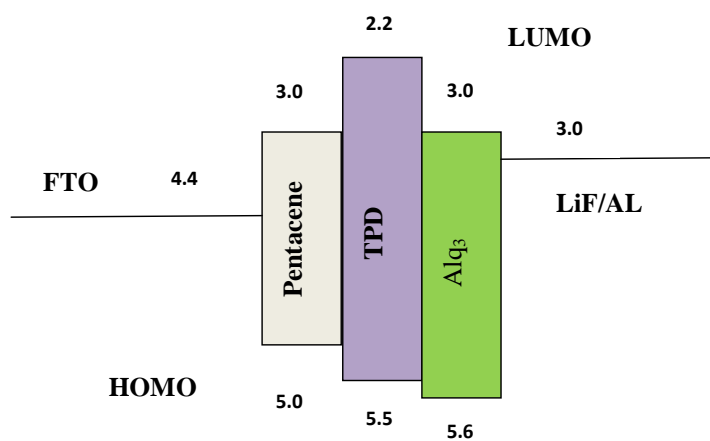


Figure 4.1 (b): Energy band structure of OLED device

### 4.1.3 Result and discussion

The output characteristics of all the OLED devices with buffer thickness of 4nm, 7nm, 9nm and 11nm are discussed in this section. The structures of the different set of bilayer anodes used in this study are as follows:

Set 1. FTO/Pentacene (0nm)

Set 2. FTO/Pentacene (4nm)

Set 3. FTO/Pentacene (7nm)

Set 4. FTO/Pentacene (10nm)

Set 5. FTO/Pentacene (14nm)

The J-V-L characteristics of OLED devices having configuration FTO/ Pentacene (varying thickness) /TPD (40 nm) /Alq3 (45 nm) /Lif (4nm) /Al (110 nm) are given in Fig 4.1 (c) and 4.1 (d) respectively. Our observation shows that the presence of interlayer has a direct effect of blocking the hole current by controlling the flow of positive charge carrier towards the organic layer. In our work, we found that the device with 9nm buffer layer provides the maximum device efficiency of 4.12Cd/A compared to the other OLED devices. Thus it is clear that the current efficiency value is increased compared to the device without a buffer layer (2.3 Cd/A). Due to the high thickness of buffer layer, there is a gradual decrease of

luminance and increase of device efficiency is observed. This is due to the proper balancing of charge carrier injection. Therefore it is understood that the presence of interlayer enhanced the

device efficiency by affecting the hole injection. This organic buffer layer also prevents the diffusion of oxygen and metallic ion into the organic layer from the anode and hence reduces the possibility of an electrical breakdown of the OLED device. From the earlier report, it is clear that the mobility of electron is always lower in the electron transport layer (ETL) than the mobility of holes in the hole transport layer (HTL) [251]. So, Here we balance the mobility of positive charge carrier by inserting a thin buffer layer between the FTO and TPD layer. Therefore the buffer can increase the probability of electron-hole pair recombination by preventing the accumulation of excess holes in the luminance layer. From the characteristics graphs, it is clear that efficiency of the devices is found to be increased continuously although the current density and the luminance value of the devices decrease with increasing interlayer thickness. In our work optimized result of the device is found to be at the thickness of 10nm buffer layer. After this critical thickness of the buffer layer efficiency of the device is decreased considerably due to more reduction of charge tunnelling mechanism at the higher thickness.

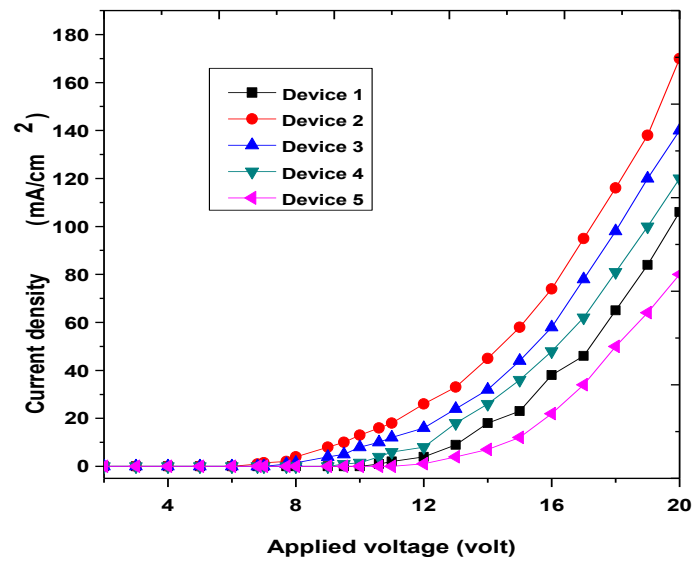


Figure 4.1 (c): Graph of applied voltage vs current density

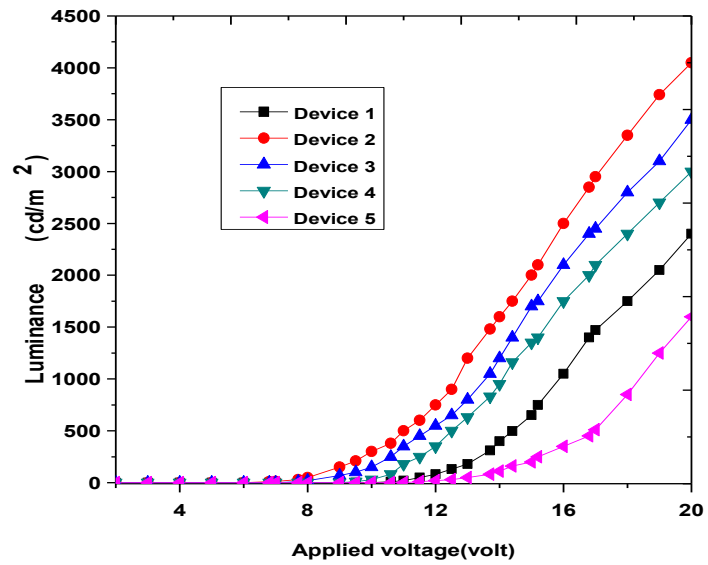


Figure 4.1 (d): Graph of applied voltage vs luminance

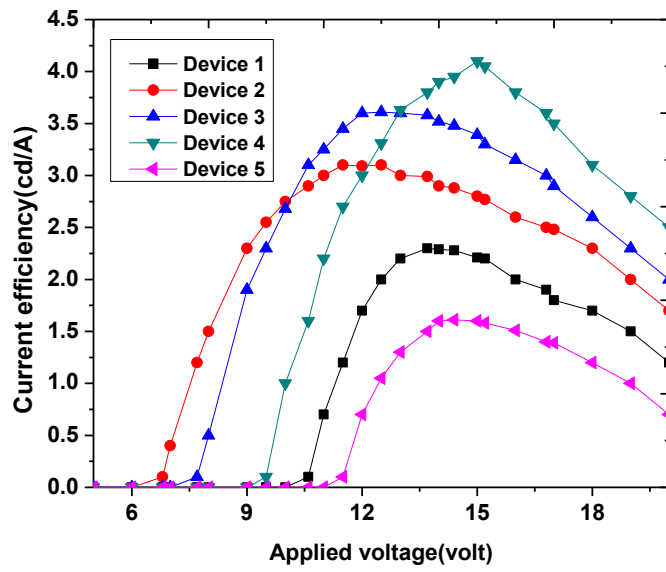


Figure 4.1 (e): Graph of applied voltage vs. current efficiency

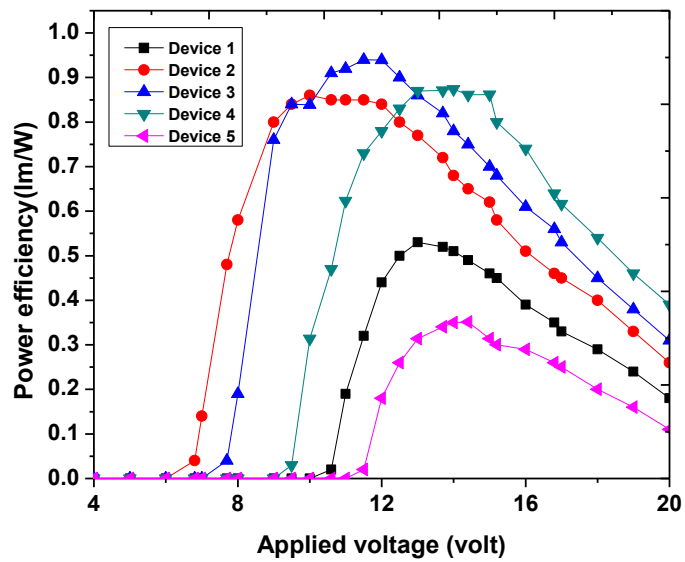


Figure 4.1 (f): Graph of applied voltage vs power efficiency



Figure 4.1 (e) represents the current efficiency and voltage characteristics of the OLED devices. From this figure, it is clear that device 4 shows the maximum efficiency and whereas device 5 has the lowest efficiency. This situation is directly linked to the proper charge injection process from electrode to the organic layer. Similarly, the variation of power efficiency vs voltage characteristics for all the devices is also shown in figure 4.1 (f) in which device 4 shows the highest value where the maximum charge balancing is achieved. The variation of optical transmittance and sheet resistance with different thickness of buffer layer over FTO film is given in figure 4.1 (g). The following table shows the summary of the result of five OLED devices along with the electrical and optical properties with different bilayer anode combination.

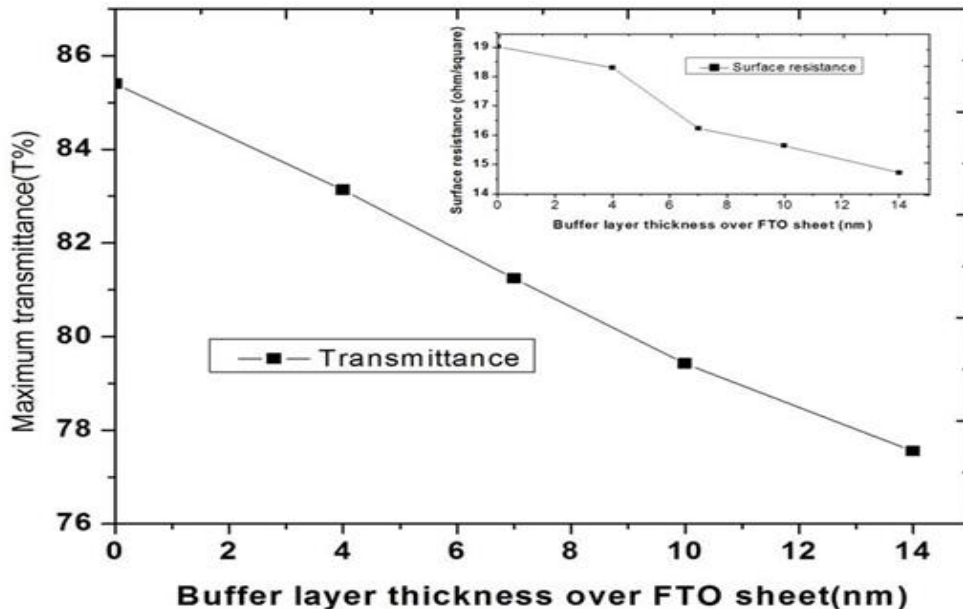


Figure 4.1 (g): Variation of maximum optical transmittance and sheet resistance of buffer layer over FTO surface

**Table -4.1:** Luminance and efficiency characteristics of the devices with different pentacene buffer layer thicknesses at the current density of 30 mA/cm<sup>2</sup>.

S. N	Pentacene thickness	Luminance (cd/m <sup>2</sup> )	Turn-on voltage(volt)	Luminous efficiency (cd/A)	Standard deviation of current efficiency(cd/A)	Standard deviation of power efficiency(lm/W)
1	0nm	750	10.6	2.30	0.95	0.20
2	4nm	900	6.8	3.1	0.83	0.23
3	7nm	1050	7.7	3.58	1.21	0.30
4	10nm	1160	9.5	4.12	1.56	0.33
5	14nm	450	11.5	1.40	0.67	0.143

From this table, it is observed that there is a tendency that the turn-on voltage increases with the growth of buffer layer thickness. This situation is linked to the larger voltage dropped across the oxide buffer layer [252]. On the other hand performance of the OLED is highly dependent on the surface morphology of electrode surface. For that purpose we analysis the surface morphology of both the single and double layer of FTO surface and is carried out with the help of FE- SEM images, which are given in figure 4.1 (h) and 4.1 (i) respectively.

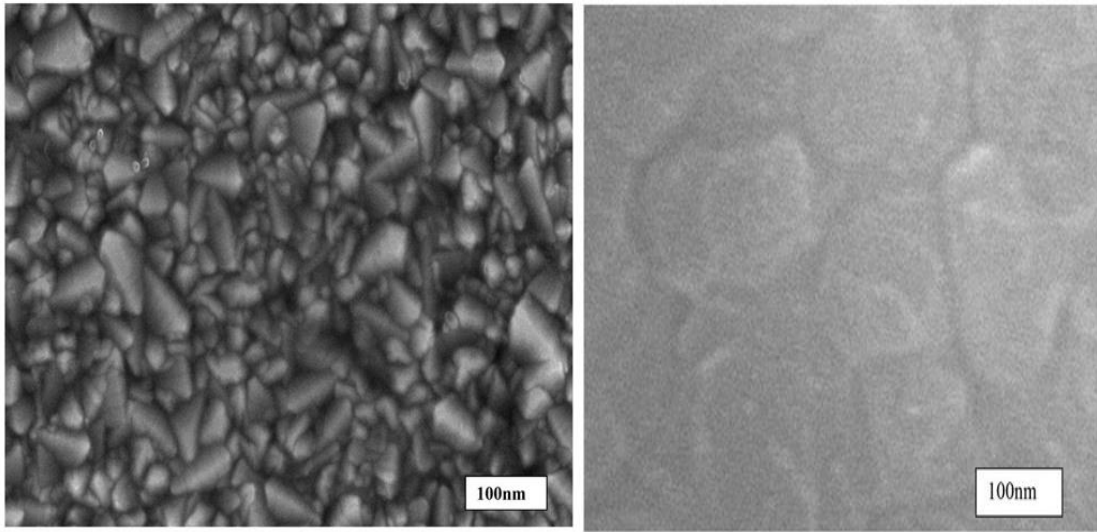


Figure 4.1 (h): FE-SEM images of bare FTO surface      Figure 4.1 (i): FE-SEM images of FTO+Pentacene surface

From the study of SEM images, it is found that the surface of bilayer anode became smoother compared to the single anode due to the presence of the oxide layer. This provides a uniform field distribution over the entire anode region and also reduces the probability of the formation of the non-emissive area in the active region. It implies a better contact of anode surface to the organic layer.

#### **4.1.4 Conclusion**

1. In this work, we used Pentacene buffer layer which has been systematically studied for FTO based OLED structure.
2. We concluded that too thick buffer films lead to higher turn-on voltage along with lower device efficiency.

3. Our result revealed that there is an optimum thickness of organic interlayer at which OLED efficiency is highly enhanced.
4. In this investigation, the 10nm buffer layer has resulted in enhancement in current efficiency compared to the single layer FTO anode.

## **4.2) Organic light emitting diode using Perylene interlayer between the electrode and an organic interface region**

In this work, we have studied the performance of Organic light-emitting diode (OLED) with vacuum deposited Perylene layer over Fluorine-doped Tin Oxide (FTO) surface. To investigate the effect of Perylene layer on device performance of OLED, different thicknesses of Perylene are deposited on the FTO surface and studied their current density, luminance and device efficiency characteristics at their respective thickness. Study of optical transmittance, sheet resistance and surface morphology of the bilayer anode film are carried out with the help of UV-VISIBLE double beam spectrophotometer unit, four probe resistivity unit and field emission scanning electron microscope. In this investigation, the maximum value of current efficiency is found to be 5.25Cd/A.

### **4.2.1 Fabrication of the OLEDs**

As mentioned earlier we used the only bottom emitting OLED structure. In this study, we also fabricated the Alq<sub>3</sub> based OLED device by using FTO+Perylene bilayer combination for anode structure. These types of bottom emitting OLEDs were fabricated by the Multiple Pump Down (MPD) method after cleaning the FTO coated glass substrates. In every deposition, thoroughly cleaned masks were used to achieve the different geometrical patterns. Initial substrates are cleaning, cleaning of the vacuum coating unit and masks after each deposition was achieved by the same procedure as described in chapter 2.

The AL cathode electrode was evaporated using tungsten helix filament while the thin layer of Perylene was evaporated using a cone-shaped filament. In our work for deposition of both the inorganic and organic layer, we used a high vacuum chamber unit having vacuum better than  $5 \times 10^{-6}$  Torr. The deposition rate for Perylene was about  $12 \text{ \AA}/\text{sec}$ , and for another layer, it was about  $15 \text{ \AA}/\text{sec}$ . Sheet resistance and optical transmittance are measured by four probe and UV-VISIBLE double beam spectrophotometer unit. The current-voltage-luminance characteristics of the fabricated OLEDs were measured by digitally controlled source-meter (SMU) and luminance meter unit. In our work active area of the samples was  $3 \times 6 \text{ mm}^2$  and thickness of the thin film was confirmed profilometer set up as mentioned in section 2.7.1(b).

Here we have fabricated the OLED structures by using Perylene as hole injection layer(HIL), N,N'-bis ( 3-methyl phenyl )-N,N'(phenyl)- benzidine(TPD) as hole transport layer, Tris ( 8-hydroxy quinolinato) aluminium (Alq3) as emitting layer and lithium fluoride (LiF) as electron transport layer respectively. We have compared the J-V-L characteristics of OLEDs with different thickness of HIL and HIL free OLED. Here we used LiF electron injection layer otherwise it is difficult for electron injection to take place from AL cathode to the Alq3 layer. The structures of the different set of bilayer anodes used in this study are as follows:

Set 1. FTO/Perylene (0nm)

Set 2. FTO/Perylene (3nm)

Set 3. FTO/Perylene (6nm)

Set 4. FTO/Perylene (9nm)

Set 5. FTO/Perylene (12nm)

## 4.2.2 Backing and ageing

Clean electric oven was used to air-baked the fabricated OLEDs up to a temperature of 200°C. The OLEDs were taken in the thoroughly cleaned petridishes of suitable sizes and placed in the electric oven at the pre-set temperature for the required time of baking.

## 4.2.3 Schematic representation and energy level alignment

**diagram:**

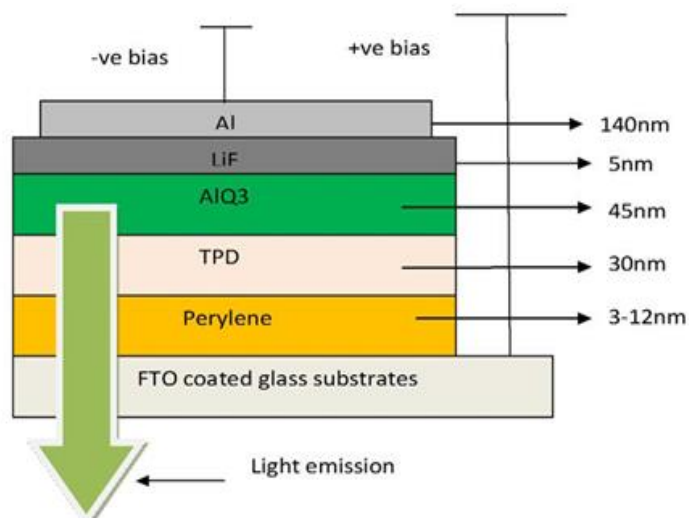


Figure 4.2 (a): Schematic presentation of OLED

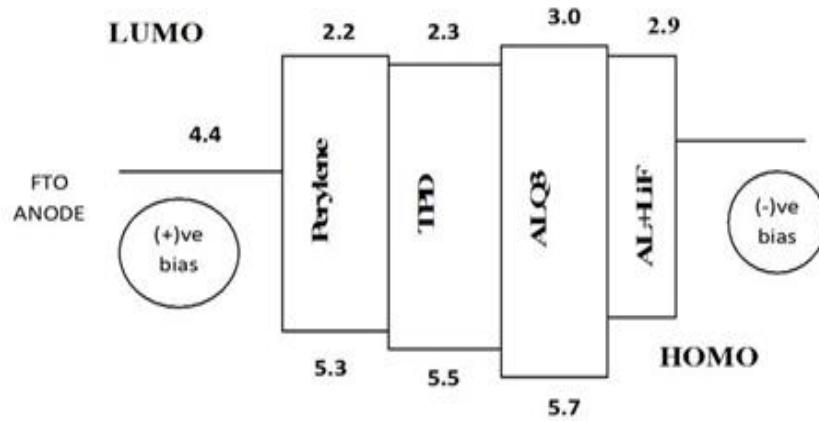


Figure 4.2 (b): Energy band structure of OLED device

#### 4.2.4 Result and discussion:

Following figure 4.2 (c) indicates the spectrum of optical transmittance of FTO-coated glass as a function of the thickness of Perylene layer (0-12nm). The optical transmittance of FTO-coated glass with 3nm Perylene layer is almost close (within the green wavelength region) to the single FTO anode surface. After that transmittance slowly tends to decrease with the increasing thickness of the hole injection layer. Therefore, the increase of buffer layer thickness over the anode region blocks the light transmission property which agrees with theoretical formulation (i.e., T% is inversely proportional to the thickness of thin film). When the thickness of Perylene layer is 6nm, then the maximum transmittance value is nearly 82.9%. Similarly, at the 9nm range, its value becomes 82.2%. For the thickness of 12nm Perylene film, the average transmittance of bilayer anode (within 500-600nm) is larger than 80%. The variation of sheet resistance vs thickness of Perylene layer over FTO surface is also shown here.



It shows a decreasing trend of surface resistance with increasing thickness of buffer layer.

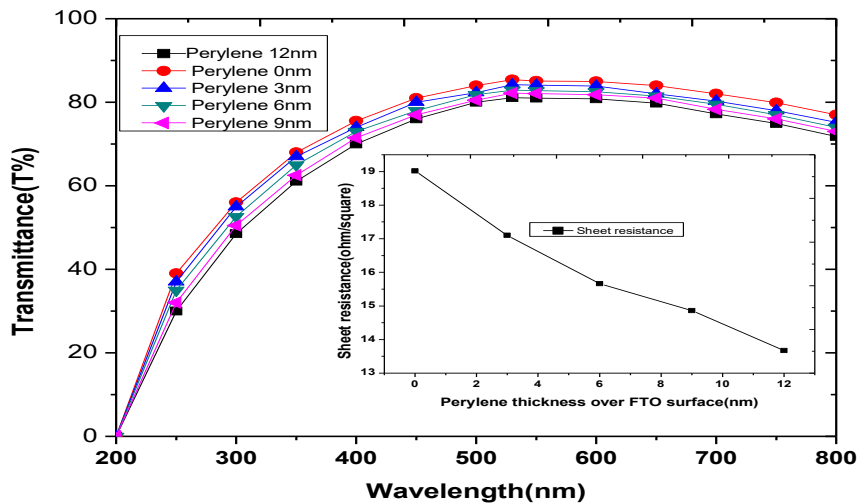


Figure 4.2 (c): Variation of optical transmittance and sheet resistance with Perylene thickness

The current-voltage and the luminance-voltage characteristics of OLEDs having configuration FTO/ Buffer layer (3nm-12nm) /TPD (30 nm)/Alq3 (45 nm)/Lif(5nm)/Al (140 nm) is discussed here. In our work, we varied the operational voltage from 0 to 22 volt. It is found that OLED with a Perylene layer of 9 nm thickness has a relatively higher efficiency at the same applied voltage compared with other devices. It is found that when the thickness of the buffer layer is continuously increased, then there is a decreasing tendency of the current density of the

devices. This indicated that this interlayer has the direct effect of blocking the hole current by

controlling the flow of positive charge carrier injection across the organic layer. In our work, it is found that the device with 9nm Perylene buffer layer has the highest efficiency of 5.25Cd/A compared to the other OLED devices. Therefore, current efficiency increases compared to the device without a buffer layer (2.52 Cd/A). With the increasing thickness of buffer layer, there is a gradual decrease of luminance and increases the efficiency of the devices which is due to the blocking of positive charge carrier current by the high thickness of organic buffer layer. Therefore it can be said that the insertion of Perylene interlayer enhanced the efficiency by controlling the hole injection. This interlayer also prevents the diffusion of metal and oxygen into the organic layer from the anode side and hence reduces the probability of an electrical breakdown of the device. From the characteristics graph as shown in figure 4.2 (d), figure 4.2 (e) and figure 4.2 (f) it is clear that although the value of current density and luminance is decreased, their efficiency is more improved continuously with the increasing thickness of the buffer layer.

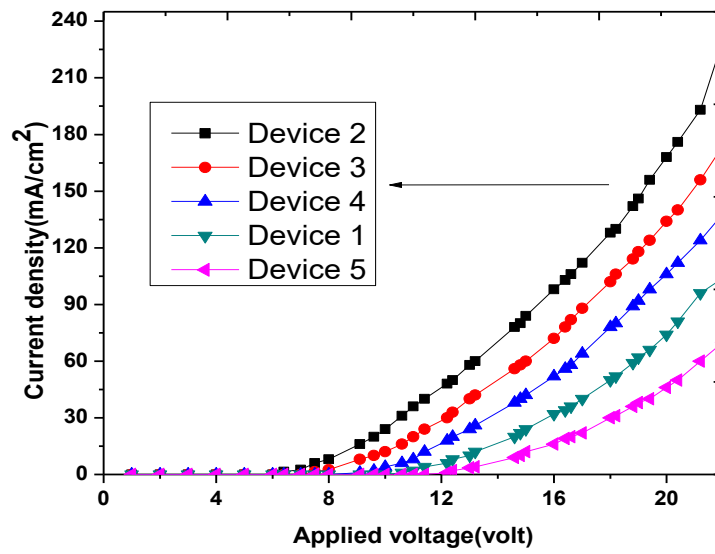


Figure 4.2 (d): Graph of applied voltage vs current density

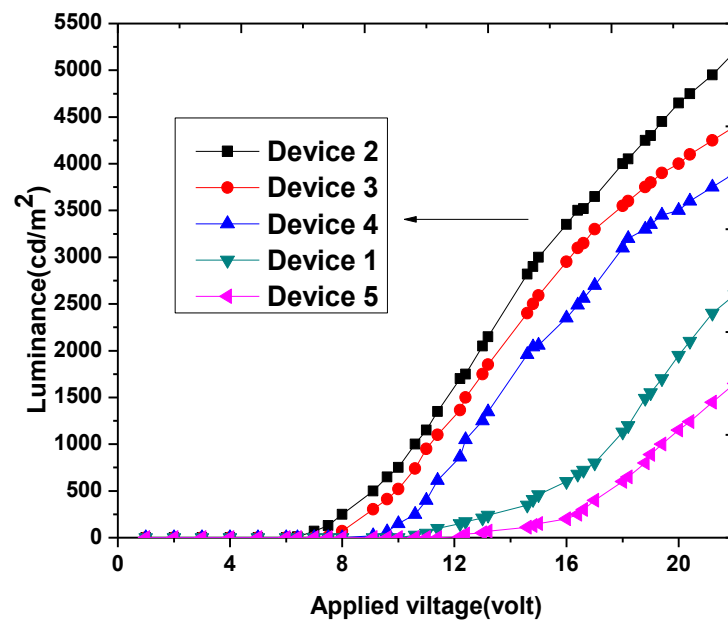


Figure 4.2 (e): Graph of applied voltage vs luminance

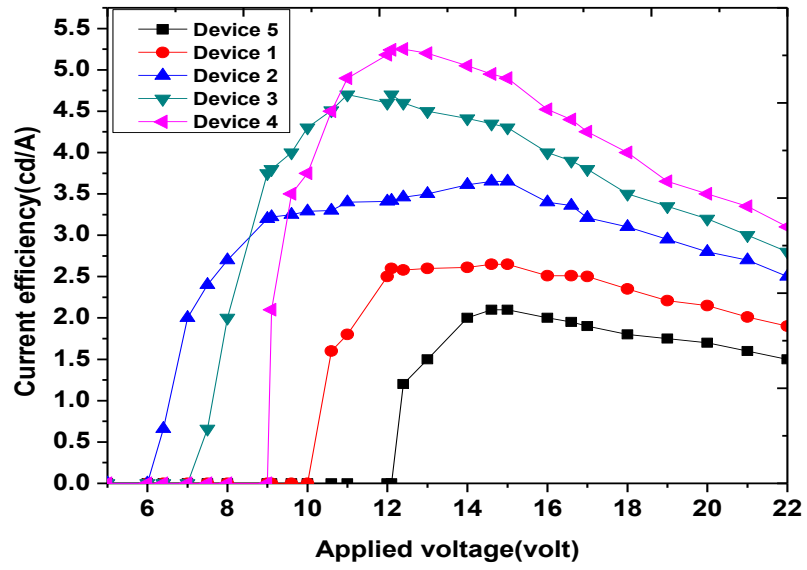


Figure 4.2 (f): Graph of applied voltage vs current efficiency

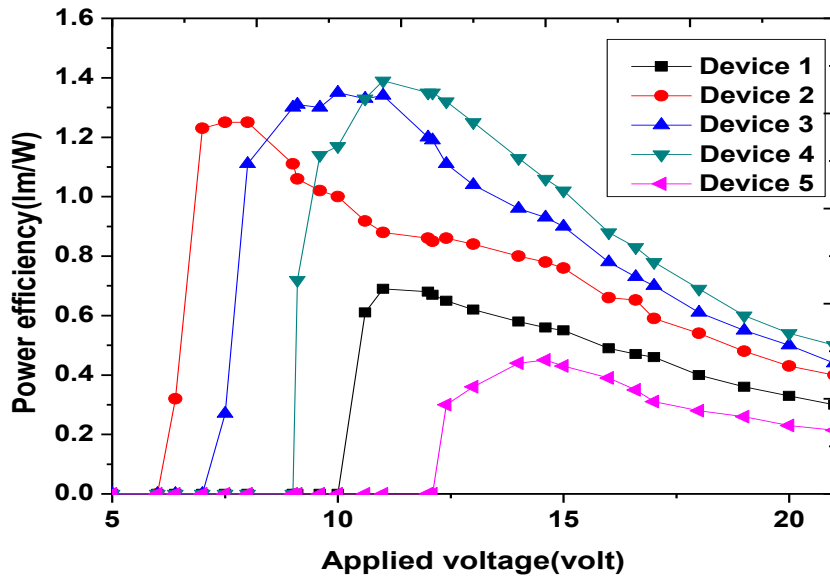


Figure 4.2 (g): Graph of applied voltage vs power efficiency

Similarly, the variation of power efficiency vs applied voltage characteristics for all the devices is shown in figure 4.2 (g) in which device 4 shows the highest value of power efficiency where the maximum balance of holes and electron injection takes place. Table 4.2 shows the summary of the result of five OLED devices along with their average value (mean value) and standard deviation value of current efficiency.

Following figure 4.2 (h) shows the Electroluminescence (EL) spectrum of all the OLED devices in our work at 17 volts which is measured by Spectrometer unit. It can be seen that all the five devices have the maximum peak in their EL spectra within the same wavelength region from 520nm to 530nm (i.e., green wavelength region). This indicated that all the emissions of the devices are coming from the Alq<sub>3</sub>, which implies that wavelength of emitted light is fall in the green wavelength region.

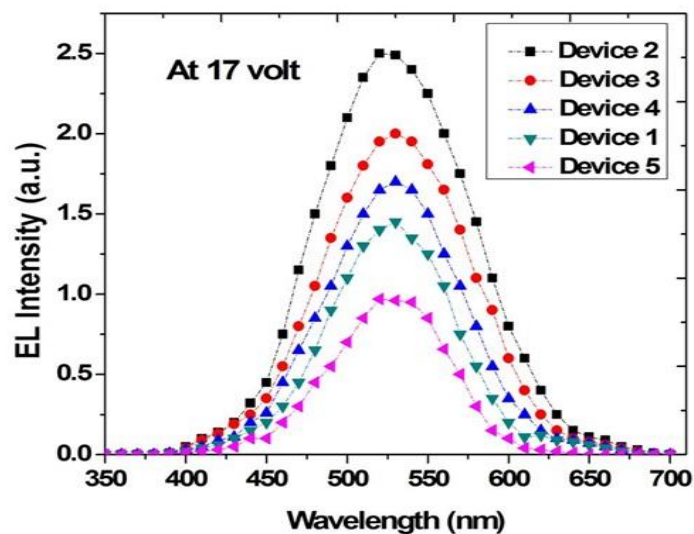


Figure 4.2 (h): Electroluminescence (EL) spectrum of all the OLED devices

**Table 4.2: Summary of the property of OLED devices at a current density of 20mA/cm<sup>2</sup>**

S.N.	Buffer layer thickness (nm)	Luminance (cd/m <sup>2</sup> )	Turn-on voltage (volt)	Luminance efficiency (cd/A)	Average value of current efficiency (cd/A)	Standard deviation of current efficiency (cd/A)
1	0	350	10.6	1.75	1.28	1.20
2	3	650	6.4	3.25	2.39	1.41
3	6	950	7.5	4.75	2.79	1.87
4	9	1050	9.1	5.25	2.75	2.18
5	12	300	12.4	1.50	0.745	0.907

From this table, the turn-on voltages of the devices with buffer layer are found to be lower than that of the device without a buffer layer. However, there is a tendency to increase the turn-on voltages with the increasing thickness of anode buffer layer, because of the larger voltage dropped across the buffer layer. Also when the thickness of Perylene is increased to 12nm, both the value of luminance and luminance efficiency is found to be more decrease due to more reduction of tunnelling mechanism across the interface layer. Along with these, after the insertion of Perylene layer over FTO electrode, the surface becomes smoother which is necessary for the achievement of a good OLED device and also for providing better contact with organic TPD layer. The surface morphology of both the single and double layer of FTO film is shown in figure 4.2 (i) and figure 4.2 (j) respectively.

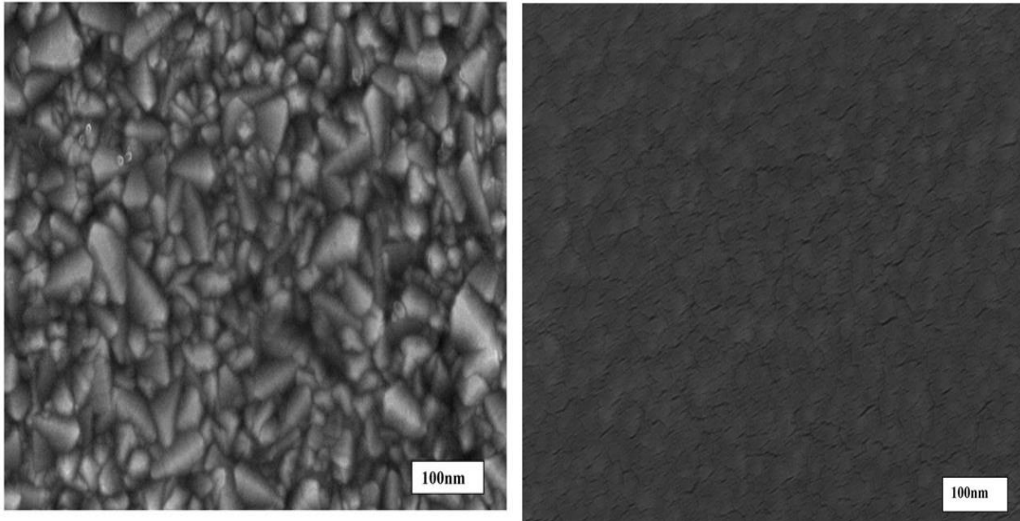


Fig. 4.2 (i): FE-SEM images of FTO surface Fig. 4.2 (j): FE-SEM images of FTO+Perylene surface

#### **4.1.5 Conclusion:**

1. Here we reported that the insertion of the proper thickness of perylene buffer layer in the interface region leads to the significant enhancement of current efficiency of the organic light emitting diode.
2. Excessively thick Perylene films lead to a higher turn-on voltage along with decreasing the current efficiency of the OLED devices due to the high blocking of positive charge carrier injection.

3. The highest current efficiency of the device with 9 nm Perylene was 5.25 cd/A which is about 2.08 times than that of the device with single layer anode surface.

4. This might also be due to the high energy band gap of Perylene buffer layer. Within the charge tunnelling region, Perylene energy level acts as an effective exciton-blocking layer which mainly prevents electrons from reaching the anode due to the large energy band gap.



### **4.3 Improve performance of bottom emitting Organic Light Emitting Diode using rubrene interlayer between the electrode and organic interface**

In this study better performance of organic light-emitting diodes (OLEDs) are demonstrated with rubrene buffer layer. The luminance efficiency is found to be increased compared to the single layer electrode surface at an optimized thickness of 8nm rubrene layer. To study the performance of OLED by the buffer layer, we deposited rubrene films at different thicknesses on the FTO surface and studied their **J-V** and **L-V** characteristics. Also, further analysis was carried out by measuring sheet resistance, optical transmittance and surface morphology with the FE-SEM and AFM images. Here the maximum value of current efficiency is found to be 6.35Cd/A.

#### **4.3.1 Fabrication of the OLEDs**

In this study, we also fabricated the Alq<sub>3</sub> based OLED device by using FTO+Rubrene bilayer combination for anode structure. These types of bottom emitting OLEDs were fabricated by the Multiple Pump Down (MPD) method after cleaning the FTO coated glass substrates as earlier mentioned. In every deposition, thoroughly cleaned masks were used to achieve the different geometrical patterns. Initial substrates are cleaning, cleaning of the vacuum coating unit and masks after each deposition was achieved by the same procedure as described in chapter 2.

Tungsten helix filament was used for Al deposition while the thin layer of Rubrene was evaporated using a boat-shaped filament. For deposition of both the inorganic and

organic layer, we used a high vacuum chamber unit having vacuum better than  $5 \times 10^{-6}$  Torr. The deposition rate for Rubrene was about  $12 \text{ \AA}/\text{sec}$ , and for another layer, it was about  $15 \text{ \AA}/\text{sec}$ . Sheet resistance and optical transmittance are measured by four probe and UV-VISIBLE double beam spectrophotometer unit. The current-voltage-luminance characteristics of the fabricated OLEDs were measured by digitally controlled source-meter (SMU) and luminance meter unit.

The structures of the different set of bilayer anodes used in this study are as follows:

Device: 1. FTO/ Rubrene (0nm)/ TPD (35nm)/Alq3 (40nm)/Lif(3nm)/Al (130nm)

Device: 2. FTO/Rubrene (3nm)/TPD (35nm)/Alq3 (40nm)/Lif(3nm)/Al (130nm)

Device: 3. FTO/Rubrene (5nm)/TPD (35nm)/Alq3 (40nm)/Lif(3nm)/Al (130nm)

Device: 4. FTO/Rubrene (8nm)/TPD (35nm)/Alq3 (40nm)/Lif(3nm)/Al (130nm)

Device: 5. FTO/Rubrene (11nm)/TPD (35nm)/Alq3 (40nm)/Lif(3nm)/Al (130nm)

### **4.3.2 Backing and ageing**

Clean electric oven was used to air-baked the fabricated OLEDs up to a temperature of  $200^\circ\text{C}$  for 3-4 hours. The OLEDs were taken in the thoroughly cleaned petridishes of suitable sizes and placed in the electric oven at the pre-set temperature for the required time of baking. These were then stored in a clean dessicator charged with fused  $\text{CaCl}_2$  for OLED characterization.

### **4.3.3 Schematic representation and energy level alignment diagram:**

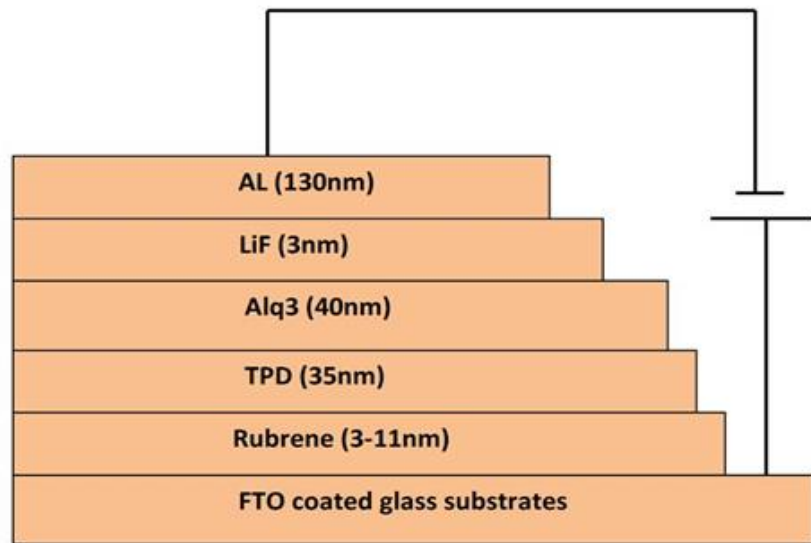


Figure 4.3 (a): Schematic representation of Organic Light Emitting Diode

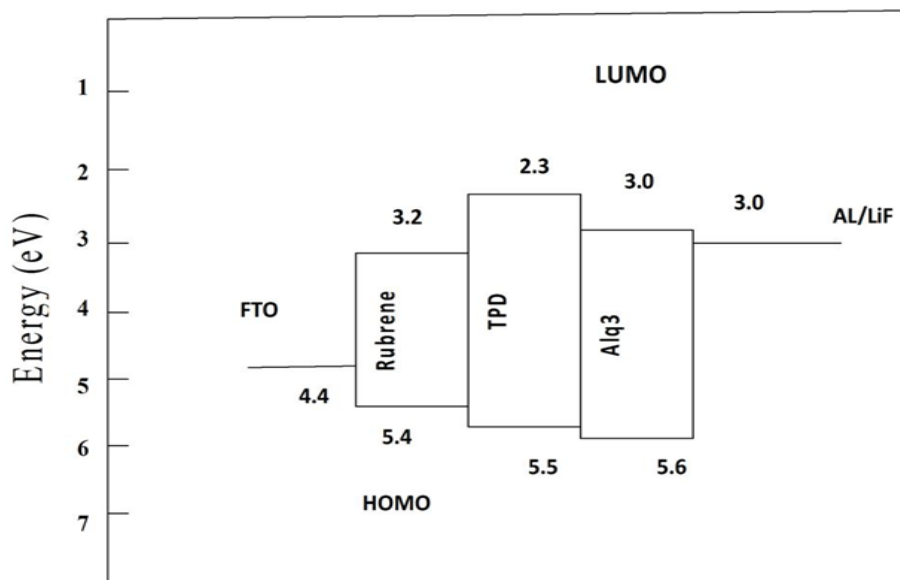


Figure 4.3 (b): Energy level alignment of OLED structure

### 4.3.4 Result and discussion

Following figure 4.3 (c) represents the transmittance spectra of bilayer anode for Rubrene layer over FTO electrode. Here the maximum value of optimized FTO/Rubrene bilayer anode is higher than 80% (average value of 81% within 530-560nm wavelength region) which is a good indicator for transparent electronics. Similarly, the variation of sheet resistance vs thickness of rubrene layer over FTO surface is shown here. This shows a decreasing trend of surface resistance along with increasing thickness of buffer layer over the electrode surface.

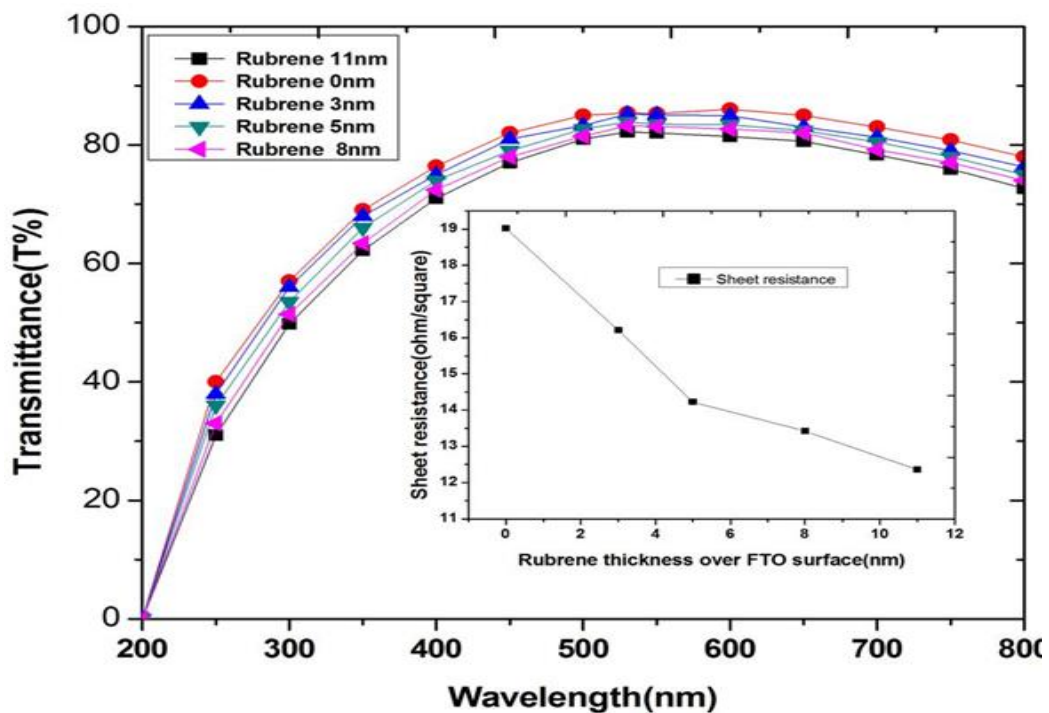


Figure 4.3 (c) Transmission spectrum and a sheet resistance of bilayer FTO/Rubrene film

The current-voltage and the luminance-voltage characteristics of OLEDs having configuration FTO/ Buffer layer (3nm-11nm) /TPD (35 nm)/Alq3 (40nm)/Lif(3nm)/Al (130 nm) is discussed here. In our work, we varied the operational voltage from 0 to 22 volt. It is found that OLED with a Rubrene layer of 8 nm thickness has a relatively higher efficiency at the same applied voltage compared with other devices. It is found that when the thickness of the buffer layer is continuously increased, then there is a decreasing tendency of the current density of the devices. This indicated that this interlayer has the direct effect of blocking the hole current by controlling the flow of positive charge carrier injection across the organic layer. In our work, it is found that the device with 8nm Rubrene buffer layer has the highest efficiency of 6.35 Cd/A compared to the other OLED devices. Therefore, current efficiency increases compared to the device without a buffer layer (3.61 Cd/A). With the increasing thickness of buffer layer, there is a gradual decrease of luminance and increases the efficiency of the devices which is due to the blocking of positive charge carrier current by the high thickness of organic buffer layer. Therefore it can be said that the insertion of Rubrene interlayer enhanced the efficiency by controlling the hole injection. From the characteristics graph as shown in following figures it is clear that although the value of current density and luminance is decreased, their efficiency is more improved continuously with the increasing thickness of the buffer layer.

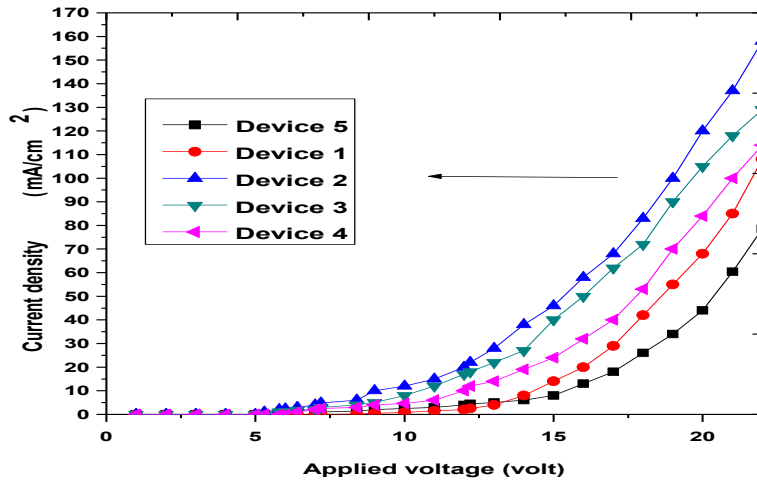


Figure 4.3 (d): Graph of applied voltage vs current density

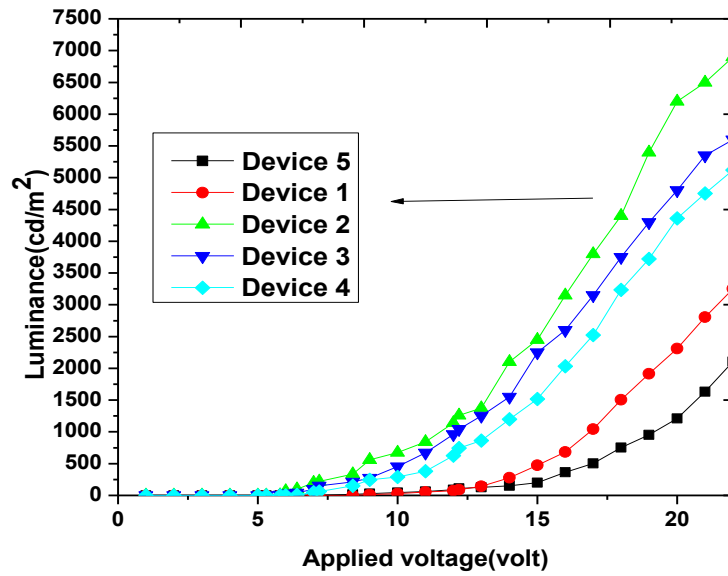


Figure 4.3 (e): Graph of applied voltage vs luminance

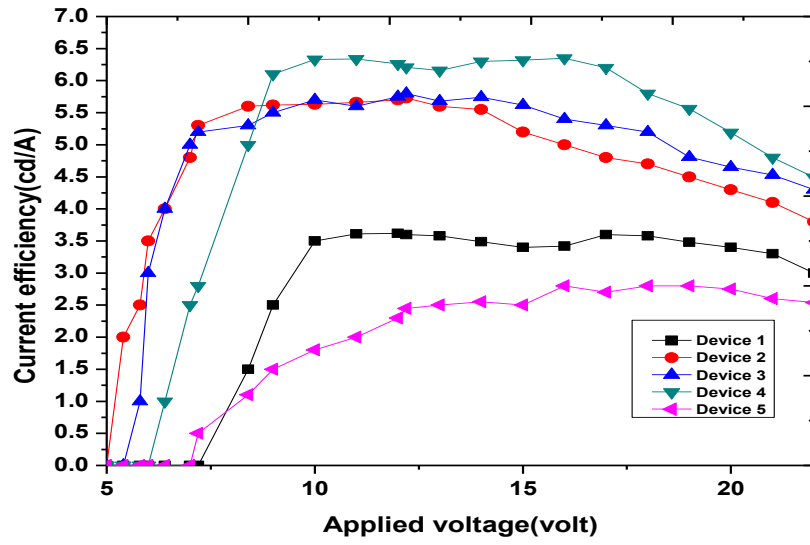


Figure 4.3 (f): Graph of applied voltage vs current efficiency

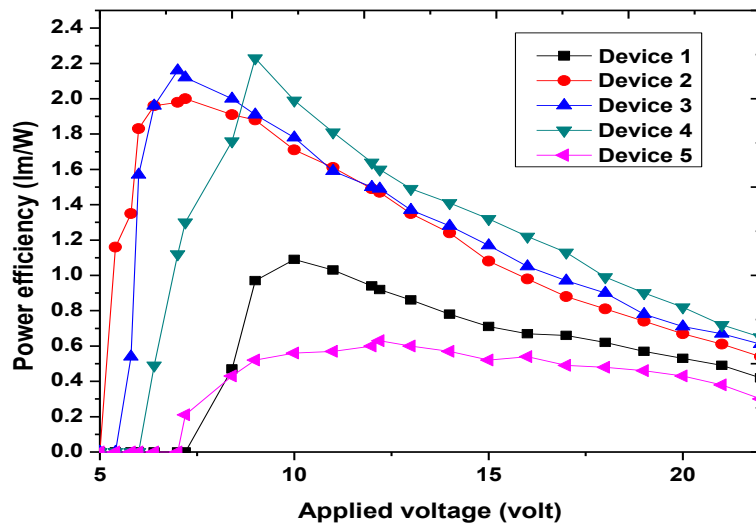


Figure 4.3 (g): Graph of applied voltage vs power efficiency

Similarly, the variation of power efficiency vs applied voltage characteristics for all the devices is shown in figure 4.3 (g) in which device 4 shows the highest value of power efficiency where the maximum balance of holes and electron injection takes place. The graph of standard deviation (which is a measure of the spread of their efficiency in a set of data at different voltages from their mean value) of current and power efficiency vs OLED devices at different thickness of buffer layer is given in figure 4.3 (h). Table-4.3 shows the summary of the result of five OLED devices along with their average and standard deviation value of device efficiency.

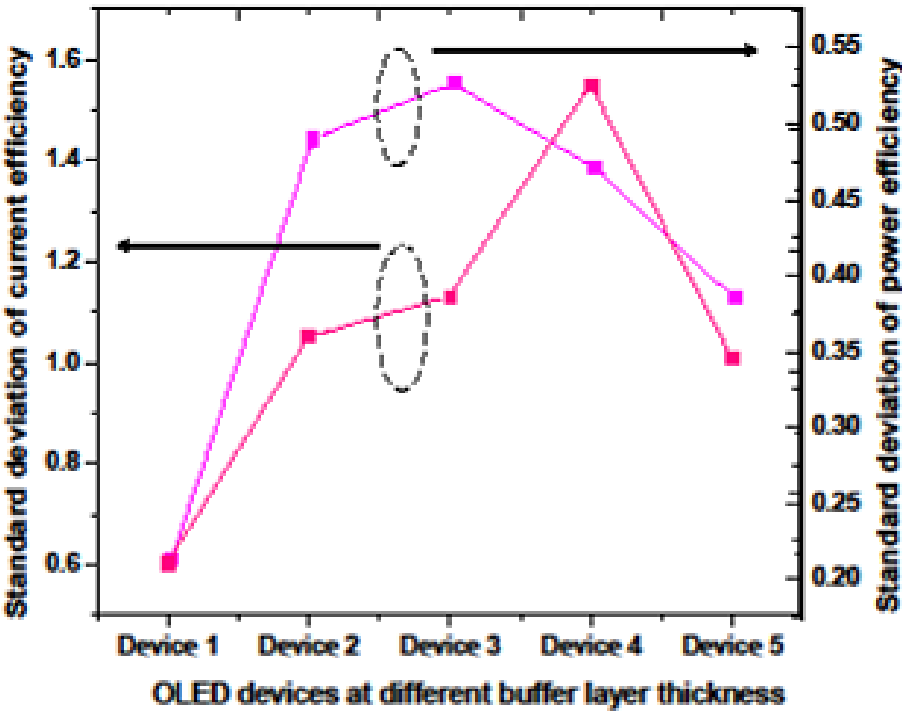


Figure 4.3 (h): Graph of standard deviation vs OLED devices



**Table -4.3:** Luminance and efficiency characteristics for the devices with different buffer layer thicknesses at the current density of 40 mA/cm<sup>2</sup>.

<b>S.N</b>	<b>Buffer layer thickness</b>	<b>Luminance (cd/m<sup>2</sup>)</b>	<b>Turn-on voltage (volt)</b>	<b>Luminous efficiency (cd/A)</b>	<b>Average value of current efficiency</b>	<b>Standard deviation value of current efficiency</b>
<b>1</b>	0nm	<b>1456</b>	<b>8.4</b>	<b>3.64</b>	<b>3.28</b>	<b>0.55</b>
<b>2</b>	3nm	<b>2212</b>	<b>5.4</b>	<b>5.53</b>	<b>4.70</b>	<b>1.05</b>
<b>3</b>	5nm	<b>2248</b>	<b>5.8</b>	<b>5.62</b>	<b>4.91</b>	<b>1.13</b>
<b>4</b>	8nm	<b>2524</b>	<b>6.2</b>	<b>6.31</b>	<b>5.24</b>	<b>1.54</b>
<b>5</b>	11nm	<b>1180</b>	<b>7.3</b>	<b>2.95</b>	<b>2.24</b>	<b>0.98</b>

From this table, it is seen that there is a tendency that the turn-on voltage increases with the increase of anode layer thickness. This is due to the relatively weak modulation of the internal field which increases the voltage drop across the interface region. Also when the thickness is increased to 11 nm of the Rubrene layer, both the value of luminance and luminance efficiency is found to be decreased due to more reduction of a tunnelling mechanism. From the study of SEM images, it can be concluded that the surface of bilayer anode became smoother compared to the single anode due to the presence of organic layer. This implies that there is a better contact of bilayer anode surface with respect to the organic HTL layer than that of the single FTO surface as smoother anode surface is necessary for better device performance. This is further confirmed by AFM images as shown in figure 4.3 (k) and 4.3 (l). From

this AFM study, it is demonstrated that the single FTO surface has a certain amount of spikes or irregular region whereas the modified FTO surface with rubrene coating is found to be a regular and smooth surface with minimizing the rough region. This is the reason because of which we get, the better device efficiency when an electrical bias is applied to the charge tunnelling region.

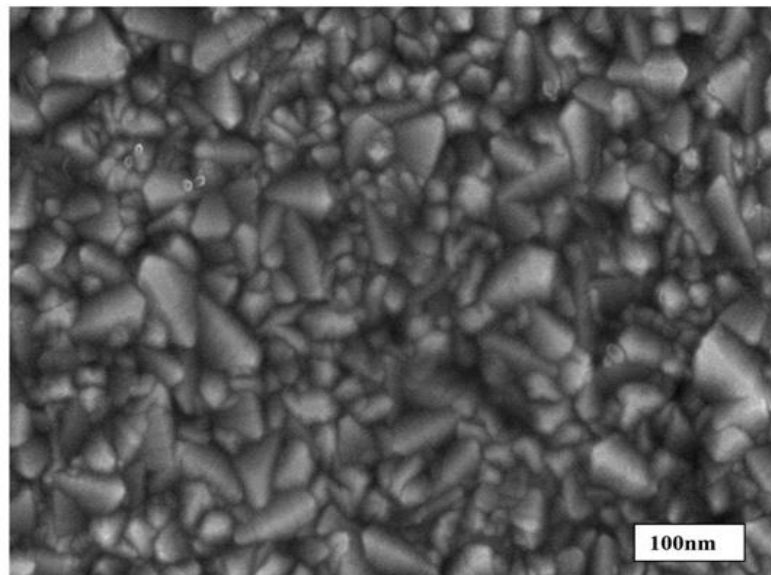


Figure 4.3 (i): FE-SEM images of single FTO surface

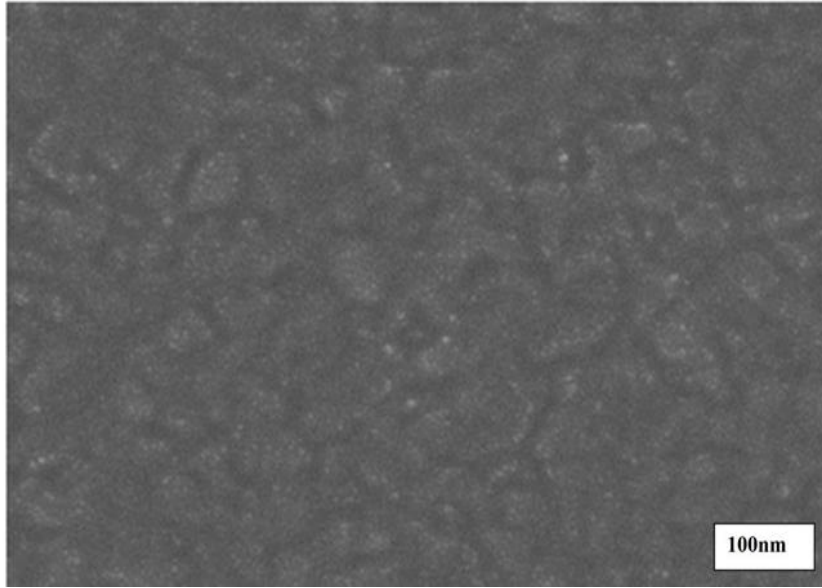


Figure 4.3 (j): FE-SEM images of FTO+Rubrene surface

### 4.3.5 Conclusions

1. In summary, the above-presented results demonstrate the fabrication of an organic electro-luminescence device on bilayer anode in which the maximum efficiency is found to be 6.35 cd/A at the optimized thickness of 8nm rubrene interlayer.
2. This result is found to be better than single layer anode under the same condition of operation. Here we conclude that excessively thick buffer layer leads to high turn-on voltage along with decreasing the current efficiency of the OLED devices due to the high blocking of positive charge carrier injection.
3. In our work optimum thickness has resulted in 1.75 times increasing the current efficiency than that of single FTO based device.

## **4.4 Organic Light Emitting Diode with Fluorine-doped Tin Oxide (FTO)/ Perylene doped PEDOT: PSS bilayer electrode**

We have investigated the performance of the Organic Light Emitting Diode(OLED) with Fluorine-doped Tin Oxide (FTO)/ Perylene doped poly (3, 4-ethylenedioxythiophene: poly (4-styrene sulfonate) (PEDOT: PSS) bilayer electrode. The solution of Perylene doped PEDOT: PSS is prepared by dissolving Perylene in a 2-Propanol solvent and mixing with PEDOT: PSS. Increasing the amount of Perylene in the polymer film, the changes in surface properties are observed. We find a decreasing tendency in both the optical transmittance and surface resistance. However, surface resistance begins to increase sharply at the doping amount of Perylene 7ml and 9ml concentration respectively. The thermal treatment in doped PEDOT: PSS film results in increasing the conductivity of the layer. The maximum luminance of 4160 cd/m<sup>2</sup> and current efficiency of 6.38 cd/A are obtained under annealing treated OLED structure of FTO/doped PEDOT: PSS/TPD/Alq3/LiF/AL.

### **4.4.1 Device fabrication**

In our work, FTO is used as anode substrate and PEDOT: PSS as a buffer layer. The FTO glass substrates are cleaned with acetone, ethanol, and isopropyl alcohol (1:1:1) for 50 minutes and then rinsed with ethanol. It is pre-patterned using etching process, and pixel area is fixed as three mm×6 mm. Both the materials are purchased from Sigma-Aldrich (USA). 2-propanol is used as a solvent agent for

perylene which is used as a doping material in this work. Similarly, N, N'-bis (3-ethyle phenyl) -N, N'(phenyl) - benzidine (TPD), Tris (8-hydroxy quinolinato) aluminium (Alq3) and lithium fluoride (LiF) use as a hole transport layer, light emitting layer, and electron injection layer respectively. Perylene solution of 1ml, 3ml, 5ml, 7ml, and 9ml are prepared by dissolve in a 2-propanol solvent by applying external heat for few minutes. To optimize the doping level of Perylene concentration, we take 10ml PEDOT: PSS solution in our work. It is found that the solution became light yellowish colour as the dissolution time increases as shown in figure 4.4(c). After preparation of organic solvent as mentioned above each composition of such solvent is mixed with 10ml PEDOT: PSS solution and stirred for 75 minutes and then spin-coated on the FTO substrate at 3650 RPM for 20 s using a digitalized spin coater. The thickness of each Perylene-doped PEDOT: PSS thin film is 30 nm for this work. We have prepared different sets. The first set is subjected to an annealing process in a vacuum oven (heating at 160°C, for 8 min, and self-cooling down to room temperature). This step helps us to investigate the effect of annealing temperature on OLED performance in bilayer anode form. The annealing treated samples are transferred to a thermal evaporator unit for the deposition of TPD (35nm) and Alq3 (45nm) layers up to the cathode layer. The TPD and Alq3 layers are deposited on other sets also. Finally, LiF (3nm) and Al(120nm) layers are deposited over all the sets to complete OLED fabrication. Here we have taken a reference OLED sample on ITO electrode by using same buffer layer and additive, without any thermal treatment to check the performance difference with the heat treated FTO based bilayer anode EL device. After completion of device fabrication, we stored all the

OLEDs samples in desiccators under dark room condition for the study of their electrical and optical characteristics measurement. J-V-L characteristics are determined by the digitally controlled SMU unit and luminance meter unit. The sheet resistance and optical transmittance of different bilayer anode films are monitored by four probe method and UV-VISIBLE double beam spectrophotometer unit. We optimize the doping level after study the sheet resistance of doped polymer film. Here it is found to be 5ml of doping level.

Following device, structures were used to study the OLED performance after optimization.

Device1: FTO/TPD/ALQ3/LiF/AL

Device 2: FTO/PEDOT: PSS/TPD/ALQ3/LiF/AL (without annealing treatment)

Device 3: FTO/PEDOT: PSS/TPD/ALQ3/LiF/AL (with annealing treatment)

Device 4: FTO/PEDOT: PSS+5ml of perylene solution/TPD/ALQ3/LiF/AL (without annealing)

Device 5: FTO/PEDOT: PSS+5ml of perylene solution/TPD/ALQ3/LiF/AL  
(annealing treatment)

Device 6: ITO/PEDOT: PSS+5ml of perylene solution/TPD/ALQ<sub>3</sub>/LiF/AL (without annealing)

#### 4.4.2 Schematic representation and energy band structure of OLED

### OLED

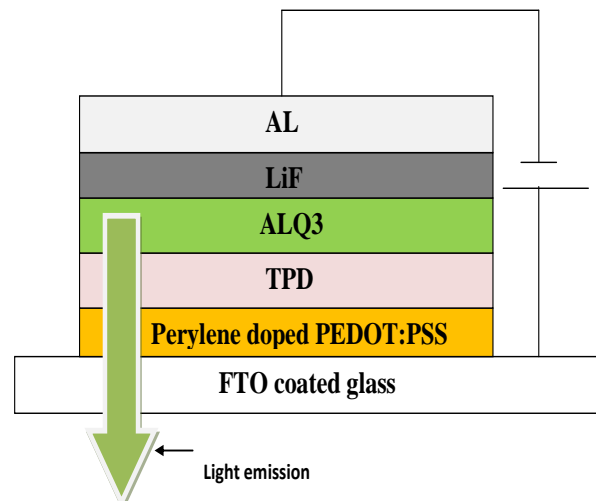


Figure 4.4 (a) : Schematic representation of OLED

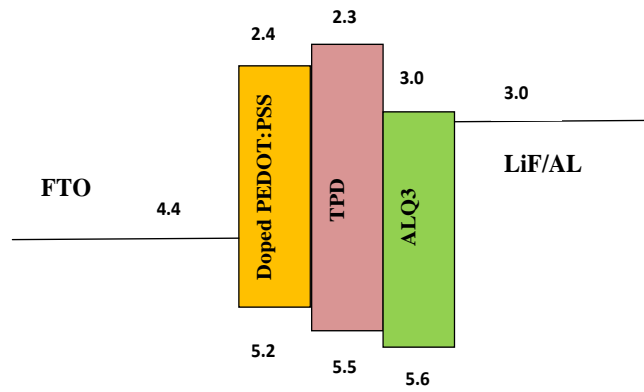


Figure 4.4 (b) : Energy band diagram of OLED

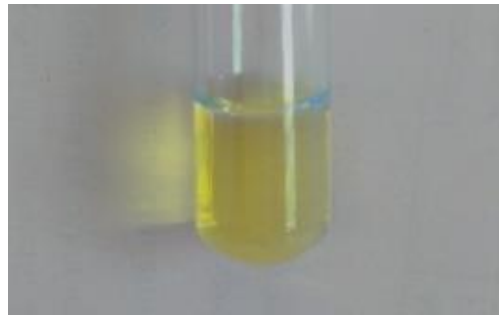


Figure 4.4 (c): Solution of Perylene doped PEDOT: PSS with 2-propanol solvent

### 4.4.3 Result and discussion

The variation of optical transmittance of PEDOT: PSS film with different ml of Perylene dopant is shown in figure 4.4 (d). Similarly, the variation of sheet resistance is also shown in figure 4.4 (e).



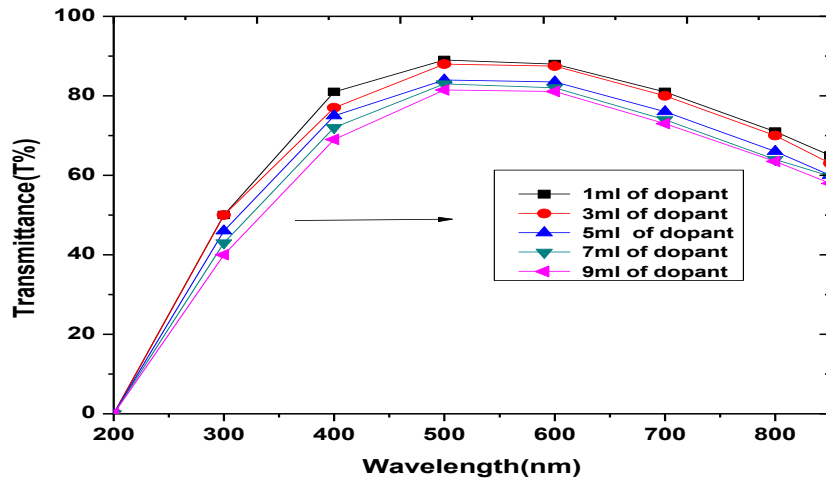


Figure 4.4 (d): Graph of variation of optical transmittance vs wavelength of a polymer film with different concentrations of dopant

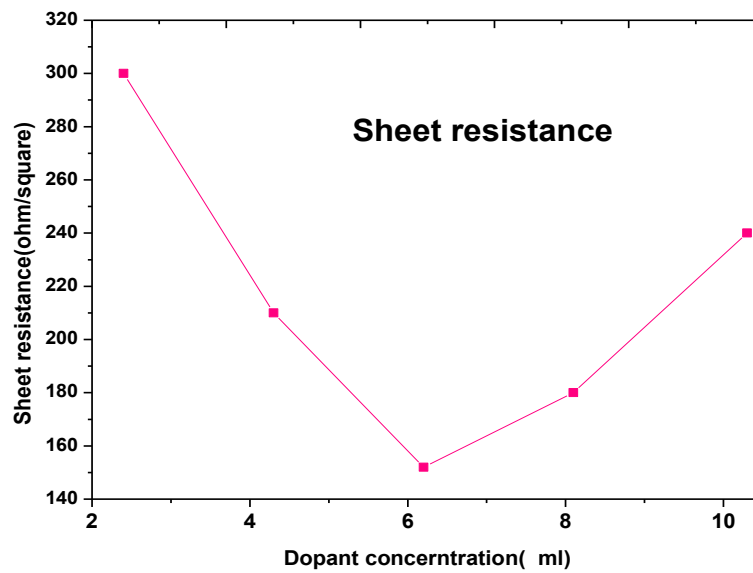


Figure 4.4 (e): Graph of doping concentrations vs sheet resistance of the polymer film

It is found that as the amount of Perylene concentration increases, a decrease of light intensity is occurred within the visible region along with the decreasing tendency of sheet resistance. Thus Perylene treated polymer film shows the light blocking behaviour. However, its average transmittance is still higher than 80% in the whole range of dopant concentration within 500-600nm wavelength region, which is a good indicator for transparent electronics. Similarly with 7ml and 9ml of Perylene solution in PEDOT: PSS films, we observed that the surface resistance is beginning to increase, which implies that the conductivity of Perylene mixed PEDOT: PSS films become decreases as the organic doping amount greater than 5ml. So in our work, we consider the doping level to be at 5ml. This result indicates that both the optical and electrical properties are affected by the doping process. Initially, when the doping amount of perylene is low, the organic solution can disperse in a polymer solution which reduces the effect on sheet resistance. The corresponding conductivity enhancement is due to the changing of carrier mobility and surface structure caused by the addition of organic solution in polymer films. When the solution is added, the interaction between PEDOT chains and solvent causes the change the structure of polymer chain. This interaction is mainly between the sulphonic acid group and organic additives [264]. As a result the charge conductivity of PEDOT: PSS thin film is increased. Further, the addition of Perylene solution enhances the electrical conductivity as surface resistance is found to decrease as shown in figure 4.4 (e). According to an earlier report, this decreasing of resistance may be linked to the incident of reducing the thickness of the

PSS molecules which enhanced the electrical conductivity through the structural changes due to the separation of insulating PSS by dopant molecules [265]. Before the addition of organic solvent, the bonding between the PEDOT cores is limited due to the insulating behaviour of PSS. However, however, after the addition of doping molecules, the PSS shells are separated by weakening the columbic attraction between PEDOT and PSS chains [266]. By the increasing of doping amount regularly in PEDOT: PSS there is an increase in the space between PEDOT and PSS chains. Because of this separation, it is difficult for the charge hopping process to take place between the polymer chains after optimizing concentration [267] which finally decreases the surface conductivity (i.e. Increasing average sheet resistance). Therefore, any addition of a higher amount of doping solvent should affect the interlayer charge mobility which reduces the film conductivity in the interface region between the two layers of the thin film devices. This result coincides with similar trends in earlier literature [268]. Fig. 4.4 (f) shows the current-voltage characteristics of the OLEDs with and without Perylene treated PEDOT: PSS film as the hole injection layer along with the ITO OLED device. From this graph, we see that initially, the value of current density and luminance of FTO devices is small compared to the reference sample. It might be due to the low work function level of FTO (4.4eV) than that of ITO (4.8eV) electrode and higher transmittance of ITO (>90%) within the visible region. However, when we add the PEDOT: PSS layer over the anode substrate its performance is found to be increased in device 2 compared to device 1. This is due to the reducing of the energy barrier between electrode/organic interface, as the charge carrier now enter the hole transport layer comparatively from a higher energy level as shown in figure 4.4

(b). There may be some hole traps exist in the hole transport layer which traps the holes before they come to light emitting region. When the holes are injected relatively from a higher energy level, the probability of their trapping is decreased. Due to this reason, we get better results in device 2 than device 1. On the other hand the addition of dopant molecule in PEDOT: PSS solution under optimized conditions enhanced the surface conductivity of the polymer film. Therefore device performance is again found to be higher in device 4 compared to device 2. Thus we observed a continuous increasing trend of performance. It is mainly due to the reducing of surface resistance at the interface region of organic HTL layer, and Perylene treated polymer film than the without Perylene treated film as shown in figure 4.4 (e). A similar trend is also observed in luminance-voltage characteristics graph as shown in figure 4.4 (g). From the efficiency-voltage characteristic curves of OLEDs, it is clear that the device efficiency is higher in device 4 compared to device 2 as shown in figures 4.4 (h) and 4.4 (i). It implies that there is more balancing of positive charge carrier injection and its recombination with the negative charge carrier within the light emitting region which increases the average luminance (i.e. larger exciton formation probability). In our work, all measurements are carried out under ambient atmospheric condition. The table-4.4 shows the summary of all the six devices fabricated in our work along with their standard deviation of current efficiency.

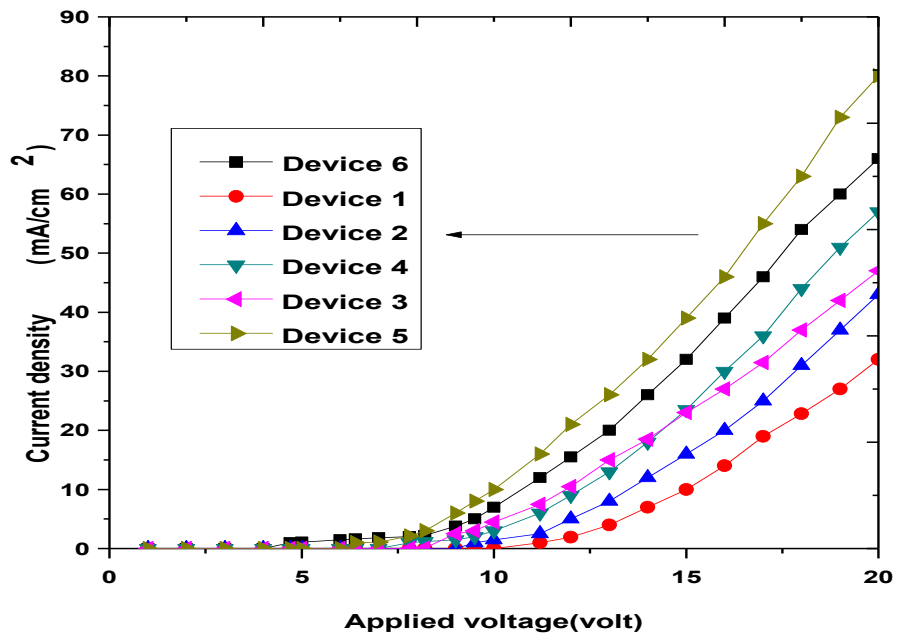


Figure 4.4 (f): Graph of current density vs. voltage

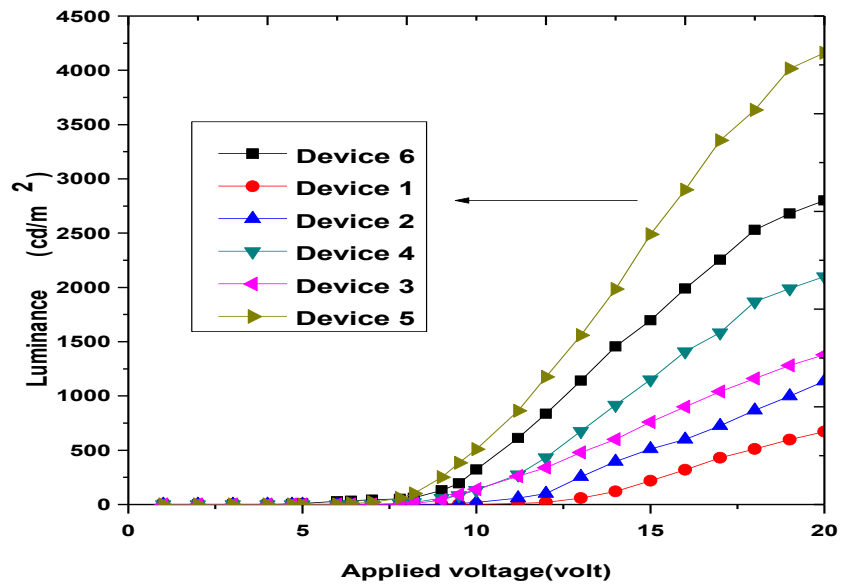


Figure 4.4 (g): Graph of Luminance vs. voltage

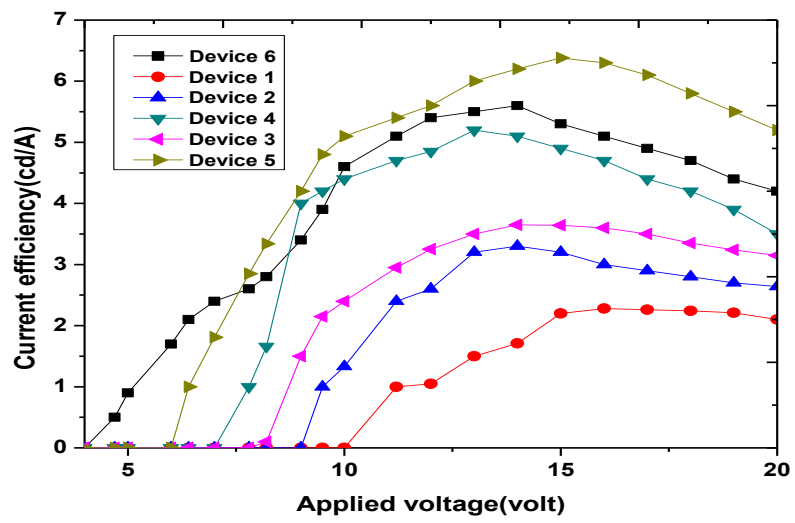


Figure 4.4 (h): Graph of current efficiency vs. applied voltage

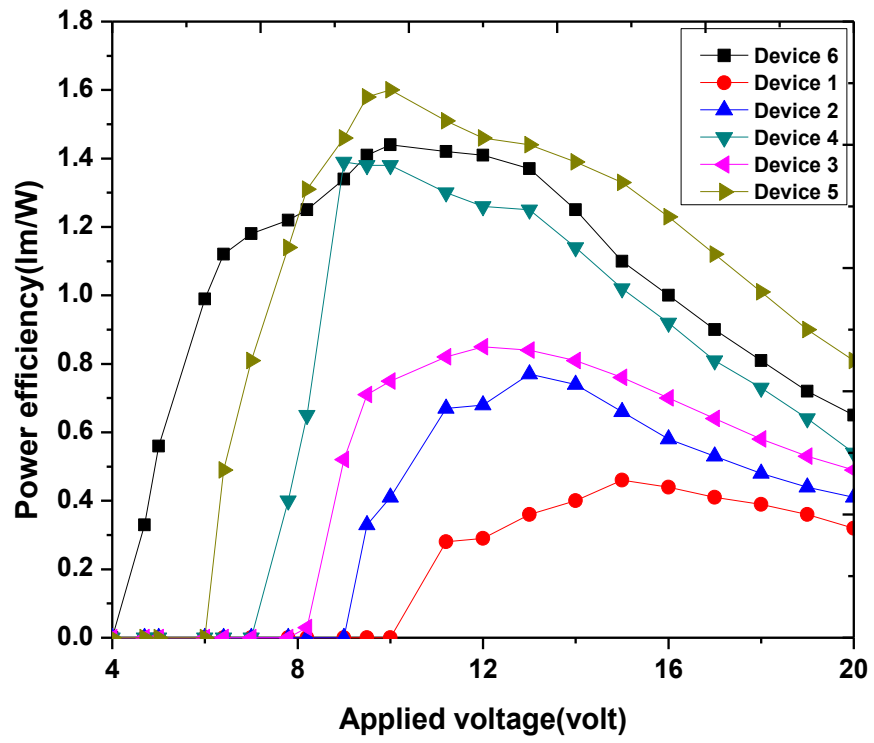


Figure 4.4 (i): Graph of power efficiency vs applied voltage

Table 4.4: Summary of the properties of OLED devices during the working period

OLED devices	PEDOT : PSS film	Optimized Perylene doping	Thermal annealing ( $^{\circ}\text{C}$ )	Maximum Luminance ( $\text{cd}/\text{m}^2$ )	Maximum Current efficiency ( $\text{cd}/\text{A}$ )	Turn on voltage (volt)	Standard deviation of current efficiency
Device 1	No	No	No	672	2.28	11.2	0.508
Device 2	Yes	No	No	1135	3.30	9.5	0.729
	Yes	No	Yes	1380	3.65	8.2	1.015
Device 3							
Device 4	Yes	Yes	No	2100	5.20	7.8	1.203
Device 5	Yes	Yes	Yes	4160	6.38	6.4	1.625
Device 6	Yes	Yes	No	2800	5.60	5.7	1.599

In our study, we take the annealing temperature  $160^{\circ}\text{C}$ . It is because the presence of such high temperature forced the PEDOT chain molecules to take a more ordered orientation compared to a lower temperature during the evaporation of additive molecules on the film of PEDOT: PSS as earlier reported [269]. Because of this orientation, the conductivity of annealed PEDOT: PSS film more increases, which



affect the charge mobility of the device by increasing the surface conductivity. For a comparative analysis, we also measure a control device 3 with PEDOT: PSS without the additive by applying such high temperature. We noticed that device performance is found to be greater than device 2. It is because of the decreasing of water content at such temperature which leads to the shrinkage of the insulating PSS shell around the conducting PEDOT grains by making a favourable ratio of their component content and hence the device performance[270]. However, this result is still found to be lower than the other dopant additive devices which imply that organic additive can take a major role in enhancing OLED performance. In our work, the maximum value of current and power efficiency is found to be 6.38 cd/A and 1.60 lm/W respectively in the device 5. This result has a similar trend with A.M. Nardes *et al.* [267]. Maximum luminance of 4160 cd/m<sup>2</sup> is obtained in the OLED device-5 at a driving voltage of 20 V. It is found that the higher current density is achieved for the doped polymer thin film under thermal annealing treatment. It implies that the interlayer resistance of the doped organic polymer film is reduced by the annealing treatment and increases the hole injection ability of the buffer layer from electrode surface to hole transport layer (HTL). This decrease of resistance of the annealing treated polymer layer ultimately reduced the bulk resistance of the OLED which provide a better conducting path for the holes to overcome the FTO/HTL interface. From the above table-1, it is clear that the turn-on voltage (i.e., the voltage from which the device can start working correctly) of device 5 is the lowest among all the FTO based devices which are found to be 6.4 volts. This value is close to the turn-on voltage of ITO-based reference device 6 (turn-on voltage 5.7 volts). This lower value is due to the reducing of contact

resistance between the anode and hole transport layer which is suitable for charge injection to the organic layer and hence the device performance. Thus the bilayer anode with a thermally treated polymer film is found to be better for electrical and optical performance. In our work, the performance of optimized FTO OLED is considered to be better than other FTO OLEDs. It may be due to the reason of higher conductivity at the interface region of FTO/organic interface under thermal treatment condition. We study the surface morphology with the field emission scanning electron microscope (FESEM) for four different situations, as the smoother anode surface is necessary to enhance the charge injection and mobility [271]. The figure 4.4 (j), 4.4 (k) and 4.4 (l) show the images of anode surface at the different situation as mentioned above discussion.

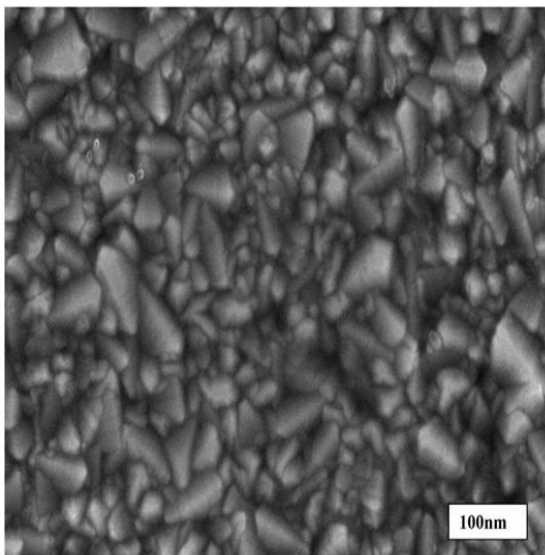


Figure 4.4 (j): FE-SEM images of bare FTO surface

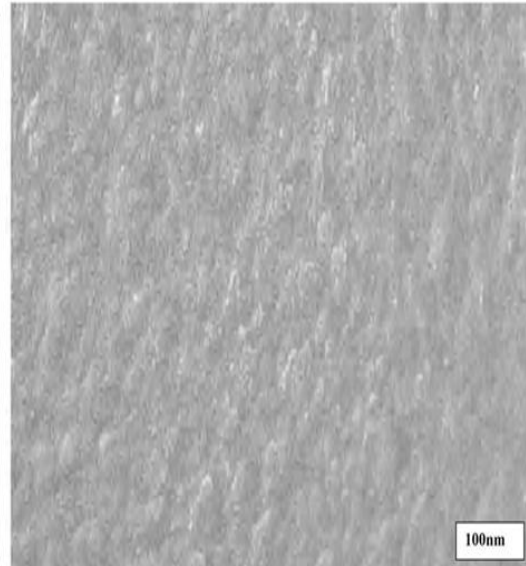


Figure 4.4 (k): FE-SEM image of non annealing doped polymer film over FTO surface

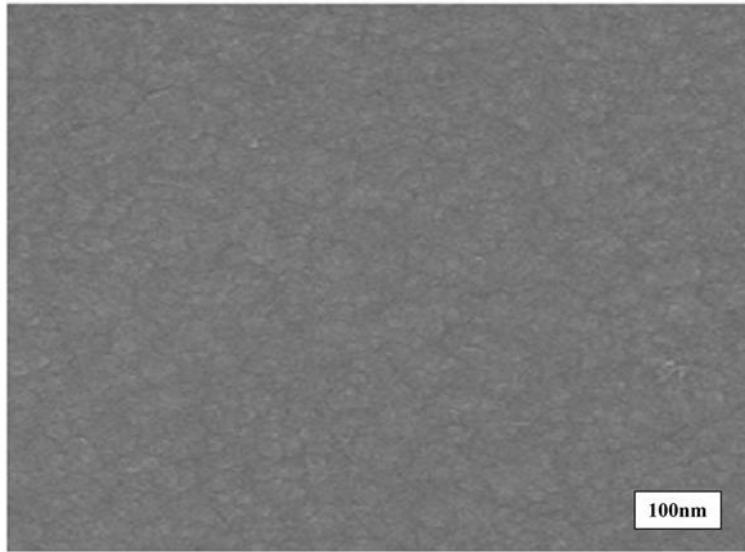


Figure 4.4 (1): FE-SEM image of annealing doped polymer film over FTO surface

From the above morphology pictures, it is clear that the surface of annealed doped PEDOT:

PSS shows better surface smoothness with more ordered (i.e. planarizes) film pattern compared to the single FTO anode and without thermally treated film. It provides a uniform field distribution over the entire anode region and also reduces the probability of the formation of the non-emissive area in the active region. Therefore, this thermally treated buffer layer provides better organic-organic contact compared to the direct contact of FTO with the HTL layer.

#### **4.4.4 Conclusions:**

1. In our work, the performance characteristics of perylene doped PEDOT: PSS as a buffer layer in OLED has been investigated. Doping of perylene solvent influences the luminance and the efficiency into PEDOT: PSS layer.

2. The surface resistance of the polymer films is decreased with the increase of the amount of perylene. Similarly from the morphological point of view the annealing treatment of doped PEDOT: PSS improves the hole injection ability along with a decrease in the contact resistance of the OLED device.

3. In our work maximum luminance of  $4160 \text{ cd/m}^2$  and current efficiency ( $6.38 \text{ cd/A}$ ) with a turn-on voltage of 6.4 volts have been achieved for device-5 with doping 5ml of perylene solution into a PEDOT: PSS film under thermal annealing condition.

4. We can reveal that the solution process perylene doped buffer layer can be used to solve the problem of high turn-on voltage and low efficiency of FTO based EL device. Therefore this non-conventional bilayer anode structure should be a good competitor with popularly known conventional ITO electrode in OLED society.

## 4.5 Stability of the devices:

For stability investigation of the devices, the OLEDs were stored in clean desiccators (charged with  $\text{CaCl}_2$ ) for almost 3 months and the current-voltage –luminance was noted periodically under dark room conditions. The corresponding characteristics graph of FTO+Pentacene, FTO+Perylene, FTO+Rubrene, and FTO+PEDOT: PSS are shown in the figures 4.5 (a)- (h). Similarly, the variation of maximum current efficiency with respect to time is also shown in figure 4.5 (i). From this figure it is clear that the value of current efficiency varies from 4.12cd/A to 0.9 cd/A, 5.25 cd/A to 1.18 cd/A, 6.35 cd/A to 1.7 cd/A and 6.40 cd/A to 2.11 cd/A respectively for the sample 1, 2, 3 and 4. This result demonstrated the degradation of the device performance.

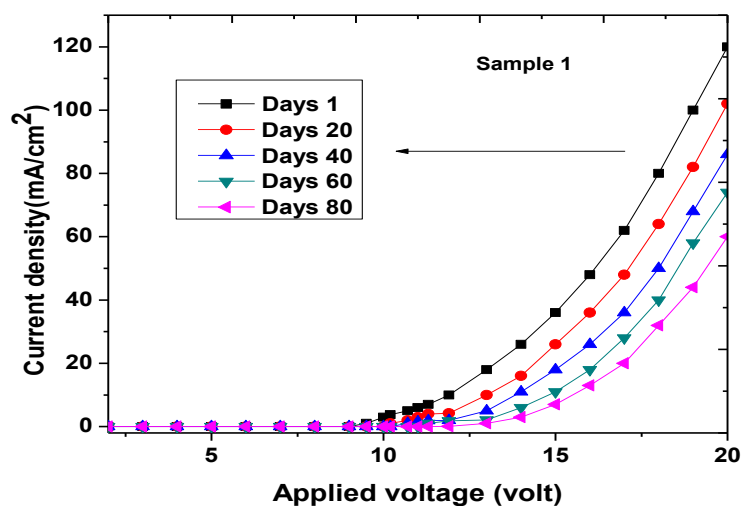


Figure 4.5 (a) : Variation of current density vs applied voltages w.r.t time (in days) for sample no.1

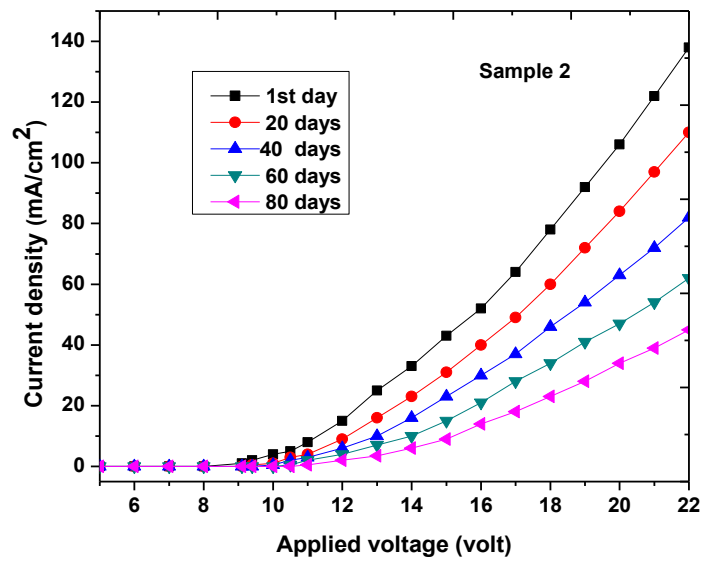


Figure 4.5 (b) : Variation of current density vs applied voltages w.r.t time (in days) for sample no.2

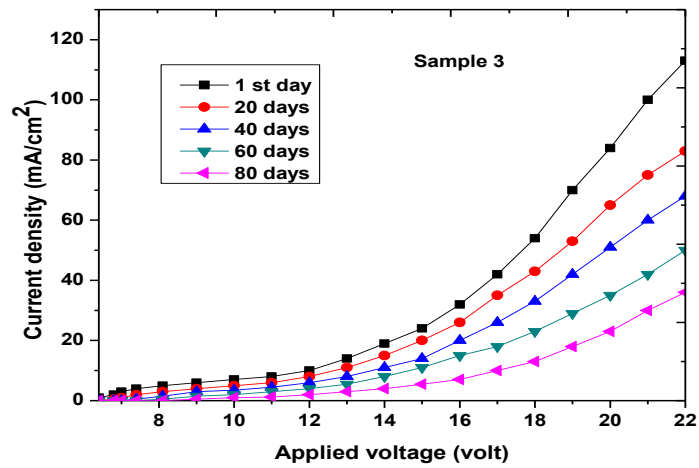


Figure 4.5 (c): Variation of current density vs applied voltages w.r.t time (in days) for sample no.3

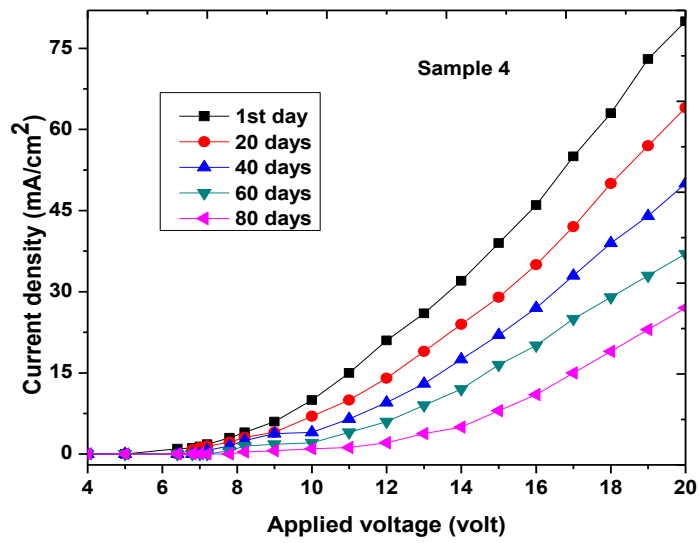


Figure 4.5 (d) : Variation of current density and voltage w.r.t time of sample-4

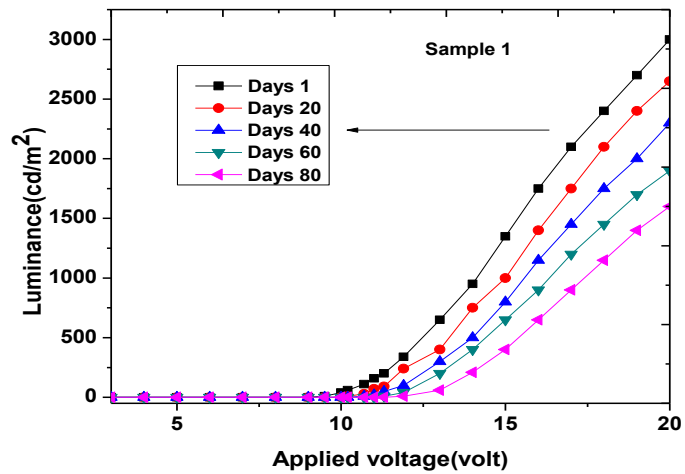


Figure 4.5 (e): Variation of luminance and voltage w.r.t time of sample-1

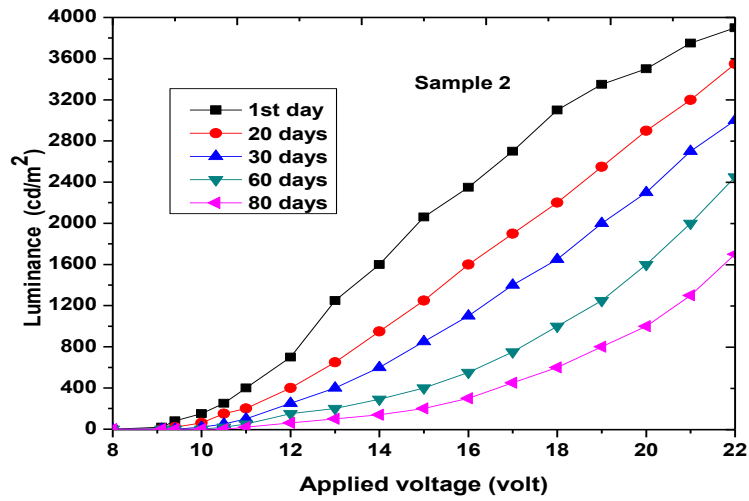


Figure 4.5 (f) : Variation of luminance and voltage w.r.t time of sample-2

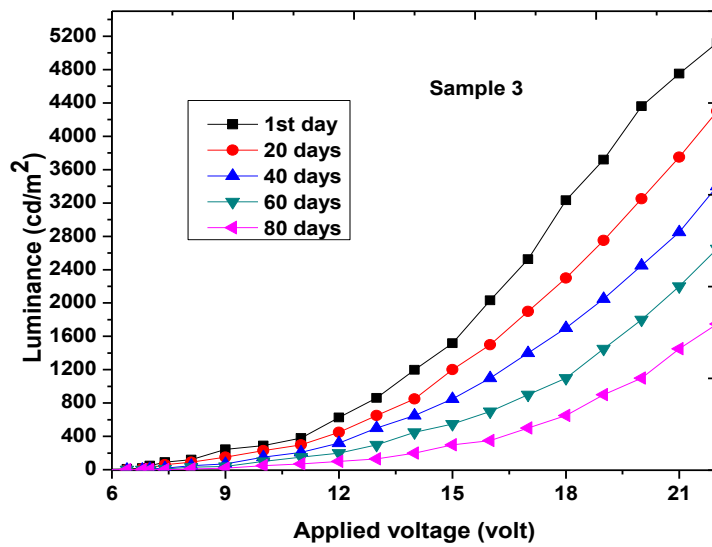


Figure 4.5 (g) : Variation of luminance and voltage w.r.t time of sample-3



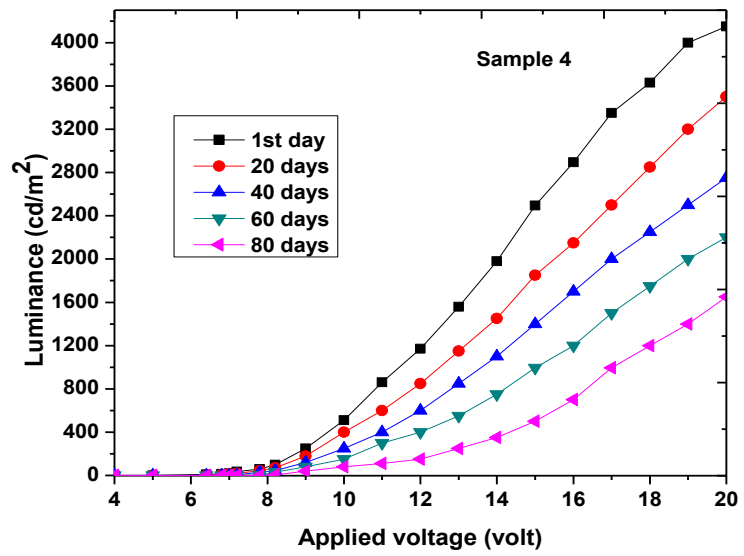


Figure 4.5 (h): Variation of luminance and voltage w.r.t time of sample-4

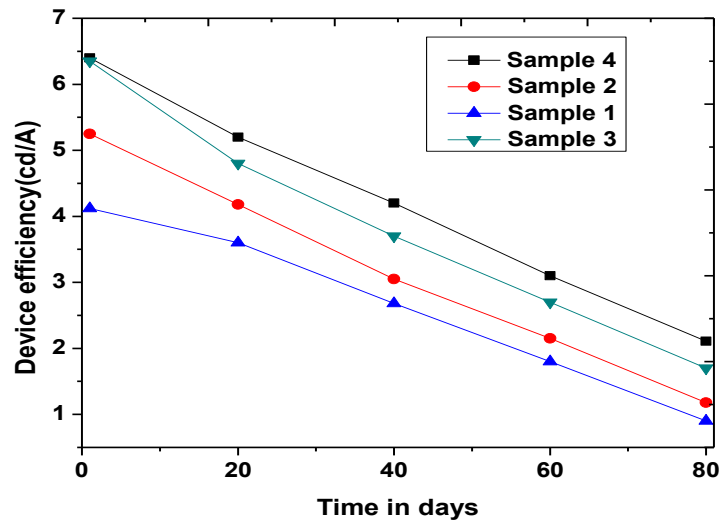


Figure 4.5 (i): Variation of maximum device efficiency w.r.t time (in days) for four different OLED sample

The decreasing values of these device parameters indicate that the existence of charge trapped in the devices with a considerable density which increases the device degradation tendency over a period and contributes to the reduced lifetime of OLEDs. In this MPD method of device fabrication, the release of vacuum after every deposition might facilitate trapping of contaminations or a layer of air in between the thin films. A layer of trapped air slowly oxidizes the films. Again the contaminants trapped between the substrates and the buffer layer may gradually migrate towards the organic layers through the grain boundaries [272] and increase the surface states. Defect produced in the vacuum evaporated thin films significantly influenced the stability of the devices. De Vos [273] observed a diffusion phenomenon at the metal/organic interface of the organic device, which increases the surface states density. Therefore in our work different bilayer anode combinations used by us are also not free from this defect. In our work, the readings were noted at different period till the devices were collapsed. From the above stability curves, it is clear that device performance continuously decreased with respect to time.

Kashiwada et al. [274] while investigating the behavior of thin film based organic devices observed that oxygen and water vapour were the main causes of device degradation. Oxygen absorption naturally brings about an increase in resistance of thin film which is responsible for the low mobility of the thin film devices. Moreover, organic materials are more sensitive to water vapour. Therefore water vapour might have contributed rapid deterioration of our devices in this highly humid region. On the

other hand, heat generated during the operation of the OLED device also accelerates the oxidation because of the presence of water vapour in the air.

## **4.6 Observations:**

(i) Out of 12 OLEDs, sample fabricated in a batch only 7 or 8 samples exhibited diode characteristics. This might be due to the non-uniform deposition of materials layers over the whole shadow mask region due to the random scattering of materials during the thermal deposition process.

(ii) Device deterioration even in vacuum desiccators indicated the presence of built-in defects in our fabricated samples.

(iii) The variation of current density and luminance with applied voltage was not found to be same in all the fabricated devices. Therefore despite the similar diode nature of the fabricated devices, about each variety was observed.

(iv) Device performance is highly depending on the fabricated condition of deposition layers. Therefore making the time of exposure of thin film layers to the ambient, before deposition of the device as small as possible.

## 4.7 Conclusions

(i) It is possible to realize OLEDs with the bilayer anode combinations FTO+Pentacene, FTO+Perylene and FTO+Rubrene by thermal vacuum evaporation method and polymer PEDOT: PSS by spin coating techniques.

(ii) Surface states together with grain boundaries trapping play an important role in the OLED behaviour.

(iii) Some built-in defects are also responsible for the decay of OLED device characteristics.

(iv) Suitable encapsulation and the use of the SPD procedure for fabrication might increase the longevity of the devices and make them suitable for use in flat-panel display technology.

(v) In this investigation, we used doping method to optimize the device for PEDOT: PSS layer whose result is found to be greater than the simple FTO+PEDOT: PSS bilayer structure. Therefore it can be said that suitable doping of the buffer layer and also the use of other deposition techniques like sputtering, chemical deposition, etc. might enable to have a deeper insight into the factors controlling the performance of these OLEDs.

(vi) It is found that organic materials are often highly disordered in the amorphous state and hence their charge carrier trapping tendency is higher than the inorganic material. In these organic materials, there is also the existence of weak interactive

force, i.e., weakly held Vander Walls force as a result of which there is a more charge trapping is occur near the interface region [275-280] compared to inorganic transition metal oxide. In our work, this might be the reason for which the efficiency of inorganic-organic based bilayer anode OLED device is smaller than inorganic-inorganic based bilayer anode OLED devices.

## 5.1 Summary and conclusions

Overall it can be summarised that performance of bilayer anode OLED is higher than that of the single electrode based device. In this work we studied the performance of interface layer between the metallic electrode and organic hole transport layer (HTL). This interface region limits the device performance mostly in thin film based EL devices. In the literature, it has been reported that diffusion of the metallic ion into the hole transport layer reduced the efficiency of the OLED devices. It is shown that the contact between the metallic electrode and hole transport layer can be improved by inserting buffer layer in the interface region. Transition metal oxide such as Vanadium Pentoxide ( $V_2O_5$ ), Nickel Oxide (NiO), Molybdenum Trioxide ( $MoO_3$ ) and Tungsten oxide ( $WO_3$ ) and organic buffer layer such as Pentacene, Perylene, Rubrene and PEDOT: PSS offers better contact behavior along with high work function value which increases the charge injection properties in OLED devices compared to the single electrode based OLED devices. Therefore by introducing these buffer layers it is possible to modify the electrode/organic interfaces which prevent the direct contact of electrode surface with organic hole transport layer and hence significantly reduces the contact resistance and provide better protection from oxygen and metallic ion diffusion towards hole transport layer and also other chemical reactions which finally increases the device performance compared with the single layer electrode surface.

On the other hand, the present study on the thin film based organic light emitting diode (OLED) using bilayer anode configuration gives valuable information about the LED

performance and the influence of traps, surface states and inbuilt defects on the device performance.

Here we have fabricated and characterized both single and double layer electrode based organic light emitting diode( OLED) using both inorganic and organic materials by using proper procedure. As mentioned above here we have chosen eight bilayer anode combinations i.e. FTO+V<sub>2</sub>O<sub>5</sub> (sample 1), FTO+NiO (sample 2), FTO+MoO<sub>3</sub> (sample 3), FTO+WO<sub>3</sub> (sample 4), FTO+Pentacene (sample 5), FTO+Perylene (sample 6), FTO+Rubrene (sample 7) and FTO+Doped PEDOT: PSS (sample 8) for investigation. The results obtained on these combinations (chapter 3 and chapter 4) are found to be greater than the single FTO based device indicating that the performance of bilayer anode OLED is higher than the single layer electrode based OLED devices.

In our study, all the varieties of thin film based OLEDs were fabricated on FTO coated glass substrates by the MPD method with the help of mechanically produced shadow mask. It is the reason that the active areas of the devices were almost remaining same in all cases. Fabricated OLEDs were stored in clean desiccators charged with fused CaCl<sub>2</sub> for few days. Then their properties were studied to evaluate their performances.

The current-voltage characteristics of each variety were obtained by the plots of current density versus applied voltage from the starting voltage of zero volts. In our work, all the fabricated OLEDs are bottom emitting type in which turn-on voltage is greater than 5 volts. The various OLEDs parameters such as current density, luminance, current efficiency and power efficiency are shown in tables 3.1, table 3.2, table 3.3, table 3.4, table 4.1,table 4.2, table 4.3 and table 4.4 for sample 1, sample 2,

sample 3, sample 4, sample 5, sample 6 sample 7 and sample 8 respectively ( chapter 3 and chapter 4). Such parameters obtained by the other investigators for the devices fabricated by the MPD/SPD etc. procedure is shown in Table-5 in this section. The comparison of these parameters with those obtained by earlier result [37, 75, 87, 90, 100] shows that the values obtained by us are found to be better. Therefore we can say that these FTO based bilayer anode structure should be a good competitor with popularly known ITO electrode in OLED society. The current efficiency and power efficiency values of the fabricated devices were obtained by considering the Lambertian Emission Pattern [281]. Current density and luminance values were found to be increased with the increasing values of applied voltages. This is a good indicator of diode behaviour of the fabricated devices. At higher current density (or voltage region) region the efficiency values of the devices were decreased due to quenching phenomenon as reported by earlier workers [49, 69, 107, 114]. Here again, among the different set of bilayer anode configuration, FTO+WO<sub>3</sub> OLED showed better device efficiency compared to the other varieties of the fabricated OLEDs. The comparatively low values of the efficiency of a different set of OLED is associated with the energy level alignment (i.e., work function) of the bilayer anode structure with respect to the organic hole transport layer (HTL) and the presence of trapping charge carriers due to the existence of surface states in the MPD fabricated device. This result is higher than the among all the organic buffer layer based devices as discussed in above section 4.7.



**Table-5** Turn-on voltage, current efficiency and power efficiency of the Organic Light Emitting Diode (OLED) in bilayer anode structure by other workers:

<b>Structure of bilayer anode</b>	<b>Workers</b>	<b>Turn-on voltage (volt)</b>	<b>Current efficiency (cd/A)</b>	<b>Power efficiency (lm/W)</b>
FTO+SPAN	Adriano R. V. Benvenho et. al. [90]	11.2	0.80	0.25
ITO+Al <sub>2</sub> O <sub>3</sub>	L. Zhou et.al [37]	7.92	3.53	1.30
ITO+ TiO <sub>2</sub>	Zhang Zhi-Feng et.al [75]	11.3	6.01	1.44
ITO+ WO <sub>3</sub>	Jingze Li et.al [87]	7.50	2.01	0.83
ITO+CBP	Huishan Yang et.al [100]	10.1	5.60	2.79

The stability investigation on the OLEDs stored in dry air for a certain period and then exposed to the ambient atmosphere indicated the existence of surface states in these devices. The parameters of the devices were found to decrease significantly with respect to the variation of time. The rate of decrement of the current density of each optimized OLED device at ambient atmosphere under dark room conditions is as follows:

$$\frac{dj}{dt} = 2.56(\text{ mA/cm}^2) \text{ per day [ Sample 1]} \quad \frac{dj}{dt} = 0.56(\text{ mA/cm}^2) \text{ per day [ Sample$$

2],

$$\frac{dj}{dt} = 0.47(\text{ mA/cm}^2) \text{ per day [ Sample 3]}, \quad \frac{dj}{dt} = 0.85(\text{ mA/cm}^2) \text{ per day [ Sample$$

4],

$$\frac{dj}{dt} = 0.75(\text{ mA/cm}^2) \text{ per day [ Sample 5]} \quad \frac{dj}{dt} = 1.16(\text{ mA/cm}^2) \text{ per day [ Sample$$

6],

$$\frac{dj}{dt} = 0.96(\text{ mA/cm}^2) \text{ per day [ Sample 7]}, \quad \frac{dj}{dt} = 0.66(\text{ mA/cm}^2) \text{ per day [Sample$$

8],

The rate of decrement of the luminance of each optimized OLED device at ambient atmosphere under dark room conditions is as follows:

$$\frac{dl}{dt} = 44.68(\text{ cd/m}^2) \text{ per day [ Sample 1]}, \quad \frac{dl}{dt} = 31.77(\text{ cd/m}^2) \text{ per day [ Sample 2]},$$

$$\frac{dl}{dt} = 14.37(\text{ cd/m}^2) \text{ per day [ Sample 3]}, \quad \frac{dl}{dt} = 26.25(\text{ cd/m}^2) \text{ per day [ Sample 4]},$$

$$\frac{dl}{dt} = 17.50(\text{ cd/m}^2) \text{ per day [ Sample 5]}, \quad \frac{dl}{dt} = 27.50(\text{ cd/m}^2) \text{ per day [ Sample 6]},$$

$$\frac{dl}{dt} = 42.12(\text{ cd/m}^2) \text{ per day [ Sample 7]}, \quad \frac{dl}{dt} = 31.25(\text{ cd/m}^2) \text{ per day [ Sample 8]}$$

Similarly the rate of decrement of the current efficiency of each optimized OLED device at ambient atmosphere under dark room conditions is as follows:

$$\frac{d\gamma}{dt} = 0.026 \text{ ( cd/A ) per day [ Sample 1]}, \quad \frac{d\gamma}{dt} = 0.051 \text{ ( cd/A ) per day [ Sample 2]}$$

$$\frac{d\gamma}{dt} = 0.047 \text{ ( cd/A ) per day [ Sample 3]}, \quad \frac{d\gamma}{dt} = 0.053 \text{ ( cd/A ) per day [ Sample 4]},$$

$$\frac{d\gamma}{dt} = 0.040 \text{ ( cd/A ) per day [ Sample 5]}, \quad \frac{d\gamma}{dt} = 0.50 \text{ ( cd/A ) per day [ Sample 6]},$$

$$\frac{d\gamma}{dt} = 0.058 \text{ ( cd/A ) per day [ Sample 7]} \quad \frac{d\gamma}{dt} = 0.048 \text{ ( cd/A ) per day [ Sample 8]}$$

The present investigation reported the different electrode-buffer layer combinations and tests their feasibility in OLEDs manufactured by the MPD procedure. It is concluded that the fabrication of the OLEDs by the MPD method using bilayer electrode combinations given in chapter 3 and 4, might increase the lifetime of the OLEDs by preventing the increase of surface states with the help of suitable encapsulation. However to arrive at ultimate conclusion regarding the usefulness and viability of these devices in practical circuitry further studies would be required. Photolithography which is known to give finest resolution of the patterns may also be used for pattern delineation. Therefore it can be said that improved facilities in the laboratory is useful for better development of OLED device with improved properties.

No encapsulation (as mentioned above) was used for the fabricated devices. As such harmful contaminants might have diffused into the devices and caused the ultimate

deterioration. Thus suitable encapsulation and the use of the other deposition techniques may give the OLEDs long-term stability and make them suitable for widespread use in electronic devices.

## **5.2 Recommendations for Future Work**

The result or findings of this work are not only interesting, but it also demonstrated the utility of non-conventional and less popularly FTO electrode towards the application of OLED society. Highly performance of FTO based OLED was realized for the first time as an outcome of this thesis. However, still, there are several issues that need to be explored for further development of OLED performance over this non-conventional FTO electrode. Some significant point of future work which should be performed to continue development of FTO based OLEDs is mentioned below:

(a) Here we consider Al as a cathode material because of its low cost and provide a better charge transport path for the negative charge carrier regarding the formation of exciton inside the light emitting region. However, it is also known that Al oxidized quickly. As a result of which it leads to the formation aluminium oxide barrier between the organic and LiF thin film. This will increase the device capacitance which finally increases the bias voltage to generate the considerable current through the device. Therefore, it will be possible to increase the stability of FTO based OLED by using an Au thin film by replacing Al which has more resistant to oxide formation.

(b) It is also possible to enhance the OLED performances through device engineering, such as a mixed host, stepwise doping or double emissive layer structure. Depending on device structures, different dopants and host materials for emissive layer should be used along with various thickness and inducer layer to optimize the electrical and optical performances of FTO devices.

(c) Similarly, from the literature report, it is known to us that proper incorporation of an interlayer between the hole transport layer and an emitting layer (HTL/EML) interface dramatically enhanced the ITO based OLED performances by blocking triplet exciton quenching and reducing the charge overflow. Therefore it is also possible to increase the FTO based device performance by using this interlayer concept within the HTL and EML region.

(d) In our work, we enhanced the device performance by adjusting the hole injection layer or buffer layer over the electrode surface by making it bilayer anode. From the recent report, we come to know that multilayer anode structure over ITO surface has also possessed the good potential for increasing device efficiency. Because these structures provide very low sheet resistance and higher optical transparency under optimized condition. This work over FTO surface has not been carried out yet and will be one of the focuses in the further work.

Thus it is possible to further study the different direction to enhance the OLED performances over non-conventional FTO electrode substrates.

### **5.3. Paper published and papers presented**

#### **(a) Papers published:**

(i) Improved performance of organic light-emitting diode with vanadium pentoxide layer on the FTO surface, [Pramana – J. Phys. DOI 10.1007/s12043-017-1389-9].

(ii) A comparative study of the influence of nickel oxide layer on the FTO surface of organic light emitting diode [ Indian J Phys. DOI 10.1007/s12648-017-1103-2]

(iii) Fabrication of organic light emitting diode using Molybdenum Trioxide interlayer between the electrode and organic interface (Under Communicated)

(iv) Organic Light Emitting Diode with Perylene interlayer between electrode-organic interface [Journal of ELECTRONIC MATERIALS, DOI: 10.1007/s11664-017-5806-0]

(v) Improve Performance of Bottom Emitting Organic Light Emitting Diode using Rubrene interlayer between the electrode and organic interface (Under Communicated)

(vi) Organic Light Emitting Diode with Fluorine-doped Tin Oxide (FTO)/ Perylene doped PEDOT: PSS bilayer electrode ( Under Communicated)

## **(b) Papers presented:**

(i) National Conference on Role of Optics and Philosophy in Environment Protection (ROPEP-2015), 10 and 11 March 2015. Woman college, Tinsukia

(ii) 4<sup>th</sup> International Conference on Advanced Nanomaterials and Nanotechnology, December 08-11 2015. Centre for Nanotechnology, Indian Institute of Technology Guwahati( IITG).

(iii) Eleventh National Conference on Solid State Ionics ( NCSSI-11), Department of Physics, Tezpur University December 21-23, 2015.

(iv) International Conference on Light and Light-Based Technologies (ICLLT), November 26-28, 2016 Tezpur University, Assam, India.

(v) X<sup>th</sup> Biennial National Conference of Physics Academy of North-East (PANE) on the theme of “ Recent Advances in Physics Research and its Relevance” 10<sup>th</sup>-12<sup>th</sup> November 2016.

(vi) International Conference on Emerging Trends in Nanomaterials Science and Technology (ICETNMST-2017), January 4-6, 2017, National Institute of Technology (NIT) Nagaland.

## **5.4 Workshop attended:**

- (I) IUCAA sponsored Workshop on “Introductory Astronomy and Astrophysics,” Department of Physics, Jagannath Barooah College, Jorhat, Assam, March 13 and 14 2015.
- (II) IUCAA sponsored Workshop on “Astronomical Data Analysis,” Department of Physics, Jagannath Barooah College, Jorhat, Assam, March 17-19, 2016.
- (III) National Seminar cum Workshop on advances in science and technology and pertinent need of instrumentation, 9-11<sup>th</sup> September 2016, Department of Physics and IQAC, Sibsagar College, Joysagar in association with CSIR-NEIST, JORHAT.



## 5.5 Bibliography:

- [1]. W. Helfrich and W. G. Schneider, *Phys. Rev. Lett.*, **14**, 229 (1965)
- [2]. H. P. Schwob, J. Fuenfschilling, and I. Zschokke-Gränacher, *Mol. Cryst. and Liq. Cryst.*, **20**, 39 (1970)
- [3]. P. S. Vincentt, W. A. Barlow, R. A. Hann, and G. G. Roberts, *Thin Solid Films*, **94**, 171 (1982)
- [4]. C W Tang and S A Vanslyke, *Appl. Phys. Lett.* **51**, 913 (1987).
- [5]. Ching W Tang, Chin H Chen, Ramanuj Goswami, , Ramanuj Goswami, US Patent 4,769,292, (1988)
- [6]. SA VanSlyke, CW Tang, LC Roberts - US Patent 4,720,432, (1988)
- [7]. C.W. Tang, S.A.VanSlyke, and C.H.Chen, *J.Appl.Phys.* 65 (9), 1 May, (1989)
- [8]. Ching W Tang and Steven A VanSlyke, US Patent 4,885,211, (1989)
- [9]. J H Burroughes, D D C Bradley, A R Brown, R N Marks, K Mackay, R H Friend, P L Burns and A B Holmes, *Nature* 347, 539 (1990)
- [10]. D. Braun, A.J. Heeger, *Applied Physics Letters* 58, (1991).
- [11]. SA VanSlyke, CW Tang, ME O'brien, CH Chen - US Patent 5,061,569, (1991).
- [12]. Li, Changjiang, Song and Zhigang, *Synthetic Metals* 40(1), 23-8 (1991).
- [13]. Zhang, Hao and Li Changjiang, *Synthetic Metals*, 44(2), 143-6, (1991).

- [14]. G. Gustafsson, Y. Cao, G. M. Treacy, F. Klavetter, N. Colaneri & A. J. Heeger, *Nature* 357, 477 – 479, (1992).
- [15]. P. L. Burn, A. B. Holmes, A. Kraft, D. D. C. Bradley, A. R. Brown, R. H. Friend & R. W. Gymer, *Nature* 356, 47 – 49,( 1992).
- [16]. Paul L. Burn, Andrew B. Holmes, Arno Kraft, Donal D. C. Bradley, Adam R. Brown and Richard H. Friend, *J. Chem. Soc., Chem. Commun.*, 32-34, (1992).
- [17]. Yutaka Ohmori, Akihiko Fujii, Masao Uchida, Chikayoshi Morishima, and Katsumi Yoshino, *Appl. Phys. Lett.* 63, 1871 (1993)
- [18]. Kock Yee Law, *Chem. Rev.*, 93 (1), pp 449–486 (1993).
- [19]. S. Saito, T. Tsutsui, M. Era, N. Takada, C. Adachi, T. W. Y. Hamada, *Proc. SPIE*, 1910, 212–221, (1993).
- [20]. N. Takada, T. Tsutsui, and S. Saito, *Appl. Phys. Lett.*, vol. 63, 2032-2034 (1993)
- [21]. P. E. Burrows, V. Bulovic, S. R. Forrest, L. S. Sapochak, D. M. McCarthy, and M. E. Thompson, *Appl. Phys. Lett.* , **65**, 2922 (1994).
- [22]. Greenham NC, Friend RHand Bradley DDC, *AdvMater* **6**:491 (1994).
- [23]. A. Dodabalapur, L. J. Rothberg, T. Miller, and E. W. Kwock, *Appl. Phys. Lett.*, vol. 64, 2486- 2488 (1994)
- [24]. T. Tsutsui, N. Takada, S. Saito, and E. Ogino, *Appl. Phys. Lett.* vol. 65, 1868-1870 (1994)
- [25]. Hosokawa C, Hiigashi H, Nakamura H and Kutomoto T, *Appl. Phys. Lettr.* , **67**,3853, (1995).

- [26]. N.C. Greenham, I.D. W. Samuel, G.R. Hayes, R. T. Phillips, Y.A.R.R. Kessener, S.C. Moratti, A.B. Holmes and R.H. Friend, *Chern. Phys. Lett.* 241, 89 (1995).
- [27]. M. Onoda, K. Yoshino, *Jpn. J. Appl. Phys.* **34**, L260 (1995)
- [28]. J. H. P. Utley, Y. P. Gao, J. Gruber, Y. Zhang, and A. Munoz- Escalona, *J. Mater. Chem.* **5**, 1297 (1995)
- [29]. J. Gao, A. J. Heeger, J. Y. Lee, and C. K. Kim, *Synth. Met.* 82, 221 (1996).
- [30]. Christian Amatore, Florence Gaubert, Anny Jutand and James H. P. Utley , *J. Chem. Soc., Perkin Trans. 2*, 2447-2452, (1996).
- [31]. Tsuyoshi Kawai, Takahiro Yamaue, Kazuya Tada, Mitsuyoshi Onoda, Sung-Ho Jin, Sam-Kwon Choi and Katsumi Yoshino , *Japanese Journal of Applied Physics*, 35, 2, (1996).
- [32]. Stanislav Nespurek, Vera Cimrova , Jiri Pflieger and Ivan Kminek, *Polymer for advanced technoly*, 7, 459–470, (1996).
- [33]. Burroows PE, Gu G, Bulovic V, Shen Z, Forrest SR and Thompson ME, *IEEE Transactions on electron devices* **44**:1188 (1997)
- [34]. Wu CC, Wu CI, Sturm JC and Kahn A, *Appl Phys Lett* **70**:1348 (1997)
- [35]. Wakimoto T, Fukuda Y, Nagayama K, Yokoi A, Nakada H and Tsuchida M, *IEEE Transactions on Electron Devices* **44**:1245 (1997)
- [36]. Hung LS, Tang CW and Mason MG, *Appl Phys Lett* **70**:152 (1997)
- [37]. Li F, Tang H. Anderegg J and Shinar J, *Appl Phys Lett* **70**:1233 (1997)
- [38]. Jabbour GE, Kippelen B, Armstrong NR and Peyghambarian N, *Appl Phys Lett* **73**:1185 (1998).

- [39]. Baldo MA, O'Brien DF, You Y, Shoustikov A, Sibley S, Thompson ME and Forrest SR, *Nature* **395**:151 (1998)
- [40]. S. T. Lee, X. Y. Hou, M. G. Mason, and C. W. Tang, *Appl. Phys. Lett.* **72**, 1593 (1998).
- [41]. S.T. Mori, H. Fujikawa, S. Tokito, and V. Taga, *Appl. Phys. Lett.* **73**, 2763 (1998).
- [42]. Kraft, A., Grimsdale A. C., Holmes A. B., *Angew., Electroluminescent Conjugated Polymers-Seeing Polymers in a New Light*, in *Chem. Int. Ed.*, 37, 402, (1998).
- [43]. G. Parthasarathy, P.E. Burrows, V. Khalfin, V.G. Kozlov, S.R. Forrest, in *Applied Physics Letters* 72, 2138-2140, (1998).
- [44]. O'Brien DF, Baldo MA, Thompson ME and Forrest SR, *Appl Phys Lett* **74**:442 (1999)
- [45]. Gu G, Parthasarathy G and Forrest SR, *Appl Phys Lett* **74**:305 (1999)
- [46]. S. K., Choi, W. K., Leung, L. M., and Neyts, K., *Applied Physics Letters* **74**(14), 1939 – 1941 (1999).
- [47]. M. Stossel, J. Staudigel, F. Steuber, J. Simmerer and A. Winnacker, *Appl. Phys. A* 68, 387–390 (1999).
- [48]. X. Zhou, J. He, L. S. Liao, M. Lu, Z. H. Xiong, X. M. Ding, and X. Y. Hou, *Appl. Phys. Lett.*, 74, 4, (1999).
- [49]. X.M.Ding, L.M.Hung, L.G.Cheng and S.T.Lee, *Appl. Phys. Lett.* **76**, 2704 (2000)
- [50]. Huang J, Yang K, Liu S and Jiang H, *Appl Phys Lett* **77**:1750 (2000)

- [51]. Wasey, J. A. E. and Barnes, W. L., *Journal of Modern Optics* **47**(4), 725 – 741 (2000).
- [52]. A. Elschner, F. Bruder, H.-W. Huer, F. Jonas, A. Karbach, S. Kirchmeyer, S. Thurm, and R. Wehrmann, *Synt. Met.*, vol. 111-112, 139–143, (2000).
- [53]. H. Fujikawa, T. Mori, K. Noda, M. Ishii, S. Tokito, and Y. Taga, *J. of Lumin.*, vol. 87–89, 1177–1179, (2000).
- [54]. P. Piromreun, H. Oh, Y. Shen, G. G. Malliaras, J. C. Scott, and P. J. Brock, *Appl. Phys. Lett.*, vol. 77, 2403–2405, (2000).
- [55]. H. C. F. Martens, J. N. Huiberts, and P. W. M. Blom, *Appl. Phys. Lett.*, vol. 77, 1852–1854, (2000).
- [56]. A. J. Ma'kinen, I. G. Hill, R. Shashidhar, N. Nikolov, and Z. H. Kafaf, *Appl. Phys. Lett.*, 79, 5, (2001).
- [57]. J. Shi, Eur. Patent 1 156 536, Nov. 21, (2001).
- [58]. Adachi C, Baldo MA, Thompson ME and Forrest SR, *J Appl Phys* **90**:5048 (2001)
- [59]. Ikai M, Tokito S, Sukamoto Y, Suzuki T and Taga Y, *Appl Phys Lett* **79**:156 (2001)
- [60]. Junqing Zhao , Shijie Xie , Shenghao Han , Zhiwei Yang, Lina Ye and Tianlin Yang *phys. stat. sol. (a)* 184, No. 1, 233–238 (2001)
- [61]. Chengfeng Qiu, Haiying Chen, Man Wong, *IEEE TRANSACTIONS ON ELECTRON DEVICES*, 48, 9, (2001).

- [62]. Ji Cui, Qinglan Huang, Jonathan C. G. Veinot, †He Yan, Qingwu Wang, Geoffrey R. Hutchison, Andrew G. Richter, Guennadi Evmenenko, Pulak Dutta, and Tobin J. Marks, *Langmuir*, 18, 9958-9970, (2002).
- [63]. Maria A. and Diaz-Garcia, *Appl. Phys. Lett.* **81**, 3924 (2002)
- [64]. J Cui, Q Huang, JCG Veinot, H Yan, Q Wang, GR Hutchison and AG Richter, *Langmuir* 18 (25), 9958-9970, (2002).
- [65]. Kang SJ, Park DS, Kim SY, Whang CN, Jeong K and Im S, *Appl Phys Lett* **81**:2581 (2002)
- [66]. Qiu Y, Gao Y, Wang L, Wei P, Duan L and Zhang D, *Appl Phys Lett* **81**:3540 (2002)
- [67]. Chengfeng Qiu, Haiying Chen, Zhiliang Xie, Man Wong,a) and Hoi Sing Kwok, *Appl Phys Lett* 80, 19, (2002).
- [68]. W. H. Kim, G. P. Kushto, H. Kim and Z. H. Kafafi, *Journal of polymer physics*, 41, 21, 2522–2528, (2003).
- [69]. J. Lee and Y. Park, D. Y. Kim, H. Y. Chu, H. Lee, and L.-M. Do, *Appl Phys Lett*, 82, 2, (2003).
- [70]. J. Campbell Scott, *J. Vac. Sci. Technol. A* 21, 521 (2003)
- [71]. I-Min Chan, Franklin C. Hong, *Thin Solid Films* 450 (2003) 304–311
- [72]. Beat Ruhstaller, Tilman Beierlein, Heike Riel, Siegfried Karg, J. Campbell Scott, and Walter Riess, *IEEE journal of selected topics in quantum electronics*, 9, 3, (2003).

- [73]. Pfeiffer M, Leo K, Zhou X, Huang JS, Hofmann M, Werner A and Blochwitz-Ninot J, *Org Electron* **4**:89 (2003)
- [74]. Z. H. Kafafi, W. H. Kim, G. P. Kushto and H. Kim *Journal of polymer physics*, **41**, 21, 2522–2528, (2003).
- [75]. Zhang Zhi-Feng, Deng Zhen-Bo, Liang Chun-Jun, Zhang Meng-Xin and Xu Deng-Hui, *Displays* **24** (2003) 231–234.
- [76]. Heike Riel, Tilman A. Beierlein, Siegfried Karg and Walter Riess, *Proc. SPIE* **4800**, Organic Light-Emitting Materials and Devices VI, 148, (2003).
- [77]. W. H. Kim, G. P. Kushto, H. Kim and Z. H. Kafafi *Journal of Polymer Science: Part B: Polymer Physics*, Vol. **41**, 2522–2528 (2003)
- [78]. Lin Ke, Ramadas Senthil Kumara, Keran Zhang, Soo Jin Chua, AND A.T.S. Wee, *Synthetic Metals* **140**, 295–299, (2004).
- [79]. Haifeng WANG, Liduo WANG, Yudi GAO, Deqiang ZHANG and Yong QIU, *Japanese Journal of Applied Physics*, **43**, 10B, 1353–1355, (2004).
- [80]. Abhishek P. Kulkarni, Christopher J. Tonzola, Amit Babel, and Samson A. Jenekhe, *Chem. Mater.* **16**, 4556-4573, (2004).
- [81]. S. T. Zhang, Z. J. Wang, J. M. Zhao, Y. Q. Zhan, Y. Wu, Y. C. Zhou, X. M. Ding, and X. Y. Hou, *APPLIED PHYSICS LETTERS*, VOLUME **84**, NUMBER **15**, (2004).
- [82]. Samson A. Jenekhe, Abhishek P. Kulkarni, Christopher J. Tonzola, Amit Babel, and *Chem. Mater.* **16**, 4556-4573, (2004).

- [83]. R.M. Montereali , S. Gambino , S. Loreti, S. Gagliardi , A. Pace , G. Baldacchini , F. Michelotti, *Synthetic Metals* 143, 171–174, (2004).
- [84]. Aparna Misra, Pankaj Kumar, S. K. Dhawan, M.N. Kamalasanan and Subhas Chandra, OLED Lab, Polymeric & Soft Material Section, National Physical Laboratory, Dr. K. S. Krishnan Road, New Delhi-110 012 , (2004).
- [85]. Jung SH, Nam WJ and Han MK, *IEEE Electron Device Lett* 25:690 (2004).
- [86]. S.H. Jeong , S.B. Lee and J.-H. Boo , *Current Applied Physics* , 4, 655–658, (2004).
- [87]. Jingze Li , Masayuki Yahiro , Kenji Ishida , Hirofumi Yamada and Kazumi Matsushige, *Synthetic Metals* 151, 141–146, (2004).
- [88]. H. J. Peng, X. L. Zhu, J. X. Sun, X. M. Yu, M. Wong and H. S. Kwok, *ISSSSNN//00000055--00996666XX//0055//33660021--10006066-*, (2005).
- [89]. J. X. Sun, X. L. Zhu, H. J. Peng, M. Wong, and H. S. Kwok, *APPLIED PHYSICS LETTERS* 87, 093504, (2005).
- [90]. Adriano R. V. Benvenho, Jos´e P. M. Serbena, Rudolf Lessmann and Ivo A. Hummelgen, *Brazilian Journal of Physics*, 35, 4A, ( 2005).
- [91]. Yu, Mingxin; Wang, Meijun; Chen, Xiaohang; Hong, Bingbing; Zhang, Xiaoyan; Cheng, Chienhong, *Journal of Chemical Research*, 9, 558-560(3), (2005).
- [92]. Yoon-Chang Kim and Young Rag Do, *Optic Express*, vol.13.Issue 5, 1598-1603 (2005).
- [93]. S Shi, D Ma, *Applied Surface Science* 253 (3), 1551-1554, (2006).
- [94]. Jianfeng Li, Liangbing Hu, Lian Wang, Yangxin Zhou, George Gru1ner, and Tobin J. Marks, *Nano Letters*, 6, 8, 2472-2477, (2006).



- [95]. Bernard Geffroy, Philippe Roy and Christophe Prat, *Polym Int* 55:572–582 (2006)
- [96]. Monica Katiyar , Asha Sharma, Deepak, Organic Ultraviolet Light Emitting Diodes, Proc. of ASID '06, 8-12 Oct, New Delhi, (2006).
- [97]. By Sean W. Culligan, Andrew C.-A. Chen, Jason U. Wallace, Kevin P. Klubek, Ching W. Tang, and Shaw H. Chen, *Adv. Funct. Mater.* 16, 1481–1487, (2006).
- [98]. John E. Knox, Mathew D. Halls, Hrant P. Hrachianz and H. Bernhard Schlege, *Phys. Chem. Chem. Phys.*, 8, 1371–1377, (2006).
- [99]. Y. Sun, N.C. Giebink, H. Kanno, B. Ma, M.E. Thompson, S.R. Forrest, *Nature*, 440 , 908,(2006).
- [100]. Huishan Yang , Wenfa Xie , Yi Zhao , Jingying Hou and Shiyong Liu, *Solid-State Electronics* 51, 111–114, (2006).
- [101]. Juo-Hao Li, Jinsong Huang, and Yang Yang, *Appl. Phys. Lett.* 90, 173505, (2007).
- [102]. Pabitra K. Nayak, Neeraj Agarwal, N. Periasamy, Meghan P. Patankar and K. L.Narasimhan, *IEEE*, 978-1-4244-1727-8/07/ (2007).
- [103]. Ping-I Shih, Chen-Han Chien, Chu-Ying Chuang, Ching-Fong Shu, Cheng-Han Yang, Jian-Hong Chen and Yun Chi, *J. Mater. Chem.*, 17, 1692–1698, (2007).
- [104]. Qingjiang Sun, Yongfang Li, and Qibing Pei, *JOURNAL OF DISPLAY TECHNOLOGY*, 3, 2, ( 2007).
- [105]. Anne Köhnen, Malte C. Gather, Nina Riegel, Philipp Zacharias, and Klaus Meerholz, *APPLIED PHYSICS LETTERS* 91, 113501, (2007).

- [106]. Kwang-Hyuk Choi, Jin-A Jeong, Han-Ki Kim, Jae-Young Lee, Jung-Hwan Lee, Hyo-Dae Bae, Yoon-Heong Tak, Se-Hyung Lee, Dong-Seok Leem and Jang-Joo Kim, *The Electrochemical Society*, 155, 0013-4651 (2008).
- [107]. Fengxia Wang, Xianfeng Qiao, Tao Xiong, ma Dongge, *Organic Electronics*, 9, 6, 985-993, (2008).
- [108]. Sung-Woo Cho, Jin-A Jeong, Jung-Hyeok Bae, Han-Ki Kim, *Thin solid films*, 516, 7881-7885 (2008).
- [109]. Jin Woo Huh, Young Min Kim, Young Wook Park, Jin Hwan Choi, Jin Woo Lee, *Journal of Applied Physics* 103, 044502 (2008)
- [110]. By Henk J. Bolink, Eugenio Coronado, Diego Repetto, Michele Sessolo, Eva M. Barea, Juan Bisquert, Germà Garcia-Belmonte, Jan Prochazka and Ladislav Kavan, *Adv. Funct. Mater.* 18, 145–150, (2008).
- [111]. S. Chen, X. Li, W. Huang, *Organic Electronics*, 9, 1112–1117, (2008).
- [112]. Z. W. Liu, M. G. Helander, Z. B. Wang, and Z. H. Lu, *Appl. Phys. Lett.* 94, 113305 (2009).
- [113]. Guang-Feng Wang Xiao-Ming Tao, John H. Xin, Bin Fei, *Nanoscale research letter*, 4, 613, (2009).
- [114]. Jeongho Kim, Yeonjin Yi, Jeong Won Kim, Seok Hwan Noh and Heon Kang, *J. Phys. D: Appl. Phys.* 45 455304, (2009).
- [115]. Michael Thomschke, Robert Nitsche, Mauro Furno, and Karl Leo, *APPLIED PHYSICS LETTERS*, 94, 083303, (2009).

- [116]. J. mija and M.J. Matachowski, World Academy of Materials and Manufacturing Engineering, Volume 40 , (2009 ).
- [117]. Kanchan Saxena, V.K. Jain and Dalip Singh Mehta, Optical Materials 32, 221–233, (2009).
- [118]. Yu-Cheng Chen, Po-Ching Kao, and Sheng-Yuan Chu, OPTICS EXPRESS A167, 21, 18, (2010).
- [119]. Pabitra K Nayak, Neeraj Agarwal, Farman Ali, Meghan Patankar, K L Narasimhan and N P erisamy, J. Chem. Sci., 122, 6, 847–855, (2010).
- [120]. G. Luka, P. Stakhira, V. Cherpak, D. Volynyuk, Z. Hotra, M. Godlewski, E. Guziewicz, B. Witkowski, W. Paszkowicz, and A. Kostruba, JOURNAL OF APPLIED PHYSICS 108, 064518 , (2010).
- [121]. N. Thejo Kalyani , S.J. Dhoble , R.B. Pode, Adv. Mat. Lett. , 2(1), 65-70, (2011).
- [122]. Lian Duan,<sup>a</sup> Liudong Hou,<sup>a</sup> Tae-Woo Lee,<sup>b</sup> Juan Qiao,<sup>a</sup> Deqiang Zhang,<sup>a</sup> Guifang Dong,<sup>a</sup> Liduo Wanga and Yong Qiu, J. Mater. Chem., 20, 6392–6407, (2010).
- [123]. Tae Gu Kim, Hwan Sool Oh, You-Hyun Kim and Woo Young Kim, Transactions On Electrical and Electronics Materials, 11, 2, 85-88, (2010)
- [124]. Yongbiao Zhao, Jiangshan Chen, and Dongge Ma, APPLIED PHYSICS LETTERS 99, 163303 (2011)

- [125]. S. Cheylan , D.S. Ghosh , D. Krautz , T.L. Chen , V. Pruneri, *Organic Electronics* 12 , 818–822, (2011).
- [126]. Jonghee Lee, Jeong-Ik Lee, Joo-Won Lee, and Hye Yong Chu, *ETRI Journal*, 33, 1, (2011).
- [127]. S. A. Bagnich, Th. Unger, F. Jaiser, D. Neher, M. W. Thesen, and H. Krueger, *Journal of applied physics*, 110, 033724 (2011).
- [128]. J. Żmija and M.J. Małachowski, *Journal of Achievements in Materials and Manufacturing Engineering*, 48/1, 14-23, (2011).
- [129]. S.W. Liu, Y. Divayana, X.W. Sun, Y. Wang, K.S. Leck, and H.V. Demir, *OPTICS EXPRESS*, 19, 5 , 4513, (2011).
- [130]. Kihyon Hong, and Jong-Lam Lee, *Electronic Materials Letters*, 7, 2 , 77-9, (2011).
- [131]. S. Touihri , L. Cattinb , D-T. Nguyenb, M. Morsli , G. Louarnb , A. Bouteville , V.Froger , J.C. Bernède, doi:10.1016/j.apsusc.2011.10.146, (2011).
- [132]. Fei Xu, Ji-Young Kwon, Ji-Hoon Kim, Hee Un Kim, Jong Min Lim, Hyunduck Cho, Changhee Lee, Jonghee Lee, Jeong-Ik Lee, Do-Hoon Hwang, *Synthetic Metals* , 162, 1421-1428, (2012).
- [133]. TH Han, Y Lee, MR Choi, SH Woo, SH Bae, BH Hong, JH Ahn, TW Lee *Nature Photonics* 6 (2), 105-110, (2012).
- [134]. K. Narayan , S. Varadharajaperumal, G. Mohan Rao, M. Manoj Varma, T. Srinivas, *Current Applied Physics* 13 , 1825, (2012).

- [135]. A. Behjata , M. Neghabi, Proceedings of the 4th International Conference on Nanostructures (ICNS4)12-14 March, Kish Island, I.R. Iran, (2012).
- [136]. O. Rana, R. Srivastava, G. Chauhan, M. Zulfequar, M. Husain, P. C. Srivastava, and M. N. Kamalasanan, *Phys. Status Solidi A* , 209, 12, 2539–2545 (2012).
- [137]. Yu-Fan Chang , Chun-Yu Chen , Fang-Tsai Luo , Yu-Chiang Chao , Hsin-Fei Meng, Hsiao-Wen Zan , Hao-Wu Lin , Sheng-Fu Horng , Teng-Chih Chao , Han-Cheng Yeh and Mei-Rurng Tseng, *Organic Electronics* ,13, 388–393, (2013).
- [138]. Jun Ho Youn, Su Jin Baek, Hyeong Pil Kim, Dong Hee Nam, Younggu Lee, Jueng Gil Leeb and Jin Jang, *J. Mater. Chem. C*, 1, 3250, (2013).
- [139]. Chia-Cheng Huang, Fang-Hsing Wang, Chia-Ching Wu, Hong-Hsin Huang, and Cheng-Fu Yang, *Nanoscale Res Lett.* 8(1), 206, (2013).
- [140]. L. Zhou, J. Y. Zhuang, S. Tongay, W. M. Su, and Z. Cui, *J. Appl. Phys.* 114, 074506 (2013).
- [141]. Lucia Petti, Massimo Rippa, Rossella Capasso, Giuseppe Nenna, Anna De Girolamo Del Mauro, Giuseppe Pandolfi, Maria Grazia Maglione, and Carla Minarini, *ACS Appl. Mater. Interfaces* , 5, 4777–4782, (2013).
- [142]. Lucia Petti<sup>1</sup>, Massimo Rippa<sup>1</sup>, Rossella Capasso<sup>1</sup>, Giuseppe Nenna<sup>2</sup>, Anna De Girolamo Del Mauro<sup>2</sup>, Maria Grazia Maglione<sup>2</sup> and Carla Minarini, *Nanotechnology* 24 315206, (2013).

- [143]. Keigo Sato, Katsuyuki Shizu, Kazuaki Yoshimura, Atsushi Kawada, Hiroshi Miyazaki, and Chihaya Adachi, *Phys. Rev. Lett.* 110, 247401, (2013).
- [144]. Pen-Cheng Wang<sup>a,†</sup>, Li-Hung Liu<sup>a</sup>, Desalegn Alemu Mengistie<sup>a,b,c</sup>, Kuan-Hsun Li<sup>a</sup>, Bor-Jiunn Wen<sup>d,e</sup>, Tzong-Shi Liu<sup>e</sup>, Chih-Wei Chu, *Displays* 34, 301–314, (2013).
- [145]. Mark T Greiner<sup>1</sup> and Zheng-Hong Lu, *NPG Asia Materials*, 5, (2013).
- [146]. Jiajie Liang, Lu Li, Xiaofan Niu, Zhibin Yu, and Qibing Pei, *J. Phys. Chem. C*, 117 (32), 16632–16639, (2013).
- [147]. Y. Karzazi, *J. Mater. Environ. Sci.* 5 (1), 1-12, (2014).
- [148]. Ehsan Najafabadi, Georgia Institute of Technology DECEMBER (2014).
- [149]. Jun-Hyuk Choi ; Sang-Keun Sung ; Chul-Hyun Kim ; Yeon-Ho Jung ; Joo-Yun Jung ; Jun-Ho Jeong ; Eung-Sug Lee, *J. Nanophoton.* 8(1), 083089, (2014).
- [150]. Carolin Isenberg and Tobat P. I. Saragi, *J. Mater. Chem. C*, 2, 8569–8577, (2014).
- [151]. Kasinath Ojha<sup>1</sup>, Oruganti Anjaneyulu<sup>1</sup> and Ashok K. Ganguli, *CURRENT SCIENCE*, VOL. 107, NO. 3, 10, ( 2014).
- [152]. Jun Wang, Weizhi Li and Chong Wang, *Journal of Nanomaterials*, Article No. 1, January 2014.
- [153]. Kazuyuki Yamae, Varutt Kittichungchit, Nobuhiro Ide, Masayuki Ota, Takuya Omoda, Volume 45, San Diego, CA, June 1–6, 682–685, (2014).

- [154]. Chizu Sekine, Yoshiaki Tsubata, Takeshi Yamada, Makoto Kitano and Shuji Doi, *Sci. Technol. Adv. Mater.* 15, 034203, (2014).
- [155]. Hongli Zhu, Zhiqiang Fang, Colin Preston, Yuanyuan Li and Liangbing Hu, *Energy Environ. Sci.*, 7, 269-287, (2014).
- [156]. Wenya Xu, Jianwen Zhao, Long Qian, Xianying Han, Liangzhan Wu, Weichen Wu, Minshun Song, Lu Zhou, Wenming Su, Chao Wang, Shuhong Nie and Zheng Cui, *Nanoscale*, 6, 1589-1595 (2014).
- [157]. Tae-Hee Han, Su-Hun Jeong, Yeongjun Lee, Hong-Kyu Seo, Sung-Joo Kwon, Min-Ho Park & Tae-Woo Lee, *Journal of Information Display*, 16, 2, 71–84, (2015).
- [158]. BOUANATI Sidi Mohammed , N. E. CHABANE SARI , MOSTEFA KARA Selma, *Transactions on Electrical and Electronic Materials.* 16(3): 124-129, (2015).
- [159]. Eliot F. Gomez and Andrew J. Steckl, *ACS Photonics*, 2 (3), 439–445, (2015).
- [160]. Xiaolong Yang, Xianbin Xu and Guijiang Zhou, *J. Mater. Chem. C*, 3, 913-944 , (2015).
- [161]. Hironori Kaji , Hajime Suzuki , Tatsuya Fukushima , Katsuyuki Shizu , Katsuaki Suzuki and Shosei Kubo, *Nature Communications* 6, Article number: 8476, (2015)
- [162]. Malte C. Gathera and Sebastian Reineke, *Journal of Photonics for Energy* 057607-1-19, Vol. 5, (2015).

- [163]. Andrzej Danell<sup>1</sup>, Łukasz Chacaga<sup>1</sup>, Tomasz Uchacz<sup>2</sup>, Monika Pokladko-Kowar<sup>3</sup>, Ewa Gondek<sup>3</sup>, Paweł Karasin'ski<sup>4</sup> and Bouchta Sahraou, *Adv. Device Mater.*, 1, 17-22,(2015).
- [164]. Jae-Hyun Lee; Min-Hoi Kim; Haechul Choi and Yoonseuk Choi, *Proc. SPIE 9668, Micro+Nano Materials, Devices, and Systems*, 966829 (2015).
- [165]. Young hoon kim, Himchan cho, Jin Hyuck Heo, Tae-Sik Kim and No Soung Myoung, *Advanced materials*, 27, 7 ,1248–1254, (2015).
- [166]. Korwin M. Schelkle, Markus Bender, Krischan Jeltsch, Tiago Backup and Klaus Mullen, *Angewandte*, 54, 48, 14545–14548, (2015).
- [167]. Akanksha Uniyal, Srishti, Poornima Mittal, *International Conference on Computing, Communication and Automation (ICCCA)*, 2016.
- [168]. Bo Wang, Lei Zhang, Yun Hu, Xiao-Bo Shi, Zhao-Kui Wang and Liang-Sheng Liao, *J. Mater. Chem. C*, 4, 6570-6574, (2016).
- [169]. Yuan Li, Ying Wu, Weimei Zeng, Yuda Li, Lijia Xu, Xueqing Qiu, Runfeng Chen, and Wei Huang, *ACS Sustainable Chem. Eng.*, 4 (4), 2004–2011, (2016).
- [170]. E. Angioni, M. Chapran, K. Ivaniuk, N. Kostiv, V. Cherpak, P. Stakhira, A. Lazauskas, S. Tamulevičius, D. Volyniuk, N. J. Findlay, T. Tuttle, J. V. Grazulevicius and P. J. Skabara, *J. Mater. Chem. C*, 4, 3851-3856, (2016).
- [171]. Daniel Volz; Thomas Baumann, *Proc. SPIE 9941, Organic Light Emitting Materials and Devices XX*, 994102 (3 November 2016).



- [172]. Adam F. Henwood, Ashu K. Bansal, David B. Cordes, Alexandra M. Z. Slawin, Ifor D. W. Samuelb and Eli Zysman-Colman ,*J. Mater. Chem. C*, DOI: 10.1039/c6tc00151c, (2016).
- [173]. Jin-Woong Honga, and Yi-Wei Guo, TRANSACTIONS ON ELECTRICAL AND ELECTRONIC MATERIALS, 17, 1, 37-40, (2016).
- [174]. Rafael Gómez-Bombarelli,, Jorge Aguilera-Iparraguirre,, Timothy D. Hirzel,, David Duvenaud,, Dougal Maclaurin,, Martin A. Blood-Forsythe,, Hyun Sik Chae,, Markus Einzinger,, Dong-Gwang Ha, *Nature Materials*, 15, 1120–1127, doi:10.1038/nmat4717, (2016).
- [175]. Tae-Hee Han, Mi-Ri Choi, Chan-Woo Jeon, Yun-Hi Kim, Soon-Ki Kwon, Tae-Woo Lee , *Sci. Adv.*, 2, 1601428, (2016).
- [176]. Jie Yang, Jing Huang, Qianqian Li and Zhen Li, *J. Mater. Chem. C*, 4, 2663-2684, (2016).
- [177]. Yonggang Yao, Jinsong Tao, Jianhua Zou, Bilun Zhang, Tian Li, Jiaqi Dai, Mingwei Zhu, Sha Wang, Kun Kelvin Fu, Doug Henderson, Emily Hitz, Junbiao Peng and Liangbing Hu, *Energy Environ. Sci.*, 9, 2278-2285, (2016).
- [178]. Yilin Xu, Haojian Yu, Cong Wang, Jin Cao, Yigang Chen, Zhongquan Ma, Ying You, Jixiang Wan, Xiaohong Fang, and Xiaoyuan Chen, *Nanoscale Res Lett.*, 12: 254 (2017).
- [179]. Zhike Liu, Shu Ping Lau and Feng Yan, *Chem. Soc. Rev.*, 44, 5638-5679, (2017).

- [180]. Meiling Shan, Haipeng Jiang, Yu Guan, Dongsu Sun, Yu Wang, Jie Hua and Jin Wang, *RSC Adv.*, **7**, 13584-13589, (2017).
- [181]. Bao-jia Li, Huang Li, Li-jing Huang, Hai-di Cao, Wei Zu, Nai-fei Ren, Hua Ding, Xia Kong, Jie-lu Zhang, *Ceramics International* , **43**, **9** , 7329-7337, (2017).
- [182]. Heng Zhang, Siting Wang, Xiaowei Sun, Shuming Chen *SID*, **25**, **3** , 143–150, (2017).
- [183]. Qingchen Dong, Feifei Tai, Hong Lian, Bo Zhao, Zheng Zhong, Zheng Chen, Jianxin Tang and Furong Zhu, *Nanoscale*, **9**, 2875-2882, (2017).
- [184]. Heng Zhang, Siting Wang, Xiaowei Sun, Shuming Chen *SID*, **25**, **3** , 143–150, (2017).
- [185]. Xingliang Dai, Yunzhou Deng, Xiaogang Peng, Yizheng Jin, *Advanced Materials*, **29**, **14**, (2017).
- [186]. Amos Egel , Guillaume Gomard, Siegfried W Kettlitz and Uli Lemmer, IOP Publishing Ltd *Journal of Optics*, **19**, **2** , (2017).
- [187]. C. Schmitz, H. W. Schmidt and M. Thelakkat, *Proceedings of SPIE* **4105**, 183 (2001)
- [188]. Z. Liu, O. V. Satata and N. Male, *Synth. Met.* **128**, 211 (2002).
- [189]. S. Barth, P. Muller, H. Riel, P. F. Seidler, W. Rieb, H. Vestweber and H. Bassler, *J. Appl. Phys.* **89**, 3711 (2001).
- [190]. M. Stolka, J. F. Yanus and D. M. Pai, *J. Phys. Chem.* **88**, 4707 (1984).

- [191]. L. S. Liao, X. H. Sun, L. F. Cheng, N. B. Wong, C. S. Lee and S. T. Lee, Chem.Phys. Lett. **333**, 212 (2001).
- [192]. B. J. Chen, W. Y. Lai, Z. Q. Gao, C. S. Lee, S. T. Lee and W. A. Gambling, Appl. Phys. Lett. **75**, 4010 (1999).
- [193]. R. G. Kepler, P. M. Beeson, S. J. Jacobs, R. A. Anderson, M. B. Sinclair, V.S. Valencia and P. A. Cahill, Appl. Phys. Lett. **66**, 3618 (1995).
- [194]. G. G. Malliaras, Y. Shen, D. H. Dunlap, H. Murata and Z. H. Kafafi, Appl. Phys. Lett. **79**, 2582 (2001).
- [195]. Oxtoby, D.W., W.A. Freeman, and T.F. Block, *Chemistry: Science of Change*. Pacific Grove: Thomson-Brook, 4th ed. (2003).
- [196]. Adachi, C., et al., J Appl Phys, **90**(10), 5048-5051, (2001).
- [197]. Baldo, M.A., et al., Nature, **395**(6698), 151-154, (1998).
- [198]. Baldo, M.A., et al Applied Physics Letters, **75**(1), 4-6 (1999).
- [199]. Thompson, M.E., P.E. Burrows, and S.R. Forrest, Current Opinion in Solid State & Materials Science, **4**(4): p. 369-372, (1999).
- [200]. Yoo, S., B. Domercq, and B. Kippelen, Applied Physics Letters, **85**(22), 5427-5429 (2004)
- [201]. Bassler, H., et al., Synthetic Metals, **91**(1-3) 173-179, (1997).
- [202]. Adachi, C., et al., Applied Physics Letters, **79**(13) 2082-2084, (2001).
- [203]. Mark, P. and W. Helfrich, Journal of Applied Physics, **33**(1) 205-215, (1962).
- [204]. M. Pope, H.P. Kallmann, and P. Magnante, Journal of Chemical Physics **38**, 2042 (1963).
- [205]. M. A. Lampert, Phys. Rev. **103**, 1648 (1956).

- [206]. M. A. Lampert and P. Mark, *Current injection in Solids* (New York Academic, (1970).
- [207]. S. M. Sze, *Physics of Semiconductor Devices* (A Wiley Interscience Publication, Newyork, 1981).
- [208]. J. C. Scott and G. G. Malliaras, *Chem. Phys. Lett.* **299**,115, (1999).
- [209]. Y. Shen, M. W. Klein, D. B. Jacobs, J. C. Scott and G. G. Malliaras, *Phys. Rev. Lett.* **86**, 3867 (2001).
- [210]. M. A. Abkowitz, H. A. Mizes and J. S. Facci, *Appl. Phys. Lett.* **66**, 1288 (1995).
- [211]. S. E. Shaheen, G. E. Jabbour, M. M. Morrell, Y. Kawabe, B. Kippelen, N. Peyghambarian, M. F. Nabor, R. Schlaf, E. A. Mash and N. R. Armstrong, *J. Appl. Phys.* **84**, 2324 (1998).
- [212]. Y. Q. Zhan, Z. H. Xiong, H. Z. Shi, S. T. Zhang, Z. Xu, G. Y. Zhong, J. He, J. M. Zhao, Z. J. Wang, E. Obbard, H. J. Ding, X. J. Wang, X. M. Ding, W. Huang and X. Y. Hou, *Appl. Phys. Lett.* **83**, 1656 (2003).
- [213]. C. Herring and M. H. Nichols, *Rev. Mod. Phys.* **21**, 185 (1949).
- [214]. H. D. Hagstrum, *Surf. Sci.* **54**, 197 (1976).
- [215]. P. Van Rysselberghe, *Chem. Phys.* **21**, 1550 (1953).
- [216]. H. Ishii, K. Sugiyama, E. Ito and K. Seki, *Adv. Mater.* **11**, 605 (1999).
- [217]. H. Ishii, K. Sugiyama, D. Yoshimura, E. Ito, Y. Ouchi and K. Seki, *IEEE journal of Selected Topics in Quantum Electronics*, **4**, 24 (1998).
- [218]. H. Ishii and K. Seki, *IEEE Trans. Electron Devices* **44**, 1295 (1997).

- [219]. H. Ishii, D. Yoshimura, K. Sugiyama, S. Narioka, Y. Hamatani, I. Kawamoto, T. Miyazaki, Y. Ouchi and K. Seki, *Synth. Met.* **85**, 1389 (1997).
- [220]. I. G. Hill, A. Rajagopal and A. Khan, *Appl. Phys. Lett.* **73**, 662 (1998).
- [221]. I. G. Hill, A. J. Makinen and Z. H. Kafafi, *Appl. Phys. Lett.* **77**, 1825 (2000).
- [222]. K. Sugiyama, D. Yoshimura, E. Ito, T. Miyazaki, Y. Hamatani, I. Kawamoto, H. Ishii, Y. Ouchi and K. Seki, *Synth. Met.* **86**, 2425 (1997).
- [223]. S. T. Lee, X. Y. Hou, M. G. Mason and C. W. Tang, *Appl. Phys. Lett.* **72**, 1593 (1998).
- [224]. T. Mori, H. Fujikawa, S. Tokito and Y. Taga, *Appl. Phys. Lett.* **73**, 2763 (1998).
- [225]. A. Rajagopal and A. Khan, *J. Appl. Phys.* **84**, 355 (1998).
- [226]. A. Rajagopal, C. I. Wu. and A. Khan, *J. Appl. Phys.* **83**, 2649 (1998).
- [227]. Q. T. Le, L. Yan, Y. Gao, M. G. Mason, D. J. Giesen and C. W. Tang, *J. Appl. Phys.* **87**, 375 (2000).
- [228]. H. Ishii, K. Sugiyama, E. Ito and K. Seki, *Adv. Mater.* **11**, 605 (1999).
- [229]. G. Paasch, H. Peisert, M. Knupfer, J. Fink and S. Scheinert, *J. Appl. Phys.* **93**, 6084 (2003).
- [230]. S. C. Chang, J. Liu, J. Bharathan, Y. Yang, J. Onohara, and J. Kido, *Advanced Materials*, **11**, 734-737, (1999).
- [231]. D. A. Pardo, G. E. Jabbour, and N. Peyghambarian, *Advanced Materials*, vol. **12**, 1249-1252, (2000).
- [232]. D. F. O'Brien, P. E. Burrows, S. R. Forrest, B. E. Koene, D. E. Loy, and M. E. Thompson, *Advanced Materials*, **10**, 1108- 1112, (1998).

- [233]. E. Bellmann, S. E. Shaheen, R. H. Grubbs, S. R. Marder, B. Kippelen, and N. Peyghambarian, *Chemistry of Materials*, **11**, pp. 399-407, (1999).
- [234]. Stolka, J.F. Yanus, and D.M. Pai, *Journal of Physical Chemistry* **88**, 4707 (1984).
- [235]. R.G. Kepler, P.M. Beeson, S.J. Jacobs, R.A. Anderson, M.B. Sinclair, V.S. Valencia, and P.A. Cahill, *Applied Physics Letters* **66**, 3618 (1995).
- [236]. Electron Display Central Home Page. 23 February( 2005).
- [237]. J. Zhao, S. Xie, S. Han, Z. Yang, L. Ye, T. Yang, *Physica Status Solidi (a)* **184**, 238 (2001).
- [238]. H. Aziz, Z. Popovic, S. Xie, A.M. Hor, N.X. Hu, C. Tripp, G. Xu, *Applied Physics Letters* **72**, 756 (1998).
- [239]. L Zhou, J Y Zhuang, S Tongay, W M Su and Z Cui, *J. Appl. Phys.* **114**, 074506 (2013)
- [240]. W P Hu, K Manabe, T Furukawa and M Matsumuda, *Appl. Phys. Lett.* **80**, 2640 (2002)
- [241]. D Kabra, L P Lu, M H Song, H J Snaith and R H Friend, *Adv. Mater.* **22**, 3194 (2010).
- [242]. S. R. Jawalekar, in Proc. of the Third Int. Workshop on Physics of Semiconductor Devices (Eds: S. C. Jain, S. Radhakrishna), World Scientific, Singapore 1985, pp. 147
- [243]. Kim, Yong Hyun, Sachse, Christoph, Machala, Michael L, May, Christian, Müller-Meskamp, Lars, Leo and Karl, *Advanced Functional Materials*. 21 (6), (2011).

- [244]. Kim, J. Y. Jung, J. H., Lee, D. E. and Joo J., *Synthetic Metals*. 126 (2–3), (2002).
- [245]. S. Tokito, K. Noda, Y. Taga, *J. Phys. D: Appl. Phys.* 29, 2750, (1996).
- [246]. K.J. Reynolds, J.A. Barker, N.C. Greenham, R.H. Friend, G.L. Frey, *J. Appl. Phys.* 92 7556, (2002).
- [247]. J. H. Ikeda, J. Sakata, M. Hayakawa, T. Aoyama, T. Kawakami, K. Kamata, Y. Iwaki, S. Seo, Y. Noda, R. Nomura, S. Yamazaki, *SID 06 DIGEST P-185*, 923, (2006).
- [248]. K. Miyake, H. Kaneko, M. Sano, N. Suedomi, *J. Appl. Phys.* 55, 2747, (1984).
- [249]. Z B Deng, X M Ding, L S Liao, X Y Hou and S T Lee, *Display***21**, 79 (2000)
- [250]. Z B Deng, X M Ding and S T Lee, *Appl. Phys. Lett.* **74**, 2227 (1999)
- [251]. A K Havari, M Can, S Demic, M Kus and S Icli, *Synth. Met.* **161**, 2397 (2012)
- [252]. H H Kim *et al*, *J. Lightwave Technol.* **12**(12), 2107, (1994)
- [253]. M. M. da Silva, A. R. Vaz, S. A. Moshkalev and J. W. Swart, *ECS Transactions*, **9**, 235, (2007).
- [254]. Van Calster A. and De Vos A., *Electrocomp.Sci. Technology*, 6, 131 (1980).
- [255]. Brody, T.P., *IEEE Trans. Electron Devices*, ED 31: 1614 ( 1984).
- [256]. Sze, S.M., *Physics of Semiconductor Devices*, John Wiley and Sons, New York (1969).
- [257]. Cerofolini, G.F. and Rovere, C., *Thin solid films*, 47, 83, (1977).
- [258]. Weimer, P.K., *Phys. Thin films*, 2 : 147. (1964b).

- [259]. Blech, I., Sello, H. and Gregor, L.V., Handbook of thin film technology 23-1, McGraw-Hill, New York, (1970).
- [260]. Erskine, J.C. and Cserhati, A., J. Vac. Sci. Technology, 15, 1823, (1978).
- [261]. Chan, D.S.H. and Hill, A.E., Thin solid films, 35, 337, (1976).
- [262]. W. J. Kim., Appl. Surface Sci., vol. 252, pp. 1332–1338, 2005.
- [263] W. J. Kim *et al.* *Electrochem. Solid-State Lett.*, 8, 12, 341– 344, (2005).
- [264]. Ouyang J., Chu C. W., Chen F. C., Xu Q. and Yang, Y. *Adv. Funct. Mater.* 15 203 ( 2005).
- [265]. Crispin, X., Marciniak and SO sikowicz *J. Polym. Sci., Part B: Polym. Phys.* 41 2561 (2003)
- [266]. Wu. X., Liu J. and Wu D., *J. Mater. Chem. C* 2 4044 (2014).
- [267]. A.M. Nardes, M. Kemerink, M.M. de Kok *et al.*, *Org. Electron.* 9 727 (2008).
- [268]. Na, S.-I., Wang, G., Kim, S.-S. *et al.*, *J. Mater. Chem.* 19 9045 (2009).
- [269]. Ali Kemal Havare, Mustafa Can, Serafettin Demic *et al.*, *Synthetic Metals.* 161 2397 (2011).
- [270]. G. Greczynski, T. Kugler, and W. R. Salaneck, *Thin Solid Films*, 354 129 (1999).
- [271]. Zhang Zhi-Feng, Deng Zhen-Bo, Liang Chun-Jun, Zhang Meng-Xin and Xu Deng-Hui 24 231 (2003).



- [272]. S. Amelincks and W. Dekeyser, *Solid state Physics (Advances in Res. and Appl.)*, 8 : 327, (1959).
- [273]. D.A. Vos, *Solid state electron*, 18 : 895 (1975).
- [274]. Y. Kashiwada, K. Miyashita, T. Seki and M. Wada, *Electronic Commun. Jpn.*, 52-C:157 (1969).
- [275]. R. Rohloff, N. B. Kotadiya, N. I. Crăciun, P. W. M. Blom, and G. A. H. Wetzelaer, *APPLIED PHYSICS LETTERS* 110, 073301 (2017)
- [276]. Debdutta Ray, Lorenzo Burtone, Karl Leo, and Moritz Riede, *PHYSICAL REVIEW B* **82**, 125204 (2010).
- [277]. Benjie N. Limketkai, *Charge carrier transport in amorphous organic semiconductor*, (2008).
- [278]. L. G. Kaake, P. F. Barbara, and X.-Y. Zhu, *J. Phys. Chem. Lett.* 2010, 1, 628–635
- [279]. Arne Fleissner, Hanna Schmid, Christian Melzer, and Heinz von Seggern, *Appl Phys Lett* **91**, 242103, (2007).
- [280]. Sandro Lattante, *Electronics*, 3, 132-164; [doi:10.3390/electronics3010132](https://doi.org/10.3390/electronics3010132), (2014).
- [281]. J S Kim, P K H Ho, N C Greenham and R H Friend, *J. Appl. Phys.* **88**(2), 1073 (2002)